University of Naples *Federico II*

Philosophical Doctor in

INGEGNERIA DELLE COSTRUZIONI

25° CYCLE

College of Teachers
Proff.: Antonio De Luca, Aldo Evangelista, Flavia Fascia, Renato Iovino, Raffaele Landolfo, Claudio Mancuso, Francesco Marotti de Sciarra, Maurizio Nicolella, Marco Valerio Nicotera, Luciano Nunziante, Mario Pasquino, Pasquale Petrella, Luciano Rosati, Gianpiero Russo, Giorgio Serino, Federico Massimo Mazzolani.

Coordinator: Prof. Luciano Rosati

MARZO 2010 – FEBBRAIO 2013

Coordinator	Tutor	Candidate
Prof. Luciano Rosati	Prof. Massimiliano Fraldi	Dott. Luca Esposito
……	……	……

INDEX

MOTIVATION OF THE WORK

The idea at the basis of this work is the extent of the utilization of Topology Optimization strategies, implemented with custom-made algorithms, totally integrate in a commercial numeric code, to multi-physic fields as biomechanics and poro-elasticity where this procedure is not usually adopted.

INTRODUCTION

The scientific literature on research and applications in civil, chemical and mechanical engineering, as well as in material science has recently shown great interest in computational strategies aimed to optimize structures and materials at different levels of scale. Composites, polymers, fiber reinforced elements, porous media, micro-and nano-structured materials have been indeed widely used in many industry realms, covering applications in both traditional frameworks, say civil and mechanical engineering, and pioneer fields, such as aerospace, biomechanics and tissue engineering.

Along with technological advances associated with the production systems, an increasing interest has been recorded, in recent years, in the development of numerical techniques and software providing design criteria for the topology (TO) and structural (DO) optimization of components for the design and engineering of specific industrial products. These strategies are planned to determine, under given constraints, the shape and stiffness-weight ratio ideal for a given material, also by employing logics inspired by the evolutionary processes of functional reorganization of biological structures (tissue remodeling, healing processes). These ways have been then utilized to explore the possibility of building up innovative protocols for the manufacturing of mechanical parts or to design biomaterials matching performance requirements through structural modification (change in the distribution of mass within the volume of the component, optimal orientation of fibers in composites, etc.) from the original material. In this specific framework, closely connected to the interest

of the different industrial sectors mentioned above, the topology optimization plays a central role in the processes of technological innovation. In fact, as demonstrated by the scientific community that has recently given more and more interest to these issues, it is expected that the introduction of these logics to optimize the processes of industrial production may open new scenarios in providing solutions with high technology and low ambient impact.
In particular, Topology Optimization has, as objective function, the purpose of maximizing a given mechanical characteristic, minimizing at the same time the weight of the component; in this way it is possible to contemporarily obtain structural performance required by specific applications for which the material is designed, and – via the reduction of the weight – to respond to the urgent demand for decreasing in the amount of raw material with the effect of reducing consumption and costs.
Moreover, if the adoption of strategies based on Topology Optimization was used in designing structures for automotive, aerospace or naval in large scale, the result would be a huge reduction of the overall amount of material and production costs per unit of product with consequent advantages for both the manufacturer – in terms of competitiveness and profit – and the consumer, due to a significant advantage in terms of overall savings and ambient impact.
A similar line of reasoning could be applied with reference to products with applications to structural and biomedical fields, where once again the process of Topology Optimization could provide a strategic reply to requirement of balancing the need of increasing the standard of quality and of reducing invasiveness, cost and environmental impact. This strategy has been applied in hip arthroplasty in order to minimize the probability of failure of prosthetic implants in the case of aseptic loosening, i.e. the separation of the stem of the prosthesis from the femoral canal in the non-infection; this objective is often achieved by minimizing the stresses at the implant-bone interface. Aseptic loosening of the prosthetic implant is indeed mainly caused by bone absorption that is determined by the phenomenon of stress-shielding, i.e. the stress protection produced by the prosthesis due to its greater stiffness that overpasses the bone causing the absorption. A computational strategy based on Topology Optimization has been used to reduce this phenomenon.
Finally, by looking towards multi-physics applications and forcing a thermo-mechanical commercial code to perform poro-elastic analyses by exploiting a duality principle between the theories, the present work shows two examples of poro-elasticity problems of relevant interest in biomechanical applications: the modeling of the osteon, basis cellular unit of the bone, and drug infusion in solid tumor spheroids.
The Ph.D. dissertation is articulated in ten chapters.
Chapter I furnishes some basic remarks on theory of elasticity, recalling the concepts of finite deformation and kinematical compatibility, equilibrium and Cauchy's and Piola-Kirchhoff's stress tensors, with some key notes on linear anisotropic elasticity.

Chapter II describes continuum mechanics approaches for heterogeneous media, also presenting some recent results aimed to obtain closed-form solutions for inhomogeneous, anisotropic elastostatic problems. At the end, a micromechanical approach based on second order Fabric Tensors is treated, with reference to the most recent literature results.
Chapter III provides an introduction to the theory of homogenization. In particular, some mathematically well-posed homogenization approaches are presented such as the direct method, the Eshelby's solution and the variational methods, based on the Hashin-Shtrikman variational principles. Micro-mechanics of porous materials is also finally shown.
Chapter IV introduces the Finite Element Method additionally giving some basic remarks and describing it is possible to run mechanical analyses with the numerical commercial code Ansys®, specifically adopted here to perform the analyses.
Chapter V illustrates the Topology Optimization theory based on Solid Isotropic Material Penalization (SIMP) by essentially following the approach by Bendsøe; the formulation of the problem in the case of depleted media have been proposed with some basic statements. Finally, the Topology Optimization problems for anisotropic media have been discussed.
Chapter VI describes how Topology Optimization have been applied to an hip prosthesis in order to reduce the Stress Shielding phenomenon and at the end insights on the restrictions of the numerical code Ansys® used to perform Topology Optimization have been highlighted; moreover the limits in terms of setting of the bone material properties and of building the finite element-based model have been underlined.
In chapter VII the first innovative and original custom-made algorithm, developed to perform Topology Optimization, have been explained in details with different examples; furthermore parts of numerical codes written in APDL (Ansys Parametric Design Language) in the case of macros and in UIDL (User Interface Design Language) in the case of menu have been reported and commented. Finally, in order to underline how the numeric code Ansys® is able to perform Topology Optimization only for structure subjected to applied forces, a comparison between Ansys® and custom-made algorithm have been proposed.
Chapter VIII describes the second innovative and original custom-made procedure able to acquire information about densities in biological structure as bones or levels of matrices fractions in microstructured materials by means of vector graphics files or DICOM (Digital Imaging and Communications in Medicine) files, in this way transforming automatically and in real time these information in stiffness and strength values to which one can associate mechanical contents and thus generate finite element-based models.
Chapter IX, looking towards multi-physics applications, gives some remarks on the duality between the theory of poro-elasticity and thermo-elasticity and – on this basis – an *ad hoc* finite element-based procedure has been constructed in

order to force a thermo-mechanical commercial code to perform poro-elastic analyses.
Among the different possible perspectives, in chapter X are selected two examples of multi-physics problems and, in particular, an application of poro-elasticity to osteon structures, basis cellular units of the bone, and another to simulate the drug infusion in solid tumor spheroids.

1 REMARKS ON THEORY OF ELASTICITY

Linear elasticity is one of the more successful theories of mathematical physics. Its pragmatic success in describing the small deformations of many materials is uncontested.

The origins of the three-dimensional theory go back to the beginning of the 19th century and the derivation of the basic equations by Cauchy, Navier and Poisson. The theoretical development of the subject continued at a brisk pace until the early 20th century with the work of Beltrami, Betti, Boussinesq, Kelvin, Kirchhoff, Lamè, Saint-Venant, Somigliana, Stokes and others. These authors established the basic theorems of the theory, namely compatibility, reciprocity and uniqueness and deduced important general solutions of the underlying field equations.

In the 20th century the emphasis shifted to the solution of boundary-value problems and the theory itself remained relatively dormant until the middle of the century when new results appeared concerning, among other things, Saint-Venant's principle, stress functions, variational principles and uniqueness.

Marquis Pierre-Simon de Laplace (1759-1827): "Thus, we must consider the present state of the universe as the effect of its previous state and as the cause of those states to follow. An intelligent being which, for a given point in time, knows all the forces acting upon the universe and the positions of the objects of which it is composed, supplied with facilities large enough to

submit these data to numerical analysis, would include in the same formula the movements of the largest bodies of the universe and those of the lightest atom. Nothing would be uncertain for it and the past and future would be known to it".

Herbert Callen, in his book on thermodynamics, introduces the conservation of energy and the concept of internal energy: the development of the principle of conservation of energy has been one of the most significant achievements in the evolution of physics. The present form of the principle was not discovered in one magnificent stroke of insight but has been slowly and laboriously developed over two and a half centuries. The first recognition of a conservation principle, by Leibnitz in 1693, referred only to the sum of the kinetic energy and the potential energy of a simple mechanical mass point in the terrestrial gravitational field. As additional types of systems were considered, the established form of the conservation principle repeatedly failed, but in each case it was found possible to revive it by the addition of a new mathematical term a "new kind of energy". The energy conservation principle is now accepted as one of the most fundamental, general, and significant principles of physical theory. By essentially following the books by Ciarlet and Timoshenko, synthetic continuum mechanical foundations have been proposed.

1.1. KINEMATICAL FOUNDATIONS

1.1.1. Deformations in $\mathbf{R}^3$

In three-dimensional Euclidean space, which will therefore be identified with the space $\mathbf{R}^3$, an origin O and an orthonormal basis $\{\mathbf{e}_1, \mathbf{e}_2, \mathbf{e}_3\}$ have been chosen. From the notational viewpoint, we identify the point $\mathbf{x}$ with the vector $\mathbf{ox}$. Whenever we consider components of vectors in $\mathbf{R}^3$ or elements of matrices in $\mathbf{M}^3$, we make the convention that Latin indices {i, j, p} always take their values in the set {1,2,3} and we combine this rule with the standard summation convention. Let there be given a bounded, open and connected subset Ω of $\mathbf{R}^3$ with a sufficiently smooth boundary.

We shall think of the closure $\overline{\Omega}$ of the set Ω as representing the volume occupied by a body before it is deformed; for this reason, the set $\overline{\Omega}$ is called the *reference configuration*.

A deformation of the reference configuration $\overline{\Omega}$ is a vector field:

$$\varphi : \overline{\Omega} \to \mathbf{R}^3 \tag{1.1}$$

that is smooth enough, injective possibly on the boundary of the set Ω and orientation-preserving. We denote by $\mathbf{x}$ a generic point in the set $\overline{\Omega}$, by x_i its components with respect to the basis $\{\mathbf{e}_i\}$ and by $\partial_i = \partial/\partial x_i$ the partial derivative with respect to variable x_i.
Given a deformation $\boldsymbol{\varphi} = \varphi_i \mathbf{e}_i$, we define at each point of the set Ω the matrix:

$$\nabla\boldsymbol{\varphi} := \begin{pmatrix} \partial_1\varphi_1 & \partial_2\varphi_1 & \partial_3\varphi_1 \\ \partial_1\varphi_2 & \partial_2\varphi_2 & \partial_3\varphi_2 \\ \partial_1\varphi_3 & \partial_2\varphi_3 & \partial_3\varphi_3 \end{pmatrix} \tag{1.2}$$

The matrix $\nabla\boldsymbol{\varphi}$ is called the *deformation gradient*.
Since a deformation is orientation-preserving by definition, the determinant of the deformation gradient satisfies the orientation-preserving condition:

$$\det \nabla\boldsymbol{\varphi}(\mathbf{x}) > 0 \quad \text{for all} \quad x \in \overline{\Omega}$$

In particular, the matrix $\nabla\boldsymbol{\varphi}(\mathbf{x})$ is invertible at all points $\mathbf{x}$ of the reference configuration $\overline{\boldsymbol{\Omega}}$. Together with a deformation φ, it is often convenient to introduce the displacement $\mathbf{u}$, which is the vector field:

$$\mathbf{u} : \overline{\Omega} \to \mathbf{R}^3 \tag{1.3}$$

defined by the relation:

$$\boldsymbol{\varphi} = \mathbf{id} + \mathbf{u} \tag{1.4}$$

where $\mathbf{id}$ denotes the identity map from $\mathbf{R}^3$ onto $\mathbf{R}^3$. Notice that the displacement gradient is:

$$\nabla\mathbf{u} := \begin{pmatrix} \partial_1 u_1 & \partial_2 u_1 & \partial_3 u_1 \\ \partial_1 u_2 & \partial_2 u_2 & \partial_3 u_2 \\ \partial_1 u_3 & \partial_2 u_3 & \partial_3 u_3 \end{pmatrix} \tag{1.5}$$

and the deformation gradient is related by the equation:

$$\nabla \boldsymbol{\varphi} = \mathbf{I} + \nabla \mathbf{u} \tag{1.6}$$

Given a reference configuration $\bar{\Omega}$ and a deformation $\boldsymbol{\varphi} : \bar{\Omega} \to \mathbf{R}^3$, the set $\boldsymbol{\varphi}(\bar{\Omega})$ is called a *deformed configuration*.

At each point: $\mathbf{x}^{\varphi} := \boldsymbol{\varphi}(\mathbf{x})$ of a deformed configuration, we define the three vectors (Fig.1.1):

$$\partial_j \boldsymbol{\varphi}(\mathbf{x}) = \partial_j \varphi_i(\mathbf{x}) \mathbf{e}_i \tag{1.7}$$

Each vector $\partial_j \boldsymbol{\varphi}(\mathbf{x})$ measures the local deformation in the direction of the vector $\mathbf{e}_j$ in the sense that, to within the first order with respect to dt, the vector $\mathbf{e}_j dt$ is transformed into the vector $\partial_j \boldsymbol{\varphi}(\mathbf{x}) dt$.

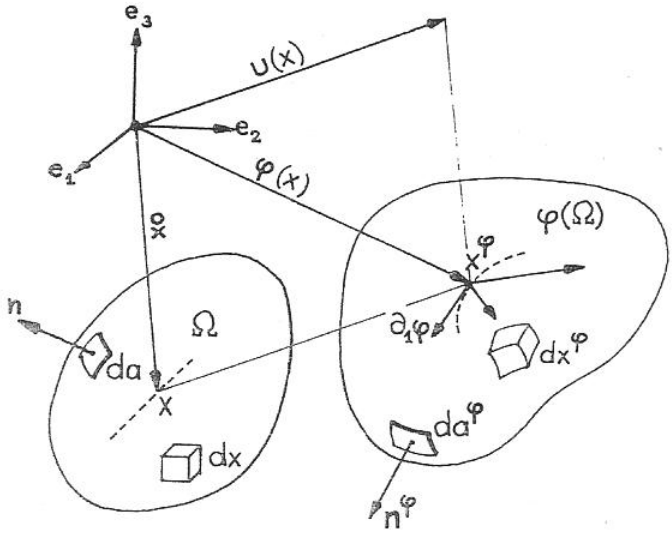

Fig. 1.1 – Geometry of a deformation: the volume element, the area element and the unit outer normal are denoted $dx, da, \mathbf{n}$ in the reference configuration $\bar{\Omega}$ and dx^{φ}, da^{φ}, $\mathbf{n}^{\varphi}$ in the deformed configuration $\boldsymbol{\varphi}(\bar{\Omega})$. The vectors $\partial_j \boldsymbol{\varphi}(\mathbf{x})$ define the deformation at a point $x \in \bar{\Omega}$ to within the first order.

Equivalently, the vector $\partial_j \boldsymbol{\varphi}(\mathbf{x})$ is the tangent vector to the j-th coordinate line passing through the point $\mathbf{x}^{\varphi}$ (i.e. the image by the deformation $\boldsymbol{\varphi}$ of a segment parallel to the vector $\mathbf{e}_j$ containing the point $\mathbf{x}$ in its interior and parameterized by t). Since the vector $\partial_j \boldsymbol{\varphi}(\mathbf{x})$ is precisely the j-th column of the matrix $\nabla \boldsymbol{\varphi}(\mathbf{x})$

the knowledge of the deformation gradient completely defines the local deformation to within the first order.

Note that, while the deformation gradient $\nabla\boldsymbol{\varphi}(\mathbf{x})$ clearly depends upon the basis $\mathbf{e}_i$, it is possible to exhibit the intrinsic geometrical character of the deformation at the point $\mathbf{x}$ by means of the polar factorization of the matrix $\nabla\boldsymbol{\varphi}(\mathbf{x})$, which appears as the product of a rotation tensor by a stretch tensor.

Moreover, the points $\mathbf{x} \in \Omega$ and the corresponding points $\mathbf{x}^{\varphi} \in \boldsymbol{\varphi}(\Omega)$ are often called *material points* and *spatial points* respectively and they are often respectively denoted X and $\mathbf{x}$ in the continuum mechanics literature.

We next compute the volume, area and length elements in the deformed configuration: in each case, the objective is, for a given deformation, to express quantities (volumes, surfaces and lengths) defined over the deformed configuration in terms of the same quantities, but defined over the reference configuration.

To emphasize the crucial distinction between both types of quantities, we adopt the superscript "$\boldsymbol{\varphi}$" notational device. This correspondence between a quantity defined as a function of the Lagrange variable $\mathbf{x}$ and a similar quantity defined as a function of the Euler variable $\mathbf{x}^{\varphi} = \boldsymbol{\varphi}(\mathbf{x})$, can be extended to other quantities as volume, surfaces and lengths.

1.1.2. Volume Element in the Deformed Configuration

Let φ be a deformation.

If dx denotes the volume element at the point $\mathbf{x}$ of the reference configuration, the volume element dx^{φ} at the point $\mathbf{x}^{\varphi} = \boldsymbol{\varphi}(\mathbf{x})$ of the deformed configuration (Fig. 1.1) is given by:

$$dx^{\varphi} = \det \nabla\boldsymbol{\varphi}(x)\, dx \tag{1.8}$$

since $\left|\det \nabla\boldsymbol{\varphi}(x)\right| = \det \nabla\boldsymbol{\varphi}(x) > 0$ by assumption.

The volume element dx^{φ} is used for computing volumes in the deformed configuration.

If A denotes a measurable subset of the reference configuration $\bar{\Omega}$, the volume of the set A and the volume of the deformed set $A^{\varphi} := \varphi(A)$ are respectively given by:

$$vol\ A := \int_A dx, \quad vol\ A^{\varphi} := \int_{A^{\varphi}} dx^{\varphi} = \int_A \det \nabla \boldsymbol{\varphi}(x)\, dx \tag{1.9}$$

1.1.3. Length Element in the Deformed Configuration: the Strain Tensor

If a deformation $\boldsymbol{\varphi}$ is differentiable at a point $\mathbf{x} \in \overline{\Omega}$, then we can write for all points $x + \boldsymbol{\delta}\mathbf{x} \in \overline{\Omega}$:

$$\boldsymbol{\varphi}(x + \boldsymbol{\delta}\mathbf{x}) - \boldsymbol{\varphi}(x) = \nabla \boldsymbol{\varphi}(x)\boldsymbol{\delta}\mathbf{x} + o(|\boldsymbol{\delta}\mathbf{x}|) \tag{1.9}$$

whence:

$$|\boldsymbol{\varphi}(x + \boldsymbol{\delta}\mathbf{x}) - \boldsymbol{\varphi}(x)|^2 = \boldsymbol{\delta}\mathbf{x}^T \nabla \boldsymbol{\varphi}^{\boldsymbol{T}}(x) \nabla \boldsymbol{\varphi}(x) \boldsymbol{\delta}\mathbf{x} + o(|\boldsymbol{\delta}\mathbf{x}|^2) \tag{1.10}$$

The symmetric tensor:

$$C := \nabla \boldsymbol{\varphi}^{\boldsymbol{T}} \nabla \boldsymbol{\varphi} \tag{1.11}$$

in the above expression is called the *right Cauchy-Green Strain Tensor*. Notice that the associated quadratic form:

$$(\boldsymbol{\xi}, \boldsymbol{\xi}) \in \mathbf{R}^3 \times \mathbf{R}^3 \rightarrow \boldsymbol{\xi}^T \mathbf{C}(x) \boldsymbol{\xi} = |\nabla \boldsymbol{\varphi}(x) \boldsymbol{\xi}^2| \tag{1.12}$$

is positive definite at all points $\mathbf{x} \in \overline{\Omega}$, since the deformation gradient $\nabla \boldsymbol{\varphi}$ is everywhere invertible by assumption. As expected, this quadratic form is used for computing lengths. Let:

$$\gamma = f(I), \quad f : I \rightarrow \overline{\Omega}, \text{ I: compact interval of R} \tag{1.13}$$

be a curve in the reference configuration. Denoting by f_i the components of the mapping $\mathbf{f}$, the length of the curve γ is given by $\left(f' = \frac{df}{dt} \right)$:

$$\text{length } \gamma := \int_L |f'(t)|\, dt = \int_L \{ f'(t) f'(t) \}^{1/2}\, dt \tag{1.14}$$

while the length of the deformed curve $\gamma^{\varphi} : \boldsymbol{\varphi}(\gamma)$ is given by:

$$\text{length } \gamma^{\varphi} := \int_L \left|\boldsymbol{\varphi} \circ f'(t)\right| dt = \int_L \left\{C_{ij}\left(f(t)\right) f'(t) f'(t)\right\}^{1/2} dt \qquad (1.15)$$

Consequently, the length elements dl and dl^{φ} in the reference and in the deformed configurations may be symbolically written as (Fig. 1.2):

$$dl = \left\{\mathbf{dx}^T \mathbf{dx}\right\}^{1/2}, \quad dl^{\varphi} = \left\{\mathbf{dx}^T \mathbf{C}\, \mathbf{dx}\right\}^{1/2} \qquad (1.16)$$

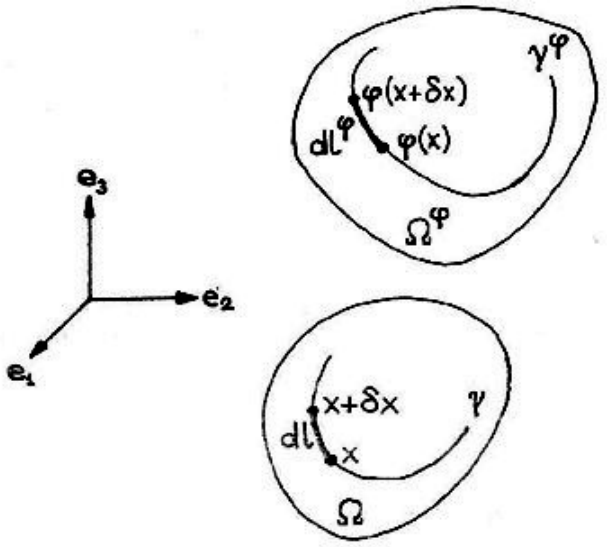

Fig. 1.2 – The length elements $dl = \left\{\mathbf{dx}^T \mathbf{dx}\right\}^{1/2}$ and $dl^{\varphi} = \left\{\mathbf{dx}^T \mathbf{C}\, \mathbf{dx}\right\}^{1/2}$ in the reference and deformed configurations. The tensor $\mathbf{C} = \nabla \boldsymbol{\varphi}^{\boldsymbol{T}} \nabla \boldsymbol{\varphi}$ is the right Cauchy-Green tensor.

If in particular $\mathbf{dx} = dt\, \mathbf{e}_j$, the corresponding length element in the deformed configuration is $\left\{\mathbf{C}_{jj}\right\}^{1/2} dt = \left|\partial_j \boldsymbol{\varphi}\right| dt$.

In view of showing that the tensor $\mathbf{C}$ is indeed a good measure of strain, let us first consider a class of deformations inducing no strain. A deformation is called a *rigid deformation* if it is of the form:

$$\boldsymbol{\varphi}(x) = \mathbf{a} + \mathbf{Q}\, o\, \mathbf{x}, \quad \mathbf{a} \in \mathbf{R}, \quad \mathbf{Q} \in \mathbf{O}^3_+, \text{ for all } \mathbf{x} \in \bar{\Omega} \qquad (1.17)$$

where $\mathbf{O}^3_+$ denotes the set of rotations in $\mathbf{R}^3$.

Observe that (Fig. 1.3) the rotation $\mathbf{Q}$ may be performed around any point $\tilde{\mathbf{x}} \in \mathbf{R}^3$, since we can also write:

$$\boldsymbol{\varphi}(x) = \boldsymbol{\varphi}(\tilde{x}) + \mathbf{Q}\,\tilde{\mathbf{x}}\,\mathbf{x} \tag{1.18}$$

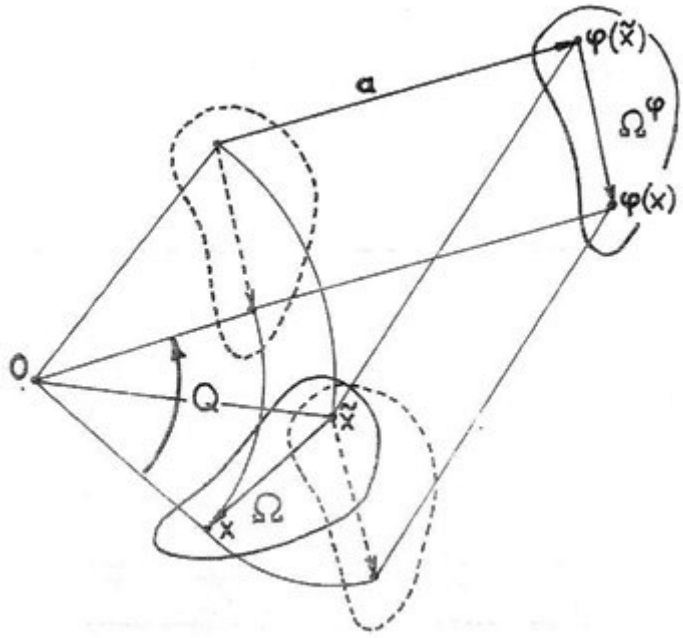

Fig. 1.3 – A rigid deformation is a translation, followed by a rotation (or viceversa) of the reference configuration.

If $\boldsymbol{\varphi}$ is a rigid deformation, then $\nabla\boldsymbol{\varphi}(x) = \mathbf{Q} \in \mathbf{O}^3_+$ at all points $\mathbf{x} \in \bar{\Omega}$, and therefore:

$$\mathbf{C} = \mathbf{I} \text{ in } \bar{\Omega}, \text{ i.e. , } \nabla\boldsymbol{\varphi}(x)^T \nabla\boldsymbol{\varphi}(x) = I \text{ for all } \mathbf{x} \in \bar{\Omega} \tag{1.19}$$

It is remarkable that conversely, if $\mathbf{C} = \mathbf{I}$ in $\bar{\Omega}$ and $\det\nabla\boldsymbol{\varphi} > 0$, the corresponding deformation is necessarily rigid.
We let $\mathbf{O}^n$ denote the set of all orthogonal matrices of order n.
The difference:

$$2\mathbf{E} := \mathbf{C} - \mathbf{I} \tag{1.20}$$

is a measure of the deviation between a given deformation and a rigid deformation, since $\mathbf{C} = \mathbf{I}$ if and only if the deformation is rigid.

Two deformations corresponding to the same tensor C differ by a rigid deformation.
The knowledge of the tensor field $\mathbf{C}:\Omega\to\mathbf{S}^3$ completely determines the deformation, up to composition with rigid deformations.
These considerations are illustrated in the following figure 1.4.

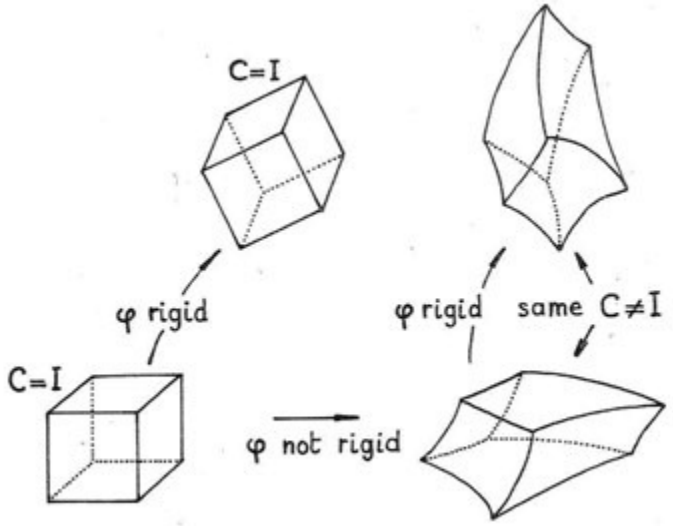

Fig. 1.4 – The right Cauchy-Green tensor $\mathbf{C}$ is equal to $\mathbf{I}$ if and only if the deformation is rigid. Two deformations corresponding to the same tensor C differ by a rigid deformation

The tensor $\mathbf{E}$ is called the *Green-Lagrange strain tensor*. Expressed in terms of the displacement gradient $\nabla\mathbf{u}$, in lieu of the deformation gradient $\nabla\boldsymbol{\varphi}=\mathbf{I}+\nabla\mathbf{u}$ (recall that $\boldsymbol{\varphi}=\mathbf{id}+\mathbf{u}$), the strain tensor $\mathbf{C}$ becomes:

$$\mathbf{C}=\nabla\boldsymbol{\varphi}^T\nabla\boldsymbol{\varphi}=\mathbf{I}+\nabla\mathbf{u}^T+\nabla\mathbf{u}+\nabla\mathbf{u}^T\nabla\mathbf{u}=\mathbf{I}+2\mathbf{E} \tag{1.21}$$

With:

$$\mathbf{E}(\mathbf{u}):=\mathbf{E}=\frac{1}{2}\left(\nabla\mathbf{u}^T+\nabla\mathbf{u}+\nabla\mathbf{u}^T\nabla\mathbf{u}\right) \tag{1.22}$$

For future use, we record the formulas:

$$C_{ij}=\partial_i\varphi_k\partial\varphi_k,\quad E_{ij}=\frac{1}{2}\left(\partial_i u_j+\partial_j u_i+\partial_i u_k\partial_j u_k\right) \tag{1.23}$$

where $\boldsymbol{\varphi} = \varphi_i \mathbf{e}_i$, $\mathbf{u} = u_i \mathbf{e}_i$. Note that the introduction of the factor ½ in the definition of the tensor $\mathbf{E}$ is motivated by the requirement that its first order part $\frac{1}{2}\left(\nabla \mathbf{u}^T + \nabla \mathbf{u}\right)$ coincide with the linearized strain tensor. Besides, the tensor $\left(\mathbf{C}^{1/2} - \mathbf{I}\right)$ was sometimes advocated as an alternative measure of strain and the factor ½ had the effect that the first order parts of both tensor $\mathbf{E}$ and $\left(\mathbf{C}^{1/2} - \mathbf{I}\right)$ coincide.

1.2. STATIC FOUNDATIONS

1.2.1. The Equations of Equilibrium

A body occupying a deformed configuration $\bar{\Omega}^{\varphi}$, subjected to applied body forces in its interior Ω^{φ} and to applied surfaces forces on a portion $\Gamma_1^{\varphi} = \varphi\left(\Gamma_1\right)$ of its boundary, is in static equilibrium if the fundamental stress principle of Euler and Cauchy is satisfied.
This axiom is the basis of continuum mechanics and implies the celebrated Cauchy theorem, according to which there exists a symmetric tensor field $\mathbf{T}^{\varphi} : \bar{\Omega}^{\varphi} \to \mathbf{S}^3$ such that:

$$\begin{cases} -div^{\varphi}\mathbf{T}^{\varphi} = \mathbf{f}^{\varphi} & in \quad \Omega^{\varphi} \\ \mathbf{T}^{\varphi}\mathbf{n}^{\varphi} = \mathbf{g}^{\varphi} & in \quad \Gamma_1^{\varphi} \end{cases} \tag{1.24}$$

where $\mathbf{f}^{\varphi}$ and $\mathbf{g}^{\varphi}$ are the densities of the applied body and surface forces respectively and $\mathbf{n}^{\varphi}$ is the unit outer normal vector along Γ_1^{φ}.
These equations are called the equilibrium over the deformed configuration and the tensor $\mathbf{T}^{\varphi}$ is called the *Cauchy Stress Tensor*.
A remarkable feature of these equations is their divergence structure, which makes them amenable to a variational formulation; a disadvantage is that they are expressed in terms of the unknown $\mathbf{x}^{\varphi} = \varphi\left(\mathbf{x}\right)$.
In order to obviate this difficulty while retaining the divergence structure of the equations, we use the Piola transform $\mathbf{T} : \bar{\Omega} \to \mathbf{M}^3$ of the Cauchy stress tensor field, which is defined by $\mathbf{T}\left(\mathbf{x}\right) = \mathbf{T}^{\varphi}\left(\mathbf{x}^{\varphi}\right) Cof \nabla \boldsymbol{\varphi}\left(\mathbf{x}\right)$.
In this way, it is found that the equilibrium equations over $\bar{\Omega}^{\varphi}$ are equivalent to the equilibrium equations over the reference configuration $\bar{\Omega}$:

$$\begin{cases} -div\,\mathbf{T} = \mathbf{f} & in \quad \Omega \\ \mathbf{T}\mathbf{n} = \mathbf{g} & in \quad \Gamma_1 \end{cases} \tag{1.25}$$

where $\mathbf{n}$ denotes the unit outer normal vector along Γ_1.

The fields $\mathbf{f}:\Omega \to \mathbf{R}^3$ and $\mathbf{g}:\Gamma_1 \to \mathbf{R}^3$ are related to the fields $\mathbf{f}^\varphi:\Omega^\varphi \to \mathbf{R}^3$ and $\mathbf{g}^\varphi:\Gamma_1^\varphi \to \mathbf{R}^3$ by the simple formulas $\mathbf{f}\,dx = \mathbf{f}^\varphi dx^\varphi$ and $\mathbf{g}\,dx = \mathbf{g}^\varphi dx^\varphi$. Because they are still in divergence form, these equations can be given a variational formulation, known as the *Principle of Virtual Work*. The tensor $\mathbf{T}$ is called the *first Piola-Kirchhoff Stress Tensor*.

We also introduce the symmetric *second Piola-Kirchhoff Stress Tensor* $\mathbf{\Sigma} = \nabla\boldsymbol{\varphi}^{-1}\mathbf{T}$, which naturally arises in the expression of the constitutive equations of elastic materials.

The applied forces describe the action of the outside world on the body. An elementary force $\mathbf{f}^\varphi(x)dx^\varphi$ is exerted on the elementary volume dx^φ at each point x^φ of the deformed configuration. Likewise, an elementary force $\boldsymbol{g}^\varphi(x^\varphi)da^\varphi$ is exerted on the elementary area da^φ at each point x^φ of the subset Γ_1^φ of the boundary of the deformed configuration (Fig 1.5). Such forces generally represent the action of another body along the portion Γ_1^φ of the boundary.

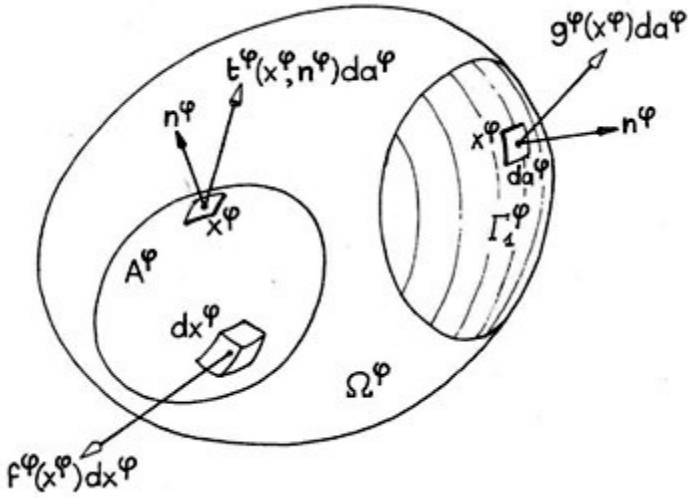

Fig. 1.5 – Applied forces comprise applied body forces $\mathbf{f}^\varphi(x)dx^\varphi$, $x^\varphi \in \Omega^\varphi$ and applied surface forces $\mathbf{g}^\varphi(x)dx^\varphi$, $x^\varphi \in \Gamma_1^\varphi$.

1.2.2. The Stress Principle of Euler and Cauchy

Continuum mechanics for static problems is founded on the following axiom, named after the fundamental contributions of Euler and Cauchy. The exterior product in $\mathbf{R}^3$ is denoted by $\wedge$.
Consider a body occupying a deformed configuration $\bar{\Omega}^\varphi$ and subjected to applied forces represented by densities $\boldsymbol{f}^\varphi := \Omega^\varphi \to R^3$ and $\boldsymbol{g}^\varphi := \Omega^\varphi \to \mathbf{R}^3$. Then there exists a vector field:

$$\mathbf{t}^\varphi : \Omega^\varphi \times S_1 \to R^3, \text{ where } S_1 = \left\{ v \in \mathbb{R}^3; |\mathbf{v}| = 1 \right\} \tag{1.26}$$

Such that:

(a) for any sub-domain A^φ of $\bar{\Omega}^\varphi$ and at any point $\mathbf{x}^\varphi \in \Gamma_1^\varphi \cap \partial A^\varphi$ where the unit outer normal vector $\mathbf{n}^\varphi$ exists: $\mathbf{t}^\varphi\left(\mathbf{x}^\varphi, \mathbf{n}^\varphi\right) = \mathbf{g}^\varphi\left(\mathbf{x}^\varphi\right)$

(b) Axiom of Force Balance: for any sub-domain A^φ of $\bar{\Omega}^\varphi$:

$$\int_{A^\varphi} \mathbf{f}^\varphi\left(\mathbf{x}^\varphi\right) dx^\varphi + \int_{\partial A^\varphi} \mathbf{t}^\varphi\left(\mathbf{x}^\varphi, \mathbf{n}^\varphi\right) dx^\varphi = \mathbf{0}, \tag{1.27}$$

where $\mathbf{n}^\varphi$ denotes the unit outer normal vector along ∂A^φ.

(c) Axiom of Moment Balance: for any sub-domain A^φ of $\bar{\Omega}^\varphi$:

$$\int_{A^\varphi} \mathbf{o}\mathbf{x}^\varphi \wedge \mathbf{f}^\varphi\left(\mathbf{x}^\varphi\right) dx^\varphi + \int_{\partial A^\varphi} \mathbf{o}\mathbf{x}^\varphi \wedge \mathbf{t}^\varphi\left(\mathbf{x}^\varphi, \mathbf{n}^\varphi\right) dx^\varphi = \mathbf{0} \tag{1.28}$$

Thus the stress principle first asserts the existence of elementary surface forces $\mathbf{t}^\varphi\left(\mathbf{x}^\varphi, \mathbf{n}^\varphi\right) da^\varphi$ along the boundaries of all domains of the reference configuration.
Secondly, the stress principle asserts that at a point $\mathbf{x}^\varphi$ of the boundary ∂A^φ of a sub-domain A^φ, the elementary surface force depends on the sub-domain A^φ, only via the normal vector $\mathbf{n}^\varphi$ to ∂A^φ at $\mathbf{x}^\varphi$.
Thirdly, the stress principle asserts that any sub-domain A^φ of the deformed configuration $\bar{\Omega}^\varphi$, including $\bar{\Omega}^\varphi$ itself, is in static equilibrium, in the sense that the torsor formed by the elementary forces $\mathbf{t}^\varphi\left(\mathbf{x}^\varphi, \mathbf{n}^\varphi\right) da^\varphi$, $x^\varphi \in \partial A^\varphi$, $\mathbf{n}^\varphi$ normal to ∂A^φ at $\mathbf{x}^\varphi$ and the body forces $\mathbf{f}^\varphi\left(\mathbf{x}^\varphi\right) d\mathbf{x}^\varphi$, $\mathbf{x}^\varphi \in A^\varphi$, is equivalent to zero. This means that both the resultant vector and its resulting moment with respect

to the origin (and thus with respect to any other point, by a classical property of torsos) vanish.
Hence the stress principle mathematically express, in the form of an axiom, the intuitive idea that the static equilibrium of any sub-domain A^φ of $\bar{\Omega}^\varphi$, already subjected to given applied body forces $\mathbf{f}^\varphi\left(\mathbf{x}^\varphi\right)d\mathbf{x}^\varphi$, $\mathbf{x}^\varphi \in A^\varphi$ and to given applied surface forces $\mathbf{g}^\varphi\left(\mathbf{x}^\varphi\right)da^\varphi$, at those points $\mathbf{x}^\varphi \in \Gamma_1^\varphi \cap \partial A^\varphi$ where the outer normal vector to $\Gamma_1^\varphi \cap \partial A^\varphi$ exists, is made possible by the added effect of elementary surfaces forces of the specific form indicated, acting on the remaining part of the boundary ∂A^φ.
Gurtin called system of forces the set formed by the applied body forces, corresponding to the vector field $\boldsymbol{f}^\varphi := \Omega^\varphi \to \mathbf{R}^3$ and by the surface forces, corresponding to the vector field $\boldsymbol{t}^\varphi := \Omega^\varphi \times S_1 \to \mathbf{R}^3$.
Let $\mathbf{x}^\varphi$ be a point of the deformed configuration. The vector $\mathbf{t}^\varphi\left(\mathbf{x}^\varphi, \mathbf{n}^\varphi\right)$ is called the Cauchy stress vector across an oriented surface element with normal $\mathbf{n}^\varphi$ or the density of the surface force per unit area in the deformed configuration.

1.2.3. Cauchy's Theorem and the Cauchy Stress Tensor

The dependence of the Cauchy stress vector $\mathbf{t}^\varphi\left(\mathbf{x}^\varphi, \mathbf{n}^\varphi\right)$ with respect to its second argument $\mathbf{n} \in S_1$ is linear, i.e., at each point $\mathbf{x}^\varphi \in \Omega^\varphi$, there exists a tensor $\mathbf{T}^\varphi\left(\mathbf{x}^\varphi\right) \in \mathbf{M}^3$ such that $\mathbf{t}^\varphi\left(\mathbf{x}^\varphi, \mathbf{n}^\varphi\right) = \mathbf{T}^\varphi\left(\mathbf{x}^\varphi\right)\mathbf{n}$ for all $\mathbf{n} \in S_1$; moreover at each point $\mathbf{x}^\varphi \in \Omega^\varphi$, the tensor $\mathbf{T}^\varphi\left(\mathbf{x}^\varphi\right)$ is symmetric; finally the tensor field $\mathbf{T}^\varphi : \Omega^\varphi \to \mathbf{M}^3$ and the vector fields $\boldsymbol{f}^\varphi := \Omega^\varphi \to R^3$, and $\boldsymbol{g}^\varphi := \Gamma_1^\varphi \to \mathbf{R}^3$ are respectively related by a partial differential equation in Ω^φ and by a boundary condition on Γ_1^φ. Assume that the applied body force density $\boldsymbol{f}^\varphi := \Omega^\varphi \to \mathbf{R}^3$, is continuous and that the Cauchy stress vector field:

$$\mathbf{t}^\varphi : \left(\mathbf{x}^\varphi, \mathbf{n}^\varphi\right) \in \bar{\Omega}^\varphi \times S_1 \to \mathbf{t}^\varphi\left(\mathbf{x}^\varphi, \mathbf{n}\right) \in \mathbf{R}^3 \tag{1.29}$$

is continuously differentiable with respect to the variable $\mathbf{x}^\varphi \in \bar{\Omega}^\varphi$ for each $\mathbf{n} \in S_1$ and continuous with respect to the variable $\mathbf{n} \in S_1$ for each $\mathbf{x}^\varphi \in \bar{\Omega}^\varphi$. Then the axioms of force and moment balance imply that there exists a continuously differentiable tensor field:

$$\mathbf{T}^{\varphi} : \mathbf{x}^{\varphi} \in \bar{\Omega}^{\varphi} \rightarrow \mathbf{T}^{\varphi}\left(\mathbf{x}^{\varphi}\right) \in \mathbf{M}^{3} \tag{1.30}$$

such that the Cauchy stress vector satisfies:

$$\mathbf{t}^{\varphi}\left(\mathbf{x}^{\varphi}, \mathbf{n}\right) = \mathbf{T}^{\varphi}\left(\mathbf{x}^{\varphi}\right)\mathbf{n} \quad \text{for all } \mathbf{x}^{\varphi} \in \bar{\Omega}^{\varphi} \text{ and all } \mathbf{n} \in S_1 \tag{1.31}$$

and such that:

$$-div^{\varphi}\mathbf{T}^{\varphi}\left(\mathbf{x}^{\varphi}\right) = \mathbf{f}^{\varphi}\left(\mathbf{x}^{\varphi}\right) \text{ for all } \mathbf{x}^{\varphi} \in \Omega^{\varphi} \tag{1.32}$$

$$\mathbf{T}^{\varphi}\left(\mathbf{x}^{\varphi}\right) = \mathbf{T}^{\varphi}\left(\mathbf{x}^{\varphi}\right)^{T} \text{ for all } \mathbf{x}^{\varphi} \in \bar{\Omega}^{\varphi} \tag{1.33}$$

$$\mathbf{T}^{\varphi}\left(\mathbf{x}^{\varphi}\right)\mathbf{n}^{\varphi} = \mathbf{g}^{\varphi}\left(\mathbf{x}^{\varphi}\right) \text{ for all } \mathbf{x}^{\varphi} \in \Gamma_1^{\varphi} \tag{1.34}$$

where $\mathbf{n}^{\varphi}$ is the unit outer normal vector along Γ_1^{φ}. The symmetric tensor $\mathbf{T}^{\varphi}$ is called the *Cauchy Stress Tensor* at the point $\mathbf{x}^{\varphi} \in \bar{\Omega}^{\varphi}$.

It is helpful to keep in mind the interpretation of the elements $\mathbf{T}_{ij}^{\varphi}\left(\mathbf{x}^{\varphi}\right)$. Since $\mathbf{t}^{\varphi}\left(x^{\varphi}, \mathbf{e}_j\right) = \mathbf{T}_{ij}^{\varphi}\left(\mathbf{x}^{\varphi}\right) \cdot \mathbf{e}_i$, the elements of the j-th row of the tensor $\mathbf{T}^{\varphi}\left(x^{\varphi}\right)$ represent the components of the Cauchy stress vector $\mathbf{t}^{\varphi}\left(x^{\varphi}, \mathbf{n}\right)$ at the point $\mathbf{x}^{\varphi}$ corresponding to the particular choice $\mathbf{n} = \mathbf{e}_j$ (see Fig. 1.6):

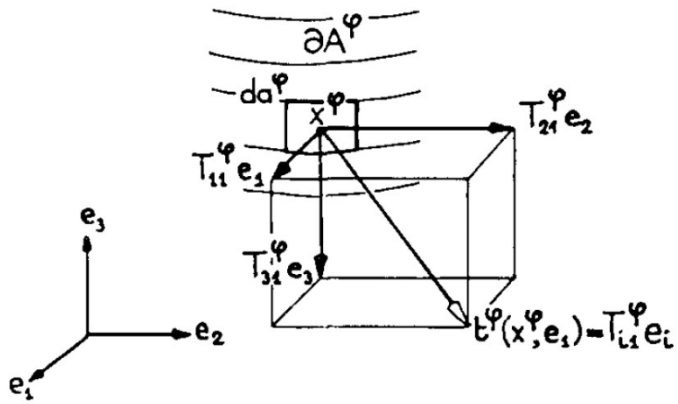

Fig. 1.6 – Interpretation of the elements $\mathbf{T}_{i1}^{\varphi}$ of the Cauchy stress tensor $\mathbf{T}^{\varphi} = \left(T_{ij}^{\varphi}\right)$

The knowledge of the three vectors $\mathbf{t}^{\varphi}\left(x^{\varphi}, \mathbf{e}_j\right)$ in turn completely determines the Cauchy stress vector $\mathbf{t}^{\varphi}\left(x^{\varphi}, \mathbf{n}\right)$ for an arbitrary vector $\mathbf{n} = n_i \mathbf{e}_i \in S_1$, since:

$$\mathbf{t}^{\varphi}\left(x^{\varphi}, \mathbf{n}\right) = n_j \mathbf{t}^{\varphi}\left(x^{\varphi}, \mathbf{e}_j\right) \tag{1.35}$$

The Cauchy stress vector is often represented on three mutually perpendicular faces of a rectangular parallelepiped as in fig. 1.6. The following three special cases of Cauchy stress tensors are particularly worthy of interest, where in each case it is assumed that the Cauchy stress tensor is constant in the particular region considered.
First, if:

$$\mathbf{T}^{\varphi}\left(x^{\varphi}\right)=-\pi\,\mathbf{I},\quad \pi\in\mathbb{R} \tag{1.36}$$

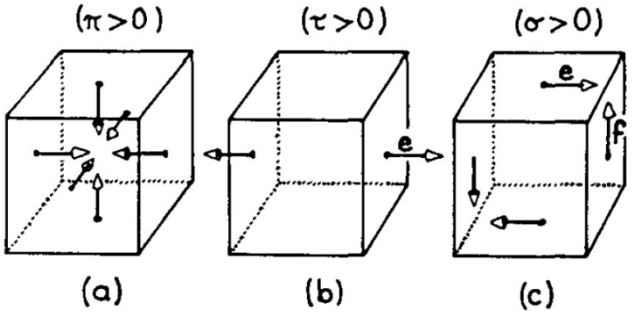

Fig. 1.7 – Three important special case of Cauchy stress tensor: (a) Pressure $\mathbf{T}^{\varphi}=-\pi\,\mathbf{I}$; (b) Pure tension in the direction $\mathbf{e}:\mathbf{T}^{\varphi}=\tau\,\mathbf{e}\otimes\mathbf{e}$; (c) Pure shear relative to the directions $\mathbf{e}$ and $\mathbf{f}:\mathbf{T}^{\varphi}=\sigma\left(\mathbf{e}\otimes\mathbf{f}+\mathbf{f}\otimes\mathbf{e}\right)$

the Cauchy stress tensor is a pressure. In this case, the Cauchy stress vector:

$$\mathbf{t}^{\varphi}\left(x^{\varphi},\mathbf{n}\right)=-\pi\,\mathbf{n} \tag{1.37}$$

is always normal to the elementary surface element and its length is constant and it is directed inward if π is <0 (see Fig. 1.7a). Secondly, if:

$$\mathbf{T}^{\varphi}\left(x^{\varphi}\right)=\tau\,\mathbf{e}\otimes\mathbf{e},\quad \tau\in\mathbf{R},\quad \mathbf{e}\in\mathbf{R}^{3},\quad \left|\mathbf{e}\right|=1 \tag{1.38}$$

the Cauchy stress tensor is a pure tension if τ is >0, or a pure compression if τ is <0, in the direction $\mathbf{e}$, with tensile stress τ. In this case, the Cauchy stress vector:

$$\mathbf{t}^{\varphi}\left(x^{\varphi},\mathbf{n}\right)=-\tau\left(\mathbf{e}\cdot\mathbf{n}\right)\mathbf{e}, \tag{1.39}$$

which is always parallel to the vector $\mathbf{e}$, is directed outward if $\tau > 0$, or inward if $\tau < 0$, on the faces with normal $\mathbf{n} = \mathbf{e}$ or $\mathbf{n} = -\mathbf{e}$ and it vanishes on the faces whose normal is orthogonal to the vector $\mathbf{e}$ (see Fig. 1.7b).
Thirdly (see Fig. 1.7c), if:

$$\mathbf{T}^{\varphi}\left(x^{\varphi}\right) = \sigma\left(\mathbf{e}\otimes\mathbf{f} + \mathbf{f}\otimes\mathbf{e}\right), \quad \sigma \in \mathbf{R}, \quad \mathbf{e},\mathbf{f} \in \mathbf{R}^3, \quad |\mathbf{e}| = |\mathbf{f}| = 1, \quad \mathbf{e}\cdot\mathbf{f} = 0, \tag{1.40}$$

The Cauchy stress tensor is a pure shear, with shear stress τ, relative to the directions $\mathbf{e}$ and $\mathbf{f}$. In this case, the Cauchy stress vectors are given by:

$$\mathbf{t}^{\varphi}\left(x^{\varphi},\mathbf{n}\right) = \sigma\left\{\left(\mathbf{f}\cdot\mathbf{n}\right)\mathbf{e} + \left(\mathbf{e}\cdot\mathbf{n}\right)\mathbf{f}\right\} \tag{1.41}$$

The Cauchy stress tensors corresponding to these three special cases are respectively given by (for definiteness, we assume that $\mathbf{e} = \mathbf{e}_1$ and $\mathbf{f} = \mathbf{e}_2$):

$$\begin{pmatrix} -\pi & 0 & 0 \\ 0 & -\pi & 0 \\ 0 & 0 & -\pi \end{pmatrix}, \quad \begin{pmatrix} \tau & 0 & 0 \\ 0 & 0 & 0 \\ 0 & 0 & 0 \end{pmatrix}, \quad \begin{pmatrix} 0 & \sigma & 0 \\ \sigma & 0 & 0 \\ 0 & 0 & 0 \end{pmatrix} \tag{1.42}$$

1.3. CONSTITUTIVE ASSUMPTION

1.3.1. Introduction to the Behaviour of the Materials

1.3.1.1. Tensile Strength and Tensile Stress

An elastic material is one that deforms immediately upon loading, maintains a constant deformation as long as the load is held constant and returns immediately to its original undeformed shape when the load is removed.
The most natural test of a material's mechanical properties is the Tension Test, in which a strip or cylinder of the material, having length L and cross-sectional area A, is anchored at one end and subjected to an axial load P – a load acting along the specimen's long axis – at the other (See Fig. 1.8).
As the load is increased gradually, the axial deflection δ of the loaded end will increase also. Eventually the test specimen breaks, often fracturing suddenly into two or

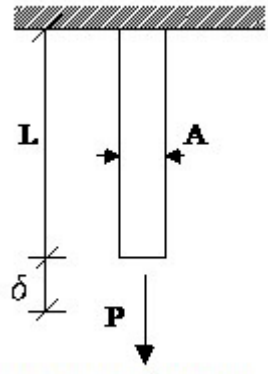

Fig. 1.8 – The Tension Test.

more pieces. One of the pivotal historical developments in our understanding of material mechanical properties was the realization that the strength of a uniaxially loaded specimen is related to the magnitude of its cross-sectional area. This notion is reasonable when one considers the strength to arise from the number of chemical bonds connecting one cross section with the one adjacent to it, where each bond is visualized as a spring with certain stiffness and strength. Obviously, the number of such bonds will increase proportionally with the section's area. The axial strength of a piece of blackboard chalk will therefore increase as the square of its diameter. In contrast, increasing the length of the chalk will not make it stronger. Galileo is said to have used this observation to note that giants, should they exist, would be very fragile creatures. Their strength would be greater than ours, since the cross-sectional areas of their skeletal and muscular systems would be larger by a factor related to the square of their height. But their weight, and thus the loads they must sustain, would increase as their volume, which is by the cube of their height. A simple fall would probably do them great damage. When reporting the strength of materials loaded in tension, it is customary to account for this effect of area by dividing the breaking load by the cross-sectional area:

$$\sigma_f = \frac{P_f}{A_0} \tag{1.43}$$

where σ_f is the Ultimate Tensile Stress, P_f is the load at fracture and A_0 is the original cross-sectional area. The units of stress are obviously load per unit area, N/m^2 (also called Pascal, or Pa) in the SI system. If the specimen is loaded by an axial force P less than the breaking load P_f, the tensile stress is developed by analogy with equation (1.43) as:

$$\sigma = \frac{P}{A_0} \tag{1.44}$$

The tensile stress, the force per unit area acting on a plane transverse to the applied load, is a fundamental measure of the internal forces within the material.

1.3.1.2. Stiffness

It is important to distinguish stiffness, which is a measure of the load needed to induce a given deformation in the material, from the strength, which usually refers to the material's resistance to failure by fracture or excessive deformation. The stiffness is usually measured by applying relatively small loads and measuring the resulting deformation. Since the deformations in most materials are very small for these loading conditions, the experimental problem is largely

one of measuring small changes in length accurately. Hooke made a number of such measurements on long wires under various loads and observed that to a good approximation the load P and its resulting deformation δ were related linearly as long as the loads were sufficiently small. This relation, generally known as *Hooke's Law*, can be written algebraically as:

$$P = k\delta \tag{1.45}$$

where k is a constant of proportionality called the *Stiffness* and having units of N/m.

The stiffness is not a function of the material alone, but is also influenced by the specimen shape. An useful way to adjust the stiffness so as to be a purely materials property is to normalize the load by the cross-sectional area; i.e. to use the tensile stress rather than the load.

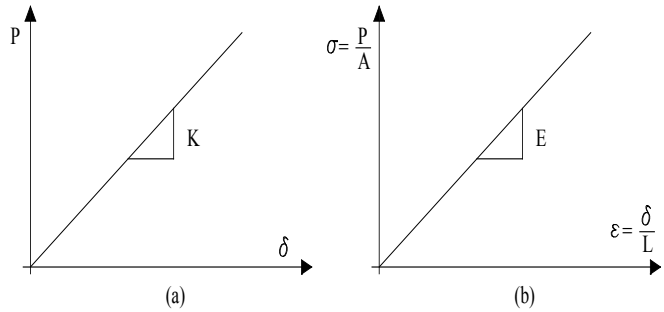

Fig. 1.9 – Hooke's law in terms of (a) load-displacement and (b) stress-strain.

Further, the deformation δ can be normalized by noting that an applied load stretches all parts of the wire uniformly, so that a reasonable measure of *stretching* is the deformation per unit length:

$$\varepsilon = \frac{\delta}{L_0} \tag{1.46}$$

Here L_0 is the original length and ε is a dimensionless measure of stretching called the strain. Using these more general measures of load per unit area and displacement per unit length, Hooke's Law becomes:

$$\frac{P}{A_0} = E\frac{\delta}{L_0} \tag{1.47}$$

or:

$$\sigma = E\varepsilon \tag{1.48}$$

The constant of proportionality E, called *Young's Modulus* or the modulus of elasticity, is one of the most important mechanical descriptors of a material.
It has the same units as stress, Pa or psi. As shown in Fig. 1.9, Hooke's law can refer to either of equations. (1.45) or (1.48).
The Hookean stiffness k is now recognizable as being related to the Young's modulus E and the specimen geometry as:

$$k = \frac{EA}{L} \tag{1.49}$$

Another useful relation is obtained by solving Eqn. (1.47) for the deflection in terms of the applied load as:

$$\delta = \frac{PL}{EA} \tag{1.50}$$

Note that the stress σ developed in a tensile specimen subjected to a fixed load is independent of the material properties, while the deflection depends on the material property E. Hence the stress σ in a tensile specimen at a given load is the same whether it's made of steel or polyethylene, but the strain ε would be different: the polyethylene will exhibit much larger strain and deformation, since its modulus is two orders of magnitude less than steel's. A material that obeys Hooke's Law is called *Hookean*. Such a material is elastic according to the description of elasticity given in the introduction (immediate response, full recovery), and it is also linear in its relation between stress and strain (or equivalently, force and deformation). Therefore a Hookean material is linear elastic. It is important to keep in mind that not all elastic materials are linear (rubber is elastic but nonlinear), but not all linear materials are elastic (viscoelastic materials can be linear in the mathematical sense, but do not respond immediately and are thus not elastic). The linear proportionality between stress and strain given by Hooke's law is not nearly general, but it's really just an approximation that is observed to be reasonably valid for many materials as long the applied stresses are not too large. As the stresses are increased, eventually more complicated material response will be observed. If we were to push on the specimen rather than pulling on it, the loading would be described as compressive rather than tensile. In the range of relatively low loads, Hooke's law holds for this case as well. By convention, compressive stresses and strains are negative, so the expression $\sigma = E\varepsilon$ holds for both tension and compression.

1.3.2. Elasticity, Groups of Symmetry, Anisotropic Solids with Fourth Rank Tensors

1.3.2.1. Linear Costitutive Law for Hyperelastic Solids

The heterogeneous materials can be characterized by both inhomogeneity and anisotropy, since the first aspect is due to the multi-phase composition of the medium, while the second one is due to the geometrical arrangement of the different constituents within the examined heterogeneous volume. A linear anisotropic elastic material, as known, can have as many as 21 elastic constants. However, this number can be opportunely reduced when the examined material possesses certain material symmetry. Moreover, it is also reduced, in most cases, when a two-dimensional deformation is considered. It is worth to remember that the matrices of the elastic constants must be positive definite, because the strain energy must be positive. Hence, referring to a fixed rectangular coordinate system $\mathbf{e}_1, \mathbf{e}_2, \mathbf{e}_3$, let $\mathbf{T}$ and $\mathbf{E}$ be the stress and the strain fields, respectively, in an anisotropic hyperelastic material. The stress-strain relation can be written in the following form:

$$\mathbf{T} = \mathbf{C} : \mathbf{E} \tag{1.51}$$

or, in components:

$$\sigma_{ij} = C_{ijhk}\varepsilon_{hk} \tag{1.52}$$

where $\mathbf{C}$ is the fourth rank elastic stiffness tensor and where, for the hypothesis of iperelasticity, the components C_{ijhk} satisfy the following conditions of full symmetry:

$$C_{ijhk} = C_{jihk} = C_{hkij} \tag{1.53}$$

The above written equation (1.53) groups in it the following equalities:

$$C_{ijhk} = C_{jihk} = C_{ijkh} = C_{jikh} \tag{1.54}$$

and:

$$C_{ijhk} = C_{hkij} \tag{1.55}$$

where the (1.54) follows directly from the symmetry of the stress and the strain tensors, while the (1.55) is due to the assuming hypothesis of existence of the

elastic potential ϕ. In other word, the strain energy ϕ per unit volume of the material, given by:

$$\phi = \int_0^{\varepsilon} \sigma_{ij} d\varepsilon_{ij} \tag{1.56}$$

is independent of the loading path, i.e. the path that ε_{ij} takes from 0 to ε while it depends on the final value of ε, only.
In linear elasticity, the (1.56) may be written as:

$$\phi = \frac{1}{2}\sigma_{ij}\varepsilon_{ij} = \frac{1}{2}C_{ijhk}\varepsilon_{ij}\varepsilon_{hk} \tag{1.57}$$

and since the strain energy must be positive, it has to be:

$$C_{ijhk}\varepsilon_{ij}\varepsilon_{hk} > 0 \tag{1.58}$$

for any real, non zero, symmetric tensor ε_{ij}. Hence, as said before, the stiffness tensor **C** is defined positive. Analogously, the stress-strain relation can be written in the following form, inverse of (1.51):

$$\mathbf{E} = \mathbf{S} : \mathbf{T} \tag{1.59}$$

or, in components:

$$\varepsilon_{ij} = S_{ijhk}\sigma_{hk} \tag{1.60}$$

Where **S** fourth rank elastic compliance tensor and where, for the hypothesis of iper-elasticity, the components S_{ijhk} satisfy the following conditions of full symmetry:

$$S_{ijhk} = S_{jihk} = S_{hkij} \tag{1.61}$$

The above written equation (1.61) groups in it the following equalities:

$$S_{ijhk} = S_{jihk} = S_{ijkh} = S_{jikh} \tag{1.62}$$

and:

$$S_{ijhk} = S_{hkij} \tag{1.63}$$

where the (1.62) follows directly from the symmetry of the stress and the strain tensors, while the (1.63) is due to the assuming hypothesis of existence of the elastic complementary potential ψ .

In other word, the stress energy ψ per unit volume of the material, given by:

$$\psi = \int_0^{\sigma} \varepsilon_{ij} d\sigma_{ij} \tag{1.64}$$

It is independent of the loading path, i.e. the path that σ_{ij} takes from 0 to σ while it depends on the final value of σ , only.

In linear elasticity, the (1.64) may be written as:

$$\psi = \frac{1}{2}\sigma_{ij}\varepsilon_{ij} = \frac{1}{2}S_{ijhk}\sigma_{ij}\sigma_{hk} \tag{1.65}$$

and since the stress energy must be positive, it has to be:

$$S_{ijhk}\sigma_{ij}\sigma_{hk} > 0 \tag{1.66}$$

for any real, non zero, symmetric tensor σ_{ij} .

Hence, as said before, the compliance tensor **S** is defined positive. Introducing the contract notation, such that:

$$\begin{aligned}
&\sigma_{11} = \sigma_1, \quad \sigma_{22} = \sigma_2, \quad \sigma_{33} = \sigma_3, \\
&\sigma_{32} = \sigma_4, \quad \sigma_{31} = \sigma_5, \quad \sigma_{12} = \sigma_6, \\
&\varepsilon_{11} = \varepsilon_1, \quad \varepsilon_{22} = \varepsilon_2, \quad \varepsilon_{33} = \varepsilon_3, \\
&2\varepsilon_{32} = \varepsilon_4, \quad 2\varepsilon_{31} = \varepsilon_5, \quad 2\varepsilon_{12} = \varepsilon_6
\end{aligned} \tag{1.67}$$

the stress-strain laws (1.52) and (1.60) may be respectively written as:

$$\sigma_\alpha = C_{\alpha\beta}\varepsilon_\beta, \quad C_{\alpha\beta} = C_{\beta\alpha} \tag{1.68}$$

and:

$$\varepsilon_\alpha = S_{\alpha\beta}\varepsilon_\beta, \quad S_{\alpha\beta} = S_{\beta\alpha} \tag{1.69}$$

In particular, with reference, to the equation (1.68), it may be expressed in a matrix form where, as well known, the upperscript T means for traspost matrix and the sign **:** means a tensor product:

$$\mathbf{T} = \mathbf{C} : \mathbf{E}, \quad \mathbf{C} = \mathbf{C}^T \tag{1.70}$$

The stress and the strain tensors, ***T*** and ***E***, are expressed in form of 6x1 column matrices, while the stiffness tensor $\mathbf{C}$ is expressed in form of 6x6 symmetric matrix in order to simplify the tensorial products.
Ultimately with this kind of transformation the tensorial products become matrix product, where:

$$\mathbf{C} = \begin{bmatrix} C_{11} & C_{12} & C_{13} & C_{14} & C_{15} & C_{16} \\ C_{12} & C_{22} & C_{23} & C_{24} & C_{25} & C_{26} \\ C_{13} & C_{23} & C_{33} & C_{34} & C_{35} & C_{36} \\ C_{14} & C_{24} & C_{34} & C_{44} & C_{45} & C_{46} \\ C_{15} & C_{25} & C_{35} & C_{45} & C_{55} & C_{56} \\ C_{16} & C_{26} & C_{36} & C_{46} & C_{56} & C_{66} \end{bmatrix} \tag{1.71}$$

where the transformation between C_{ijhk} and $C_{\alpha\beta}$ is accomplished by replacing the subscripts *ij* (or *hk*) by α or β, by using the following rules:

$$\begin{aligned} & ij(or\ hk) \leftrightarrow \alpha\left(or\ \beta\right) \\ & 11 \ \leftrightarrow \ 1 \\ & 22 \ \leftrightarrow \ 2 \\ & 33 \ \leftrightarrow \ 3 \\ & 32 \ \ or \ \ 23 \ \leftrightarrow \ 4 \\ & 31 \ \ or \ \ 13 \ \leftrightarrow \ 5 \\ & 12 \ \ or \ \ 21 \ \leftrightarrow \ 6 \end{aligned} \tag{1.72}$$

We may write the transformation (1.72) as:

$$\alpha = \begin{cases} i & if\ i = j \\ 9 - i - j & if\ i \neq j \end{cases} \qquad \beta = \begin{cases} h & if\ h = k \\ 9 - h - k & if\ h \neq k \end{cases} \tag{1.73}$$

Analogously, the stress-strain law (1.59) may be expressed in a matrix form:

$$\mathbf{E} = \mathbf{S} : \mathbf{T}, \quad \mathbf{S} = \mathbf{S}^T \tag{1.74}$$

where also the compliance tensor $\mathbf{S}$ is expressed in form of 6x6 symmetric matrix:

$$S = \begin{bmatrix} S_{11} & S_{12} & S_{13} & S_{14} & S_{15} & S_{16} \\ S_{12} & S_{22} & S_{23} & S_{24} & S_{25} & S_{26} \\ S_{13} & S_{23} & S_{33} & S_{34} & S_{35} & S_{36} \\ S_{14} & S_{24} & S_{34} & S_{44} & S_{45} & S_{46} \\ S_{15} & S_{25} & S_{35} & S_{45} & S_{55} & S_{56} \\ S_{16} & S_{26} & S_{36} & S_{46} & S_{56} & S_{66} \end{bmatrix} \tag{1.75}$$

Here, the transformation between S_{ijhk} and $S_{\alpha\beta}$ is similar to that one between C_{ijhk} and $S_{\alpha\beta}$ except the following:

$$\begin{aligned} &S_{ijhk} = S_{\alpha\beta} \quad \textit{if both} \quad \alpha,\beta \le 3 \\ &2S_{ijhk} = S_{\alpha\beta} \quad \textit{if either} \quad \alpha \textit{ or } \beta \le 3 \\ &4S_{ijhk} = S_{\alpha\beta} \quad \textit{if both} \quad \alpha,\beta > 3 \end{aligned} \tag{1.76}$$

From (1.70) and (1.74), it is obtained the expression of the strain energy:

$$\phi = \frac{1}{2}\mathbf{E}^T\mathbf{C}\,\mathbf{E} = \frac{1}{2}\mathbf{T}^T\,\mathbf{E} = \frac{1}{2}\mathbf{T}^T\,\mathbf{S}\,\mathbf{T} \tag{1.77}$$

and, by considering that ϕ has to be positive, it must be:

$$\begin{aligned} &\mathbf{E}^T\mathbf{C}\,\mathbf{E} > 0 \\ &\mathbf{T}^T\mathbf{S}\,\mathbf{T} > 0 \end{aligned} \tag{1.78}$$

This implies that the matrices $\mathbf{C}$ and $\mathbf{S}$ are both positive definite. Moreover, by substituting of the (1.74) in the (1.70) yields:

$$\mathbf{C}\cdot\mathbf{S} = \mathbf{I} = \mathbf{S}\cdot\mathbf{C} \tag{1.79}$$

where the second equality follows from the first one which says that $\mathbf{C}$ and $\mathbf{S}$ are the inverses of each other and, hence, their product commutes. For a linear anisotropic elastic material the matrices $\mathbf{C}$ and $\mathbf{S}$ have 21 elastic independent constants. The number of the independent elastic constants of the 6x6 matrices $\mathbf{C}$ and $\mathbf{S}$ can be opportunely reduced when the examined anisotropic material possesses certain material symmetry. Hence, with reference to a new rectangular coordinate system $\{\mathbf{e}_1^*, \mathbf{e}_2^*, \mathbf{e}_3^*\}$, obtained from the initial fixed one $\{\mathbf{e}_1, \mathbf{e}_2, \mathbf{e}_3\}$ under an orthogonal transformation:

$$\mathbf{e}^* = \mathbf{Q} \cdot \mathbf{e} \tag{1.80}$$

or, in components:

$$e_i^* = Q_{ij} e_j \tag{1.81}$$

in which $\mathbf{Q}$ is an orthogonal matrix that satisfies the following relations:

$$\mathbf{Q} \cdot \mathbf{Q}^T = \mathrm{I} = \mathbf{Q}^T \mathbf{Q} \tag{1.82}$$

or:

$$Q_{ij} Q_{kj} = \delta_{ik} = Q_{ji} Q_{jk} \tag{1.83}$$

a material is said to possess a *symmetry* with respect to $\mathbf{Q}$ if the elastic fourth rank stiffness tensor $\mathbf{C}^*$ referred to the $\mathbf{e}_i$ coordinate system is equal to that one $\mathbf{C}$ referred to the coordinate system $\mathbf{e}_i$, i.e.:

$$\mathbf{C}^* = \mathbf{C} \tag{1.84}$$

or in components:

$$\mathbf{C}^*_{ijhk} = \mathbf{C}_{ijhk} \tag{1.85}$$

where:

$$\mathbf{C}^*_{ijhk} = Q_{ip} Q_{jq} Q_{hr} Q_{ks} \mathbf{C}_{pqrs} \tag{1.86}$$

In other words, when:

$$C_{ijhk} = Q_{ip} Q_{jq} Q_{hr} Q_{ks} C_{pqrs} \tag{1.87}$$

the material possesses a symmetry with respect to $\mathbf{Q}$.
Some authors adopt the transformation law for $C_{\alpha\beta}$:

$$C^*_{\alpha\beta} = K_{\alpha r} K_{\beta t} C_{rt} \tag{1.88}$$

where $\mathbf{K}$ is a 6x6 matrix, whose elements are obtained by means of suitable assembly of the components Q_{ij}, according to proposals by Mehrabadi, Cowin et al (1995), and Mehrabadi and Cowin (1990).
Then, an anisotropic material possesses the symmetry of *central inversion* (*C*) if the (1.87) is satisfied for:

$$\mathbf{Q} = \begin{bmatrix} -1 & 0 & 0 \\ 0 & -1 & 0 \\ 0 & 0 & -1 \end{bmatrix} = -\mathbf{I} \tag{1.89}$$

The (1.87) is obviously satisfied by the $\mathbf{Q}$ given in the (1.89) for any C_{ijhk}. Therefore, all the anisotropic materials have the symmetry of central inversion.
If $\mathbf{Q}$ is a proper orthogonal matrix, the transformation (1.80) represents a rigid body rotation about an axis. So, an anisotropic material is said to possess a *rotational symmetry* if the (1.87) is satisfied for:

$$\mathbf{Q}^r(\theta) = \begin{bmatrix} \cos\theta & \sin\theta & 0 \\ -\sin\theta & \cos\theta & 0 \\ 0 & 0 & 1 \end{bmatrix} \tag{1.90}$$

which represents, for example, a rotation about the $\mathbf{e}_3$-axis an angle θ, as shown in the following figure:

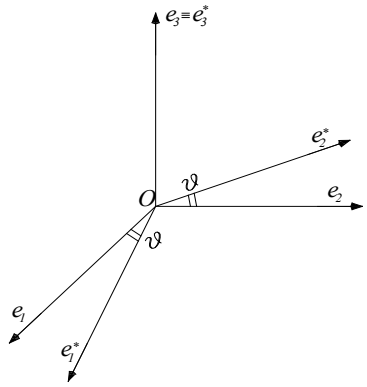

Fig. 1.10 – Rigid rotation about the $\mathbf{e}_3$-axis.

By extending this property, i.e. if the (1.87) is satisfied by the $\mathbf{Q}$ as given through the (1.90) for any θ, then the material possesses a rotational symmetry with respect at any rotation in the $\mathbf{e}_3 = 0$ plane. In this case, it is said that the

$\mathbf{e}_3 = 0$ is the *plane of transverse isotropy* or that $\mathbf{e}_3$ is *axis of elastic symmetry* with order $p = \infty\,(L\infty)$. More in general, instead, by indicating with:

$$\theta = \frac{2\pi}{p} \tag{1.91}$$

the rotation angle about an axis, this latter is defined as *axis of elastic symmetry* with order *p*. Since *p* may assume values equal to 2, 3, 4,6 and ∞, the axis of elastic symmetry has indicated, respectively, with *L*2 , *L*3 , *L*4 , *L*6 and *L*∞. If $\mathbf{Q}$ is, instead, an orthogonal matrix as defined below:

$$\mathbf{Q} = \mathbf{I} - 2\,\mathbf{n} \otimes \mathbf{n}^T \tag{1.92}$$

where ***n*** *is* a unit vector, the transformation (1.80) represents a reflection about a plane whose normal is ***n***, defined as *reflection plane or symmetry plane* (*P*). In particular, if ***m*** is any vector on the plane, the following relation is satisfied:

$$\mathbf{Q}\,\mathbf{n} = -\mathbf{n}, \quad \mathbf{Q}\,\mathbf{m} = -\mathbf{m} \tag{1.93}$$

According to such orthogonal matrix, therefore, a vector normal to the reflection plane reverses its direction after the transformation while a vector belonging to the reflection plane remains unchanged.
So, an anisotropic material is said to possess a *symmetry plane* if the (1.87) is satisfied by the $\mathbf{Q}$ as given by (1.92).

1.3.2.2. Anisotropy and Material Symmetries

The existence of various combinations of the different symmetry forms implies a corresponding classification of the anisotropy classes of the materials. In particular, two extreme cases of anisotropic elastic materials are the *triclinic* materials and the *isotropic* ones.
The first material possesses no rotational symmetry or a plane of reflection symmetry, while the second material possesses infinitely many rotational symmetries and planes of reflection symmetry.
For such materials, it can be shown that:

$$C_{ijhk} = \lambda\delta_{ij}\delta_{hk} + G\left(\delta_{ih}\delta_{jk} + \delta_{ik}\delta_{jh}\right) \tag{1.94}$$

where λ and *G* are the Lamè constants, satisfies the (1.87) for any orthogonal $\mathbf{Q}$.

It is possible to demonstrate that if an anisotropic elastic material possesses a material symmetry with the orthogonal matrix $\mathbf{Q}$, then it also possesses the material symmetry with $\mathbf{Q}^T = \mathbf{Q}^{-1}$. This means, for example, that if the material has rotational symmetry with rotation about the x_3-axis an angle θ, it also has the symmetry about the x_3-axis an angle $-\theta$. Moreover, it is possible to demonstrate that if an anisotropic elastic material possesses symmetry with $\mathbf{Q}'$ and $\mathbf{Q}''$, then it also possesses symmetry with $\mathbf{Q} = \mathbf{Q}'\mathbf{Q}''$. These statements, valid either for linear or nonlinear material, is useful in determining the structure of the stiffness tensor when the material possesses symmetries.
Depending on the number of rotations and/or reflection symmetry a crystal possesses, Voigt (1910) in fact classified crystals into 32 classes.
However, in terms of the 6x6 matrix $\mathbf{C}$, there are only 8 basic groups, since different combinations of symmetry forms may lead to the same structure of the stiffness tensor.
This classification maid for crystals can be extended for non-crystalline materials, so that for them the structure of $\mathbf{C}$ can also be represented by one of the 8 basic groups.

- **Triclinic Materials**

They represent the most general case, in which no symmetry form exists. The number of independent constants is, therefore, 21 and the matrix $\mathbf{C}$ assumes the following form:

$$\mathbf{C} = \begin{bmatrix} C_{11} & C_{12} & C_{13} & C_{14} & C_{15} & C_{16} \\ C_{12} & C_{22} & C_{23} & C_{24} & C_{25} & C_{26} \\ C_{13} & C_{23} & C_{33} & C_{34} & C_{35} & C_{36} \\ C_{14} & C_{24} & C_{34} & C_{44} & C_{45} & C_{46} \\ C_{15} & C_{25} & C_{35} & C_{45} & C_{55} & C_{56} \\ C_{16} & C_{26} & C_{36} & C_{46} & C_{56} & C_{66} \end{bmatrix} \quad n° = 21 \tag{1.95}$$

which is equal to that one of the equation (1.71).

- **Monoclinic Materials**

The symmetry forms are: L^2, P, L^2PC.
The number of the independent elastic constants is 13 and the matrix $\mathbf{C}$ assumes the following expressions:

a) Symmetry plane coinciding with $\mathbf{e}_1 = 0$, i.e., $\theta = 0$:

$$\mathbf{C} = \begin{bmatrix} C_{11} & C_{12} & C_{13} & C_{14} & 0 & 0 \\ C_{12} & C_{22} & C_{23} & C_{24} & 0 & 0 \\ C_{13} & C_{23} & C_{33} & C_{34} & 0 & 0 \\ C_{14} & C_{24} & C_{34} & C_{44} & 0 & 0 \\ 0 & 0 & 0 & 0 & C_{55} & C_{56} \\ 0 & 0 & 0 & 0 & C_{56} & C_{66} \end{bmatrix} \quad n^\circ = 13 \qquad (1.96)$$

b) Symmetry plane coinciding with $\mathbf{e}_2 = 0$, i.e., $\theta = \frac{\pi}{2}$ or $\varphi = 0$:

$$\mathbf{C} = \begin{bmatrix} C_{11} & C_{12} & C_{13} & 0 & C_{15} & 0 \\ C_{12} & C_{22} & C_{23} & 0 & C_{25} & 0 \\ C_{13} & C_{23} & C_{33} & 0 & C_{35} & 0 \\ 0 & 0 & 0 & C_{44} & 0 & C_{46} \\ C_{15} & C_{25} & C_{35} & 0 & C_{55} & 0 \\ 0 & 0 & 0 & C_{46} & 0 & C_{66} \end{bmatrix} \quad n^\circ = 13 \qquad (1.97)$$

c) Symmetry plane coinciding with $\mathbf{e}_3 = 0$, i.e., $\varphi = \frac{\pi}{2}$:

$$\mathbf{C} = \begin{bmatrix} C_{11} & C_{12} & C_{13} & 0 & 0 & C_{16} \\ C_{12} & C_{22} & C_{23} & 0 & 0 & C_{26} \\ C_{13} & C_{23} & C_{33} & 0 & 0 & C_{36} \\ 0 & 0 & 0 & C_{44} & C_{45} & 0 \\ 0 & 0 & 0 & C_{45} & C_{55} & 0 \\ C_{16} & C_{26} & C_{36} & 0 & 0 & C_{66} \end{bmatrix} \quad n^\circ = 13 \qquad (1.98)$$

- **Orthotropic (or Rhombic) Materials**

The symmetry forms are: $3P, 3L^2, L^2 2P, 3L^2 3PC$.
With reference to the symmetry form $3P$, it means that the three coordinate planes, $\theta = 0$, $\theta = \frac{\pi}{2}$ and $\varphi = \frac{\pi}{2}$ are the symmetry planes.

The number of the independent elastic constants is 9 and the matrix $\mathbf{C}$ assumes the following form:

$$\mathbf{C}=\begin{bmatrix} C_{11} & C_{12} & C_{13} & 0 & 0 & 0 \\ C_{12} & C_{22} & C_{23} & 0 & 0 & 0 \\ C_{13} & C_{23} & C_{33} & 0 & 0 & 0 \\ 0 & 0 & 0 & C_{44} & 0 & 0 \\ 0 & 0 & 0 & 0 & C_{55} & 0 \\ 0 & 0 & 0 & 0 & 0 & C_{66} \end{bmatrix} \quad n^{\circ}=9 \tag{1.99}$$

- **Trigonal Materials**

The symmetry forms are $L^3 3L^2, L^3 3P, L_6^3 3L^2 3PC$.
With reference to the symmetry form $3P$, it is verified that the three coordinate planes, $\theta=0$, $\theta=+\frac{\pi}{3}$ and $\theta=-\frac{\pi}{3}$ are the symmetry planes.
The number of the independent elastic constants is 6 and the matrix $\mathbf{C}$ assumes the following form:

$$\mathbf{C}=\begin{bmatrix} C_{11} & C_{12} & C_{13} & C_{14} & 0 & 0 \\ C_{12} & C_{11} & C_{13} & -C_{14} & 0 & 0 \\ C_{13} & C_{13} & C_{33} & 0 & 0 & 0 \\ C_{14} & -C_{14} & 0 & C_{44} & 0 & 0 \\ 0 & 0 & 0 & 0 & C_{44} & C_{14} \\ 0 & 0 & 0 & 0 & C_{14} & \dfrac{(C_{11}-C_{12})}{2} \end{bmatrix} \quad n^{\circ}=6 \tag{1.100}$$

- **Tetragonal Materials**

The symmetry forms are: $L^4, L^4 PC, L_4^2$.
Iit is verified that the tetragonal materials show five symmetry planes at $\theta=0$, $\theta=+\frac{\pi}{4}$, $\theta=-\frac{\pi}{4}$, $\theta=+\frac{\pi}{2}$ and $\varphi=+\frac{\pi}{2}$.
The number of the independent elastic constants is 6 and the matrix $\mathbf{C}$ assumes the following form:

$$\mathbf{C}=\begin{bmatrix} C_{11} & C_{12} & C_{13} & 0 & 0 & 0 \\ C_{12} & C_{11} & C_{13} & 0 & 0 & 0 \\ C_{13} & C_{13} & C_{33} & 0 & 0 & 0 \\ 0 & 0 & 0 & C_{44} & 0 & 0 \\ 0 & 0 & 0 & 0 & C_{44} & 0 \\ 0 & 0 & 0 & 0 & 0 & C_{66} \end{bmatrix} \quad n^{\circ}=6 \qquad (1.101)$$

- **Transversely Isotropic (or Exagonal) Materials**

The forms are: $L^3P, L^3 3L^2P, L^6, L^6 6L^2, L^6PC, L^6 6P, L^6 6L^2 7PC$.

For the transversely isotropic materials the symmetry planes are $\varphi=+\frac{\pi}{2}$, i.e. $\left(\mathbf{e}_3=0\right)$, and any plane that contains the $\mathbf{e}_3$-axis. So, the $\mathbf{e}_3$-axis is the axis of symmetry.
The number of the independent elastic constants is 5 and the matrix $\mathbf{C}$ assumes the following form:

$$\mathbf{C}=\begin{bmatrix} C_{11} & C_{12} & C_{13} & 0 & 0 & 0 \\ C_{12} & C_{11} & C_{13} & 0 & 0 & 0 \\ C_{13} & C_{13} & C_{33} & 0 & 0 & 0 \\ 0 & 0 & 0 & C_{44} & 0 & 0 \\ 0 & 0 & 0 & 0 & C_{44} & 0 \\ 0 & 0 & 0 & 0 & 0 & \frac{\left(C_{11}-C_{12}\right)}{2} \end{bmatrix} \quad n^{\circ}=5 \qquad (1.102)$$

- **Cubic Materials**

The forms are $3L^2 4L^3, 3L^2 4L_6^3 3PC, 3L_4^2 4L^3 6P, 3L^4 4L^3 6L^2, 3L^4 4L_6^3 6L^2 9PC$.
For the cubic materials there are nine symmetry planes, whose normal vectors are on the three coordinate axes and on the coordinate planes making an angle $\varphi=+\frac{\pi}{4}$ with coordinate axes.
The number of the independent elastic constants is 3 and the matrix $\mathbf{C}$ assumes the following form:

$$\mathbf{C}=\begin{bmatrix} C_{11} & C_{12} & C_{12} & 0 & 0 & 0 \\ C_{12} & C_{11} & C_{12} & 0 & 0 & 0 \\ C_{12} & C_{12} & C_{11} & 0 & 0 & 0 \\ 0 & 0 & 0 & C_{44} & 0 & 0 \\ 0 & 0 & 0 & 0 & C_{44} & 0 \\ 0 & 0 & 0 & 0 & 0 & C_{44} \end{bmatrix} \quad n^{\circ}=3 \qquad (1.103)$$

- **Isotropic Materials**

For the isotropic materials any plane is a symmetry plane.
The number of the independent elastic constants is 2 and the matrix $\mathbf{C}$ assumes the following form:

$$\mathbf{C}=\begin{bmatrix} C_{11} & C_{12} & C_{12} & 0 & 0 & 0 \\ C_{12} & C_{11} & C_{12} & 0 & 0 & 0 \\ C_{12} & C_{12} & C_{11} & 0 & 0 & 0 \\ 0 & 0 & 0 & \dfrac{C_{11}-C_{12}}{2} & 0 & 0 \\ 0 & 0 & 0 & 0 & \dfrac{C_{11}-C_{12}}{2} & 0 \\ 0 & 0 & 0 & 0 & 0 & \dfrac{C_{11}-C_{12}}{2} \end{bmatrix} \quad n^{\circ}=2 \qquad (1.104)$$

If λ and μ are the Lamè constants, the (1.104) becomes:

$$\mathbf{C}=\begin{bmatrix} 2\mu+\lambda & \lambda & \lambda & 0 & 0 & 0 \\ \lambda & 2\mu+\lambda & \lambda & 0 & 0 & 0 \\ \lambda & \lambda & 2\mu+\lambda & 0 & 0 & 0 \\ 0 & 0 & 0 & 2\mu & 0 & 0 \\ 0 & 0 & 0 & 0 & 2\mu & 0 \\ 0 & 0 & 0 & 0 & 0 & 2\mu \end{bmatrix} \quad n^{\circ}=2 \qquad (1.105)$$

It is remarkable that, for isotropic materials, it needs only three planes of symmetry to reduce the number of elastic constants from 21 to 2.

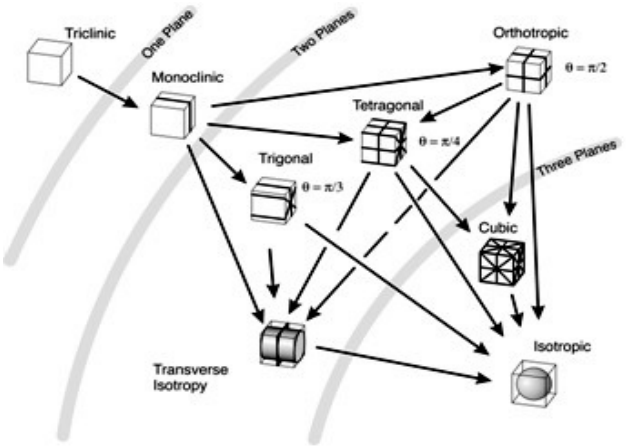

Fig. 1.11 – Hierarchical organization of the eight material symmetries of linear elasticity

The previous figure shows the hierarchical organization of the eight material symmetries of linear elasticity.

It is organized so that the lower symmetries are at the upper left and, as one moves down and across the table to the right, one encounters crystal systems with greater and greater symmetry.

It is worth to underline that the structure of the matrix $\mathbf{C}$ above obtained for each class of materials is referred to the specified coordinate system.

When different coordinate systems are employed, the transformation law (1.86) has to be used for obtaining the structure of the new matrix $\mathbf{C}$, in which, while the number of nonzero elements may increase, the number of independent elastic constants remains constant since it does not depend on the choice of the coordinate systems.

In engineering applications the matrix $\mathbf{S}$ for isotropic materials is written as:

$$\mathbf{S} = \frac{1}{E}\begin{bmatrix} 1 & -\nu & -\nu & 0 & 0 & 0 \\ -\nu & 1 & -\nu & 0 & 0 & 0 \\ -\nu & -\nu & 1 & 0 & 0 & 0 \\ 0 & 0 & 0 & 1+\nu & 0 & 0 \\ 0 & 0 & 0 & 0 & 1+\nu & 0 \\ 0 & 0 & 0 & 0 & 0 & 1+\nu \end{bmatrix} \tag{1.106}$$

where, as well known, E is the Young's modulus and υ is the Poisson ratio. These constant values are related with the Lamè constants, λ and μ, in the following way:

$$E = \frac{\mu(3\lambda + 2\mu)}{\mu + \lambda}, \quad \nu = \frac{\lambda}{2(\lambda + \mu)} \tag{1.107}$$

It can be shown that:

$$\lambda = \frac{\nu E}{(1+\nu)(1-2\nu)}, \quad \mu = \frac{E}{2(1+\nu)} \tag{1.108}$$

The strong convexity condition which is equivalent to the positive definiteness of the strain energy (1.66), yields that the stiffness tensor **C** is defined positive, as well as, the positive definiteness of the stress energy (1.66), yields that the compliance tensor **S** is defined positive.
In particular, in the contracted notation, the (1.66) implies that the 6x6 matrix **C** is also positive definite; for this reason, all its principal minors are positive, that is:

$$C_{ii} > 0 \quad (i \text{ not summed}) \tag{1.109}$$

$$\det\begin{bmatrix} C_{ii} & C_{ij} \\ C_{ij} & C_{jj} \end{bmatrix} > 0 \quad (i, j \text{ not summed}) \tag{1.110}$$

$$\det\begin{bmatrix} C_{ii} & C_{ij} & C_{ih} \\ C_{ij} & C_{jj} & C_{jh} \\ C_{ih} & C_{jh} & C_{hh} \end{bmatrix} > 0 \quad (i, j, k \text{ not summed}) \tag{1.111}$$

$$\det\begin{bmatrix} C_{ii} & C_{ij} & C_{ik} & C_{ih} \\ C_{ij} & C_{jj} & C_{jk} & C_{jh} \\ C_{ik} & C_{jk} & C_{kk} & C_{kh} \\ C_{ih} & C_{jh} & C_{kh} & C_{hh} \end{bmatrix} > 0 \quad (i, j, k, h \text{ not summed}) \tag{1.112}$$

$$\det\begin{bmatrix} C_{ii} & C_{ij} & C_{ik} & C_{ih} & C_{im} \\ C_{ij} & C_{jj} & C_{jk} & C_{jh} & C_{jm} \\ C_{ik} & C_{jk} & C_{kk} & C_{kh} & C_{km} \\ C_{ih} & C_{jh} & C_{kh} & C_{hh} & C_{hm} \\ C_{im} & C_{jm} & C_{km} & C_{hm} & C_{mm} \end{bmatrix} > 0 \quad (i, j, k, h, m \text{ not summed}) \tag{1.113}$$

$$\det[\mathbf{C}] > 0 \tag{1.114}$$

where i, j, h are distinct integers which can have any value from 1 to 6.

In particular, according to the theorem which states that a real symmetric matrix is positive definite if and only if its leading principal minors are positive, the necessary and sufficient conditions for the 6x6 matrix $\mathbf{C}$ to be positive definite are the positivity of its 6 leading principal minors, i.e..
The above done anisotropic classification of the materials according to the number of symmetry planes is based on the assumption that, for each material, the number and the locations of the symmetry planes are known. However, this is not the case when considering an unknown material. So, often, the elastic stiffness and the elastic compliances of the material have to be determined to an arbitrarily chosen coordinate system.
The result is that, if there exists a symmetry plane, it may not be one of the coordinate planes. Consequently, all elements of the matrices $\mathbf{C}$ and $\mathbf{S}$ can be nonzero. The problem is to locate the symmetry planes if they exist when $\mathbf{C}$ (or $\mathbf{S}$) is given.
When a plane of symmetry exists, as already seen, the (1.87) is satisfied by the $\mathbf{Q}$ given in (1.92), which has the properties given in (1.93) where $\boldsymbol{n}$ is a unit vector normal to the plane symmetry and $\boldsymbol{m}$ is any vector perpendicular to $\boldsymbol{n}$. Cowin and Mehrabadi (1987) have demonstrated that a set of necessary and sufficient conditions for $\boldsymbol{n}$ to be a unit normal vector to a plane of symmetry is:

$$C_{ijhh}n_j = \left(C_{pqss}n_p n_q\right)n_i \tag{1.115}$$

$$C_{ikhk}n_h = \left(C_{pqpq}n_p n_q\right)n_i \tag{1.116}$$

$$C_{ijhk}n_j n_k n_h = \left(C_{pqrs}n_p n_q n_r n_s\right)n_i \tag{1.117}$$

$$C_{ijhk}m_j m_k m_h = \left(C_{pqrs}n_p m_q n_r m_s\right)n_i \tag{1.118}$$

More in general, the equations from (1.115) to (1.118) tell that $\boldsymbol{n}$ is an eigenvector of the 3x3 symmetric matrices U, V, $R(\boldsymbol{n})$ and $R(\boldsymbol{m})$ whose elements are:

$$U_{ij} = C_{ijhh}, \quad V_{ih} = C_{ikhk}, \quad R_{ih}\left(\mathbf{n}\right) = C_{ijhk}n_j n_k \tag{1.119}$$

An anisotropic elastic material with given elastic stiffness C_{ijhk} has a plane of symmetry if and only if $\boldsymbol{n}$ is an eigenvector of $R(\boldsymbol{n})$ and $R(\boldsymbol{m})$, or of U and $R(\boldsymbol{m})$ or of V and $R(\boldsymbol{m})$. The vector $\boldsymbol{n}$ is normal to the plane of symmetry, while $\boldsymbol{m}$ is any vector on the plane of symmetry. An anisotropic elastic material with given

elastic stiffness C_{ijhk} has a plane of symmetry if and only if $\boldsymbol{n}$ (normal vector to the plane of symmetry) is a common eigenvector of U and V and satisfies:

$$C_{ijhk} m_i n_j n_h n_k = 0 \tag{1.120}$$

$$C_{ijhk} m_i m_j m_h n_k = 0 \tag{1.121}$$

or any two independent vectors $\mathbf{m}^{\alpha}$ $(\alpha = 1,2)$ on the plane of symmetry that do not form an angle a multiple of $\pi / 3$.

REFERENCES

Ciarlet PG, 1988. Three-Dimensional Elasticity. Elsevier.

Cowin SC, Mehrabadi MM, 1987. On the identification of material symmetry for anisotropic elastic materials. Quarterly Journal of Mechanics and Applied Mathematics. 40: 451-476.

Cowin SC, Mehrabadi, MM, 1995. Anisotropic symmetries in linear elasticity. Applied Mechanics Review. 48: 247-285.

Cowin SC, 2001. Tissue Mechanics. Springer.

Mehrabadi MM, Cowin SC, 1990. Eigentensors of linear anisotropic elastic materials. Quarterly Journal of Mechanics and Applied Mathematics. 43: 15-41.

Timoshenko S, Goodier JN. 1951. Theory of Elasticity. McGraw-Hill.

Voigt W. 1928. Lehrbuch der Kristallphysik. Leipzig: BG Teubner Verlag.

2 HETEROGENEOUS MATERIALS

It is well known the difficulty to find solutions to anisotropic inhomogeneous material problems. A very few restricted classes of these problems are solved in a general way.

One example of these solutions is for cylinders subjected to pure torsion and possessing cylindrical orthotropy, with a variation of the shear moduli with the local normal direction to the family of curves of which the lateral boundary is a member (Cowin, 1987). This solution is a generalization, to a set of arbitrary cross-sectional shapes, of a problem solved by Voigt (Voigt, 1928) for a circular cross-section with radial variation of its cylindrical anisotropy. These cylinders are said to possess shape intrinsic orthotropy since it is the boundary of the cylinder that establishes the possible directional variation of the elastic moduli. A second example was given by Chung & Ting (Chung & Ting, 1995) who presented an exact solution for the case of an anisotropic half-space with elastic moduli dependent upon one coordinate, the angle θ, when the loads on the half-space are represented by a straight line of force. These kinds of problems were called angularly inhomogeneous problems by the authors. Closely related to these solutions is a third example called radially inhomogeneous problems (Alshits and Kirchner, 2001). As the name suggests, the variation of the elastic constants is in the radial direction in this case.

In spite of this difficulty, in the last years, it has been a growing interest about the mechanical behaviour of anisotropic and inhomogeneous solids, above all in biomechanics. Moreover, the necessity to build thermodynamically consistent theories for this kind of materials, by means the employment of the mathematical theory of the homogenization, has determined the necessity to find exact analytical solutions in the ambit of this more complex section of the theory of elasticity, (Lions, 1985), (Maugin, 1993).
In the next sections, it is presented a useful method enables one to find solutions for inhomogeneous, anisotropic elastostatic problems under particular conditions by means of the use of two theorems, S.A.S. theorem and D.A.S. theorem (Fraldi and Cowin, 2004).

2.1. STRESS ASSOCIATED SOLUTIONS THEOREM FOR INHOMOGENEOUS ELASTICITY

The Stress Associated Solution (SAS) Theorem lets to find solutions for inhomogeneous, anisotropic elastostatic problems if two conditions are satisfied:

(1) a knowledge of the solution for a homogeneous elastic *reference* problem (the *associated problem*) whose solution has a stress state with a zero eigenvalue everywhere in the domain of the problem, and

(2) an inhomogeneous anisotropic elastic tensor related to the homogeneous anisotropic elastic tensor of (1) by:

$$\mathbb{C}^I = \varphi(\boldsymbol{x})\mathbb{C}^H, \qquad \varphi(\boldsymbol{x}) \Big| \ \forall \boldsymbol{x} \in B,\ \varphi(\boldsymbol{x}) > \alpha > 0,\ \alpha \in \mathbb{R}^+ \qquad (2.1)$$

where $\mathbb{C}^H = \mathbb{C}^{H^T}$ is the elasticity tensor of a generic anisotropic homogeneous elastic material of the *reference problem*, $\mathbb{C}^I$ is the elasticity tensor of the corresponding anisotropic inhomogeneous elastic problem, B is the domain occupied by both the homogeneous object B^H and the inhomogeneous one B^I, $\alpha \in \mathbb{R}^+$ is an arbitrary positive real number, while $\varphi(\boldsymbol{x})$ is a $C^2(B)$ scalar function.
The assumption (2.1) means that the inhomogeneous character of the material is due to the presence of a scalar parameter producing the inhomogeneity in the elastic coefficients.
This method makes it possible to find analytical solutions for an *inhomogeneous* anisotropic elastic problem if the elastic solution of the corresponding *homogeneous* anisotropic *reference* problem is known and characterized everywhere by a stress state with a zero eigenvalue.

The solutions to the *inhomogeneous* anisotropic elastic problem are called the *associated solutions* of the *homogeneous problem.*

2.1.1. Zero-Eigenvalue Stress and Zero-Eigenvalue Strain Fields

A zero-eigenvalue stress state (zero-eigenvalue strain state) is characterized by the condition that the determinant of the stress (strain) is zero:

$$\det \boldsymbol{T} = 0, \qquad (\det \boldsymbol{E} = 0)\,. \tag{2.2}$$

It is easy to show that a zero-eigenvalue stress (strain) state is a necessary condition for a plane stress (strain) state. The components of the stress tensor $\boldsymbol{T}$ (strain tensor $\boldsymbol{E}$) are denoted by σ_{ij} (ε_{ij}). The strain tensor $\boldsymbol{E}$ is related to the displacement field $\boldsymbol{u}$ by:

$$\boldsymbol{E} = \frac{1}{2}[(\nabla \otimes \boldsymbol{u}) + (\nabla \otimes \boldsymbol{u})^T] = sym\nabla \otimes \boldsymbol{u} \qquad \forall \boldsymbol{x} \in B \tag{2.3}$$

in which $grad\,\boldsymbol{u} = (\nabla \otimes \boldsymbol{u})$ and the symbol $\otimes$ represents the *tensor product*. In components we have:

$$\varepsilon_{ij} = \frac{1}{2}(u_{i,j} + u_{j,i})\,, \tag{2.4}$$

where the comma denotes differentiation and $\boldsymbol{u}$ is the displacement field.

2.1.2. Stress Associated Solutions (SAS) Theorem

Consider the following mixed boundary-value elastostatic homogeneous and anisotropic problem P^H in the absence of action-at-a-distance forces:

$$\nabla \cdot \boldsymbol{T}(\boldsymbol{u}) = \boldsymbol{0} \quad \text{in } B^H,\ \boldsymbol{T}(\boldsymbol{u}) \cdot \boldsymbol{n} = \boldsymbol{t} \text{ on } \partial B_t^H,\ \boldsymbol{u} = \boldsymbol{u}_0 \text{ on } \partial B_u^H \tag{2.5}$$

where B^H is the domain occupied by the homogeneous elastic object, $\partial B^H = \{\partial B_t^H \cup \partial B_u^H\}$ is its boundary and $\boldsymbol{t}$ and $\boldsymbol{u}_0$ are the traction field and the displacements assigned on the corresponding partition of the boundary, respectively (Barber, 1992; Gurtin, 1972). The notation for the divergence of the stress tensor is $\nabla \cdot \boldsymbol{T}(\boldsymbol{u}) = div\,\boldsymbol{T}(\boldsymbol{u})$, where the *del operator* is a vectorial

differential operator defined by $\nabla \equiv \partial_i \boldsymbol{e}_i$, $\partial_i \equiv \partial / \partial x_i = (*)_{,i}$ is the partial differential operator and $\boldsymbol{e}_i$ is the base unit vector of the *i*-axis.
The anisotropic Hooke's law is written:

$$\boldsymbol{T}(\boldsymbol{u}) = \mathbb{C}^H : \boldsymbol{E}(\boldsymbol{u}) = \mathbb{C}^H : sym(\nabla \otimes \boldsymbol{u}) = \mathbb{C}^H : (\nabla \otimes \boldsymbol{u}) \tag{2.6}$$

or, in components:

$$\sigma_{ij} = C^H_{ijhk} \varepsilon_{hk} = C^H_{ijhk} u_{h,k} . \tag{2.7}$$

Let $\mathfrak{S}^H = \{\boldsymbol{u}^H, \boldsymbol{E}^H, \boldsymbol{T}^H\}$ be the solution of the homogeneous problem (2.5).
Consider now an associated anisotropic elastic inhomogeneous problem P^I, described by modifying the system (2.5), with $\boldsymbol{t}^I = \varphi \boldsymbol{t}$ representing the traction field applied on ∂B^I_t and the inhomogeneous anisotropic elasticity tensor given by (2.1), thus:

$$\nabla \cdot \boldsymbol{T}(\boldsymbol{u}) = \boldsymbol{0} \quad \text{in } B^I, \ \boldsymbol{T}(\boldsymbol{u}) \cdot \boldsymbol{n} = \boldsymbol{t}^I \ \text{on } \partial B^I_t, \ \boldsymbol{u} = \boldsymbol{u}_0 \ \text{on } \partial B^I_u \tag{2.8}$$

The solid domains B^H and B^I, as well as their corresponding boundary partitions made on ∂B^H and ∂B^I, are geometrically the same in the homogeneous and inhomogeneous problems.
Then, if we expand the equation $(2.8)_1$ it is possible to write:

$$\begin{aligned} &\nabla \cdot \boldsymbol{T}(\boldsymbol{u}) = \nabla \cdot [\varphi(\boldsymbol{x}) \mathbb{C}^H : \boldsymbol{E}(\boldsymbol{u})] = \\ &= \varphi(\boldsymbol{x}) \nabla \cdot [\mathbb{C}^H : \boldsymbol{E}(\boldsymbol{u})] + [\mathbb{C}^H : \boldsymbol{E}(\boldsymbol{u})] \cdot \nabla \varphi(\boldsymbol{x}) = \boldsymbol{0} \end{aligned} \tag{2.9}$$

where $\nabla(*) = grad(*)$ is the gradient operator applied on a generic scalar-valued function $(*)$. Consider now the situation in which the displacements are equal for the homogeneous and inhomogeneous problems. Then, by substituting the displacement solution $\boldsymbol{u}^H$ obtained for the homogeneous problem P^H in (2.9) in place of the displacement vector $\boldsymbol{u}$, we have that:

$$\nabla \cdot \boldsymbol{T}(\boldsymbol{u}^H) = \varphi(\boldsymbol{x}) [\nabla \cdot \boldsymbol{T}^H(\boldsymbol{u}^H)] + [\boldsymbol{T}^H(\boldsymbol{u}^H)] \cdot \nabla \varphi(\boldsymbol{x}) = \boldsymbol{0} \tag{2.10}$$

But, since $\nabla \cdot [\boldsymbol{T}^H(\boldsymbol{u}^H)] = \nabla \cdot [\mathbf{C}^H : \boldsymbol{E}(\boldsymbol{u}^H)] = \boldsymbol{0}$, it follows that:

$$[\boldsymbol{T}^H(\boldsymbol{u}^H)] \cdot \nabla \varphi(\boldsymbol{x}) = \boldsymbol{0} \qquad \forall \boldsymbol{x} \in B^I \tag{2.11}$$

By excluding the trivial case in which $\varphi(\boldsymbol{x}) = \text{constant}$, it follows that:

$$\det \boldsymbol{T}^H = 0, \qquad \forall \boldsymbol{x} \in B^H \tag{2.12}$$

This means that the stress state at $\boldsymbol{x}$ of the *reference* homogeneous problem is required to be a zero eigenvalue stress state everywhere in the domain.
To investigate the geometrical meaning of the equation (2.11), since (2.11) must be true everywhere in B^I, we consider, without loss of generality, the *local principal stress reference system* $\{\xi_1, \xi_2, \xi_3\}$, in which the stress tensor $\boldsymbol{T}^H$ takes the component form:

$$\mathrm{T}^{\mathrm{H}} = \begin{bmatrix} \sigma^{\mathrm{H}}_{\xi_1} & 0 & 0 \\ 0 & \sigma^{\mathrm{H}}_{\xi_2} & 0 \\ 0 & 0 & \sigma^{\mathrm{H}}_{\xi_3} \end{bmatrix}. \tag{2.13}$$

Representing the gradient of the scalar function φ as:

$$\nabla\varphi(\boldsymbol{\xi})^{\mathrm{T}} = [\varphi_{,\xi_1} \quad \varphi_{,\xi_2} \quad \varphi_{,\xi_3}], \tag{2.14}$$

the three scalar equations implied by (2.11) are written as:

$$\sigma^H_{\xi_1}\varphi_{,\xi_1} = 0, \ \sigma^H_{\xi_2}\varphi_{,\xi_2} = 0, \ \sigma^H_{\xi_3}\varphi_{,\xi_3} = 0\,. \tag{2.15}$$

The system (2.15) is satisfied if the stress tensor $\boldsymbol{T}^H$ for the reference homogeneous problem P^H is, at each internal point $\boldsymbol{x} \in B^H$, a locally variable *zero eigenvalue stress* state.
If there is only one zero eigenvalue, say in the ξ_3-direction, the only non-zero component of the vector $\nabla\varphi$, is $\varphi_{,\xi_3}$ at the corresponding points $\boldsymbol{x} \in B^I$. If there are two zero eigenvalues there can be two non-zero components of $\nabla\varphi$. The case of three zero eigenvalues of the stress tensor $\boldsymbol{T}^H$ is trivial and will not be mentioned further. It follows that, at each internal point, the equipotential surfaces of φ admit as a tangent plane the plane whose normal is coaxial with the eigenvector associated with the zero stress eigenvalue (or a direction, in the case of two zero stress eigenvalues).
This is illustrated in Figure 2.1 for the case of one zero eigenvalue of stress.
The geometrical relationship (2.11) between the stress tensor $\boldsymbol{T}^H$ and the vector $\nabla\varphi$ may be rewritten in the form:

$$\{\boldsymbol{T}^H \cdot \nabla\varphi = \boldsymbol{0}\} \Leftrightarrow \{\forall \boldsymbol{v} \in V, \quad \boldsymbol{T}^H : (\nabla\varphi \otimes \boldsymbol{v}) = 0\} \tag{2.16}$$

where $\boldsymbol{v}$ is any unit vector defined in the three-dimensional Euclidean space $\mathbb{E}^3$ and V represents the corresponding vector space.
It follows that the stress vector on the plane whose normal is $\boldsymbol{v}$ is always orthogonal to the vector $\nabla\varphi$.

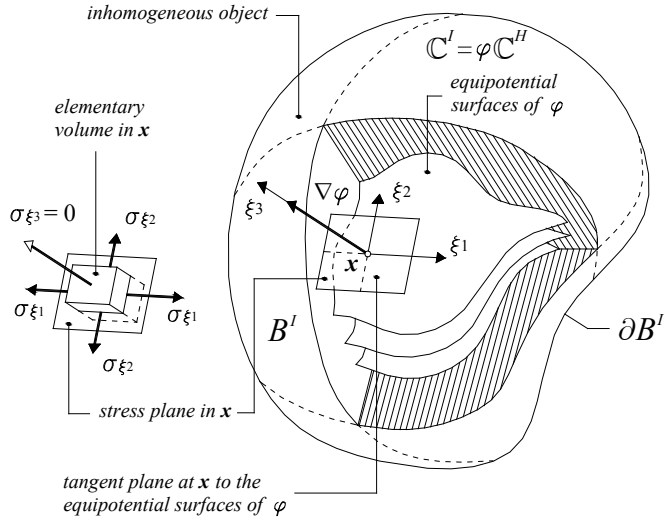

Fig. 2.1 – *Geometrical interpretation of the relationship between the equipotential surfaces of φ and the distribution of the planes of stresses in the associated anisotropic problem*

Then, it is possible to establish the following theorem:

Stress Associated Solution (SAS) Theorem. *Consider two geometrically identical elastic objects B^H and B^I, one homogeneous and the other inhomogeneous, respectively*. Let $\mathbb{C}^H$ *and* $\mathbb{C}^I = \varphi(\boldsymbol{x})\mathbb{C}^H$ *be the corresponding elasticity tensors* (Figure 2.2.). *The two elastostatic problems associated with the two objects are:*

$$P^H: \quad \{\nabla\cdot\boldsymbol{T}(\boldsymbol{u}) = \boldsymbol{0} \quad \text{in } B^H,\ \boldsymbol{T}(\boldsymbol{u})\cdot\boldsymbol{n} = \boldsymbol{t} \text{ on } \partial B_t^H,\ \boldsymbol{u} = \boldsymbol{u}^0 \text{ on } \partial B_u^H\},$$
$$P^I: \quad \{\nabla\cdot\boldsymbol{T}(\boldsymbol{u}) = \boldsymbol{0} \quad \text{in } B^I,\ \boldsymbol{T}(\boldsymbol{u})\cdot\boldsymbol{n} = \varphi\boldsymbol{t} \text{ on } \partial B_t^I,\ \boldsymbol{u} = \boldsymbol{u}^0 \text{ on } \partial B_u^I\},$$

where:

$$\varphi(\boldsymbol{x}) \in C^2(B)\Big|\ \forall\boldsymbol{x}\in B,\ \varphi(\boldsymbol{x}) > \alpha > 0, \quad \alpha\in\mathbb{R}^+.$$

If $\boldsymbol{u}^H$ is the solution of the homogeneous problem P^H, then $\boldsymbol{u}^I = \boldsymbol{u}^H$ if and only if $\{\boldsymbol{T}^H : (\nabla\varphi\otimes\boldsymbol{v}) = 0, \quad \forall\boldsymbol{v}\in V\}$, i.e.:

$$\{\forall \boldsymbol{x} \in B^I,\ \forall \boldsymbol{v} \in V,\ \boldsymbol{T}^H:(\nabla\varphi \otimes \boldsymbol{v}) = 0\} \ \Leftrightarrow\ \boldsymbol{u}^I = \boldsymbol{u}^H .$$

It is convenient to increase the similarity between the elastic problems for the homogeneous and the inhomogeneous materials by writing the boundary conditions in the same way.
Thus we substitute for the prescribed boundary tractions a corresponding prescribed displacement field; this converts the portion of the boundary upon which the surface tractions are prescribed to a portion of the boundary upon which the displacements are prescribed.
Due to uniqueness of solution, this is always possible in a linear elastic problem. Then, the two problems may be written in the equivalent forms as:

$$P^H:\ \{\nabla\cdot\boldsymbol{T}(\boldsymbol{u}) = \boldsymbol{0} \quad \text{in } B^H,\ \boldsymbol{u} = \boldsymbol{u}^t \ \text{on } \partial B_t^H,\ \boldsymbol{u} = \boldsymbol{u}^0 \ \text{on } \partial B_u^H\},$$
$$P^I:\ \{\nabla\cdot\boldsymbol{T}(\boldsymbol{u}) = \boldsymbol{0} \quad \text{in } B^I,\ \boldsymbol{u} = \boldsymbol{u}^t \ \text{on } \partial B_t^I,\ \boldsymbol{u} = \boldsymbol{u}^0 \ \text{on } \partial B_u^I\},$$

where $\boldsymbol{u}^t$ represents the prescribed displacement on ∂B_t and where, now, the tractions $\boldsymbol{t}$ and $\varphi\boldsymbol{t}$ represent the reactions of the constraints on ∂B_t specified by $\boldsymbol{u}^t$. It follows that, when a solution $\mathfrak{S}^H = \{\boldsymbol{u}^H, \boldsymbol{E}^H, \boldsymbol{T}^H\}$ for an anisotropic homogeneous elastic problem P^H is known, the *Stress Associated Solution Theorem* yields the corresponding solution for an inhomogeneous problem P^I as $\mathfrak{S}^I = \{\boldsymbol{u}^H, \boldsymbol{E}^H, \varphi\boldsymbol{T}^H\}$, if and only if $\boldsymbol{T}^H\cdot\nabla\varphi = \boldsymbol{0}$ everywhere in the object and the displacement boundary conditions are the same for both the homogeneous and the inhomogeneous objects. Thus the solution $\mathfrak{S}^H = \{\boldsymbol{u}^H, \boldsymbol{E}^H, \boldsymbol{T}^H\}$ is used to construct a solution of the associated inhomogeneous problem.
Finally we note that the restriction (2.1) may be relaxed in many different ways. For example the *Associated Solutions* could involve only some selected elastic moduli of the homogeneous elasticity tensor, so that the solutions do not depend on all stiffness coefficients.
This means that it is possible to extend the validity of the proposed theorem by rewriting the assumption (2.1) in the weaker form:

$$\hat{C}^I_{ijhk} = \varphi\,\hat{C}^H_{ijhk},$$

where $\hat{C}^H_{ijhk}$ represents only those elastic coefficients explicitly involved in the specific anisotropic homogeneous problem used to construct the associated solution. In the next section it is shown that components of the elasticity tensor not involved in the solution of the homogeneous problem will not be involved in the solution of the associated inhomogeneous problem.

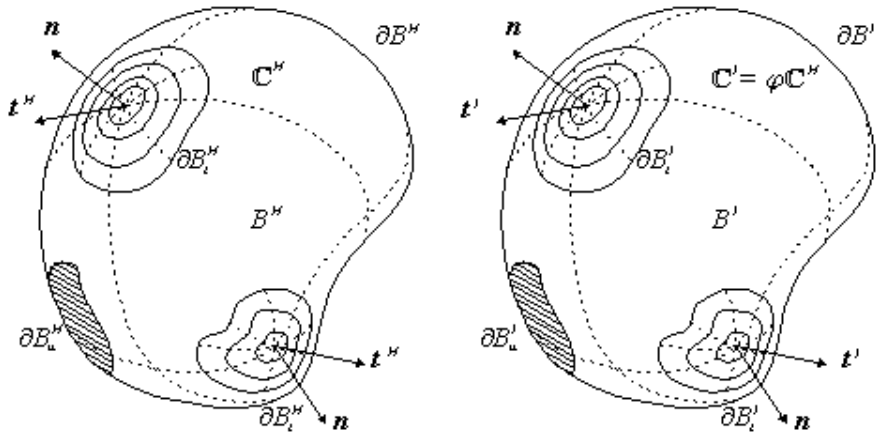

Fig. 2.2 – The homogeneous (a) on the left and inhomogeneous (b) on the right bodies with their boundary conditions

2.2. GENERALIZATION OF THE SAS THEOREM TO PIECEWISE INHOMOGENEITIES

Two types of composite materials are considered in this section, one in which φ is *constant*, but piecewise *discontinuous* and another in which φ is a *piecewise continuous function*.
These two cases extend the domain of applicability of the condition (2.1), and therefore the domain of applicability of the SAS theorem.
In the first case the extension is to composite materials for which each phase is characterized by elastic moduli that are constant within their own phase, but are different from the constant elastic moduli of the other phases. In the second case the extension is to composite materials for which each phase is characterized by the possibility of each phase having variable elastic coefficients inside the phase domain and discontinuous elastic coefficients across phase boundaries. The next section treats the case where φ is constant, but piecewise discontinuous.

2.2.1. Composite Materials where φ is Constant, but Piecewise Discontinuous

In the following two sections we extend the SAS theorem to heterogeneous materials where there is not a smooth variation of the elastic moduli. To achieve this, we will make reference to some results obtained previously and formulate new hypotheses about the features of composite inhomogeneous bodies

considered. In particular, for each phase p present of a composite material, we will assume here that the elasticity tensor can be written as:

$$\mathbb{C}_p^H = \varphi_p \mathbb{C}^H, \qquad p = \{1,2,...,n\} \subset \mathbb{N} \tag{2.17}$$

where $\mathbb{C}^H$ is the elasticity tensor of a reference isotropic or anisotropic homogeneous material and φ_p is a positive scalar parameter. This hypothesis does not constitute the most general case for describing the relation between the elastic tensors of the different phases for a composite material, but it is widely utilized in literature because many artificial and natural composites exhibit mechanical properties that are well represented by the proposed assumption (Lekhnitskii, 1963; Ting, 1996; Fraldi and Guarracino, 2001; Nemat-Nasser and Hori, 1993). Let us consider a partition of the inhomogeneous body $\{\Omega_p(B) \big| \ B \equiv \bigcup_{p=1}^{n} \Omega_p(B)\}$, where $\partial\Omega_{(p,q)}$ represents the interface boundary between two generic sub-domains Ω_p and Ω_q of the partition, with elasticity tensors $\mathbb{C}_p^H$ and $\mathbb{C}_q^H$, respectively. If we assume that the solution for the anisotropic homogeneous reference problem is known, and the geometries of the homogeneous and composite material objects are the same, we can study the conditions under which the stress tensor for the inhomogeneous material (multi-phase material) assumes the form:

$$\boldsymbol{T}_p^H = \varphi_p \boldsymbol{T}^H, \qquad \forall \boldsymbol{x} \in \Omega_p(B) \tag{2.18}$$

required by the SAS theorem. Note that the stress (2.18) satisfies the equilibrium equations in each sub-domain of the partition:

$$\nabla \cdot \boldsymbol{T}_p^H = \varphi_p \nabla \cdot \boldsymbol{T}^H = \boldsymbol{0}, \quad \forall \boldsymbol{x} \in \Omega_p(B). \tag{2.19}$$

Moreover, by virtue of the assumed constitutive relationships:

$$\boldsymbol{E}_p^H = \mathbb{C}_p^{H-1} \boldsymbol{T}_p^H = \mathbb{C}^{H-1} \boldsymbol{T}^H = \boldsymbol{E}^H, \quad \{\forall p \in \mathbf{N}, \forall \boldsymbol{x} \in \Omega_p\} \tag{2.20}$$

the satisfaction of the compatibility condition on the surfaces of discontinuity between the different materials of the composite object is automatic.
From the force equilibrium on the interfaces between two adjacent phases, it follows that:

$$\boldsymbol{T}_p^H \cdot \boldsymbol{n}_{(p,q)} = \boldsymbol{T}_q^H \cdot \boldsymbol{n}_{(p,q)}, \qquad \{\forall \{p,q\} \in \mathbf{N}, \forall \boldsymbol{x} \in \partial\Omega_{(p,q)}\} \tag{2.21}$$

where $\boldsymbol{n}_{(p,q)}$ is the unit normal vector to the interface between the phases p and q. By virtue of (2.18), the equation (2.21) is satisfied if:

$$\boldsymbol{T}^H \cdot \boldsymbol{n}_{(p,q)} = \boldsymbol{0}, \qquad \forall \boldsymbol{x} \in \partial\Omega_{(p,q)}. \tag{2.22}$$

Equation (2.22) requires that for each point belonging to the interface surfaces between two phases, the stress tensor $\boldsymbol{T}^H$ must possess at least one zero-eigenvalue, that is $\{\det \boldsymbol{T}^H = 0, \quad \forall \boldsymbol{x} \in \partial\Omega_{(p,q)}\}$.

This hypothesis is necessary in order to orient the plane of the stress on the interface surfaces such that the eigenvector associated with a zero eigenvalue of the stress tensor is coaxial with the unit normal vector to the tangent plane to the interface. For structures sometimes consistent with this hypothesis one can consider the interfaces between layers of certain plant structures, for example, onions and leeks. In the literature of this subject examples that conform to this hypothesis include the piece-wise angularly inhomogeneous elastic wedges considered by Ting (Ting, 1996), the intrinsically orthotropic layered cylinders under torsion, described by Cowin (Cowin, 1987), as well as in other examples analyzed by Lekhnitskii (Lekhnitskii, 1963).

To complete the elastic solution for the composite material (2.17) using the known solution of a homogeneous reference problem, we note the satisfaction of the compatibility and equilibrium conditions on the external boundary. The satisfaction of the compatibility conditions is easily verified by virtue of (2.20). The equilibrium equation on the part of the external boundary where the tractions are prescribed is given by:

$$\boldsymbol{T}_e^H \cdot \boldsymbol{n} = \boldsymbol{t}_e^H = \varphi_e \boldsymbol{t}^H, \quad \forall \boldsymbol{x} \in \partial B_{t(e)} \tag{2.23}$$

where $\partial B_{t(e)}$ represents a typical element of the partition of the external boundary on which the tractions $\boldsymbol{t}^H$ are prescribed in the homogeneous reference problem. The total stress boundary is the sum over all the typical distinct boundaries, $\partial B_t = \bigcup_{e=1}^{k} \partial B_{t(e)}$, where k represents the total number of phases that have a projection of their boundary on the external boundary on which the tractions are assigned.

Then, if the conditions (2.22) and (2.23) are satisfied, we can build the elastic solution of composite multi-phase materials from a knowledge of the displacements and the stresses for a homogeneous object with analogous geometry using the extension of the SAS theorem. Note that, in order to utilize the results of the proposed theorem for inhomogeneous materials in which φ

was assumed to be a continuous scalar function, the stress tensor $\boldsymbol{T}^H$ had to exhibit a zero-eigenvalue at each point of the body.
However, in order to generalize the SAS theorem to composite materials where φ is constant, but piecewise discontinuous, it is sufficient that the stress tensor $\boldsymbol{T}^H$ related to the associated homogeneous problem possesses a zero-eigenvalue $\left(\det \boldsymbol{T}^H = 0\right)$ only in the points belonging to the internal interfaces between the different phases.
This means that, in the case of materials where φ is a constant, but piecewise discontinuous, $\boldsymbol{T}^H$ can be a three-dimensional stress field in any other point of the solid domain.

2.2.2. Composite Materials where φ is Piecewise Continuous

In this subsection we consider the new and more general situation in which each phase p of the heterogeneous solid (composite material) can be represented by the following elasticity tensor:

$$\mathbb{C}_p^H = \varphi_p(\boldsymbol{x}_p)\mathbb{C}^H, \quad \forall \boldsymbol{x}_p \in \Omega_p \subset B \tag{2.24}$$

where $\mathbb{C}^H$ is the elasticity tensor of a homogeneous reference material, while φ_p is now a positive scalar function, not necessarily constant, but continuous inside each phase (or sub-domain defined by the partition described above).
We relax some of the hypotheses for the situation when φ is constant, but retain the previous notation; $\{\Omega_p(B) \,\big|\, B \equiv \bigcup_{p=1}^{n} \Omega_p(B)\}$ is again the partition of the inhomogeneous object, with $\partial\Omega_{(p,q)}$ representing the interface boundary between two generic adjacent sub-domains Ω_p and Ω_q of the partition whose elasticity tensors are $\mathbb{C}_p^H$ and $\mathbb{C}_q^H$, respectively, see Figure 2.3..
The representation of the stress tensor of the phase p required by the SAS theorem is:

$$\boldsymbol{T}_p^H = \varphi_p(\boldsymbol{x}_p)\boldsymbol{T}^H, \qquad \forall \boldsymbol{x}_p \in \Omega_p(B). \tag{2.25}$$

Equilibrium is satisfied if the divergence of the stress for each phase is zero:

$$\nabla \cdot \boldsymbol{T}_p^H = \varphi_p \nabla \cdot \boldsymbol{T}^H + \boldsymbol{T}^H \cdot \nabla \varphi_p = \boldsymbol{0} \Rightarrow \boldsymbol{T}^H \cdot \nabla \varphi_p = \boldsymbol{0}, \quad \forall \boldsymbol{x}_p \in \Omega_p(B) \tag{2.26}$$

From this result it follows, using (2.17) and (2.20), that $\boldsymbol{E}_p^H = \boldsymbol{E}^H$, $\{\forall p \in \mathbf{N}, \forall \boldsymbol{x}_p \in \Omega_p\}$. The equilibrium conditions (2.21)-(2.22) across the interface between two phases are then satisfied as well the external boundary conditions (2.23) considered previously. This means that, in order to extend the SAS theorem to piecewise continuous composite materials, one has to first establish two facts about the stress tensor $\boldsymbol{T}^H$, namely: 1) at each internal point of each phase *p*, the stress tensor $\boldsymbol{T}^H$ possesses at least one zero-eigenvalue and 2) at every point in the interface between two adjacent phases the normal to the tangent plane has to be coincident with the direction of the eigenvector associated with the zero eigenvalue.

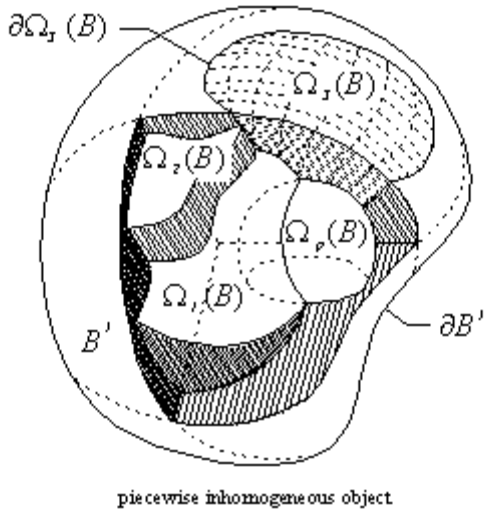

Fig. 2.3 – A representation of a possible spatial distribution of the phases inside a piecewise inhomogeneous material.

2.3. DISPLACEMENT ASSOCIATED SOLUTIONS (DAS) THEOREM FOR INHOMOGENEOUS ELASTICITY

Analogously to the SAS theorem, the *Displacement Associated Solution* (D.A.S.) theorem lets to find solutions for inhomogeneous anisotropic elastostatic problems, if two conditions are satisfied, (Fraldi, Cowin, 2004): (3) the solution of the homogeneous elastic *reference* problem *(the associated* one) is known and it has a local plane strain state, with a zero eigenvalue everywhere in the domain of the problem and (4) the inhomogeneous anisotropic compliance tensor is in relation with the homogeneous associated one according to the following equation:

$$\mathbb{S}^I = \frac{1}{\varphi(\boldsymbol{x})}\mathbb{C}^{H^{-1}} = \lambda(\boldsymbol{x})\mathbb{S}^H, \qquad \lambda(\boldsymbol{x})\Big|\ \forall \boldsymbol{x} \in B,\ \lambda(\boldsymbol{x}) > \beta > 0,\ \beta \in \mathbb{R}^+ \quad (2.27)$$

where $\mathbb{S}^H = \mathbb{S}^{H^T}$ is the compliance tensor of the anisotropic homogeneous elastic *reference problem*, $\mathbb{S}^I$ is the compliance tensor of the corresponding anisotropic inhomogeneous elastic problem, B is the domain occupied by both the homogeneous object B^H and the inhomogeneous one B^I, $\beta \in \mathbb{R}^+$ is an arbitrary positive real number, while $\lambda(\boldsymbol{x})$ is a $C^2(B)$ scalar function.
The second condition implies that the inhomogeneous character of the material is due to the presence of a scalar parameter, $\lambda(\boldsymbol{x})$, producing the inhomogeneity in the compliance coefficients. It can be also relaxed and, so, written in a weaker form:

$$\hat{S}^I_{ijhk} = \lambda \hat{S}^H_{ijhk} \quad (2.28)$$

where $\hat{S}^H_{ijhk}$ represents only those compliance coefficients explicitly involved in the specific anisotropic homogeneous problem used to construct the associated solution. This means that components of the compliance tensor not involved in the solution of the homogeneous problem will not be involved in that one of the associated inhomogeneous problem. If the conditions (3) and (4) are satisfied, starting from the known solution of the homogeneous problem, the *associated solution,* that is the solution to the inhomogeneous problem, is derived.
In particular, the stress field solution is identical with the stress field of the homogeneous reference solution, while the strain field of the inhomogeneous problem is equal to $\lambda(\boldsymbol{x})$ times the strain field of the homogeneous problem. The advantage of this method is in the fact that its use yields exact solutions for several new interesting inhomogeneous and anisotropic problems.
More in detail, let us to consider an anisotropic homogeneous elastic object, that occupies a volume B^H, with mixed boundary-value (see Figure 2.2.a).
In presence of action-at-a-distance forces and taking into account the compatibility of the solution by writing the equilibrium equations in terms of displacements, the following equilibrium equations can be written:

$$\begin{aligned} &\nabla \cdot \boldsymbol{T}(\boldsymbol{u}) = \boldsymbol{0} \quad \text{in } B^H \\ &\boldsymbol{T}(\boldsymbol{u}) \cdot \boldsymbol{n} = \boldsymbol{t} \quad \text{on } \partial B^H_t \\ &\boldsymbol{T}(\boldsymbol{u}) \cdot \boldsymbol{n} = \boldsymbol{0} \quad \text{on } \partial B^H_0 \end{aligned} \quad (2.29)$$

where $\nabla = \partial_i \boldsymbol{e}_i$ is a vectorial differential operator, ∂B_t^H is the boundary partition of the homogeneous continuum on which the traction field is assigned, ∂B_0^H is the boundary partition of the homogeneous continuum in absence of both traction and displacements fields. On the boundary partition on which the displacements field is assigned, the following relation has to be satisfied:

$$\boldsymbol{u} = \boldsymbol{0} \quad \text{on } \partial B_u^H \tag{2.30}$$

where ∂B_u^H is the boundary partition of the homogeneous continuum on which the displacements field is assigned. The anisotropic Hooke's law, in a linear elastic stress-strain relation, is written in the form:

$$\boldsymbol{T}(\boldsymbol{u}) = \mathbb{C}^H : \boldsymbol{E}(\boldsymbol{u}) = \mathbb{C}^H : sym(\nabla \otimes \boldsymbol{u}) = \mathbb{C}^H : (\nabla \otimes \boldsymbol{u}) \tag{2.31}$$

or:

$$sym(\nabla \otimes \boldsymbol{u}) = \boldsymbol{E}(\boldsymbol{u}) = \mathbb{S}^H : \boldsymbol{T}(\boldsymbol{u}) \tag{2.32}$$

in components:

$$\sigma_{ij} = C_{ijhk}^H \varepsilon_{hk} = C_{ijhk}^H u_{h,k} \tag{2.33}$$

or:

$$\varepsilon_{ij} = S_{ijhk}^H \sigma_{hk} \,. \tag{2.34}$$

Let us to consider, now, an anisotropic inhomogeneous elastic object, that occupies a volume B^I, geometrically the same of B^H, with mixed boundary-value (see Figure 2.2.b). In presence of action-at-a-distance forces and taking into account the compatibility of the solution by writing the equilibrium equations in terms of displacements, in an analogous manner to what has been done before, the following equilibrium equations can be written:

$$\begin{aligned} &\nabla \cdot \boldsymbol{T}(\boldsymbol{u}) = -\mathbf{b} && \text{in } B^I \\ &\boldsymbol{T}(\boldsymbol{u}) \cdot \boldsymbol{n} = \boldsymbol{t} && \text{on } \partial B_t^I \\ &\boldsymbol{T}(\boldsymbol{u}) \cdot \boldsymbol{n} = \boldsymbol{0} && \text{on } \partial B_0^I \end{aligned} \tag{2.35}$$

where ∂B_t^I is the boundary partition of the inhomogeneous continuum on which the traction field is assigned. It is geometrically the same of that one in the

homogeneous problem and ∂B_0^I is the boundary partition of the inhomogeneous continuum in absence of both traction and displacements fields. It is geometrically the same of that one in the homogeneous problem.
On the boundary partition on which the displacements field is assigned, the following relation has to be satisfied:

$$\boldsymbol{u} = \boldsymbol{0} \quad \text{on } \partial B_u^I \tag{2.36}$$

where ∂B_u^I is the boundary partition of the inhomogeneous continuum on which the displacements field is assigned. It is geometrically the same of that one in the homogeneous problem.
Let us to assume the stress tensor $\boldsymbol{T}^H$ as the solution for the homogeneous problem, and let us to assume, also, the hypothesis that:

$$\boldsymbol{T}^I = \boldsymbol{T}^H . \tag{2.37}$$

In this way, the equations in the differential system (2.29) are automatically satisfied. Moreover, if $\boldsymbol{T}^H$ is the solution of the first anisotropic and homogeneous problem, we have that the compatibility condition:

$$\nabla \times \left[\nabla \times \left(\mathbb{S}^H : \boldsymbol{T}^H \right) \right] = \boldsymbol{0} \tag{2.38}$$

has to be also satisfied. As well-known, this ensures that a displacement field $\boldsymbol{u}^H$ exists. So, it is possible to write the strain-displacement relationship:

$$\boldsymbol{E}^H = \mathbb{S}^H : \boldsymbol{T}^H = sym\left(\nabla \otimes \boldsymbol{u}^H \right) \tag{2.39}$$

where $\boldsymbol{u}^H$ is displacements field, solution of the homogeneous problem. Then, in order to accept the hypothesis (2.37), the following equation:

$$\nabla \times \left[\nabla \times \left(\mathbb{S}^I : \boldsymbol{T}^I \right) \right] = \nabla \times \left[\nabla \times \left(\lambda \, \mathbb{S}^H : \boldsymbol{T}^H \right) \right] = \boldsymbol{0} \tag{2.40}$$

becomes necessary and sufficient condition for the existence of a displacement field $\boldsymbol{u}^I$, where $\boldsymbol{u}^I$ is the displacements field, solution of the inhomogeneous problem, and it is given by:

$$sym\left(\nabla \otimes \boldsymbol{u}^I \right) = \boldsymbol{E}^I = \mathbb{S}^I : \boldsymbol{T}^I = \lambda \, \mathbb{S}^H : \boldsymbol{T}^H . \tag{2.41}$$

The compatibility condition (2.40), in general, is not satisfied. Therefore, it is necessary to find the conditions under whose it becomes true, (Fraldi, Cowin, 2004). Without loss of generality, let us consider:

$$\lambda = \lambda(\boldsymbol{x}_3) \tag{2.42}$$

that means that the $\boldsymbol{x}_3$ is the direction locally coaxial with the gradient of λ, i.e.:

$$\nabla\lambda^T = \left[0, 0, \partial\lambda/\partial x_3\right]. \tag{2.43}$$

So, by recalling that $\boldsymbol{u}^H$ is the solution of the homogeneous problem, and by operating some algebraic manipulations, the set of compatibility equations (2.40) can be reduced to five differential equations as it is shown:

$$\begin{cases} \lambda_{,33}u^H_{1,1} + \lambda_{,3}\left(u^H_{1,3} - u^H_{3,1}\right)_{,1} = 0 \\ \lambda_{,33}u^H_{2,2} + \lambda_{,3}\left(u^H_{2,3} - u^H_{3,2}\right)_{,2} = 0 \\ \lambda_{,3}\left(u^H_{1,2} - u^H_{2,1}\right)_{,1} = 0 \\ \lambda_{,3}\left(u^H_{1,2} - u^H_{2,1}\right)_{,2} = 0 \\ \lambda_{,33}\left(u^H_{1,2} + u^H_{2,1}\right) + \lambda_{,3}\left[\left(u^H_{1,3} - u^H_{3,1}\right)_{,2} + \left(u^H_{2,3} - u^H_{3,2}\right)_{,1}\right] = 0 \end{cases} \tag{2.44}$$

where, obviously, is absent any prescribed constraints about the relation between the first and the second derivatives of the parameter λ.

It can be noted that the terms in the parentheses represent the skew components of the $\nabla \otimes \boldsymbol{u}^H$, that are local rotations, while the only present strain components are $\left(1-\delta_{i3}\right)\left(1-\delta_{j3}\right)u^H_{i,j}$, having indicated with δ_{hk} the standard Kronecker operator. It has to be noted that:

1. the displacement field for the reference homogeneous problem has to be related, at each internal point $\boldsymbol{x} \in B^H$, with a local plane strain field, where any plane with support the axis $\boldsymbol{x}_3$ can be the plane of the strains;
2. $$\det \boldsymbol{E}^H = 0; \tag{2.45}$$
3. the vector $\nabla\lambda$, the corresponding points $\boldsymbol{x} \in B^I$, has to be coaxial with the support axis $\boldsymbol{x}_3$ of plane of the strains in the homogeneous problem;
4. $curl\left(\boldsymbol{u}^H\right)$ must be independent from $\boldsymbol{x}_3$-direction, i.e. the $\nabla\lambda$-direction.

In the previous statements, analogously to what has been done with the stress state, it has been implicitly considered the definition about the *plane strain:* a strain state will be *said plane* if, in a fixed point $\boldsymbol{x}$ of the solid, there is *a plane*

of the strains to which all the strain components ε_{ij} belong. It is easy to demonstrate that this plane exists if the strain tensor $\boldsymbol{E}$ has a zero eigenvalue. So, if $\{\xi_1,\xi_2,\xi_3\}$ is the orthogonal *principal* reference frame of the strain tensor $\boldsymbol{E}$ and if ξ_3 is assumed, for example, as the eigenvector associated to the zero eigenvalue of $\boldsymbol{E}$, *the plane of the strains* must coincide with $\xi_1-\xi_3$ plane. It follows that a necessary and sufficient condition for the existence of a *plane strain* is given by:

$$\det\boldsymbol{E}=0\,. \tag{2.46}$$

It has to be noted that the satisfaction of the compatibility condition (2.40) yields that the displacements field of the homogeneous problem has to satisfy the equations (2.44). This compatibility condition (2.40), therefore, may be rewritten in the form:

$$\begin{aligned}&\left\{curl\left[\,curl\left(\lambda\,\mathbb{S}^H:\boldsymbol{T}^H\right)\right]=\boldsymbol{0}\right\}\Leftrightarrow\\&\left\{\forall\boldsymbol{h}\in V:\nabla\lambda\cdot\boldsymbol{h}=0,\left(\nabla\otimes curl\,\boldsymbol{u}^H\right)\boldsymbol{h}=\boldsymbol{0},\,sym\left(\nabla\otimes\boldsymbol{u}^H\right)\boldsymbol{h}\cdot\boldsymbol{h}=0\right\}\end{aligned} \tag{2.47}$$

where $\lambda(\boldsymbol{x})\in C^2\left(B\right)\Big|\,\forall\boldsymbol{x}\in B,\ \lambda(\boldsymbol{x})>\alpha>0,\ \alpha\in\mathbb{R}^+,\ \boldsymbol{h}$ is any unit vector defined in the three-dimensional Euclidean space $\mathbb{E}^3$ and V is the corresponding vector space. Moreover, it is worth to note that the assumed position (2.27) and the hypothesis (2.37), that is true if the equation (2.40) is satisfied, imply:

$$\boldsymbol{E}^I=\lambda\boldsymbol{E}^H\,. \tag{2.48}$$

So, at this point, it can be stated that any anisotropic and homogeneous elastic problem that possesses a solution represented by the displacement equations can be considered a *Displacement Auxiliary Solution* for the corresponding dual inhomogeneous elastic problem.
In other words, it can be possible to demonstrate the following theorem:

Displacement Associated Solution (DAS) Theorem

Consider two geometrically identical anisotropic elastic objects, one homogeneous, B^H, and the other inhomogeneous, B^I, respectively. Let be $\mathbb{S}^H$ and $\mathbb{S}^I=\lambda\left(\boldsymbol{x}\right)\mathbb{S}^H$ the corresponding compliance tensors. The two elastostatic

Cauchy problems associated with the two objects, in presence of the body forces and of mixed boundary-value, are:

$$\begin{aligned} P^H : \{ & \nabla \cdot \boldsymbol{T}(\boldsymbol{u}) = -\mathbf{b} \text{ in } B^H, \ \boldsymbol{T}(\boldsymbol{u}) \cdot \boldsymbol{n} = \boldsymbol{t} \text{ on } \partial B_t^H, \\ & \boldsymbol{T}(\boldsymbol{u}) \cdot \boldsymbol{n} = \mathbf{0} \text{ on } \partial B_0^H, \ \boldsymbol{u} = \mathbf{0} \text{ on } \partial B_u^H \}, \\ P^I : \{ & \nabla \cdot \boldsymbol{T}(\boldsymbol{u}) = -\mathbf{b} \text{ in } B^I, \ \boldsymbol{T}(\boldsymbol{u}) \cdot \boldsymbol{n} = \boldsymbol{t} \text{ on } \partial B_t^I, \\ & \boldsymbol{T}(\boldsymbol{u}) \cdot \boldsymbol{n} = \mathbf{0} \text{ on } \partial B_0^H, \ \boldsymbol{u} = \mathbf{0} \text{ on } \partial B_u^H \} \end{aligned} \tag{2.49}$$

If $\boldsymbol{T}^H$ is the solution of the homogeneous problem p^H, then $\boldsymbol{T}^I = \boldsymbol{T}^H$ if and only if the second part of the equation (2.47) is verified, i.e. if:

$$\boldsymbol{w}^H = curl\, \boldsymbol{u}^H \Big| \forall \boldsymbol{v}, \ \ skew\left(\nabla \otimes \boldsymbol{u}^H\right)\boldsymbol{v} = \boldsymbol{w}^H \wedge \boldsymbol{v}$$

we have that:

$$\forall \boldsymbol{h} \in V \Big| \nabla\lambda \cdot \boldsymbol{h} = 0, \begin{Bmatrix} \left(\nabla \otimes curl\, \boldsymbol{u}^H\right)\boldsymbol{h} = \mathbf{0}, \\ sym\left(\nabla \otimes \boldsymbol{u}^H\right)\boldsymbol{h} \cdot \boldsymbol{h} = 0 \end{Bmatrix} \Leftrightarrow \left\{\boldsymbol{T}^I = \boldsymbol{T}^H\right\}. \tag{2.50}$$

In other words, when a solution $\boldsymbol{B}_\varepsilon^H = \left\{\boldsymbol{u}^H, \boldsymbol{E}^H, \boldsymbol{T}^H\right\}$ for an anisotropic homogeneous elastic problem p^H is known, the DAS theorem yields the corresponding solution for an inhomogeneous elastic problem p^I as $\boldsymbol{B}_\varepsilon^I = \left\{\lambda \boldsymbol{E}^H, \boldsymbol{T}^H\right\}$, if and only if the anisotropic and homogeneous elastic problem possesses, everywhere in the object, a displacement solution satisfying the equations (2.44) and if the displacements boundary conditions are the same for both the homogeneous and inhomogeneous objects.

The solution $\boldsymbol{u}^I$, for the inhomogeneous problem, in general, have to be integrated with reference to the specific case. It is worth to underline that in the case where displacement boundary-value $\boldsymbol{u}$ is not equal to zero, the elastic mixed problem can be rewritten as the corresponding first type one, in which only the traction and reaction fields are considered. For more details on D.A.S. demonstration, see (Fraldi, Cowin, 2004). It is useful to underline, now and again, the geometrical interpretation of the result of the theorem, constituted by the observation that, in order to find an analytical solution for a given elastic inhomogeneous and anisotropic body in the form $\boldsymbol{B}_\varepsilon^I = \left\{\lambda \boldsymbol{E}^H, \boldsymbol{T}^H\right\}$, a necessary and sufficient condition is that the displacement solution for the corresponding anisotropic and homogeneous problem is related with a local plane strain field that has as plane of the strains any plane with support an axis coaxial with the

gradient of λ, with rotational part depending on this gradient direction, only. The D.A.S. theorem can be generalized to comprise different types of composite materials. For example, it is possible to consider the case of a multi-linear law for λ, i.e.:

$$\lambda = \lambda_0 + \lambda_1 \boldsymbol{x}_1 + \lambda_2 \boldsymbol{x}_2 + \lambda_3 \boldsymbol{x}_3 \tag{2.51}$$

with λ_i, $i = \{0,...,3\}$ arbitrary constants.

In this case, it is obtained that the second derivatives of the differential system (2.44) go to zero, therefore, the compatibility equation system becomes as it follows:

$$\begin{cases} \lambda_1 \left(u^*_{1,2} - u^*_{2,1} \right)_{,2} = \lambda_2 \left(u^*_{1,2} - u^*_{2,1} \right)_{,1} \\ \lambda_2 \left(u^*_{2,3} - u^*_{3,2} \right)_{,3} = \lambda_3 \left(u^*_{2,3} - u^*_{3,2} \right)_{,2} \\ \lambda_3 \left(u^*_{1,3} - u^*_{3,1} \right)_{,1} = \lambda_1 \left(u^*_{1,3} - u^*_{3,1} \right)_{,3} \\ \lambda_1 \left[\left(u^*_{1,2} - u^*_{2,1} \right)_{,3} + \left(u^*_{1,3} - u^*_{3,1} \right)_{,2} \right] = \lambda_2 \left(u^*_{1,3} - u^*_{3,1} \right)_{,1} + \lambda_3 \left(u^*_{1,2} - u^*_{2,1} \right)_{,1} \\ \lambda_2 \left[\left(u^*_{2,1} - u^*_{1,2} \right)_{,3} + \left(u^*_{1,3} - u^*_{3,1} \right)_{,1} \right] = \lambda_1 \left(u^*_{2,3} - u^*_{3,2} \right)_{,2} + \lambda_3 \left(u^*_{2,1} - u^*_{1,2} \right)_{,2} \\ \lambda_3 \left[\left(u^*_{3,1} - u^*_{1,3} \right)_{,2} + \left(u^*_{3,2} - u^*_{2,3} \right)_{,1} \right] = \lambda_1 \left(u^*_{3,2} - u^*_{2,3} \right)_{,3} + \lambda_2 \left(u^*_{3,1} - u^*_{1,3} \right)_{,3} \end{cases} \tag{2.52}$$

Because of the arbitrary of the assumption about the constants in the λ law, by setting to zero all skew components of $\nabla \otimes \boldsymbol{u}^H$, a very closed solution of the system can be found in the classical *strain potential* form, (Barber, 1992), that is:

$$\boldsymbol{u}^H = \nabla \phi \tag{2.53}$$

where $\phi = \phi(\boldsymbol{x})$ is a scalar function. The displacement in the form of the equation (2.52) produces, as well-known, an irrotational deformation field and constitutes the irrotational part of the Papkovich-neuber representation in the isotropic elasticity, (Barber, 1992). The reason for which this particular case could result very useful is related to the fact that many fundamental solutions in isotropic and anisotropic elasticity have a representation as described in (2.52), as the axisymmetric, thermoelastic and heat-conduction problems.

It is, also, interesting to observe that, for the case of multi-linear law of λ, not any prescription on the form of the strain tensor $\boldsymbol{E}^H$ is necessary and, so, it is

possible to use as *Displacement Associated Solutions* all the three dimensional solutions about anisotropic elasticity, satisfying the equation (2.52), that is, all the three dimensional solutions that satisfy the equation:

$$curl\, \boldsymbol{u}^H = \mathbf{0} \tag{2.54}$$

For the examples of applicability of the DAS theorem and for more details on its formulation, let us to send to the references being in literature, (Fraldi, Cowin, 2004).
It is worth to note that the DAS theorem, like the SAS one, yields the possibility to find a closed-form solution for some inhomogeneous materials and it evidences that this possibility depends, in general, on the relation between the geometry of the strain distribution in the homogeneous material and the structural gradient, $\nabla\lambda$, of the inhomogeneous material.

2.4. ANISOTROPIC MEDIA: VOLUME FRACTION AND FABRIC TENSORS

In multiphase or damage materials, mechanical properties are closely related to the underlying microstructure or crack distribution. Although the volume fraction is the primary parameter in the geometric characterization of the microstructure of such materials, it does not provide information about the arrangement and the orientation of the microstructure. It is therefore necessary to introduce further parameters able to describe such orientations. The approach commonly use to modelling the material microstructure consists on introducing tensors of higher rank which characterize the microstructural architecture. In particular, in many applications, microstructural anisotropy seems to be sufficiently well described by a scalar and a symmetric second rank fabric tensor, which restricts the material symmetry to orthotropy. Fabric tensors may be defined in a wide number of ways but it is required to be a positive define tensor that is a quantitative stereological measure of the microstructural architecture, a measure whose principal axes are coincident with the principal microstructural direction and whose eigenvalues are proportional to the distribution of the microstructure in the associated principal direction. The fabric tensor may be measure on a finite test volume and it is considered a continuous function of the position in the material. It should be highlight that since the fabric tensor is a continuum point property, its applicability to solve real problem is really difficult because would require a wide number of measures. In other words it would be necessary evaluate the fabric tensor in each point of the material. In the next sections, some way proposed in scientific literature to construct fabric tensors are illustrated.

2.4.1. Mean Intercept Lenght (MIL) Tensor

In order to characterize the microstructural anisotropy in orthotropic materials, Harrigan and Mann (1984) proposed a particular second order tensor – the so-called mean intercept length (MIL) tensor – related to the stereological measurement of the microstructural arrangement. In particular, the MIL in a material is define as the average distance, measured along a particular straight line, between two interfaces of the two different constituents. The value of the MIL is a function of the slope θ of the line along which the measurement is made in a specific plane. If, by plotting in a polar diagram the MIL – measured in the selected plane passing through a particular point in the specimen – as function of θ, the polar diagram produced ellipses (see Figure 2.4), than the values of all MILs in the plane may be represented by a second-order tensor in two dimension.

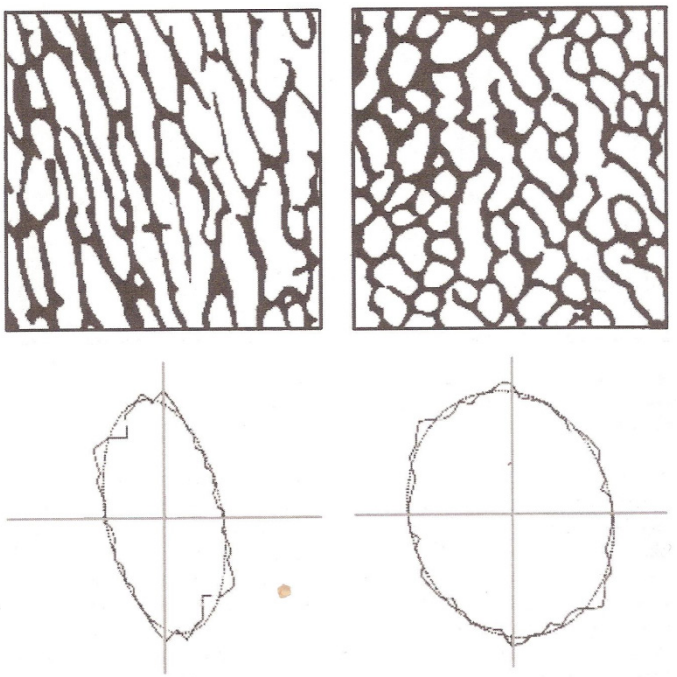

Fig. 2.4 – Polar diagram of the Mean Intercept Length function of a cancellous bone

By extending these consideration to a three-dimensional case, the MILs in all direction would be represented by an ellipsoid that is by a positive define second rank tensor $\boldsymbol{M}$ which is commonly related to the mean intercept length $L(\boldsymbol{n})$ by the relationship $1/L^2(\boldsymbol{n}) = \boldsymbol{n} \cdot \boldsymbol{M}\boldsymbol{n}$, where $\boldsymbol{n}$ is the unit vector in the direction of the mean intercept length measurement.

The MIL approach, as well as other stereological methods – e.g. the volume orientation method, the star volume distribution method – was proposed to construct the fabric tensor for biphasic materials, with particular reference to a specific porous material, the cancellous bone (Odgaard *et al.*, 1997). However, it is worth to highlight that for particular microstructure – e.g. planar fibre networks or materials made of a set of plates – the MIL distribution is not in general elliptic and so it may not be analytically expressed in terms of a second-order tensor (Tözeren and Skalak, 1989).
Cowin (Cowin,1986) defined a fabric tensor $\boldsymbol{H}$ related to the MIL tensor $\boldsymbol{M}$ by $\boldsymbol{H} = \boldsymbol{M}^{-1/2}$. Such tensor is well defined being the positive square root of the inverse of the positive define symmetric tensor $\boldsymbol{M}$. The difference between $\boldsymbol{H}$ and $\boldsymbol{M}$ is in the shape of ellipsoid while the principal axes coincide.

2.4.2. Orientation Distribution Function (ODF)

Let φ be some macroscopic scalar property of a material. At a given instant, φ generally depends on the material point, identified with the reference position vector $\boldsymbol{x}$, and on the orientation, specified by the unit vector $\boldsymbol{n}$; that is, $\varphi = \varphi(\boldsymbol{x}, \boldsymbol{n})$.
Since only the dependence of φ on $\boldsymbol{n}$ is concerned in subsequent investigations, it is convenient to consider $\boldsymbol{x}$ as fixed and drop the dependence of φ on $\boldsymbol{x}$. Then we write:

$$\varphi = f(\boldsymbol{n}), \qquad f : \mathscr{S} \to \mathscr{R} \tag{2.55}$$

and call *f*, the scalar-valued function defined on the unit sphere $\mathscr{S}$, the *orientation distribution function* (ODF) of the property φ. Concretely φ may be the effective surface density of the microdefects, Young's modulus, the wave speed, the electrical resistivity, the fatigue limit, etc. (Lemaitre *et al.*, 1987).
The function $f(\boldsymbol{n})$ must satisfy the condition:

$$f(\boldsymbol{n}) = f(-\boldsymbol{n}), \qquad \forall \boldsymbol{n} \in \mathscr{S} \tag{2.56}$$

because any material property φ in a direction is independent of the geometrical choice made between $\boldsymbol{n}$ and $-\boldsymbol{n}$ for defining that direction. It is possible to prove that the invariance requirement (2.56) is satisfied if and only if there exists a function $\hat{f}$ from $\mathscr{N} = \mathscr{S} \otimes \mathscr{S}$ to $\mathscr{R}$ such that

$$f(\boldsymbol{n}) = \hat{f}(\boldsymbol{n} \otimes \boldsymbol{n}) = \hat{f}(\boldsymbol{N}), \qquad \forall \boldsymbol{n} \in \mathscr{S} \tag{2.57}$$

In the following we only consider the function $\hat{f}(\boldsymbol{N})$ for which the condition (2.56) is verified.
Assume $\hat{f}(\boldsymbol{N})$ to be square-integrable:

$$\int_{\mathscr{S}} \left|\hat{f}(\boldsymbol{N})\right|^2 da < +\infty \tag{2.58}$$

where $da = \sin\theta\, d\theta\, d\phi$ is an infinitesimal surface element of the unit sphere $\mathscr{S}$.
It is that known (Vilenkin, 1969; Bunge, 1982; Jones, 1985) that $\hat{f}(\boldsymbol{N})$ can be expanded in the following Fourier series:

$$\begin{aligned} \hat{f}(\boldsymbol{N}) &= f_0(\boldsymbol{N}) + f_1(\boldsymbol{N}) + f_2(\boldsymbol{N}) + ... \\ &= g + \boldsymbol{G'} : \boldsymbol{F}(\boldsymbol{N}) + \mathbb{G'} :: \mathbb{F}(\boldsymbol{N}) + ..., \qquad \forall \boldsymbol{N} \in \mathscr{N} \end{aligned} \tag{2.59}$$

which is convergent in mean, i.e.:

$$\lim_{n\to\infty} \int_{\mathscr{S}} \left|\hat{f}(\boldsymbol{N}) - s_n(\boldsymbol{N})\right|^2 da = 0, \quad s_n(\boldsymbol{N}) := f_0(\boldsymbol{N}) + f_1(\boldsymbol{N}) + ... + f_n(\boldsymbol{N}) \tag{2.60}$$

In the equation (2.59), $\{\boldsymbol{I}, \boldsymbol{F}(\boldsymbol{N}), \mathbb{F}(\boldsymbol{N}), ...\}$ are generalized spherical harmonics (Kanatani, 1984; Onat, 1984; Jones, 1985) and form a complete orthogonal basis for the squere-integrable functions on $\boldsymbol{L}$.
The first two tensor spherical harmonics $\boldsymbol{F}(\boldsymbol{N})$ and $\mathbb{F}(\boldsymbol{N})$ are of particular interest. In view of the tensor products of Kronecker-type, they may be written in the coordinate-free forms:

$$\boldsymbol{F}(\boldsymbol{N}) = \boldsymbol{N} - \frac{1}{3}\boldsymbol{I} \tag{2.61}$$

$$\begin{aligned} \mathbb{F}(\boldsymbol{N}) = \boldsymbol{N}\otimes\boldsymbol{N} - \tfrac{1}{7}\big(\boldsymbol{I}\otimes\boldsymbol{N} + \boldsymbol{N}\otimes\boldsymbol{I} + \boldsymbol{I}\underline{\otimes}\boldsymbol{N} + \boldsymbol{N}\underline{\otimes}\boldsymbol{I} + \boldsymbol{I}\overline{\otimes}\boldsymbol{N} + \boldsymbol{N}\overline{\otimes}\boldsymbol{I}\big) + \\ \tfrac{1}{35}\big(\boldsymbol{I}\otimes\boldsymbol{I} + \boldsymbol{I}\underline{\otimes}\boldsymbol{I} + \boldsymbol{I}\overline{\otimes}\boldsymbol{I}\big) \end{aligned} \tag{2.62}$$

The orthogonality of the basis functions $\{\boldsymbol{I}, \boldsymbol{F}(\boldsymbol{N}), \mathbb{F}(\boldsymbol{N}), ...\}$ means that

$$\begin{aligned} &\int_{\mathscr{S}} \boldsymbol{F}(\boldsymbol{N})\, da = \boldsymbol{0}, \qquad \int_{\mathscr{S}} \mathbb{F}(\boldsymbol{N})\, da = \mathbb{O} \\ &\int_{\mathscr{S}} \boldsymbol{F}(\boldsymbol{N}) \otimes \mathbb{F}(\boldsymbol{N})\, da = \int_{\mathscr{S}} \mathbb{F}(\boldsymbol{N}) \otimes \boldsymbol{F}(\boldsymbol{N})\, da = \mathbb{O}_6, ... \end{aligned} \tag{2.63}$$

where $\mathbb{O}_6$ denotes the sixth-order zero tensor. It is important to remark that $\boldsymbol{F}(\boldsymbol{N})$ is symmetric and traceless:

$$\boldsymbol{F}^T = \boldsymbol{F}; \quad \boldsymbol{I} : \boldsymbol{F} = 0 \tag{2.64}$$

and that $\mathbb{F}(\boldsymbol{N})$ is completely symmetric and traceless:

$$\mathbb{F} = \left(\boldsymbol{I}\overline{\otimes}\boldsymbol{I}\right)\mathbb{F} = \mathbb{F}^T; \quad \left(\boldsymbol{Y}\overline{\otimes}\boldsymbol{X}\right) :: \mathbb{F} = \left(\boldsymbol{Y}\overline{\otimes}\boldsymbol{X}^T\right) :: \mathbb{F}, \quad \forall \boldsymbol{X}, \boldsymbol{Y} \in \mathscr{L}; \quad \mathbb{F}\boldsymbol{I} = \boldsymbol{0} \tag{2.65}$$

The first three expansion coefficients of equation (2.59) can be determined from $f(\boldsymbol{n})$ via the integrals (Kanatani, 1984):

$$\begin{aligned} g &= \frac{1}{4\pi}\int_L \hat{f}(\boldsymbol{N})\,da, \quad \boldsymbol{G}' = \frac{15}{8\pi}\int_L \hat{f}(\boldsymbol{N})\boldsymbol{F}(\boldsymbol{N})\,da, \\ \mathbb{G}' &= \frac{315}{32\pi}\int_L \hat{f}(\boldsymbol{N})\mathbb{F}(\boldsymbol{N})\,da. \end{aligned} \tag{2.66}$$

Due to equations (2.64) and (2.65), $\boldsymbol{G}'$ turns out to be symmetric and traceless and $\mathbb{G}'$ to be completely symmetric and traceless. With these properties, in the most general case, $\boldsymbol{G}'$ and $\mathbb{G}'$ contain five and nine independent components, respectively.

It is readily seen from equations (2.59) and (2.60) that any square-integrable ODF $\hat{f}(\boldsymbol{N})$ is fully characterized by its scalar and tensor expansion coefficients $\{g, \boldsymbol{G}', \mathbb{G}', ...\}$. If only the leading terms (for example, the first three ones) of the series expansion, (2.59), are retained, a finite or discrete description is then obtained for $\hat{f}(\boldsymbol{N})$. Theoretically speaking, the accuracy of such a description increases with the number of the leading terms being employed; in practice, the maximum value of this number is determined by the degree of accuracy with which the directional data of the property φ are experimentally acquired.

The importance of this result resides in the fact that only the tensors of zero or even orders are usable for a finite description of the ODF of a scalar-valued physical or mechanical property φ.

2.4.3. Relationship between Fabric Tensor and Elasticity Tensor

From a mathematical point of view, identifying the dependence of the elastic behaviour of the material on its microstructure consists in analyzing the formal relationship between the fabric tensor and the elasticity tensor.

The main attempt to relate a fabric tensor describing microstructure to a fourth rank elasticity tensor – with specific reference to porous materials – is due to Cowin (Cowin, 1985).
He proposed a model based on a normalized second rank fabric tensor and developed a general representation of $\bar{\boldsymbol{C}}$ as a function of the solid volume fraction γ and of the invariants of the fabric tensor $\boldsymbol{H}$ based on the notion that the matrix material of the porous elastic solid is isotropic and that the anisotropy of the porous elastic solid itself is due only to the geometry of microstructure represented by the fabric tensor. The mathematical statement of this notion is that the stress tensor $\boldsymbol{T}$ is an isotropic function of the strain tensor $\boldsymbol{E}$ and the fabric tensor $\boldsymbol{H}$ as well as the solid volume fraction γ. Thus, the tensor valued function:

$$\boldsymbol{T} = \boldsymbol{T}\left(\gamma, \boldsymbol{E}, \boldsymbol{H}\right) \tag{2.67}$$

has the property that:

$$\boldsymbol{Q}\boldsymbol{T}\boldsymbol{Q}^{T} = \boldsymbol{T}\left(\gamma, \boldsymbol{Q}\boldsymbol{E}\boldsymbol{Q}^{T}, \boldsymbol{Q}\boldsymbol{H}\boldsymbol{Q}^{T}\right) \tag{2.68}$$

for all orthogonal tensors $\boldsymbol{Q}$.
This definition of an isotropic tensor valued function is given, for example, by Truesdell and Noll (1965).
In accord with the isotropy assumption, the stress tensor $\boldsymbol{T}$ has the representation:

$$\begin{aligned}\boldsymbol{T} = {} & f_1\boldsymbol{I} + f_2\boldsymbol{H} + f_3\boldsymbol{H}^2 + f_4\boldsymbol{E} + f_5\boldsymbol{E}^2 + f_6\left(\boldsymbol{H}\boldsymbol{E} + \boldsymbol{E}\boldsymbol{H}\right) \\ & + f_7\left(\boldsymbol{H}^2\boldsymbol{E} + \boldsymbol{E}\boldsymbol{H}^2\right) + f_8\left(\boldsymbol{H}\boldsymbol{E}^2 + \boldsymbol{E}^2\boldsymbol{H}\right) + f_9\left(\boldsymbol{H}^2\boldsymbol{E}^2 + \boldsymbol{E}^2\boldsymbol{H}^2\right)\end{aligned} \tag{2.69}$$

where f_1 through f_9 are function of the ten invariants $Tr\boldsymbol{H}$, $Tr\boldsymbol{H}^2$, $Tr\boldsymbol{H}^3$, $Tr\boldsymbol{E}$, $Tr\boldsymbol{E}^2$, $Tr\boldsymbol{E}^3$, $Tr\boldsymbol{H}\boldsymbol{E}$, $Tr\boldsymbol{H}^2\boldsymbol{E}$, $Tr\boldsymbol{H}\boldsymbol{E}^2$, $Tr\boldsymbol{E}^2\boldsymbol{H}^2$. This representation is reduced by the requirement that $\boldsymbol{T}$ be linear in $\boldsymbol{E}$ and that $\boldsymbol{T}$ vanish when $\boldsymbol{E}$ vanishes, thus:

$$\boldsymbol{T} = f_1\boldsymbol{I} + f_2\boldsymbol{H} + f_3\boldsymbol{H}^2 + f_4\boldsymbol{E} + f_6\left(\boldsymbol{H}\boldsymbol{E} + \boldsymbol{E}\boldsymbol{H}\right) + f_7\left(\boldsymbol{H}^2\boldsymbol{E} + \boldsymbol{E}\boldsymbol{H}^2\right) \tag{2.70}$$

where f_1, f_2, f_3 must be of the form:

$$
\begin{aligned}
f_1 &= a_1 Tr\boldsymbol{E} + a_2 Tr\boldsymbol{HE} + a_3 Tr\boldsymbol{H}^2\boldsymbol{E}, \\
f_2 &= d_1 Tr\boldsymbol{E} + b_1 Tr\boldsymbol{HE} + b_2 Tr\boldsymbol{H}^2\boldsymbol{E}, \\
f_3 &= d_2 Tr\boldsymbol{E} + d_3 Tr\boldsymbol{HE} + b_3 Tr\boldsymbol{H}^2\boldsymbol{E}
\end{aligned} \tag{2.71}
$$

and where a_1, a_2, a_3, b_1, b_2, b_3, d_1, d_2 and d_3, are function of $Tr\boldsymbol{H}$, $Tr\boldsymbol{H}^2$ and $Tr\boldsymbol{H}^3$. It follows then that:

$$
\begin{aligned}
\boldsymbol{T} = {} & \boldsymbol{I}\left(a_1 Tr\boldsymbol{E} + a_2 Tr\boldsymbol{HE} + a_3 Tr\boldsymbol{H}^2\boldsymbol{E}\right) + \boldsymbol{H}\left(d_1 Tr\boldsymbol{E} + b_1 Tr\boldsymbol{HE} + b_2 Tr\boldsymbol{H}^2\boldsymbol{E}\right) \\
& + \boldsymbol{H}^2\left(d_2 Tr\boldsymbol{E} + d_3 Tr\boldsymbol{HE} + b_3 Tr\boldsymbol{H}^2\boldsymbol{E}\right) + 2c_1\boldsymbol{E} + 2c_2\left(\boldsymbol{HE} + \boldsymbol{EH}\right) \\
& + 2c_3\left(\boldsymbol{H}^2\boldsymbol{E} + \boldsymbol{EH}^2\right)
\end{aligned} \tag{2.72}
$$

where we have set $f_4 = 2c_1$, $f_6 = 2c_2$ and $f_7 = 2c_3$. This result may be expressed in indicial notation as:

$$
\begin{aligned}
T_{ij} = {} & \delta_{ij}\left(a_1 E_{kk} + a_2 H_{rp}E_{pr} + a_3 H_{rq}H_{qp}E_{pr}\right) + \\
& + H_{ij}\left(d_1 E_{kk} + b_1 H_{rp}E_{pr} + b_2 H_{rq}H_{qp}E_{pr}\right) + \\
& + H_{is}H_{sj}\left(d_2 E_{kk} + d_3 H_{rp}E_{pr} + b_3 H_{rq}H_{qp}E_{pr}\right) + \\
& + 2c_1 E_{ij} + 2c_2\left(H_{ir}E_{rj} + E_{ir}H_{rj}\right) \\
& + 2c_3\left(H_{ip}H_{pr}E_{rj} + E_{ir}H_{rp}H_{pj}\right)
\end{aligned} \tag{2.73}
$$

Comparison of this result with the constitutive equation $T_{ij} = C_{ijhk}E_{hk}$ suggests that C_{ijhk} should be of the form:

$$
\begin{aligned}
C_{ijhk} = {} & \left(a_1\delta_{ij} + d_1 H_{ij} + d_2 H_{is}H_{sj}\right)\delta_{hk} + \left(a_2\delta_{ij} + b_1 H_{ij} + d_3 H_{is}H_{sj}\right)H_{hk} \\
& + \left(a_3\delta_{ij} + b_2 H_{ij} + b_3 H_{is}H_{sj}\right)H_{hq}H_{qk} + 2c_1\delta_{hi}\delta_{kj} \\
& + 2c_2\left(H_{ih}\delta_{kj} + \delta_{ih}H_{kj}\right) + 2c_3\left(H_{ip}H_{pk}\delta_{kj} + \delta_{ih}H_{kp}H_{ps}\right).
\end{aligned} \tag{2.74}
$$

In order to satisfy the symmetry conditions (1.90) we must set $d_1 = a_2$, $d_2 = a_3$, and $d_3 = b_2$ and take the symmetric parts of the terms multiplied by $2c_1$, $2c_2$, and $2c_3$ with respect to *hk* and *ij*. The final results may be express as follow:

$$
\begin{aligned}
C_{ijhk} = {} & a_1\delta_{ij}\delta_{hk} + a_2(H_{ij}\delta_{ij} + H_{hk}\delta_{hk}) + a_3(\delta_{ij}H_{hq}H_{qk} + \delta_{hk}H_{iq}H_{qj}) + \\
& + b_1H_{ij}H_{hk} + b_2(H_{ij}H_{hq}H_{qk} + H_{is}H_{sj}H_{hk}) + b_3H_{is}H_{sj}H_{hq}H_{qk} + \\
& + c_1(\delta_{hi}\delta_{kj} + \delta_{ki}\delta_{hj}) + c_2(H_{ih}\delta_{kj} + H_{hj}\delta_{ki} + H_{ik}\delta_{hj} + H_{kj}\delta_{hi}) + \\
& + c_3(H_{ir}H_{rh}\delta_{kj} + H_{rj}H_{hr}\delta_{ki} + H_{ir}H_{rk}\delta_{hj} + H_{kr}H_{rj}\delta_{ih})
\end{aligned}
\tag{2.75}
$$

where a_1, a_2, a_3, b_1, b_2, b_3, c_1, c_2 and c_3 are functions of γ and $Tr\boldsymbol{H}$, $Tr\boldsymbol{H}^2$ and $Tr\boldsymbol{H}^3$. It is possible to show that the representation (2.75) for the fourth rank elasticity tensor is not capable of representing all possible elastic material symmetry. The last material symmetry that may be represented by is orthotropy.

In fact, expanding in indicial notation in the coordinate system that diagonalized the fabric tensor ($H_{12} = H_{13} = H_{23} = 0$), only the following nine components of the elastic tensor are non-zero and are function of the nine coefficient a_1, a_2, a_3, b_1, b_2, b_3, c_1, c_2, c_3 and of the three eigenvalues of $\boldsymbol{H}$, H_{11}, H_{22} and H_{33}:

$$
\begin{aligned}
C_{1111} &= a_1 + 2c_1 + 2(a_2 + 2c_2)H_{11} + (2a_3 + b_1 + 4c_3)H_{11}^2 + 2b_2H_{11}^3 + b_3H_{11}^4 \\
C_{2222} &= a_1 + 2c_1 + 2(a_2 + 2c_2)H_{22} + (2a_3 + b_1 + 4c_3)H_{22}^2 + 2b_2H_{22}^3 + b_3H_{22}^4 \\
C_{3333} &= a_1 + 2c_1 + 2(a_2 + 2c_2)H_{33} + (2a_3 + b_1 + 4c_3)H_{33}^2 + 2b_2H_{33}^3 + b_3H_{33}^4 \\
C_{1122} &= a_1 + a_2(H_{11} + H_{22}) + a_3(H_{11}^2 + H_{22}^2) + b_1H_{11}H_{22} + \\
&\quad + b_2(H_{11}H_{22}^2 + H_{22}H_{11}^2) + b_3H_{11}^2H_{22}^2 \\
C_{1133} &= a_1 + a_2(H_{11} + H_{33}) + a_3(H_{11}^2 + H_{33}^2) + b_1H_{11}H_{33} + \\
&\quad + b_2(H_{11}H_{33}^2 + H_{33}H_{11}^2) + b_3H_{11}^2H_{33}^2 \\
C_{3322} &= a_1 + a_2(H_{33} + H_{22}) + a_3(H_{33}^2 + H_{22}^2) + b_1H_{33}H_{22} + \\
&\quad + b_2(H_{33}H_{22}^2 + H_{22}H_{33}^2) + b_3H_{33}^2H_{22}^2 \\
C_{1212} &= c_1 + c_2(H_{11} + H_{22}) + c_3(H_{11}^2 + H_{22}^2) \\
C_{1313} &= c_1 + c_2(H_{11} + H_{33}) + c_3(H_{11}^2 + H_{33}^2) \\
C_{3232} &= c_1 + c_2(H_{33} + H_{22}) + c_3(H_{33}^2 + H_{22}^2)
\end{aligned}
\tag{2.76}
$$

Note that these nine components of the elasticity tensor are distinct if and only if the eigenvalues of $\boldsymbol{H}$ are distinct. In fact, it is easy to see that by setting $H_{22} = H_{33}$ in the (2.76), only the following six constants are different:

$$
\begin{aligned}
C_{1111} &= a_1 + 2c_1 + 2(a_2 + 2c_2)H_{11} + (2a_3 + b_1 + 4c_3)H_{11}^2 + 2b_2H_{11}^3 + b_3H_{11}^4 \\
C_{2222} &= C_{3333} = a_1 + 2c_1 + 2(a_2 + 2c_2)H_{22} + (2a_3 + b_1 + 4c_3)H_{22}^2 + 2b_2H_{22}^3 + \\
&\quad + b_3H_{22}^4 \\
C_{1122} &= C_{1133} = a_1 + a_2(H_{11} + H_{22}) + a_3(H_{11}^2 + H_{22}^2) + b_1H_{11}H_{22} + \\
&\quad + b_2(H_{11}H_{22}^2 + H_{22}H_{11}^2) + b_3H_{11}^2H_{22}^2 \\
C_{3322} &= a_1 + a_2(H_{33} + H_{22}) + a_3(H_{33}^2 + H_{22}^2) + b_1H_{33}H_{22} + \\
&\quad + b_2(H_{33}H_{22}^2 + H_{22}H_{33}^2) + b_3H_{33}^2H_{22}^2 \\
C_{1212} &= C_{1313} = c_1 + c_2(H_{11} + H_{22}) + c_3(H_{11}^2 + H_{22}^2) \\
C_{3232} &= c_1 + c_2(H_{33} + H_{22}) + c_3(H_{33}^2 + H_{22}^2)
\end{aligned}
\tag{2.77}
$$

and only five of which are independent being $C_{2222} = C_{2233} + 2C_{2323}$. Thus, the represented material symmetry is the transversely isotropy. In the same way, if the eigenvalues of $\boldsymbol{H}$ are all equal the represented material symmetry is the isotropy, being only the following three constant different

$$
\begin{aligned}
C_{1111} = C_{2222} = C_{3333} &= a_1 + 2c_1 + 2(a_2 + 2c_2)H_{11} + (2a_3 + b_1 + 4c_3)H_{11}^2 \\
&\quad + 2b_2H_{11}^3 + b_3H_{11}^4 \\
C_{1122} = C_{1133} = C_{2233} &= a_1 + a_2(H_{11} + H_{22}) + a_3(H_{11}^2 + H_{22}^2) + b_1H_{11}H_{22} \\
&\quad + b_2(H_{11}H_{22}^2 + H_{22}H_{11}^2) + b_3H_{11}^2H_{22}^2 \\
C_{1212} = C_{1313} = C_{3232} &= c_1 + c_2(H_{11} + H_{22}) + c_3(H_{11}^2 + H_{22}^2)
\end{aligned}
\tag{2.78}
$$

and only two of which are independent, being $C_{1111} = C_{1122} + 2C_{1212}$.

The nine functions a_1, a_2, a_3, b_1, b_2, b_3, c_1, c_2 and c_3 depending upon γ, $Tr\boldsymbol{H}$, $Tr\boldsymbol{H}^2$ and $Tr\boldsymbol{H}^3$, can be determine by means of experimental tests.

Following this method, Zysset and Curnier (1995) introduce a general approach for relating the material microstructure to the four rank elasticity tensor. In particular, they describe the microstructure by means of a scalar and a symmetric, traceless second rank fabric tensor. By using a representation theorem for anisotropic function with tensorial arguments, they derive a general expression for the elastic free energy and discuss the resulting material symmetry in terms of the fabric tensor. Specifically, they hypothesize that the mechanical anisotropy of the material is identical to that of a single microstructural property $f = f(\boldsymbol{N}) > 0$, where $\boldsymbol{N} = \boldsymbol{n} \otimes \boldsymbol{n}$ is the dyadic product of the unit vector $\boldsymbol{n}$ specifying the orientation (He *et al.*, 1995). By following the procedure shown in section 2.2, assuming that the function f to be square integrable, it can be expanded in a convergent Fourier series

$$f(\boldsymbol{N}) = g \cdot \boldsymbol{I} + \boldsymbol{G} : \boldsymbol{F}(\boldsymbol{N}) + \mathbb{G} :: \mathbb{F}(\boldsymbol{N}) + ..., \qquad \forall \boldsymbol{N} \qquad (2.79)$$

where $\boldsymbol{I}$, $\boldsymbol{F}(\boldsymbol{N})$ and $\mathbb{F}(\boldsymbol{N})$ are even ranked tensorial basis functions – in particular $\boldsymbol{I}$ is the second order unit tensor, while $\boldsymbol{F}(\boldsymbol{N})$ and $\mathbb{F}(\boldsymbol{N})$ are given by the **(2.61)** and (2.62), respectively – and g, $\boldsymbol{G}$ and $\mathbb{G}$ are the corresponding even ranked tensorial coefficients, called fabric tensor and given by the equations (2.66). As highlight in section 2.2., the accuracy of the series expansion improves with the number of retained leading terms.
However, in most applications, the first and second terms provide a sufficient description of material anisotropy. So, the orientation distribution function f is approximate with:

$$f(\boldsymbol{N}) = g \cdot \boldsymbol{I} + \boldsymbol{G} : \boldsymbol{F}(\boldsymbol{N}) \qquad (2.80)$$

which implies a restriction on material symmetry – that can be orthotropy if all three eigenvalues of $\boldsymbol{G}$ are distinct, transerse isotropy if only two eigenvalues of $\boldsymbol{G}$ are distinct or isotropy if the tensor $\boldsymbol{G}$ vanishes.
By using the second rank tensor representation $\boldsymbol{Q}$ of the orthogonal group *Orth*, the material symmetry group *G* can be characterized by the fabric tensors:

$$\boldsymbol{Q} \in G \Leftrightarrow \begin{cases} \boldsymbol{Q}^T g \boldsymbol{I} \boldsymbol{Q} = g\boldsymbol{I} \\ \boldsymbol{Q}^T \boldsymbol{G} \boldsymbol{Q} = \boldsymbol{G} \\ (\boldsymbol{Q} \underline{\otimes} \boldsymbol{Q})^T \mathbb{G} (\boldsymbol{Q} \underline{\otimes} \boldsymbol{Q}) = \mathbb{G} \\ \dots \end{cases} \qquad (2.81)$$

Following this hypothesis, a scalar valued function $\psi(\boldsymbol{E})$ invariant with respect to the elements of the symmetry group *G* can be identified with an isotropic function $\hat{\psi}(\boldsymbol{E}, g, \boldsymbol{G}, \mathbb{G}, \dots)$ of the same argument and the corresponding fabric tensor (Boehler, 1987):

$$\psi(\boldsymbol{E}) = \psi(\boldsymbol{Q}^T \boldsymbol{E} \boldsymbol{Q}), \qquad \forall \boldsymbol{Q} \in G,$$
$$\hat{\psi}(\boldsymbol{E}, g, \boldsymbol{G}, \mathbb{G}, \dots) = \hat{\psi}\left(\boldsymbol{Q}^T \boldsymbol{E} \boldsymbol{Q}, g, \boldsymbol{Q}^T \boldsymbol{G} \boldsymbol{Q}, (\boldsymbol{Q} \underline{\otimes} \boldsymbol{Q})^T \mathbb{G} (\boldsymbol{Q} \underline{\otimes} \boldsymbol{Q})\right), \qquad \forall \boldsymbol{Q} \in Orth$$

Representation theorems then provide the most general form of the isotropic scalar function $\hat{\psi}(\boldsymbol{E}, g, \boldsymbol{G}, \mathbb{G}, \dots)$ in terms of invariants of the arguments.

For a scalar g and two second rank tensor arguments $\boldsymbol{E}$ and $\boldsymbol{G}$, with $\boldsymbol{G}$ being traceless, a set of irreducible invariants is given by (Boehler, 1987) $Tr(\boldsymbol{E})$, $Tr(\boldsymbol{E}^2)$, $Tr(\boldsymbol{E}^3)$, g, $Tr(\boldsymbol{G}^2)$, $Tr(\boldsymbol{G}^3)$, $Tr(\boldsymbol{EG})$, $Tr(\boldsymbol{E}^2\boldsymbol{G})$, $Tr(\boldsymbol{EG}^2)$, $Tr\left((\boldsymbol{EG})^2\right)$.

Retaining only quadratic terms in $\boldsymbol{E}$ to come up with linear elasticity, general form of the elastic free energy is:

$$\begin{aligned}\psi &= \psi(\boldsymbol{E},g,\boldsymbol{G}) = \frac{c_1}{2}Tr^2(\boldsymbol{E}) + \frac{c_2}{2}Tr(\boldsymbol{E}^2) + \frac{c_3}{2}Tr^2(\boldsymbol{EG}) \\ &+c_4 Tr(\boldsymbol{E}^2\boldsymbol{G}) + \frac{c_5}{2}Tr^2(\boldsymbol{EG}^2) + \frac{c_6}{2}Tr\left((\boldsymbol{EG})^2\right) + c_7 Tr(\boldsymbol{E})Tr(\boldsymbol{EG}) \\ &+c_8 Tr(\boldsymbol{EG})Tr(\boldsymbol{EG}^2) + c_9 Tr(\boldsymbol{E})Tr(\boldsymbol{EG}^2)\end{aligned} \tag{2.82}$$

where c_i are functions of g and the two invariants of $\boldsymbol{G}$. The constitutive equation for the stress tensor is obtained by derivation of the free energy potential ψ with respect to the strain $\boldsymbol{E}$:

$$\begin{aligned}\boldsymbol{T} &= \frac{\partial\psi}{\partial\boldsymbol{E}}(\boldsymbol{E},g,\boldsymbol{G}) = c_1 Tr(\boldsymbol{E})\boldsymbol{I} + c_2\boldsymbol{E} + c_3 Tr(\boldsymbol{EG})\boldsymbol{G} + c_4(\boldsymbol{EG}+\boldsymbol{GE}) \\ &+c_5 Tr(\boldsymbol{EG}^2)\boldsymbol{G}^2 + c_6(\boldsymbol{GEG}) + c_7\left(Tr(\boldsymbol{EG})\boldsymbol{I} + Tr(\boldsymbol{E})\boldsymbol{G}\right) \\ &+c_8\left(Tr(\boldsymbol{EG}^2)\boldsymbol{G} + Tr(\boldsymbol{EG})\boldsymbol{G}^2\right) + c_9\left(Tr(\boldsymbol{EG}^2)\boldsymbol{I} + Tr(\boldsymbol{E})\boldsymbol{G}^2\right)\end{aligned} \tag{2.83}$$

The elasticity tensor is obtained by further derivation:

$$\begin{aligned}\mathbb{C} &= \frac{\partial^2\psi}{\partial\boldsymbol{E}^2}(\boldsymbol{E},g,\boldsymbol{G}) \\ &= c_1\boldsymbol{I}\otimes\boldsymbol{I} + c_2\boldsymbol{I}\underline{\overline{\otimes}}\boldsymbol{I} + c_3\boldsymbol{G}\underline{\overline{\otimes}}\boldsymbol{G} + c_4\left(\boldsymbol{G}\underline{\overline{\otimes}}\boldsymbol{I} + \boldsymbol{I}\underline{\overline{\otimes}}\boldsymbol{G}\right) + c_5\boldsymbol{G}^2\otimes\boldsymbol{G}^2 + c_6\boldsymbol{G}\underline{\overline{\otimes}}\boldsymbol{G} \\ &+c_7\left(\boldsymbol{I}\otimes\boldsymbol{G} + \boldsymbol{G}\otimes\boldsymbol{I}\right) + c_8\left(\boldsymbol{G}\otimes\boldsymbol{G}^2 + \boldsymbol{G}^2\otimes\boldsymbol{G}\right) + c_9\left(\boldsymbol{I}\otimes\boldsymbol{G}^2 + \boldsymbol{G}^2\otimes\boldsymbol{I}\right)\end{aligned} \tag{2.84}$$

The material symmetry represented by the elasticity tensor in the form (2.84), like which one in (2.75), is at least the orthotropy that may degenerate into transverse isotropy when two eigenvalues of $\boldsymbol{G}$ are identical and into isotropy when the fabric tensor $\boldsymbol{G}$ vanishes. By using the spectral decomposition of $\boldsymbol{G}$:

$$\boldsymbol{G} = g_i\boldsymbol{G}_i,\ \boldsymbol{G}_i = \boldsymbol{g}_i\otimes\boldsymbol{g}_i$$

where g_i are the eigenvalues and $\boldsymbol{g}_i$ are the unit orthogonal eigenvectors of $\boldsymbol{G}$, and the property $\boldsymbol{G}_1 + \boldsymbol{G}_2 + \boldsymbol{G}_3 = \boldsymbol{I}$, the elasticity tensor (2.84) may be translated in the general orthotropic form :

$$\mathbb{S} = \lambda_{ii}\boldsymbol{G}_i \otimes \boldsymbol{G}_i + \lambda_{ij}^{*}\left(\boldsymbol{G}_i \otimes \boldsymbol{G}_j + \boldsymbol{G}_j \otimes \boldsymbol{G}_i\right) + 2\mu_{ij}\left(\boldsymbol{G}_i \overline{\underline{\otimes}} \boldsymbol{G}_j + \boldsymbol{G}_j \overline{\underline{\otimes}} \boldsymbol{G}_i\right) \qquad (2.85)$$

where summation is performed for $i < j$ due to symmetrization of tensor products. The identification of the coefficients leads to:

$$\begin{aligned}
\lambda_{ii} &= c_1 + c_2 + c_3 g_i^2 + 2c_4 g_i + c_5 g_i^4 + c_6 g_i^2 + 2c_7 g_i + c_8 g_i^3 + 2c_9 g_i^2, \\
\lambda_{ij}^{*} &= c_1 + c_3 g_i g_j + c_5 g_i^2 g_j^2 + c_7\left(g_i + g_j\right) + c_8\left(g_i g_j^2 + g_j g_i^2\right) + c_9\left(g_i^2 + g_j^2\right), \qquad (2.86) \\
\mu_{ij} &= \tfrac{1}{2}c_2 + \tfrac{1}{2}c_4\left(g_i + g_j\right) + \tfrac{1}{2}c_6 g_i g_j
\end{aligned}$$

At this stage, additional assumptions are necessary to guide the choice of the nine functions c_i.

The hypothesis they made, consists in introducing a homogeneity property for the set of fabric tensor $\{g, \boldsymbol{G}\}$, which means that anisotropy of the elastic constitutive law is independent of the size or physical units of the microstructural properties $\mathbb{S}(\lambda \boldsymbol{G}) = \lambda^k \mathbb{S}(g, \boldsymbol{G}), \forall \lambda > 0$, where $k \neq 0$ is the degree of the homogeneity property.

By considering the isotropic elasticity tensor, $\mathbb{S} = \lambda_c \boldsymbol{I} \otimes \boldsymbol{I} + 2\mu_c \boldsymbol{I} \overline{\underline{\otimes}} \boldsymbol{I}$, and substituting the identity tensor $\boldsymbol{I}$ by the tensor $g\boldsymbol{I} + \boldsymbol{G}$:

$$\mathbb{S} = \lambda_c\left(g\boldsymbol{I} + \boldsymbol{G}\right) \otimes \left(g\boldsymbol{I} + \boldsymbol{G}\right) + 2\mu_c\left(g\boldsymbol{I} + \boldsymbol{G}\right) \overline{\underline{\otimes}} \left(g\boldsymbol{I} + \boldsymbol{G}\right) \qquad (2.87)$$

where λ_c and μ_c are Lamé like constants, a particular form of the previous model is provided:

$$\begin{aligned}
&c_1 = \lambda_c g^2, \quad c_2 = 2\mu_c g^2, \quad c_3 = \lambda_c, \\
&c_4 = 2\mu_c g, \quad c_5 = 0, \quad c_6 = 2\mu_c, \qquad (2.88) \\
&c_7 = \lambda_c g, \quad c_8 = 0, \quad c_9 = 0
\end{aligned}$$

In the principal reference frame of $\boldsymbol{G}$:

$$\begin{aligned}\mathbb{S}(g,\boldsymbol{G}) = &\left(\lambda_c + 2\mu_c\right)\left(g+g_i\right)^2\left(\boldsymbol{G}_i \otimes \boldsymbol{G}_i\right)\\ &+\lambda_c\left(g+g_i\right)\left(g+g_j\right)\left(\boldsymbol{G}_i \otimes \boldsymbol{G}_j + \boldsymbol{G}_j \otimes \boldsymbol{G}_i\right)\\ &+2\mu_c\left(g+g_i\right)\left(g+g_j\right)\left(\boldsymbol{G}_i \underline{\overline{\otimes}} \boldsymbol{G}_j + \boldsymbol{G}_j \underline{\overline{\otimes}} \boldsymbol{G}_i\right)\end{aligned} \tag{2.89}$$

Comparison with the general orthotropic form gives:

$$\begin{aligned}&\lambda_{ii} = \left(\lambda_c + 2\mu_c\right)\left(g+g_i\right)^2, \quad \forall i,\\ &\lambda^*_{ij} = \lambda_c\left(g+g_i\right)\left(g+g_j\right), \quad \forall i,j \ \ (i<j),\\ &\mu_{ij} = \mu_c\left(g+g_i\right)\left(g+g_j\right), \quad \forall i,j \ \ (i<j).\end{aligned} \tag{2.90}$$

Sufficient but not necessary to satisfy the homogeneity condition, the substitution (2.87) provides the most simple orthotropic model that degenerates into transverse isotropy if two eigenvalues of $\boldsymbol{G}$ are identical and into isotropy if $\boldsymbol{G} = 0$.

In order to generalize the previous approach, it is considered now the substitution (2.87) for an arbitrary strictly positive power *k* of the tensor $g\boldsymbol{I} + \boldsymbol{G}$. In the principal reference frame of $\boldsymbol{G}$, the elasticity tensor becomes:

$$\begin{aligned}\mathbb{S}(g,\boldsymbol{G}) = &\left(\lambda_c + 2\mu_c\right)m_i^{2k}\left(\boldsymbol{G}_i \otimes \boldsymbol{G}_i\right)\\ &+\lambda_c m_i^k m_j^k\left(\boldsymbol{G}_i \otimes \boldsymbol{G}_j + \boldsymbol{G}_j \otimes \boldsymbol{G}_i\right)\\ &+2\mu_c m_i^k m_j^k\left(\boldsymbol{G}_i \underline{\overline{\otimes}} \boldsymbol{G}_j + \boldsymbol{G}_j \underline{\overline{\otimes}} \boldsymbol{G}_i\right)\end{aligned} \tag{2.91}$$

where $m_i = g + g_i$. The coefficient exhibits the more general form:

$$\begin{aligned}&\lambda_{ii} = \left(\lambda_c + 2\mu_c\right)m_i^{2k}, \quad \forall i,\\ &\lambda^*_{ij} = \lambda_c m_i^k m_j^k, \quad \forall i,j \ \ (i<j),\\ &\mu_{ij} = \mu_c m_i^k m_j^k, \quad \forall i,j \ \ (i<j).\end{aligned} \tag{2.92}$$

In this case, the anisotropic elastic behaviour of the material is completely described by the two constants λ_c and μ_c, the exponent *k* and the fabric tensor $\{g,\boldsymbol{G}\}$ and the overall elasticity tensor assumes the form:

$$\mathbb{S} = \begin{pmatrix} \left(\lambda_c + 2\mu_c\right) m_1^{2k} & \lambda_c m_1^k m_2^k & \lambda_c m_1^k m_3^k & 0 & 0 & 0 \\ \lambda_c m_2^k m_1^k & \left(\lambda_c + 2\mu_c\right) m_2^{2k} & \lambda_c m_2^k m_3^k & 0 & 0 & 0 \\ \lambda_c m_3^k m_1^k & \lambda_c m_3^k m_2^k & \left(\lambda_c + 2\mu_c\right) m_3^{2k} & 0 & 0 & 0 \\ 0 & 0 & 0 & 2\mu_c m_2^k m_3^k & 0 & 0 \\ 0 & 0 & 0 & 0 & 2\mu_c m_3^k m_1^k & 0 \\ 0 & 0 & 0 & 0 & 0 & 2\mu_c m_1^k m_2^k \end{pmatrix}. \tag{2.93}$$

REFERENCES

Alshits VI, Kirchner OK. 2001. Cylindrically anisotropic, radially inhomogeneous elastic materials. Proc. R. Soc. A. 457: 671-693.

Barber JR. 1992. Elasticity. Kluwer Academic Publishers.

Boehler JP. 1987. Application of Tensor Functions in Solid Mechanics. Springer.

Bunge G. 1970. Texture Analysis in Material Science. Mathematical Methods. Butterworth.

Cowin SC. 1985. The Relationship between the Elasticity Tensor and the Fabric Tensor. Mechanics of Materials. 4: 137-147.

Cowin SC. 1986. Wolff's law of trabecular architecture at remodelling equilibrium. Journal of Biomechanical Engineering. 108: 83-88.

Cowin SC, 1987. Torsion of cylinders with shape intrinsic orthotropy. J. Appl. Mech. 109: 778-782.

Chung MY, Ting TCT. 1995. Line forces and dislocations in angularly inhomogeneous anisotropic piezoelectric wedges and spaces. Philos. Mag. A. 71: 1335-1343.

Fraldi M., Guarracino F. 2001. On a general property of a class of homogenized porous media. Mech.Res.Comm. 28: 213-221.

Fraldi M, Cowin SC. 2004. Inhomogeneous elastostatic problem solutions constructed from stress-associated homogeneous solutions. Journal of the Mechanics and Physics of Solids 52: 2207-2233.

Gurtin M E. 1972. The Linear Theory of Elasticity, Handbbuch der Physik. Springer.

Harrigan TP, Mann RW, 1984. Characterization of microstructural anisotropy in orthotropic materials using a second rank tensor. Journal of Material Science, 19: 761-767.

He QC, Curnier A. 1995. A more fundamental approach to damaged elastic stress-strain relations. International J. of Solids and Structures. 32: 1433-1457Jones MN. 1985. Spherical Harmonics and Tensors for Classical Field Theory. Wiley.

Kanatani K. 1984. Distribution of directional data and fabric tensors. Int. J. Engng Sci. 22: 149-164.

Lekhnitskii SG. 1963. Theory of elasticity of an anisotropic elastic body. Holden Day Inc.

Lemaitre J, Dufailly J. 1987. Damage measurement. Eng Fracture Mech. 28: 643-661.

Lions JL, 1985. Les Methodes de l'Homogeneisation: Theorie et Applications en Physique. Eyrolles Ed.

Maugin GA. 1993. Material inhomogeneities in elasticity. Chapman & Hall.

Nemat-Nasser S, Horii H. 1993. Micromechanics: Overall properies of heterogeneous materials. North-Holland.

Odgaard A, Kabel J, van Rietbergen B, Dalstra M, Huiskes R, 1997. Fabric and elastic principal directions of cancellous bone are closely related. J. Biomechanics. 30: 487-495.

Onat ET. 1984. Effective properties of elastic materials that contain penny shaped voids. Int. J. Engng Sci. 22: 1013-1021.

Ting TCT. 1996. Anisotropic elasticity. Theory and applications. Oxford.

Tözeren A, Skalak R. 1989. Does fabric tensor exist for a fabric? Journal of Material Science. 24: 1700-1706.

Truesdell C, Noll W. 1965. The non-linear field theories of mechanics. Handbuch der Physik, vol. III/3. Springer.

Vilenkin NJ. 1969. Fonctions Spéciales et Théorie de la Représentation des Groupes. Dunod.

Voigt W, 1928. Lehrbuch der Kristallphysik. Leipzig: BG Teubner Verlag.

Zysset PK, Curnier A. 1995. An alternative model for anisotropic elasticity based on fabric tensors. Mech. of Materials. 21: 243-250.

3 THEORY OF HOMOGENIZATION

Homogenization is the modelling of a heterogeneous medium by means of a unique continuous medium. A heterogeneous medium is a medium of which material properties (e. g., elasticity coefficients) vary pointwise in a continuous or discontinuous manner, in a periodic or nonperiodic way, deterministically or randomly. While, obviously, homogenization is a modelling technique that applies to all fields of macroscopic physics governed by nice partial differential equations, we focus more particularly on the mechanics of deformable bodies.

3.1. REPRESENTATIVE VOLUME ELEMENT (RVE)

Two different scales are used in the description of heterogeneous media. One of these is a *macroscopic* (x) scale at which homogeneities are weak.
The other one is the scale of inhomogeneities and is referred to as the *microscopic* (y) scale.
The latter defines the size of the representative volume element (Fig. 3.1.). The basic cell of a periodic composite is an example of RVE. From the experimental point of view, we can say that there exists a kind of statistical homogeneity in

the sense that any RVE at a specific point looks very much like any other RVE taken at random at another point.

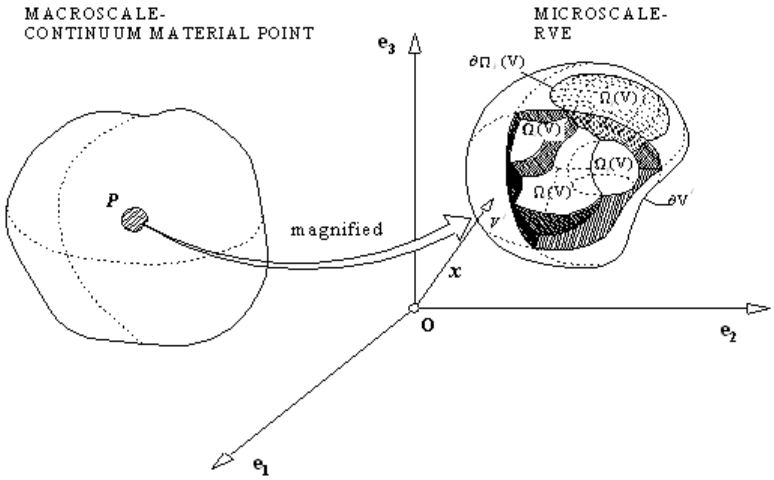

Fig. 3.1 – Representative Volume Element

The mathematical problem presents itself in the following manner. Let $\boldsymbol{\sigma}(y)$ and $\boldsymbol{\varepsilon}(y)$ be the stress and strain at the micro scale in the framework of small-perturbation hypothesis.

We denote by $\boldsymbol{\Sigma}$ and $\mathbf{E}$ the same notion at the macro scale. Let $\langle ... \rangle$ indicate the averaging operator. For a volume averaging we have:

$$\begin{aligned} \boldsymbol{\Sigma}(\boldsymbol{x}) &= \langle \boldsymbol{\sigma} \rangle = \frac{1}{|V|} \int_V \boldsymbol{\sigma}(x,y)\, dy \\ \mathbf{E}(\boldsymbol{x}) &= \langle \boldsymbol{\varepsilon} \rangle = \frac{1}{|V|} \int_V \boldsymbol{\varepsilon}(x,y)\, dy \end{aligned} \tag{3.1}$$

where V is the volume of the RVE.

It is important to notice that any quantity that is an additive function is averaged in the micro-macro transition.

Thus, if $\overline{\rho} = \langle \rho \rangle$ denotes the averaged density, then we have:

$$\begin{aligned} \overline{\rho} E &= \langle \rho e \rangle, \quad \text{internal energy,} \\ \overline{\rho} S &= \langle \rho \eta \rangle, \quad \text{entropy,} \\ \Phi &= \langle \phi \rangle, \quad \text{dissipation} \end{aligned} \tag{3.2}$$

3.2. LOCALIZATION PROBLEM

We can state the following:

- the process that relates $(\boldsymbol{\Sigma},\mathbf{E})$ by means of equations (3.1) and (3.2) and the microscopic constitutive equations is called *homogenization*;
- the inverse process that consists in determining $\boldsymbol{\sigma}(y)$ and $\boldsymbol{\varepsilon}(y)$ from $\boldsymbol{\Sigma}$ and $\mathbf{E}$ is called *localization*.

Therefore, the data are $\boldsymbol{\Sigma}$ and $\mathbf{E}$ in the localization process which corresponds to the following problem:

$$(\boldsymbol{PL})\begin{cases}\langle\boldsymbol{\sigma}\rangle=\boldsymbol{\Sigma}\\ \langle\boldsymbol{\varepsilon}\rangle=\mathbf{E}\\ \operatorname{div}\boldsymbol{\sigma}=\mathbf{0}\end{cases} \tag{3.3}$$

This problem is original, because of the following two reasons:

(i) the load is the averaged value of a field and not a prescription at points in the bulk or at a limiting surface;
(ii) there are *no* boundary conditions.

It follows from (ii) that the problem (3.3) is ill-posed. The missing boundary condition must, in some way, reproduce the internal state of the RVE in the most satisfactory manner. They therefore depend on the choice of RVE, more specifically on its size. As a rule, different choices of RVE will provide different macroscopic laws.
The following give some examples of boundary conditions:

$$\boldsymbol{\sigma}\cdot\boldsymbol{n}=\boldsymbol{\Sigma}\cdot\boldsymbol{n} \quad \text{on } \partial V \quad - \quad \text{uniform traction on } \partial V\ ; \tag{3.4}$$

$$\boldsymbol{u}=\mathbf{E}\cdot\boldsymbol{y} \quad \text{on } \partial V \quad - \quad \text{uniform traction on } \partial V \tag{3.5}$$

With this and $\operatorname{div}\boldsymbol{\sigma}=\mathbf{0}$, in V, it is verified that (3.1) holds good. Indeed, for (3.5) we have:

$$\frac{1}{2}\int_V\left(\frac{\partial u_i}{\partial y_j}+\frac{\partial u_j}{\partial y_i}\right)dv=\frac{1}{2}\int_{\partial V}\left(u_i n_j+u_j n_i\right)ds=\frac{1}{2}\int_{\partial V}\left(\mathrm{E}_{ik}y_k n_j+\mathrm{E}_{jk}y_k n_i\right)ds \tag{3.6}$$

or

$$\left\langle\boldsymbol{\varepsilon}(\boldsymbol{u})\right\rangle=\mathbf{E} \tag{3.7}$$

The proof for (3.4) is self-evident.

The above reasoning does not apply to the case of a periodic structure. In that case, $\boldsymbol{\sigma}$ and $\boldsymbol{\varepsilon}$ are locally periodic (they are only quasi-periodic for a large sample) and the periodicity condition read as follows:

- the traction $\boldsymbol{\sigma}\cdot\boldsymbol{n}$ are opposite on opposite faces of ∂V (where $\boldsymbol{n}$ corresponds to $-\boldsymbol{n}$);
- the local strain $\boldsymbol{\varepsilon}(\boldsymbol{u})$ is made of two part, the mean $\mathbf{E}$ and the fluctucation part $\boldsymbol{\varepsilon}(\boldsymbol{u}^*)$ such that:

$$\boldsymbol{\varepsilon}(\boldsymbol{u}) = \mathbf{E} + \boldsymbol{\varepsilon}(\boldsymbol{u}^*), \quad \langle \boldsymbol{\varepsilon}(\boldsymbol{u}^*) \rangle = 0 \tag{3.8}$$

where $\boldsymbol{u}^*$ can be shown to be periodic. Therefore, the conditions are:

$$\begin{cases} \boldsymbol{\sigma}\cdot\boldsymbol{n} & \text{is antiperiodic,} \\ \boldsymbol{u} = \mathbf{E}\cdot\boldsymbol{y} + \boldsymbol{u}^*, \boldsymbol{u}^* & \text{periodic} \end{cases} \tag{3.9}$$

On account of (3.4), (3.5) and (3.9), the problem (3.3) now is theoretically well-posed, but this must be verified for each constitutive behaviour.

3.3. THE HILL-MANDEL PRINCIPLE OF MACROHOMOGENEITY

Let $\bar{\boldsymbol{\sigma}}$ and $\bar{\boldsymbol{u}}$ be, respectively, a statistically admissible (SA) stress field and a kinematically admissible (KA) displacement field. Then it is possible to prove that:

$$\langle \bar{\boldsymbol{\sigma}} : \boldsymbol{\varepsilon}(\bar{\boldsymbol{u}}) \rangle = \bar{\boldsymbol{\Sigma}} : \bar{\mathbf{E}} \tag{3.10}$$

The remarkable expression (3.10) is called the *prinpiple of macrohomogeneity of Hill and Mandel* (Hill, 1965, Mandel 1971) or the Hill-Mandel relation between micro and macro scales.
In statistical theories this condition is viewed as an ergodic hypothesis. This condition, in fact, plays in the end a much more important role than the boundary conditions applied at the RVE.

3.4. THE EXAMPLE OF PURE ELASTICITY

In this section the localization problem in the case of anisotropic linear elastic components are examined.

3.4.1. The Localization Problem

This problem is written in the following form (here $\mathbb{C}(y)$ is the tensor of elasticity coefficient at the micro scale):

$$\begin{cases} \boldsymbol{\sigma}(y) = \mathbb{C}(y) : \boldsymbol{\varepsilon}(y) = \mathbb{C}(y) : \left[\mathbf{E} + \boldsymbol{\varepsilon}(\boldsymbol{u}^*(y)) \right] \\ \operatorname{div} \boldsymbol{\sigma} = \mathbf{0} \\ \text{boundary conditions} \end{cases} \tag{3.11}$$

where $\mathbf{E}$ or $\boldsymbol{\Sigma}$ is prescribed. Accordingly, the fluctuation displacement $\boldsymbol{u}^*$ is the solution of the following problem:

$$\begin{cases} \operatorname{div}\left(\mathbb{C} : \boldsymbol{\varepsilon}(\boldsymbol{u}^*) \right) = -\operatorname{div}\left(\mathbb{C} : \mathbf{E} \right) \\ \text{boundary conditions} \end{cases} \tag{3.12}$$

Whenever $\mathbf{E}$ is constant for each constituent component, it can be shown that:

$$\operatorname{div}\left(\mathbb{C} : \mathbf{E} \right) = \left([\![\mathbb{C}]\!] : \mathbf{E} \right) \boldsymbol{n} \delta(S) \tag{3.13}$$

where $[\![\mathbb{C}]\!] = \mathbb{C}^+ - \mathbb{C}^-$, $\delta(S)$ is Dirac's distribution, and $\boldsymbol{n}$ is the unit normal oriented from the '$-$' to the '$+$' side of the surface S separating components. Then we can state the following:

Proposition. Under classical working hypotheses applying to $\mathbb{C}$ (symmetry and positivity), the problem (3.12) admits a unique solution for all three types of boundary condition.

To prove this we must distinguish whether it is $\mathbf{E}$ or $\boldsymbol{\Sigma}$ which is prescribed.

3.4.2. Case where $\mathbf{E}$ is Prescribed

For the existence and uniqueness proofs one can see Suquet (1981). We shall only give the representation of the solution. As the problem is linear, the solution $\boldsymbol{\varepsilon}(\boldsymbol{u}^*)$ depends linearly on the prescribed field $\mathbf{E}$. The latter can be decomposed into six elementary states of macroscopic strains (stretch in three directions and three shears). Let $\boldsymbol{\varepsilon}(\chi_{kl})$ be the fluctation strain field induced by these six elementary states at the microscopic level. The solution $\boldsymbol{\varepsilon}(\boldsymbol{u}^*)$ for a

general macrostrain $\mathbf{E}$ is the superposition of the six elementary solutions, so that we can write (summation over *k* and *l*):

$$\boldsymbol{\varepsilon}(\boldsymbol{u}^*) = \mathrm{E}_{kl}\boldsymbol{\varepsilon}(\chi_{kl}) \tag{3.14}$$

In all we have:

$$\boldsymbol{\varepsilon}(\boldsymbol{u}) = \mathbf{E} + \boldsymbol{\varepsilon}(\boldsymbol{u}^*) = \mathbf{E}\left(\mathbf{I} + \boldsymbol{\varepsilon}(\boldsymbol{\chi})\right) \tag{3.15}$$

or, in components:

$$\varepsilon_{ij}(\boldsymbol{u}) = D_{ijkl}\mathrm{E}_{kl} = (\boldsymbol{D}:\mathbf{E})_{ij} \tag{3.16}$$

where:

$$D_{ijkl} = I_{ijkl} + \varepsilon_{ij}(\chi_{kl}) \tag{3.17}$$

Here $I_{klij} = \frac{1}{2}\left(\delta_{ik}\delta_{jl} + \delta_{il}\delta_{jk}\right)$ is the tensorial representation in $\mathbb{R}^3$ of the unity of $\mathbb{R}^6$ and D_{ijkl} is called, depending on the author, the *tensor of strain localization*, or tensor of concentrations (Mandel, 1971) or the tensor of influence (Hill, 1967).

Homogenization
We can write in an obvious manner:

$$\boldsymbol{\Sigma} = \langle\boldsymbol{\sigma}\rangle = \langle\mathbb{C}:\boldsymbol{\varepsilon}(\boldsymbol{u})\rangle = \langle\mathbb{C}:\boldsymbol{D}:\mathbf{E}\rangle = \langle\mathbb{C}:\boldsymbol{D}\rangle:\mathbf{E} \tag{3.18}$$

so that:

$$\boldsymbol{\Sigma} = \mathbb{C}^{\mathrm{hom}}:\mathbf{E}, \quad \mathbb{C}^{\mathrm{hom}} = \langle\mathbb{C}:\boldsymbol{D}\rangle \tag{3.19}$$

We note that:

$$\langle\boldsymbol{D}\rangle = \boldsymbol{I}, \quad \langle\boldsymbol{D}^T\rangle = \boldsymbol{I}$$

Equation $(3.19)_2$ shows that the tensor of 'macro' elasticity coefficients is obtained by taking the average of 'micro' elasticity coefficients, the latter being *weighted* by the tensor of strain localization. It is possible to prove that the

tensor $\mathbb{C}^{\text{hom}}$ is symmetric. For a direct proof we compute $\left\langle \boldsymbol{D}^T : \bar{\boldsymbol{\sigma}} \right\rangle$ for an admissible field $\bar{\boldsymbol{\sigma}}$, obtaining thus:

$$\left\langle \boldsymbol{D}^T : \bar{\boldsymbol{\sigma}} \right\rangle_{ij} = \left\langle D^T_{ijkl} : \bar{\sigma}_{kl} \right\rangle = \left\langle \left[I_{ijkl} + \varepsilon_{kl}\left(\chi_{ij}\right) \right] \bar{\sigma}_{kl} \right\rangle = \bar{\boldsymbol{\Sigma}}_{ij}$$

i.e.,

$$\boldsymbol{\Sigma} = \left\langle \boldsymbol{D}^T : \boldsymbol{\sigma} \right\rangle = \left\langle \boldsymbol{D}^T : \mathbb{C} : \boldsymbol{\varepsilon}\left(\boldsymbol{u}\right) \right\rangle = \left\langle \boldsymbol{D}^T : \mathbb{C} : \boldsymbol{D} \right\rangle : \mathbf{E}$$

so that:

$$\mathbb{C}^{\text{hom}} = \left\langle \boldsymbol{D}^T : \mathbb{C} : \boldsymbol{D} \right\rangle \tag{3.20}$$

which is symmetric.

3.4.3. Case where $\boldsymbol{\Sigma}$ is Prescribed

The localization problem than reads:

$$\begin{cases} \boldsymbol{\varepsilon}\left(\boldsymbol{u}\right) = \boldsymbol{\varepsilon}\left(\boldsymbol{u}^*\right) + \mathbf{E} = \mathbb{S} : \boldsymbol{\sigma} \\ \operatorname{div} \boldsymbol{\sigma} = \mathbf{0} \\ \left\langle \boldsymbol{\sigma} \right\rangle = \boldsymbol{\Sigma} \\ \text{boundary conditions} \end{cases} \tag{3.21}$$

where $\mathbb{S}$ is the tensor of the micro elastic compliance and $\mathbf{E}$ is an unknown. The existence and uniqueness of the solution may be proved (Suquet, 1981). Thus, here, we assume that a unique solution $\boldsymbol{\sigma}$ exists. This solution depends linearly on data by virtue of the linearity of the problem. Let us call S_{kl} the solution of the problem (3.21) for the datum $\boldsymbol{\Sigma} = \boldsymbol{I}_{kl}$ - note that $I_{ijkl} = \left(\boldsymbol{I}_{kl}\right)_{ij}$.
Then the general solution, obtained by superposition, is written:

$$\begin{aligned} &\boldsymbol{\sigma} = \boldsymbol{A} : \boldsymbol{\Sigma}, \quad \text{i.e.,} \quad \boldsymbol{\sigma}\left(y\right) = \Sigma_{kl} A_{kl}\left(y\right), \\ &\text{or} \quad \sigma_{ij} = A_{ijkl}\Sigma_{kl}, \quad A_{ijkl} = \left(\boldsymbol{A}_{kl}\right)_{ij} \end{aligned} \tag{3.22}$$

where $\boldsymbol{A}$ is the tensor of stress localization.

The homogenized compliance tensor $\mathbb{S}^{\text{hom}}$ is evaluated thus.
We have directly:

$$\mathbf{E} = \left\langle \boldsymbol{\varepsilon}(\boldsymbol{u}) \right\rangle = \left\langle \mathbb{S} : \boldsymbol{\sigma} \right\rangle = \left\langle \mathbb{S} : \boldsymbol{A} \right\rangle : \boldsymbol{\Sigma} = \mathbb{S}^{\text{hom}} : \boldsymbol{\Sigma} \tag{3.23}$$

whence:

$$\mathbb{S}^{\text{hom}} = \left\langle \mathbb{S} : \boldsymbol{A} \right\rangle \tag{3.24}$$

We note that:

$$\left\langle \boldsymbol{A}^{\text{T}} \right\rangle = \boldsymbol{I} \tag{3.25}$$

and for any admissible field $\left\langle \boldsymbol{\varepsilon}(\overline{\boldsymbol{u}}) \right\rangle$ we can write:

$$\left\langle \boldsymbol{A}^{\text{T}} : \boldsymbol{\varepsilon}(\overline{\boldsymbol{u}}) \right\rangle_{ij} = \left\langle A^{\text{T}}_{ijkl}\, \varepsilon_{kl}(\overline{\boldsymbol{u}}) \right\rangle = \left\langle \left(A_{ij}\right)_{kl}\, \varepsilon_{kl}(\overline{\boldsymbol{u}}) \right\rangle = \left\langle \left(A_{ij}\right)_{kl} \right\rangle \left\langle \varepsilon_{kl}(\overline{\boldsymbol{u}}) \right\rangle = \overline{\text{E}}_{ij}$$

so that:

$$\mathbf{E} = \left\langle \boldsymbol{A}^{\text{T}} : \boldsymbol{\varepsilon}(\boldsymbol{u}) \right\rangle = \left\langle \boldsymbol{A}^{\text{T}} : \mathbb{S} : \boldsymbol{\sigma} \right\rangle = \left\langle \boldsymbol{A}^{\text{T}} : \mathbb{S} : \boldsymbol{A} \right\rangle : \boldsymbol{\Sigma},$$

Whence:

$$\mathbb{S}^{\text{hom}} = \left\langle \boldsymbol{A}^{\text{T}} : \mathbb{S} : \boldsymbol{A} \right\rangle \tag{3.26}$$

and thus $\mathbb{S}^{\text{hom}}$ is symmetric.

3.4.4. Equivalence between Prescribed Stress and Prescribed Strain

First we note that $\mathbb{C}^{\text{hom}}$ and $\mathbb{S}^{\text{hom}}$ are inverse tensors (in $\mathbb{R}^6$) of one another if they correspond to the same choice of boundary conditions in the localization problem. Indeed, using the symmetry of $\mathbb{C}^{\text{hom}}$ we can write:

$$\mathbb{C}^{\text{hom}} : \mathbb{S}^{\text{hom}} = \left(\mathbb{C}^{\text{hom}}\right)^{T} : \mathbb{S}^{\text{hom}} = \left\langle \boldsymbol{D}^{T} : \mathbb{C} \right\rangle : \left\langle \mathbb{S} : \boldsymbol{A} \right\rangle \tag{3.27}$$

in which the first factor is an admissible stress field (from the definition of $\boldsymbol{D}$

and $\boldsymbol{A}$) and the second factor is an admissible strain field. The principle (3.10) therefore applies and we can write $\left(\mathbb{C}:\mathbb{S}=\mathbb{I}\right)$:

$$\mathbb{C}^{\text{hom}}:\mathbb{S}^{\text{hom}}=\left\langle \boldsymbol{D}^{T}:\mathbb{C}:\mathbb{S}:\boldsymbol{A}\right\rangle =\left\langle \boldsymbol{D}^{T}:\boldsymbol{A}\right\rangle =\left\langle \boldsymbol{D}^{T}\right\rangle :\left\langle \boldsymbol{A}\right\rangle =\boldsymbol{I}. \quad (3.28)$$

However, if *different* boundary conditions are used, one then has the estimate of Hill (1967) and Mandel (1971):

$$\mathbb{C}^{\text{hom}}:\mathbb{S}^{\text{hom}}=\mathbb{I}+O\left(\left(d/l\right)^{3}\right), \quad (3.29)$$

where $\mathbb{C}^{\text{hom}}$ is evaluated by using the condition (3.5), while $\mathbb{S}^{\text{hom}}$ is computed through use of the condition (3.4), d is a characteristic size of an inhomogeneity and l is the typical size of the RVE. If $l\gg d$, then the choice of boundary condition is very important. For *periodic* media where $d/l=O\left(1\right)$, this choice is hardly important.

3.5. COMPOSITE HETEROGENEOUS MATERIALS: DERIVATION OF COMPLIANCE AND STIFFNESS TENSORS

The overall properties of a composite material depends not only upon the constitutive properties of each phases, but also on the microstructural architecture and define a relationship between the overall field variables – such as the deformation and the stress. The determination of the overall deformation and stress obviously needs of the preventive determination of the deformation and stress, and than the solution of an elastic PDE problem which involves the equilibrium, compatibility and constitutive equations of each phase, as well as the continuity conditions of the interphase. In other words, between two different phases – called here (1) and (2) – it must results:

$$\boldsymbol{u}^{(1)}=\boldsymbol{u}^{(2)}, \quad \boldsymbol{\sigma}^{(1)}\boldsymbol{n}=\boldsymbol{\sigma}^{(2)}\boldsymbol{n} \quad (3.30)$$

being $\boldsymbol{u}^{(i)}$ the displacement field of the *i*-phase, $\boldsymbol{\sigma}^{(i)}$ the stress field of the *i*-phase and $\boldsymbol{n}$ is the outer normal vector of a point on the interphase. From such procedure – which may be seen as a direct approach to the homogenization problem – seems clear that the homogenized properties depend upon the microstructure architecture. Consequently, this procedure is often extremely difficult to apply because of the equations (3.30), and may be developed only in vary particular – and often ideal – cases.

In the following section, alternative approaches to determine the overall properties of composite materials are presented. In particular, the *direct approach* requires the exact evaluation of the microscopic fields for some specific geometries, and so it is the more efficient, the more the microstructural geometry is similar to that one used in the model.
The *variational approaches* are always able to furnish upper and lower bounds of the overall properties of the composite materials. In particular, such approaches are the only ones that may solve the homogenization problem when the microstructural geometries are particular irregular or not completely known. Obviously, the wider the range defined by the upper and lower bounds gets, the less the practical utility of these methods is.

3.5.1. Direct Methods – Eshelby Solution

Let consider an homogeneous, linearly elastic and infinitely extended medium, subjected to a uniform prescribed strain $\mathbf{E}^*$ on the domain Ω. Generally, the resulting strain $\mathbf{E}$ is variable on Ω, but Eshelby proved that if Ω is an ellipsoid then the resulting strain $\mathbf{E}$ and hence the stress $\mathbf{T}$, are also uniform in Ω, the former being given by:

$$\mathbf{E} = \mathbb{P}\mathbf{E}^* \tag{3.31}$$

where the four-order tensor $\mathbb{P}$ is called Eshelby's tensor and it shows the following properties:

- it is symmetric with respect to the first two indices and the second two indices, $P_{ijkl} = P_{jikl} = P_{ijlk}$, while, in general, it is not symmetric with respect to the exchange of ij and kl, i. e., in general, $P_{ijkl} \neq P_{klij}$;
- it is independent of the material properties of the inclusion Ω;
- it is completely defined in terms of the aspect ratios of the ellipsoidal inclusion Ω, and the elastic parameters of the surrounding matrix;
- when the surrounding matrix is isotropic, then $\mathbb{P}$ depends only on the Poisson's ratio of the matrix and the aspect ratios of Ω.

In the following this results is proving in the case of isotropic matrix with Poisson's ratio ν and shear modulus μ. Let:

$$u_i(\boldsymbol{x}) = -C_{jkmn}\varepsilon^*_{mn}\int_\Omega G_{ij/k}(\boldsymbol{x}-\boldsymbol{x}')d\boldsymbol{x}' \tag{3.32}$$

be the solution of the PDE problem of the considered problem, where the Green function $\boldsymbol{G}(\boldsymbol{x}-\boldsymbol{x}')$ for the homogeneous and isotropic medium is:

$$\boldsymbol{G}(\boldsymbol{x}-\boldsymbol{x}')=\frac{1}{16\pi\mu(1-\nu)}\left[\frac{(3-4\nu)\boldsymbol{I}}{|\boldsymbol{x}-\boldsymbol{x}'|}+\frac{(\boldsymbol{x}-\boldsymbol{x}')\otimes(\boldsymbol{x}-\boldsymbol{x}')}{|\boldsymbol{x}-\boldsymbol{x}'|^3}\right] \quad (3.33)$$

where $\boldsymbol{I}$ is the second order identity tensor. Being Ω an ellipsoid of equation:

$$\frac{x_1^2}{a_1^2}+\frac{x_2^2}{a_2^2}+\frac{x_3^2}{a_3^2}\le 1 \quad (3.34)$$

through simple algebraic manipulation it result:

$$u_i(\boldsymbol{x})=\frac{-\varepsilon^*_{jk}}{8\pi(1-\nu)}\int_\Omega g_{ijk}(\boldsymbol{l})\frac{d\boldsymbol{x}'}{|\boldsymbol{x}-\boldsymbol{x}'|^2} \quad (3.35)$$

where:

$$g_{ijk}(\boldsymbol{l})=(1-2\nu)(\delta_{ij}l_k+\delta_{ik}l_j-\delta_{jk}l_i)+3l_il_jl_k \quad (3.36)$$

being $\boldsymbol{l}$ the versor of $(\boldsymbol{x}'-\boldsymbol{x})/|\boldsymbol{x}'-\boldsymbol{x}|$.
By assuming that the point $\boldsymbol{x}$ is inside the region Ω, the integral into the (3.35) may be explicitly calculated.
To achieve this goal, the volume element $d\boldsymbol{x}'$ may be written as $r^2 dr d\omega$, being $r=|\boldsymbol{x}-\boldsymbol{x}'|$ and $d\omega$ the superficial element of a unit sphere centred in $\boldsymbol{x}$. The integration of the (3.35) with respect to *r*, yields:

$$u_i(\boldsymbol{x})=\frac{-\varepsilon^*_{jk}}{8\pi(1-\nu)}\int_\Sigma r(\boldsymbol{l})g_{ijk}(\boldsymbol{l})d\omega \quad (3.37)$$

where $r(\boldsymbol{l})$ is the positive root of:

$$(x_1+rl_1)^2/a_1^2+(x_2+rl_1)^2/a_2^2+(x_3+rl_3)^2/a_3^2=1 \quad (3.38)$$

that is:

$$r(\boldsymbol{l})=-f/g+\sqrt{f^2/g^2+e/g} \quad (3.39)$$

with:

$$\begin{aligned} g &= l_1^2/a_1^2 + l_2^2/a_2^2 + l_3^2/a_3^2 \\ f &= l_1 x_1/a_1^2 + l_2 x_2/a_2^2 + l_3 x_3/a_3^2 \\ e &= 1 - x_1^2/a_1^2 - x_2^2/a_2^2 - x_3^2/a_3^2 \end{aligned} \tag{3.40}$$

By posing $\lambda_i = l_i/a_i^2$, the (3.37) becomes:

$$u_i(\boldsymbol{x}) = \frac{x_m \varepsilon_{jk}^*}{8\pi(1-\nu)} \int_\Sigma \frac{\lambda_m g_{ijk}}{g} d\omega \tag{3.41}$$

from which the strain inside Ω may be calculated:

$$\varepsilon_{ij}(\boldsymbol{x}) = \frac{\varepsilon_{mn}^*}{16\pi(1-\nu)} \int_\Sigma \frac{\lambda_i g_{jmn} + \lambda_j g_{imn}}{g} d\omega \tag{3.42}$$

which depends upon $\boldsymbol{x} \in \Omega$.
So, the components of Eshelby's tensor $\mathbb{P}$ introduced in the equation (3.31) are:

$$\begin{aligned} P_{1111} &= \frac{3}{8\pi(1-\nu)} a_1^2 I_{11} + \frac{1-2\nu}{8\pi(1-\nu)} I_1 \\ P_{1122} &= \frac{1}{8\pi(1-\nu)} a_2^2 I_{12} - \frac{1-2\nu}{8\pi(1-\nu)} I_1 \\ P_{1133} &= \frac{1}{8\pi(1-\nu)} a_3^2 I_{13} - \frac{1-2\nu}{8\pi(1-\nu)} I_1 \\ P_{1212} &= \frac{a_1^2 + a_2^2}{16\pi(1-\nu)} I_{12} + \frac{1-2\nu}{16\pi(1-\nu)} (I_1 + I_2) \end{aligned} \tag{3.43}$$

with:

$$\begin{aligned} I_1 &= \int_\Sigma \frac{l_1^2}{a_1^2 g} d\omega \\ I_{11} &= \int_\Sigma \frac{l_1^4}{a_1^4 g} d\omega \\ I_{12} &= 3\int_\Sigma \frac{l_1^2 l_2^2}{a_1^2 a_2^2 g} d\omega \end{aligned} \tag{3.44}$$

All the non-zero components may be obtained through a cyclic permutation of the indexes (1, 2, 3). Such solution may be particularized for many cases of practical interest. By means of the solution (3.43), it is possible to determine the concentration strain tensor in an ellipsoidal inclusion of elasticity tensor $\mathbb{C}^{(2)}$ embedded in a homogeneous, isotropic and infinitely extended medium of elasticity tensor $\mathbb{C}^{(1)}$. Then, under the uniform strain field $\mathbf{E}^0$, the medium, supposed homogeneous, would be subjected to a uniform stress $\mathbf{T} = \mathbb{C}^{(1)}\mathbf{E}^0$. This uniform stress field is perturbed by the presence of the inclusion. But the stress field $\mathbf{T}^{(2)} = \mathbb{C}^{(2)}\mathbf{E}^{(2)}$ in a generic point of the inclusion is the same that we would have in the inclusion imagining to substitute the inclusion with the matrix subjected to $\mathbf{E}^0$ as well as to the strain $\mathbf{E}^*$, such as:

$$\mathbb{C}^{(2)}\mathbf{E}^{(2)} = \mathbb{C}^{(1)}\left(\mathbf{E}^{(2)} - \mathbf{E}^*\right) \tag{3.45}$$

As proved by Eshelby, a uniform strain $\mathbf{E}^*$ applied on ellipsoidal region yields – as unique equilibrated and compatible solution – a uniform strain in the region given by the equation (3.31). In this case, being also $\mathbf{E}^0$, it results:

$$\mathbf{E}^{(2)} = \overline{\mathbf{E}}^{(2)} = \mathbf{E}^0 + \mathbb{P}\mathbf{E}^* \tag{3.46}$$

The (3.46) and (3.45), yield:

$$\mathbf{E}^{(2)} = \left[\mathbb{I} + \mathbb{P}\left(\mathbb{C}^{(1)}\right)^{(-1)}\left[\mathbb{C}^{(2)} - \mathbb{C}^{(1)}\right]\right]^{-1}\mathbf{E}^0 \tag{3.47}$$

Being $\mathbf{E}^{(2)}$ uniform in Ω, the concentration strain tensor into the inclusion is:

$$\mathbb{A}^{(2)} = \left[\mathbb{I} + \mathbb{P}\left(\mathbb{C}^{(1)}\right)^{(-1)}\left[\mathbb{C}^{(2)} - \mathbb{C}^{(1)}\right]\right]^{-1} \tag{3.48}$$

3.5.2. Variational Methods – Hashin Shtrikman Variational Principle

The homogenization problem of an heterogeneous RVE is equivalent to solve one of the following variational problems:

$$\begin{aligned}\frac{1}{2}\overline{\mathbb{C}}\,\overline{\mathbf{E}}\cdot\overline{\mathbf{E}} &= \inf_{E^d\in E}\frac{1}{V}\int_V\frac{1}{2}\mathbb{C}\left(\overline{\mathbf{E}}+\mathbf{E}^d\right)\cdot\left(\overline{\mathbf{E}}+\mathbf{E}^d\right)dV \\ \frac{1}{2}\overline{\mathbb{S}}\,\overline{\mathbf{T}}\cdot\overline{\mathbf{T}} &= \inf_{T^d\in T}\frac{1}{V}\int_V\frac{1}{2}\mathbb{S}\left(\overline{\mathbf{T}}+\mathbf{T}^d\right)\cdot\left(\overline{\mathbf{T}}+\mathbf{T}^d\right)dV\end{aligned} \tag{3.49}$$

where $\mathbf{E}$ is compatible periodic strain field space, whose average value is equal to zero, $\mathbf{T}$ is equilibrated periodic stress field space, whose average value is equal to zero, $\overline{\mathbb{C}}$ is homogenized stiffness tensor, $\overline{\mathbb{S}}$ is homogenized compliance tensor, $\overline{\mathbf{T}}$ is the generic symmetric stress field, and $\overline{\mathbf{E}}$ is the generic symmetric strain field.

The first members of the $(3.49)_1$ and $(3.49)_2$ represent the elastic energy density and the complementary energy density of the homogenized material. In particular, solving the first problem of the $(3.49)_1$ is equivalent to determine, among the compatible strain fields, whose prescribed average value is $\overline{\mathbf{E}}$, the sole one that is also equilibrated. On the contrary, solving the $(3.49)_2$ is equivalent of determining, among the equilibrated stress fields, whose prescribed average value is $\overline{\mathbf{T}}$, the sole one that is also compatible.

It is possible to demonstrate that, if the stiffness tensor $\mathbb{C}$ and the compliance one $\mathbb{S}$ have, uniformly in V, all the eigenvalues lower down bounded by a positive constant, then the equations (3.49) admit one and only one solution.

Since the functionals in the first members of the (3.49) are conjugate each other, (Giangreco, 2003), it follows that the homogenized properties of the material are well defined, hence:

$$\overline{\mathbb{S}} = \overline{\mathbb{C}}^{-1} \tag{3.50}$$

In this framework, the basic physic idea of the Hashin and Shtrikman's principles is to substitute the heterogeneous medium with a reference homogeneous one, having a stiffness tensor, $\mathbb{C}^H$, and a compliance tensor, $\mathbb{S}^H$. In order to simulate the actual micro-structure, eigenstress and eigenstrain fields are prescribed on the reference homogeneous medium, as already seen in the previous section. So, the Hashin and Shtrikman's variational principles are characterized from two tumbled variational problems:

- the first problem, defined as auxiliary problem, is related to the elastostatic response of the reference homogeneous solid, subjected to a prescribed field of polarization (eigenstress or eigenstrain);
- the second problem, defined as optimization problem, has the objective to found the unknown field of polarization.
-

In the follows, the four classic Hashin and Shtrikman's variational principles are reported. It is worth to underline that two of these are minimum principles, while the other two are saddle principles. Obviously, the minimum principles are

particularly useful, because each numeric approximation of them, for example by using the Finite Element Method, represents an upper estimation of the solution. In particular, consider a reference homogeneous material which is more deformable than each phase included in the heterogeneous RVE, such that $\mathbb{C}-\mathbb{C}^H$ is positive definite everywhere in V. Hence, the following identity is verified:

$$\int_V\left(\frac{1}{2}\mathbb{C}\,\mathbf{E}\cdot\mathbf{E}-\frac{1}{2}\mathbb{C}^H\,\mathbf{E}\cdot\mathbf{E}\right)dV=\sup_{\mathbf{T}^*\in\mathbf{H}}\left\{\int_V\mathbf{T}^*\cdot\mathbf{E}-\frac{1}{2}\left(\mathbb{C}-\mathbb{C}^H\right)\mathbf{T}^*\cdot\mathbf{T}^*dV\right\} \quad (3.51)$$

where $\mathbf{H}$ is the space of symmetric second-order periodic tensors, $\mathbf{T}^*$ is polarization field (eigenstress) prescribed on the reference homogeneous medium in order to simulate the actual micro-structure of the heterogeneous RVE.
In particular, by taking:

$$\mathbf{E}=\overline{\mathbf{E}}+\hat{\mathbf{E}} \quad (3.52)$$

where $\overline{\mathbf{E}}\in Sym$ and $\hat{\mathbf{E}}\in\mathbf{E}$, and by remembering that $\mathbb{C}^H$ is constant in V, the (3.51) assumes the following form:

$$\begin{aligned}&\int_V\left[\frac{1}{2}\mathbb{C}\left(\overline{\mathbf{E}}+\hat{\mathbf{E}}\right)\left(\overline{\mathbf{E}}+\hat{\mathbf{E}}\right)-\frac{1}{2}\mathbb{C}^H\overline{\mathbf{E}}\cdot\overline{\mathbf{E}}\right]dV=\\&=\sup_{\mathbf{T}^*\in\mathbf{H}}\left\{\int_V\left[\left\langle\mathbf{T}^*\right\rangle\cdot\overline{\mathbf{E}}-\frac{1}{2}\left(\mathbb{C}-\mathbb{C}^H\right)^{-1}\mathbf{T}^*\cdot\mathbf{T}^*\right]dV\right\}+\\&+\int_V\left(\mathbf{T}^*\cdot\hat{\mathbf{E}}+\frac{1}{2}\mathbb{C}^H\hat{\mathbf{E}}\cdot\hat{\mathbf{E}}\right)dV\end{aligned} \quad (3.53)$$

where $\left\langle\mathbf{T}^*\right\rangle$ denotes the average value of $\mathbf{T}^*$ in V.

Therefore, by considering the lower bound with respect to $\hat{\mathbf{E}}$, changing the minimization with the maxim $F_{C''}^{\mathbf{T}^*}$ization and by dividing for V, it is obtained:

$$\begin{aligned}&\frac{1}{2}\overline{\mathbb{C}}\,\overline{\mathbf{E}}\cdot\overline{\mathbf{E}}-\frac{1}{2}\mathbb{C}^H\overline{\mathbf{E}}\cdot\overline{\mathbf{E}}=\\&=\frac{1}{V}\sup_{\mathbf{T}^*\in\mathbf{H}}\left\{\int_V\left(\left\langle\mathbf{T}^*\right\rangle\cdot\overline{\mathbf{E}}-\frac{1}{2}\left(\mathbb{C}-\mathbb{C}^H\right)^{-1}\mathbf{T}^*\cdot\mathbf{T}^*\right)dV+\inf_{\hat{\mathbf{E}}\in\mathbf{E}}F_{C''}^{\mathbf{T}^*}\right\}\end{aligned} \quad (3.54)$$

where the quadratic functional $F_{C''}^{\mathbf{T}^*}$ is defined by:

$$F_{C''}^{\mathbf{T}^*} = \hat{\mathbf{E}} \in E \to \int_V \left(\mathbf{T}^* \cdot \hat{\mathbf{E}} + \frac{1}{2} \mathbb{C}^H \hat{\mathbf{E}} \cdot \hat{\mathbf{E}} \right) dV \tag{3.55}$$

Now consider a reference homogeneous material which is stiffer than each phase included in the heterogeneous RVE, such that $\mathbb{C} - \mathbb{C}^H$ is negative definite everywhere in V. Hence, in analogous manner, it is obtained the following equation:

$$\begin{aligned} &\frac{1}{2} \overline{\mathbb{C}} \, \overline{\mathbf{E}} \cdot \overline{\mathbf{E}} - \frac{1}{2} \mathbb{C}^H \overline{\mathbf{E}} \cdot \overline{\mathbf{E}} = \\ &= \frac{1}{V} \inf_{\mathbf{T}^* \in \mathbf{H}} \left\{ \int_V \left(\left\langle \mathbf{T}^* \right\rangle \cdot \overline{\mathbf{E}} - \frac{1}{2} \left(\mathbb{C} - \mathbb{C}^H \right)^{-1} \mathbf{T}^* \cdot \mathbf{T}^* \right) dV + \inf_{\hat{\mathbf{E}} \in \mathbf{E}} F_{C''}^{\mathbf{T}^*} \right\} \end{aligned} \tag{3.56}$$

The equations (3.54) and (3.56) represent the Hashin and Shtrikman's variational principles, based on the eigenstress. In particular, the (3.54) is a saddle principle, while the (3.56) is a minimum principle. From them, by imposing stationariness principles with respect to $\mathbf{T}^*$, it is obtained:

$$\left(\mathbb{C} - \mathbb{C}^H \right)^{-1} \mathbf{T}^* = \hat{\mathbf{E}} + \overline{\mathbf{E}} \tag{3.57}$$

that confirms that stress field $\mathbf{T}^*$ is the correction which has to be prescribed to the reference homogeneous material stress field $\mathbb{C}^H \left(\hat{\mathbf{E}} + \overline{\mathbf{E}} \right)$ in order to obtain the stress field in the actual material $\mathbb{C} \left(\hat{\mathbf{E}} + \overline{\mathbf{E}} \right)$. It is possible to obtain other two variational principles, having similar expressions to the (3.54) and the (3.56) and involving the overall compliance tensor $\mathbb{S}$. About them, the sole results will be shown, directly, since they are reached with similar considerations to those ones already done. Therefore, consider a reference homogeneous material which is stiffer than each phase included in the heterogeneous RVE, such that $\mathbb{S} - \mathbb{S}^H$ is positive definite everywhere in V. Hence, in analogous manner, it is obtained the following equation:

$$\begin{aligned} &\frac{1}{2} \overline{\mathbb{S}} \, \overline{\mathbf{T}} \cdot \overline{\mathbf{T}} - \frac{1}{2} \overline{\mathbb{S}}^H \, \overline{\mathbf{T}} \cdot \overline{\mathbf{T}} = \\ &= \frac{1}{V} \sup_{\mathbf{E}^* \in \mathbf{H}} \left\{ \int_V \left(\left\langle \mathbf{E}^* \right\rangle \cdot \overline{\mathbf{T}} - \frac{1}{2} \left(\mathbb{S} - \mathbb{S}^H \right)^{-1} \mathbf{E}^* \cdot \mathbf{E}^* \right) dV + \inf_{\hat{\mathbf{T}} \in T} F_{S''}^{\mathbf{E}^*} \right\} \end{aligned} \tag{3.58}$$

where the quadratic functional $F_{S''}^{\mathbf{E}^*}$ is defined by:

$$F_{S''}^{\mathbf{E}^*} = \hat{\mathbf{T}} \in T \to \int_V \left(\mathbf{E}^* \cdot \hat{\mathbf{T}} + \frac{1}{2} \mathbb{S}^H \hat{\mathbf{T}} \cdot \hat{\mathbf{T}} \right) dV \tag{3.59}$$

and where $\mathbf{H}$ is the space of symmetric second-order periodic tensors, $\mathbf{E}^*$ is polarization field (eigenstrain) prescribed on the reference homogeneous medium in order to simulate the actual micro-structure of the heterogeneous RVE.
Consider, on the contrary, a reference homogeneous material which is more deformable than each phase included in the heterogeneous RVE, such that $\mathbb{S} - \mathbb{S}^H$ is positive definite everywhere in V. Hence, in similar form, it is obtained the following equation:

$$\begin{aligned} &\frac{1}{2} \overline{\mathbb{S}} \, \overline{\mathbf{T}} \cdot \overline{\mathbf{T}} - \frac{1}{2} \overline{\mathbb{S}^H} \, \overline{\mathbf{T}} \cdot \overline{\mathbf{T}} = \\ &= \frac{1}{V} \inf_{\mathbf{E}^* \in \mathbf{H}} \left\{ \int_V \left(\left\langle \mathbf{E}^* \right\rangle \cdot \overline{\mathbf{T}} - \frac{1}{2} \left(\mathbb{S} - \mathbb{S}^H \right)^{-1} \mathbf{E}^* \cdot \mathbf{E}^* \right) dV + \inf_{\hat{\mathbf{T}} \in T} F_{S''}^{\mathbf{E}^*} \right\} \end{aligned} \tag{3.60}$$

The equations (3.58) and (3.60) represent the Hashin and Shtrikman's variational principles, based on the eigenstrain. In particular, the (3.58) is a saddle principle, while the (3.60) is a minimum principle. From them, by imposing stationariness principles with respect to $\mathbf{E}^*$, it is obtained:

$$\left(\mathbb{S} - \mathbb{S}^H \right)^{-1} \mathbf{E}^* = \hat{\mathbf{T}} + \overline{\mathbf{T}} \tag{3.61}$$

that confirms that strain field $\mathbf{E}^*$ is the correction which has to be prescribed to the reference homogeneous material strain field $\mathbb{S}^H \left(\hat{\mathbf{T}} + \overline{\mathbf{T}} \right)$ in order to obtain the strain field in the actual material $\mathbb{S} \left(\hat{\mathbf{T}} + \overline{\mathbf{T}} \right)$. It has to be considered that the Hashin and Shtrikman's variational principles involve auxiliary problems, consisting in the minimization of the functionals, $F_{C''}^{\mathbf{T}^*}$ (or $F_{S''}^{\mathbf{E}^*}$). The goal is to solve an equilibrium (or a compatibility) problem, for the reference homogeneous solid, subject to a prescribed eigenstress, $\mathbf{T}^*$, (or an eigenstrain $\mathbf{E}^*$). For such problem, however, only few particular cases has a solution. In particular, it can be remembered the Eshelby's solution for the case in which the polarization field is constant and different from zero, only in an ellipsoidal region. This solution lets to use the Hashin and Shtrikman's variational principles for determining the homogenized properties of a biphasic composite,

with a low concentration of inclusions. In order to do it, the same matrix or the inclusions can be chosen as reference homogeneous material, but the matrix and the inclusions have to be well ordered, that means, $\mathbb{C}^M - \mathbb{C}^\Omega$ has to be defined in sign. In case of periodic composite, the auxiliary problem is easier to solve, because it is possible to transform the RVE domain into a Fourier domain. It is not our interest to expose this procedure, so the interested reader is referred to (Giangreco, 2003).
The calculation of the elastic energy density and of the complementary one, according to the two equations (3.49), requires the execution of very difficult minimization with respect of functionals, which are defined on unbounded space.
Operating such minimizations is equivalent to solve the elastostatic problem for the RVE, in the cases of displacements approach and tractions approach, respectively. A numeric minimization, obtained, for example, by using the Element Finite Method, can be employed on finite subspaces, E_f and T_f, of the above mentioned spaces, **E** and **T**.
Consequently, numeric minimization will yield the following expressions of the tensors, $\mathbb{C}^+$ and $\mathbb{S}^+$:

$$\begin{aligned}\frac{1}{2}\mathbb{C}^+\overline{\mathbf{E}}\cdot\overline{\mathbf{E}} &= \inf_{\mathbf{E}^d\in E_f}\frac{1}{V}\int_V\frac{1}{2}\mathbb{C}\left(\overline{\mathbf{E}}+\mathbf{E}^d\right)\left(\overline{\mathbf{E}}+\mathbf{E}^d\right)dV\\ \frac{1}{2}\mathbb{S}^+\overline{\mathbf{T}}\cdot\overline{\mathbf{T}} &= \inf_{\mathbf{T}^d\in T_f}\frac{1}{V}\int_V\frac{1}{2}\mathbb{S}\left(\overline{\mathbf{T}}+\mathbf{T}^d\right)\left(\overline{\mathbf{T}}+\mathbf{T}^d\right)dV\end{aligned} \tag{3.62}$$

which, for constructions, satisfy the following inequalities:

$$\begin{aligned}\frac{1}{2}\overline{\mathbb{C}}\,\overline{\mathbf{E}}\cdot\overline{\mathbf{E}} &\le \frac{1}{2}\mathbb{C}^+\,\overline{\mathbf{E}}\cdot\overline{\mathbf{E}}\\ \frac{1}{2}\overline{\mathbb{S}}\,\overline{\mathbf{T}}\cdot\overline{\mathbf{T}} &\le \frac{1}{2}\mathbb{S}^+\,\overline{\mathbf{T}}\cdot\overline{\mathbf{T}}.\end{aligned} \tag{3.63}$$

By naming with $\mathbb{C}^-$ and $\mathbb{S}^-$, respectively, the inverse of the tensors $\mathbb{S}^+$ and $\mathbb{C}^+$, the upper and lower limitations for the elastic energy, and the complementary one, of the homogenized material are obtained, as given by:

$$\begin{aligned}\frac{1}{2}\mathbb{C}^-\,\overline{\mathbf{E}}\cdot\overline{\mathbf{E}} \le \frac{1}{2}\overline{\mathbb{C}}\,\overline{\mathbf{E}}\cdot\overline{\mathbf{E}} \le \frac{1}{2}\mathbb{C}^+\,\overline{\mathbf{E}}\cdot\overline{\mathbf{E}}\\ \frac{1}{2}\mathbb{S}^-\,\overline{\mathbf{T}}\cdot\overline{\mathbf{T}} \le \frac{1}{2}\overline{\mathbb{S}}\,\overline{\mathbf{T}}\cdot\overline{\mathbf{T}} \le \frac{1}{2}\mathbb{S}^+\,\overline{\mathbf{T}}\cdot\overline{\mathbf{T}}.\end{aligned} \tag{3.64}$$

Elementary estimations on $\overline{\mathbb{C}}$ and $\overline{\mathbb{S}}$ are obtained by choosing the simplest E_f and T_f, i.e., coinciding with the space constituted by the sole null tensor. In this way, the well known Voigt and Reuss' estimations are reached; in particular, for a biphasic composite, they are:

$$\begin{aligned}\left(f_M\mathbb{S}_M+f_\Omega\mathbb{S}_\Omega\right)^{-1}\le\overline{\mathbb{C}}\le f_M\mathbb{C}_M+f_\Omega\mathbb{C}_\Omega\\ \left(f_M\mathbb{C}_M+f_\Omega\mathbb{C}_\Omega\right)^{-1}\le\overline{\mathbb{S}}\le f_M\mathbb{S}_M+f_\Omega\mathbb{S}_\Omega\end{aligned} \tag{3.65}$$

with:

$$\begin{aligned}&\left(f_M\mathbb{C}_M+f_\Omega\mathbb{C}_\Omega\right)^{-1}=\left(\mathbb{C}^+\right)^V,\quad \left(f_M\mathbb{C}_M+f_\Omega\mathbb{C}_\Omega\right)^{-1}=\left(\mathbb{S}^-\right)^V\\ &\left(f_M\mathbb{S}_M+f_\Omega\mathbb{S}_\Omega\right)^{-1}=\left(\mathbb{C}^-\right)^R,\quad \left(f_M\mathbb{S}_M+f_\Omega\mathbb{S}_\Omega\right)^{-1}=\left(\mathbb{S}^+\right)^R\end{aligned} \tag{3.66}$$

where the superscript V and R stands for Voigt and Reuss.
At the same manner, the Hashin and Shtrikman's variational principles (3.54), (3.56), (3.58) and (3.60) yield estimations on the stiffness and compliance tensors, if the optimization with regard to the polarization fields is employed above a finite underspace H_f, of the above unbounded mentioned space H of all possible polarization fields.
In particular, it results:

$$\frac{1}{2}\overline{\mathbb{C}}\,\overline{\mathbf{E}}\cdot\overline{\mathbf{E}}-\frac{1}{2}\mathbb{C}^H\overline{\mathbf{E}}\cdot\overline{\mathbf{E}}\ge\frac{1}{V}\sup_{\mathbf{T}^*\in H_f}\left\{\begin{aligned}&\int_V\left(\left\langle\mathbf{T}^*\right\rangle\cdot\overline{\mathbf{E}}-\frac{1}{2}\left(\mathbb{C}-\mathbb{C}^H\right)^{-1}\mathbf{T}^*\cdot\mathbf{T}^*\right)dV+\\&+\inf_{\hat{\mathbf{E}}\in E}F_{C''}^{\mathbf{T}^*}\end{aligned}\right\} \tag{3.67}$$

and:

$$\frac{1}{2}\overline{\mathbb{S}}\,\overline{\mathbf{T}}\cdot\overline{\mathbf{T}}-\frac{1}{2}\mathbb{S}^H\,\overline{\mathbf{T}}\cdot\overline{\mathbf{T}}\le\frac{1}{V}\inf_{\mathbf{E}^*\in H_f}\left\{\begin{aligned}&\int_V\left(\left\langle\mathbf{E}^*\right\rangle\cdot\overline{\mathbf{T}}-\frac{1}{2}\left(\mathbb{S}-\mathbb{S}^H\right)^{-1}\mathbf{E}^*\cdot\mathbf{E}^*\right)dV+\\&+\inf_{\hat{\mathbf{T}}\in T}F_{S''}^{\mathbf{E}^*}\end{aligned}\right\} \tag{3.68}$$

if the reference homogeneous material is more deformable than each phase included in the heterogeneous RVE.
On the contrary, it results:

$$\frac{1}{2}\overline{\mathbb{C}}\,\overline{\mathbf{E}}\cdot\overline{\mathbf{E}}-\frac{1}{2}\mathbb{C}^{H}\overline{\mathbf{E}}\cdot\overline{\mathbf{E}}\le\frac{1}{V}\inf_{\mathbf{T}^{*}\in H}\left\{\begin{array}{l}\int_{V}\left(\left\langle\mathbf{T}^{*}\right\rangle\cdot\overline{\mathbf{E}}-\frac{1}{2}\left(\mathbb{C}-\mathbb{C}^{H}\right)^{-1}\mathbf{T}^{*}\cdot\mathbf{T}^{*}\right)dV+\\+\inf_{\hat{\mathbf{E}}\in E}F_{C''}^{\mathbf{T}^{*}}\end{array}\right\}\quad(3.69)$$

and:

$$\frac{1}{2}\overline{\mathbb{S}}\,\overline{\mathbf{T}}\cdot\overline{\mathbf{T}}-\frac{1}{2}\mathbb{S}^{H}\,\overline{\mathbf{T}}\cdot\overline{\mathbf{T}}\ge\frac{1}{V}\sup_{\mathbf{E}^{*}\in H_{f}}\left\{\begin{array}{l}\int_{V}\left(\left\langle\mathbf{E}^{*}\right\rangle\cdot\overline{\mathbf{T}}-\frac{1}{2}\left(\mathbb{S}-\mathbb{S}^{H}\right)^{-1}\mathbf{E}^{*}\cdot\mathbf{E}^{*}\right)dV+\\+\inf_{\hat{\mathbf{T}}\in T}F_{S''}^{\mathbf{E}^{*}}\end{array}\right\}\quad(3.70)$$

if the reference homogeneous material is stiffer than each phase included in the heterogeneous RVE.

A numeric estimation of the inferior extreme of $F_{C''}^{\mathbf{T}^{*}}$ and of $F_{S''}^{\mathbf{E}^{*}}$ implies that only the minimum principles (3.68) and (3.69) yield upper estimations for the density of the elastic complementary energy and for the elastic one, respectively, for the homogenized material. The saddle principles (3.67) and (3.70), instead, are able to yield an estimation that cannot be read as an upper or lower estimation.

3.6. MICROMECHANICS OF POROUS MATERIALS: J-TENSOR AND DILUTE DISTRIBUTION OF VOIDS CASES

In this section, the overall stress-strain/strain stress relations are developed with reference to an RVE consisting of a linearly elastic material which contains stress-free cavities.

Consider an RVE with total volume V, bounded externally by surface ∂V. On this surface, either uniform tractions:

$$\boldsymbol{t}^{0}=\boldsymbol{n}\cdot\boldsymbol{\sigma}^{0}\qquad\text{on }\partial V\qquad(3.71)$$

or linear displacements:

$$\boldsymbol{u}^{0}=\boldsymbol{x}\cdot\boldsymbol{\varepsilon}^{0}\qquad\text{on }\partial V\qquad(3.72)$$

are assumed to be prescribed, where $\boldsymbol{\sigma}^{0}$ and $\boldsymbol{\varepsilon}^{0}$ are second-order symmetric constant stress and strain tensors for the macro-element.

It is emphasized that either (3.71) or (3.72) (4.1.1 a), but not both, can be prescribed. In other words, if the traction boundary data (3.71) corresponding to the constant macrostress $\boldsymbol{\Sigma}=\boldsymbol{\sigma}^{0}$, are prescribed, then the surface displacements on ∂V, corresponding to these tractions, in general, are not spatially linear,

being affected by the microstructure of the RVE. Similarly, if the linear displacement boundary data (3.72) corresponding to the constant macrostrain $\mathbf{E} = \boldsymbol{\varepsilon}^0$, are prescribed, then the surface tractions on ∂V, produced by these displacements, are not, in general, spatially uniform. In the sequel, therefore, the two cases are treated separately and independently, and then the relation between the results is discussed.
Assume that the material of the RVE is linearly elastic and homogeneous (but not necessarily isotropic).
The inhomogeneity, therefore, stems solely from the presence of cavities. Denote a typical cavity by Ω_α, with the boundary $\partial\Omega_\alpha$ $(\alpha = 1,2,...,\mathrm{n})$, so that there are a total of n individual cavities in V. The union of these cavities is denoted by Ω, having the boundary $\partial\Omega$ which is the union of all $\partial\Omega_\alpha$, i.e.:

$$\Omega \equiv \cup_{\alpha=1}^{n} \Omega_\alpha \qquad \partial\Omega \equiv \cup_{\alpha=1}^{n} \partial\Omega_\alpha \tag{3.73}$$

The remainder of the RVE (i.e, when Ω is excluded) is called the *matrix*. The matrix is denoted by M. The boundary of M is the sum of ∂V and $\partial\Omega$:

$$M \equiv V - \Omega \qquad \partial M \equiv \partial V - \partial\Omega \tag{3.74}$$

The total boundary surface of the RVE can include some portion of $\partial\Omega$. For simplicity, however, exclude this possibility.
Thus, all cavities are within the RVE, each being fully surrounded by the matrix material. For a typical cavity, Ω_α, two faces of its surface boundary, $\partial\Omega_\alpha$, may be distinguished, as follows:

- the exterior face of the cavity, denoted by $\partial\Omega_\alpha^{\mathrm{c}}$ which is the face toward the matrix material, denned by the direction of the exterior unit normal $\boldsymbol{n}$ of the cavity;
- the exterior face of the surrounding matrix, denoted by $\partial\Omega_\alpha^{\mathrm{M}}$, which is the face toward the interior of the cavity, denned by the direction of the exterior unit normal $(-\boldsymbol{n})$ of the matrix (i.e., the interior unit normal of the cavity); $\partial\Omega_\alpha$ coincides with $\partial\Omega_\alpha^{\mathrm{c}}$, for the cavity Ω_α, while $\partial\mathrm{M}$ at the cavity Ω_α coincides with $\partial\Omega_\alpha^{\mathrm{M}}$.

In view of this convention, the integral of a surface quantity taken over $\partial\mathrm{M}$ can always be decomposed as:

$$\begin{aligned}\int_{\partial \mathrm{M}}(.)\,dS &= \int_{\partial V}(.)\,dS + \sum_{\alpha=1}^{\mathrm{n}}\int_{\partial\Omega_\alpha^{\mathrm{M}}}(.)\,dS = \\ &= \int_{\partial V}(.)\,dS - \sum_{\alpha=1}^{\mathrm{n}}\int_{\partial\Omega_\alpha^{\mathrm{c}}}(.)\,dS = \int_{\partial V}(.)\,dS - \int_{\partial\Omega}(.)\,dS\end{aligned} \tag{3.75}$$

Thus $\partial\Omega$ always stands for the union of $\partial\Omega_\alpha^{\mathrm{c}}$ $(\alpha = 1,2,...,\mathrm{n})$. To distinguish the boundary of M at the cavities from that at the exterior of the RVE, which is ∂V, the exterior unit normal on ∂V is systematically denoted by $\boldsymbol{n}$ (as before), and the exterior unit normal on the surface $\partial\Omega_\alpha$ for a typical cavity Ω_α, by $\boldsymbol{n}$, pointing from the inside of the cavity toward the matrix M.
The matrix material is linearly elastic and homogeneous. Denote the corresponding constant elasticity tensor by $\mathbb{C}$ and the compliance tensor by $\mathbb{S}$.

3.6.1. Average Strain for Prescribed Macrostress

Suppose that uniform tractions $\boldsymbol{t}^0 = \boldsymbol{n}\cdot\boldsymbol{\sigma}^0$ are prescribed on ∂V, associated with the constant symmetric macrostress $\boldsymbol{\Sigma} = \boldsymbol{\sigma}^0$. If the RVE is homogeneous, having no cavities, then the corresponding average strain associated with the average stress $\boldsymbol{\sigma}^0$ would be:

$$\boldsymbol{\varepsilon}^0 = \mathbb{S} : \boldsymbol{\sigma}^0 \tag{3.76}$$

and hence, in conjunction with $\bar{\boldsymbol{\sigma}} = \boldsymbol{\sigma}^0$, the average strain would be $\boldsymbol{\varepsilon}^0$.
The presence of cavities disturbs the uniform stress and strain fields, producing the variable stress field $\boldsymbol{\sigma} = \boldsymbol{\sigma}(\boldsymbol{x})$ and strain field $\boldsymbol{\varepsilon} = \boldsymbol{\varepsilon}(\boldsymbol{x})$, in M, with $\boldsymbol{\sigma} = \boldsymbol{0}$ in Ω. Nevertheless, from the (3.1):

$$\bar{\boldsymbol{\sigma}} = \langle\boldsymbol{\sigma}\rangle = \frac{1}{V}\int_V \boldsymbol{\sigma}\,dv = \frac{1}{V}\int_M \boldsymbol{\sigma}\,dv = \boldsymbol{\sigma}^0 \tag{3.77}$$

On the other hand, the average strain is not, in general, equal to $\boldsymbol{\varepsilon}^0$. Instead:

$$\bar{\boldsymbol{\varepsilon}} = \langle\boldsymbol{\varepsilon}\rangle = \boldsymbol{\varepsilon}^0 + \bar{\boldsymbol{\varepsilon}}^c \tag{3.78}$$

where $\boldsymbol{\varepsilon}^0$ is defined by (3.76), and $\bar{\boldsymbol{\varepsilon}}^c$ is the additional strain due to the presence of cavities. To calculate the additional strain $\bar{\boldsymbol{\varepsilon}}^c$ due to cavities, one may apply the reciprocal theorem, as follows. Consider two sets of loads, one defined by:

$$\boldsymbol{t}^{(1)} = \begin{cases} \boldsymbol{n} \cdot \delta\boldsymbol{\sigma}^0 & \text{on } \partial V \\ -\boldsymbol{n} \cdot \delta\boldsymbol{\sigma}^0 & \text{on } \partial\Omega \end{cases} \tag{3.79}$$

which corresponds to uniform virtual stress $\delta\boldsymbol{\sigma}^0$ and strain $\delta\boldsymbol{\varepsilon}^0 = \mathbb{S} : \delta\boldsymbol{\sigma}^0$ within the entire RVE (as illustrated in Figure 3.3, $-\boldsymbol{n}$ is the interior unit normal on the cavity surface $\partial\Omega$, or the exterior unit normal to the boundary of the matrix), and the other defined by:

$$\boldsymbol{t}^{(2)} = \begin{cases} \boldsymbol{n} \cdot \boldsymbol{\sigma}^0 & \text{on } \partial V \\ \boldsymbol{0} & \text{on } \partial\Omega \end{cases} \tag{3.80}$$

which is the actual loading considered for the RVE. Denote the displacement, strain, and stress fields associated with the first loading (3.79) by:

$$\left\{\boldsymbol{u}^{(1)}, \boldsymbol{\varepsilon}^{(1)}, \boldsymbol{\sigma}^{(1)}\right\} = \left\{\left(\boldsymbol{x} . \delta\boldsymbol{\varepsilon}^0\right), \delta\boldsymbol{\varepsilon}^0, \delta\boldsymbol{\sigma}^0\right\} \tag{3.81}$$

which follows from the fact that, for loading (3.79), the strain and stress fields are both uniform throughout the matrix M and denote the fields associated with the second (i.e., the actual) loading (3.80) by:

$$\left\{\boldsymbol{u}^{(2)}, \boldsymbol{\varepsilon}^{(2)}, \boldsymbol{\sigma}^{(2)}\right\} = \left\{\boldsymbol{u}, \boldsymbol{\varepsilon}, \boldsymbol{\sigma}\right\} \tag{3.82}$$

From the reciprocal theorem, it follows that:

$$\int_{\partial V} \left(\boldsymbol{n} \cdot \boldsymbol{\sigma}^0\right) \cdot \left(\boldsymbol{x} . \delta\boldsymbol{\varepsilon}^0\right) ds = \int_{\partial V} \left(\boldsymbol{n} \cdot \delta\boldsymbol{\sigma}^0\right) \cdot \boldsymbol{u}\, ds - \int_{\partial\Omega} \left(\boldsymbol{n} \cdot \delta\boldsymbol{\sigma}^0\right) \cdot \boldsymbol{u}\, ds \tag{1.83}$$

which can be written as:

$$\delta\boldsymbol{\sigma}^0 : \left\{\int_{\partial V} \mathbb{S} : \left\{\left(\boldsymbol{x} \otimes \boldsymbol{n}\right) \cdot \boldsymbol{\sigma}^0\right\}\, ds - \int_{\partial V} \boldsymbol{n} \otimes \boldsymbol{u}\, ds + \int_{\partial\Omega} \boldsymbol{n} \otimes \boldsymbol{u}\, ds\right\} = 0 \tag{1.84}$$

Since $\delta\boldsymbol{\sigma}^0$ is an arbitrary symmetric tensor, the symmetric part of the quantity within the braces must vanish identically. Noting that the first integral within the braces yields:

$$\frac{1}{V}\int_{\partial V} \mathbb{S} : \left\{\left(\boldsymbol{x} \otimes \boldsymbol{n}\right) \cdot \boldsymbol{\sigma}^0\right\} ds = \mathbb{S} : \left\{\boldsymbol{I} \cdot \boldsymbol{\sigma}^0\right\} = \boldsymbol{\varepsilon}^0 \tag{1.85}$$

And, using the averaging scheme, it follows that:

$$\bar{\boldsymbol{\varepsilon}} = \frac{1}{V}\int_V \frac{1}{2}\left\{\nabla \otimes \boldsymbol{u} + \left(\nabla \otimes \boldsymbol{u}\right)^T\right\} dv = \boldsymbol{\varepsilon}^0 + \frac{1}{V}\int_{\partial\Omega} \frac{1}{2}\left(\boldsymbol{n} \otimes \boldsymbol{u} + \boldsymbol{u} \otimes \boldsymbol{n}\right) ds \quad (1.86)$$

Comparison with (3.78) shows that the additional strain $\bar{\boldsymbol{\varepsilon}}^c$ due to cavities, is given by:

$$\bar{\boldsymbol{\varepsilon}}^c = \frac{1}{V}\int_{\partial\Omega} \frac{1}{2}\left(\boldsymbol{n} \otimes \boldsymbol{u} + \boldsymbol{u} \otimes \boldsymbol{n}\right) ds \quad (1.87)$$

3.6.2. Overall Compliance Tensor for Porous Elastic Solids

Define *the overall compliance* $\bar{\mathbb{S}}$ of the porous RVE with a linearly elastic homogeneous matrix, through:

$$\bar{\boldsymbol{\varepsilon}} = \bar{\mathbb{S}} : \bar{\boldsymbol{\sigma}} = \bar{\mathbb{S}} : \boldsymbol{\sigma}^0, \quad (1.88)$$

where the macrostress, $\boldsymbol{\Sigma} = \boldsymbol{\sigma}^0$, is regarded prescribed, and the average strain is given by (3.78). To obtain the overall compliance in an explicit form, the strain $\bar{\boldsymbol{\varepsilon}}^c$ due to cavities will now be expressed in terms of the applied stress $\boldsymbol{\sigma}^0$. Since the matrix of the RVE is linearly elastic, for a given microstructure the displacement $\boldsymbol{u}(\boldsymbol{x})$ at a point $\boldsymbol{x}$ on $\partial\Omega$ is linearly dependent on the uniform overall stress $\boldsymbol{\sigma}^0$, as show following. By remembering that the displacement field may be expressed in terms of Green function as:

$$\boldsymbol{u}(\boldsymbol{x}) = \int_{\partial V} \boldsymbol{G}(\boldsymbol{x}, \boldsymbol{y}) \cdot \boldsymbol{t}(\boldsymbol{y}) ds \quad (1.89)$$

where $\boldsymbol{t}(\boldsymbol{y})$ are the self-equilibrating surface traction prescribed on the boundary ∂V of the RVE, if the applied tractions (3.71) are substituting into (1.89), to arrive at:

$$\boldsymbol{u}(\boldsymbol{x}) = \int_{\partial V} \boldsymbol{G}(\boldsymbol{x}, \boldsymbol{y}) \cdot \left\{\boldsymbol{n}(\boldsymbol{y}) \cdot \boldsymbol{\sigma}^0\right\} ds \quad (1.90)$$

where the integration is taken with respect to $\boldsymbol{y}$ over the boundary ∂V of the RVE. Since $\boldsymbol{\sigma}^0$ is a symmetric constant tensor, (1.90) can be expressed as:

$$u_i(\boldsymbol{x}) = K_{ijk}(\boldsymbol{x}) \sigma^0_{jk} \quad (1.91)$$

where the third-order tensor:

$$K_{ijk}(\boldsymbol{x}) = K_{ijk}(\boldsymbol{x}) = \int_{\partial V} \frac{1}{2}\left\{G_{ij}(\boldsymbol{x},\boldsymbol{y}) n_k(\boldsymbol{y}) + G_{ik}(\boldsymbol{x},\boldsymbol{y}) n_j(\boldsymbol{y})\right\} dS \qquad (1.92)$$

depends on the geometry and the elastic properties of the matrix of the RVE.
To obtain the additional overall strain, $\overline{\boldsymbol{\varepsilon}}^c$, due to the presence of cavities in terms of the prescribed overall stress, $\boldsymbol{\sigma}^0$, substitute from (1.92) into (1.87), to arrive at:

$$\overline{\varepsilon}_{ij}^c = H_{ijkl}\sigma_{kl}^0 \qquad (1.93)$$

where the *constant* fourth-order tensor, $\mathbb{H}$, is given by:

$$H_{ijkl} \equiv H_{jikl} \equiv H_{ijlk} \equiv \frac{1}{V}\int_{\partial\Omega} \frac{1}{2}\left\{n_i(\boldsymbol{x}) K_{jkl}(\boldsymbol{x}) + n_j(\boldsymbol{x}) K_{ikl}(\boldsymbol{x})\right\} dS \qquad (1.94)$$

Hence, for an RVE with a linearly elastic matrix containing cavities of arbitrary shapes and sizes, the following general result is obtained, when the overall macrostress is regarded prescribed (Horii and Nemat-Nasser, 1983):

$$\overline{\boldsymbol{\varepsilon}}^c = \mathbb{H} : \boldsymbol{\sigma}^0 \qquad (1.95)$$

It should be noted that this exact result is valid whether or not the linearly elastic constituent of the RVE is homogeneous.
The requirements are:

- the matrix of the RVE is linearly elastic;
- the microstructure of the RVE remains unchanged under the applied macrostress $\boldsymbol{\Sigma} = \boldsymbol{\sigma}^0$.

To obtain the overall elastic compliance tensor $\overline{\mathbb{S}}$, in terms of the constant compliance of the matrix, $\mathbb{S}$, and the constant tensor $\mathbb{H}$, substitute (3.76), (1.88) and (1.95) into (3.78), and noting that the resulting equation must hold for any macrostress $\boldsymbol{\sigma}^0$, arrive at:

$$\overline{\mathbb{S}} = \mathbb{S} + \mathbb{H}\,, \qquad (1.96)$$

Note that in many situation, the tensor $\mathbb{H}$ can be computer directly, using the (1.87).

3.6.3. Average Stress for Prescribed Macrostrain

Suppose that the linear displacements $\boldsymbol{u}^0 = \boldsymbol{x} \cdot \boldsymbol{\varepsilon}^0$ (associated with the constant symmetric macrostrain $\mathbf{E} = \boldsymbol{\varepsilon}^0$) are prescribed on ∂V. The matrix of the RVE is assumed to be homogeneous, as marked before. In the absence of cavities, the corresponding average stress associated with the prescribed macrostrain, $\boldsymbol{\varepsilon}^0$, would be:

$$\boldsymbol{\sigma}^0 = \mathbb{C} : \boldsymbol{\varepsilon}^0 \tag{1.97}$$

Due to the presence of cavities, the actual field quantities are nonuniform.
From the (3.6):

$$\boldsymbol{\varepsilon} = \langle \boldsymbol{\varepsilon} \rangle = \frac{1}{V}\int_V \boldsymbol{\varepsilon} dv = \frac{1}{V}\int_{\partial V} \frac{1}{2}\left(\boldsymbol{n} \otimes \boldsymbol{u} + \boldsymbol{u} \otimes \boldsymbol{n}\right) ds = \boldsymbol{\varepsilon}^0 \tag{1.98}$$

which is valid for any RVE of any material and microstructure. Note that the surface integral in (1.98) extends over the exterior boundary, ∂V, of the RVE only. It does not include the cavity boundaries $\partial\Omega$.
Equation (1.98) is the direct consequence of the fact that the average strain for an RVE is given in terms of its boundary displacements which are prescribed here to be $\boldsymbol{u}^0 = \boldsymbol{x} \cdot \boldsymbol{\varepsilon}^0$.
In general, for a prescribed macrostrain, the average stress is not equal to $\boldsymbol{\sigma}^0$ but

$$\bar{\boldsymbol{\sigma}} = \langle \boldsymbol{\sigma} \rangle = \boldsymbol{\sigma}^0 + \bar{\boldsymbol{\sigma}}^c \tag{1.99}$$

where $\boldsymbol{\sigma}^0$ is defined by (1.97), and $\bar{\boldsymbol{\sigma}}^c$ is the decrement in the overall stress due to the presence of cavities.
As in Subsection 3.1., the reciprocal theorem will be applied to calculate the average stress a in (1.99). To this end, a third set of boundary data defined by:

$$\begin{aligned} \boldsymbol{u}^{(3)} &= \boldsymbol{n} \cdot \boldsymbol{\sigma}^0 \qquad \text{on } \partial V \\ \boldsymbol{t}^{(3)} &= \mathbf{0} \qquad\quad \text{on } \partial\Omega. \end{aligned} \tag{1.100}$$

The displacement, strain, and stress fields associated with these boundary conditions are denoted by:

$$\left\{\boldsymbol{u}^{(3)}, \boldsymbol{\varepsilon}^{(3)}, \boldsymbol{\sigma}^{(3)}\right\} = \left\{\boldsymbol{u}, \boldsymbol{\varepsilon}, \boldsymbol{\sigma}\right\} \tag{1.101}$$

which are actual fields, in general, different from those given by (3.82) for the boundary conditions (3.80). The actual tractions on the boundary of the RVE now are:

$$\boldsymbol{t}(\boldsymbol{x}) = \boldsymbol{n}(\boldsymbol{x}) \cdot \boldsymbol{\sigma}(\boldsymbol{x}) \tag{1.102}$$

where $\boldsymbol{x}$ is on ∂V.
These tractions are required in order to impose the boundary displacements prescribed by (1.100).
Applying the reciprocal theorem to the two sets of loads, (3.79) and (1.100), it follows that:

$$\int_{\partial V} \boldsymbol{t} \cdot \left(\boldsymbol{x} . \delta\boldsymbol{\varepsilon}^0 \right) ds = \int_{\partial V} \left(\boldsymbol{n} \cdot \delta\boldsymbol{\sigma}^0 \right) \cdot \left(\boldsymbol{x} . \delta\boldsymbol{\varepsilon}^0 \right) ds - \int_{\partial\Omega} \left(\boldsymbol{n} \cdot \delta\boldsymbol{\sigma}^0 \right) \cdot \boldsymbol{u}\, ds \tag{1.103}$$

which can be written as:

$$\delta\boldsymbol{\varepsilon}^0 : \left\{ \int_{\partial V} \boldsymbol{t} \otimes \boldsymbol{x}\, ds - \int_{\partial V} \mathbb{C} : \left\{ \left(\boldsymbol{x} \otimes \boldsymbol{n} \right) \cdot \boldsymbol{\varepsilon}^0 \right\} ds + \int_{\partial\Omega} \mathbb{C} : \left(\boldsymbol{n} \otimes \boldsymbol{u} \right) ds \right\} = 0 \tag{1.104}$$

where, in using loading (3.81), the quantity $\delta\boldsymbol{\varepsilon}^0$ is regarded as a virtual spatially constant strain field with the corresponding stress field, $\delta\boldsymbol{\sigma}^0 = \mathbb{C} : \delta\boldsymbol{\varepsilon}^0$. Since $\delta\boldsymbol{\varepsilon}^0$ is an arbitrary symmetric tensor, the symmetric part of the quantity within the braces in (1.104) must vanish identically. Noting that the second integral within the parentheses can be expressed as:

$$\frac{1}{V} \int_{\partial V} \mathbb{C} : \left\{ \left(\boldsymbol{x} \otimes \boldsymbol{n} \right) \cdot \boldsymbol{\varepsilon}^0 \right\} ds = \mathbb{C} : \left\{ \boldsymbol{I} \cdot \boldsymbol{\varepsilon}^0 \right\} = \boldsymbol{\sigma}^0 , \tag{1.105}$$

and using the averaging procedure, it now follows that:

$$\bar{\boldsymbol{\sigma}} = \frac{1}{V} \int_{\partial V} \boldsymbol{t} \otimes \boldsymbol{x}\, ds = \boldsymbol{\sigma}^0 - \mathbb{C} : \left\{ \frac{1}{V} \int_{\partial\Omega} \frac{1}{2} \left(\boldsymbol{n} \otimes \boldsymbol{u} + \boldsymbol{u} \otimes \boldsymbol{n} \right) ds \right\} \tag{1.106}$$

Comparison with (1.99) shows that the decremental stress $\bar{\boldsymbol{\sigma}}^c$ due to the presence of cavities, is given by:

$$\bar{\boldsymbol{\sigma}}^c = -\mathbb{C} : \bar{\boldsymbol{\varepsilon}}^c \tag{1.107}$$

where $\bar{\boldsymbol{\varepsilon}}^c$ is the strain due to the presence of cavities given by (1.87), which now must be computed for the prescribed boundary displacements $\boldsymbol{u}^0 = \boldsymbol{x} \cdot \boldsymbol{\varepsilon}^0$.

3.6.4. Overall Elasticity Tensor for Porous Elastic Solids

When the overall macrostrain is regarded prescribed, $\mathbf{E} = \boldsymbol{\varepsilon}^0$, designate the overall elasticityJensor of the porous RVE with a linearly elastic and homogeneous matrix, by $\overline{\mathbb{C}}$, and define it through:

$$\overline{\boldsymbol{\sigma}} = \overline{\mathbb{C}} : \boldsymbol{\varepsilon}^0 \tag{1.108}$$

Substitution of (1.97), (1.107), and (1.108) into (1.99) then yields:

$$\left(\overline{\mathbb{C}} - \mathbb{C}\right) : \boldsymbol{\varepsilon}^0 + \mathbb{C} : \overline{\boldsymbol{\varepsilon}}^c = \mathbf{0} \tag{1.109}$$

For a given microstructure (i.e., for existing cavities with fixed shapes, sizes, and distribution), the response of the RVE is linear. Hence, the displacement field anywhere within the linearly elastic matrix of the RVE is a linear and homogeneous function of the prescribed overall constant strain $\boldsymbol{\varepsilon}^0$. Therefore, in line with results (1.91) and (1.92) for the case when the macrostresses were considered to be prescribed, at a typical point $\boldsymbol{x}$ on the boundary of the cavities, $\partial\Omega$:

$$u_i\left(\boldsymbol{x}\right) = L_{ijk}\left(\boldsymbol{x}\right)\varepsilon^0_{jk} \tag{1.110}$$

where $\boldsymbol{L}\left(\boldsymbol{x}\right)$ is a is a third-order tensor-valued function with the symmetry property, $L_{ijk} = L_{ikj}$. Now, from the definition of $\overline{\boldsymbol{\varepsilon}}^c$, given by the (1.87):

$$\overline{\varepsilon}^c_{ij} = J_{ijkl}\varepsilon^0_{kl} \tag{1.111}$$

where the constant fourth-order tensor, $\mathbb{J}$, is given by:

$$J_{ijkl} \equiv J_{jikl} \equiv J_{ijlk} \equiv \frac{1}{V}\int_{\partial\Omega}\frac{1}{2}\left\{n_i\left(\boldsymbol{x}\right)J_{jkl}\left(\boldsymbol{x}\right) + n_j\left(\boldsymbol{x}\right)J_{ikl}\left(\boldsymbol{x}\right)\right\}dS \tag{1.112}$$

Hence, for an RVE with a linearly elastic matrix (whether homogeneous or not) containing cavities of arbitrary shapes and sizes, the following general result is obtained, when the overall macrostrains are regarded prescribed:

$$\overline{\boldsymbol{\varepsilon}}^c = \mathbb{J} : \boldsymbol{\varepsilon}^0 \tag{1.113}$$

To obtain an expression for the overall elastic moduli of the porous RVE, substitute (1.113) into (1.109) and, noting that the resulting expression must be valid for any constant symmetric macrostrain $\boldsymbol{\varepsilon}^0$, arrive at

$$\bar{\mathbb{C}} = \mathbb{C} - \mathbb{C} : \mathbb{J} \tag{1.114}$$

It should be noted that in many practical problems the tensor J, similarly to the tensor $\mathbb{H}$, can be calculated directly from (1.87), and therefore, the overall elastic moduli can be estimated from (1.114). It may, however, be instructive to seek to construct the tensor $\mathbb{J}$ in terms of the Green functions $\boldsymbol{G}(\boldsymbol{x},\boldsymbol{y})$ and $\boldsymbol{G}^{-1}(\boldsymbol{x},\boldsymbol{y})$.

To this end, for the linear displacements, $\boldsymbol{u}^0 = \boldsymbol{z}\cdot\boldsymbol{\varepsilon}^0$, prescribed on the outer boundary ∂V of the RVE, by remembering that the resulting tractions, $\boldsymbol{t}(\boldsymbol{y})$, may be written as:

$$\boldsymbol{t}(\boldsymbol{y}) = \int_{\partial V} \boldsymbol{G}^{-1}(\boldsymbol{y},\boldsymbol{z})\cdot(\boldsymbol{z}\cdot\boldsymbol{\varepsilon}^0)\,ds \tag{1.115}$$

where the integration is taken with respect to $\boldsymbol{z}$ over the outer boundary ∂V of the RVE. Substituting (1.115) into (1.89), the displacement field for points on $\partial\Omega$ is obtained in terms of the prescribed macrostrain $\boldsymbol{\varepsilon}^0$, as:

$$\boldsymbol{u}(\boldsymbol{x}) = \int_{\partial V} \boldsymbol{G}(\boldsymbol{x},\boldsymbol{y})\cdot\left\{\int_{\partial V} \boldsymbol{G}^{-1}(\boldsymbol{y},\boldsymbol{z})\cdot(\boldsymbol{z}\cdot\boldsymbol{\varepsilon}^0)\,ds\right\} ds \tag{1.116}$$

where both the $\boldsymbol{y}$- and $\boldsymbol{z}$-integral are taken over ∂V. Noting that $\boldsymbol{\varepsilon}^0$ is a symmetric tensor, tensor $\boldsymbol{L}$ in (1.110) may now be written in terms of $\boldsymbol{G}$ and $\boldsymbol{G}^{-1}$, as:

$$L_{ijk}(\boldsymbol{x}) = \int_{\partial V} G_{im}(\boldsymbol{x},\boldsymbol{y})\left\{\int_{\partial V} \frac{1}{2}\left\{G^{-1}_{mj}(\boldsymbol{y},\boldsymbol{z})z_k + G^{-1}_{mk}(\boldsymbol{y},\boldsymbol{z})z_j\right\} ds\right\} ds \tag{1.117}$$

Therefore, from comparison of (1.113) with (1.117), a fourth-order tensor, $\boldsymbol{j}(\boldsymbol{x},\boldsymbol{y})$, can be introduced as:

$$j_{ijkl} = \int_{\partial V} \frac{1}{4}\begin{Bmatrix} n_i(\boldsymbol{x})G_{jm}(\boldsymbol{x},\boldsymbol{y})G^{-1}_{mk}(\boldsymbol{y},\boldsymbol{z})z_l + \\ +n_i(\boldsymbol{x})G_{jm}(\boldsymbol{x},\boldsymbol{y})G^{-1}_{ml}(\boldsymbol{y},\boldsymbol{z})z_k + \\ +n_j(\boldsymbol{x})G_{im}(\boldsymbol{x},\boldsymbol{y})G^{-1}_{mk}(\boldsymbol{y},\boldsymbol{z})z_l + \\ +n_j(\boldsymbol{x})G_{im}(\boldsymbol{x},\boldsymbol{y})G^{-1}_{ml}(\boldsymbol{y},\boldsymbol{z})z_k \end{Bmatrix} dS \tag{1.118}$$

where the integral is taken with respect to $\boldsymbol{z}$ over ∂V. The constant tensor $\mathbb{J}$ in (1.113) now becomes:

$$\mathbb{J} = \frac{1}{V}\int_{\partial\Omega}\int_{\partial V} \boldsymbol{j}(\boldsymbol{x},\boldsymbol{y})\, ds\, ds \tag{1.119}$$

where the $\boldsymbol{y}$-integration is over ∂V, and the $\boldsymbol{x}$-integration is over $\partial\Omega$.

3.7. MICROMECHANICS

Composite materials are one of the strongest candidates as a structural material for many automobile, aerospace and other applications (Agarwal et al., 1974). Recently, short fiber-reinforced composite materials have been extensively investigated because they are more economical and impact resistant (Taya et al., 1989). One of the earliest attempts to explain the reinforcing effect of fibers was described by [3], and is now referred to as the shear lag theory, which considers long straight discontinuous fibers completely embedded in a continuous matrix (Cox, 1952). Fiber-reinforced composites are often characterized by their high specific strength and specific modulus parameters (i.e., strength to weight ratios), and are widely used for applications in low-weight components. The high strength and damage resistance of the composites are very important for a number of practical applications. In order to predict the strength and other properties of composites, numerous mathematical models of deformation, damage and failure of fiber reinforced composites have been developed. Short fiber reinforced composites have several attractive characteristics that make them worthy of consideration for other applications. Therefore, short fiber reinforced composite materials have been extensively investigated because they are more economical and impact resistant.

3.7.1. Unidirectional Short Fiber Composite

A unidirectional fiber composite is highly anisotropic. Stiffness and strength in the fiber direction are of the order of the fiber value, and thus very large, while normal to the fiber direction they are of the order of the matrix value and are thus much lower. In an injection-moulded discontinuous-fiber composite, stiffness and strength are much more complex owing to the multitude of fiber orientations. The resultant properties are largely controlled by material parameters e.g. E_f (fiber elastic modulus), E_m (matrix elastic modulus), ν_f (fiber volume fraction), FLD (fiber length distribution), FOD (fiber orientation distribution) and test conditions.
The prediction of the elastic properties of discontinuous fiber reinforced materials has received much attention in the past. Three of the most commonly used methods are:

- the aggregate model;
- Cox shear-lag theory;
- the rule of mixtures

The aggregate model uses the concept of subunits, each of which possess the elastic properties of a reinforced composite in which the fibers are continuous and fully aligned. In this way, elastic moduli have been estimated for various composite systems (Halpin and Pagano, 1969).
Brody and Ward (Brody and Ward, 1971) have compared measured moduli for compression moulded 30% w/w short glass and carbon fiber polyethylene and polypropylene composites with those determined by using the aggregate model. Reasonable correlation was found although it should be remembered that the FOD was fairly isotropic compared with that produced during the injection moulding process.
More recently (Toll, 1992) a modified aggregate model was applied to plaque mouldings, identifying limitations of the previous aggregate models as:

1) the unit-cell stiffnesses require estimation by micromechanical approximations, since the unidirectional composite is normally unavailable;
2) it is reasonably accurate only at nearly unidirectional orientations

To overcome these short-comings a two-parameter model was developed which describes the unit-cell stiffnesses, easily determined from elastic constants measured for a material in a known, but arbitrary orientation state.
When measured moduli were compared with predicted values, excellent agreement was found.
Other methods have been based on various forms of the Rule of Mixtures (RoM), as:

$$E_{//} = \nu_f E_f + \nu_m E_m \quad and \quad E_{\perp} = \frac{E_f E_m}{E_m \nu_f + E_f \nu_m} \tag{3.120}$$

where $E_{||}$ and $E_{\perp}$ are moduli determined parallel and normal to the principle fiber orientation direction in a continuous unidirectional fiber system.
These equations were modified by Halpin and Tsai (Halpin and Tsai, 1967) for discontinuous-fiber materials to yield longitudinal and transverse moduli as shown below:

$$E_{\|} = E_m \left[\frac{1 + 2\frac{l}{d}\eta_{\|} v_f}{1 - \eta_{\|} v_f} \right], \quad where \quad \eta_{\|} = \left[\frac{\left(\frac{E_f}{E_m}\right) - 1}{\left(\frac{E_f}{E_m}\right) + 2\left(\frac{l}{d}\right)} \right] \tag{3.121}$$

$$E_{\perp} = E_m \left[\frac{1 + \alpha \eta_{\perp} v_f}{1 - \eta_{\perp} v_f} \right], \quad where \quad \eta_{\perp} = \left[\frac{\left(\frac{E_f}{E_m}\right) - 1}{\left(\frac{E_f}{E_m}\right) + \alpha} \right] \tag{3.122}$$

$\eta_{\|}$ and $\eta_{\perp}$ describe longitudinal and transverse efficiency factors, $\left(\frac{l}{d}\right)$ the fiber aspect ratio and α a geometric factor.

Further modifications were made to the rule of mixtures by Cox (Cox, 1952) to derive the shear lag analysis:

$$E_c = E_m \left(1 - v_f\right) + E_f v_f \left(1 - \frac{\tanh\left(\frac{\beta l}{2}\right)}{\left(\frac{\beta l}{2}\right)} \right) \tag{3.123}$$

where the last term in brackets is described as a fiber-length correction factor, l is the fiber length and β ,which governs the rate of stress build up at the fiber ends, is given by:

$$\beta = \frac{1}{r} \left[\frac{E_m}{E_f \left(1 + \nu\right) \ln\left(\frac{R}{r}\right)} \right]^{1/2} \tag{3.124}$$

where E_m is the matrix modulus, ν is Poisson's ratio, r is the fiber radius and $2R$ the mean inter-fiber spacing. For a square fiber packing system, the inter-fiber spacing is related to the volume fraction by:

$$R = r \sqrt{\frac{\pi}{4 v_f}} \tag{3.125}$$

so that β may be written as:

$$\beta = \frac{1}{r}\sqrt{\frac{E_m}{E_f\left(1+\nu\right)\ln\sqrt{\frac{\pi}{4\nu_f}}}} \tag{3.126}$$

Several assumptions were made:

1) the fiber and the matrix remain elastic in their mechanical response;
2) the interface between the fiber and the matrix is perfect;
3) no axial force is transmitted through the fiber ends.

3.7.2. Random Short Fiber Composite

To account for fiber orientation effects in short fiber materials, the RoM is adapted as:

$$E_c = E_m\left(1-\nu_f\right) + E_f\nu_f\eta_L\eta_0 \tag{3.127}$$

η_L is a fiber-length correction factor and η_0, often described as the Krenchel orientation efficiency factor (Krenchel, 1964), is given by the general form:

$$\eta_0 = \sum_n a_{fn}\cos^4\alpha_n \Big/ \sum_n a_{fn}, \quad \text{where} \quad \sum_n a_{fn} = 1 \tag{3.128}$$

where a_{fn} is the ratio between the cross-sectional area presented by a group of fibers orientated at an angle α_n respect to the applied load direction and the total area of all the fibers at a given cross-section of the composite. The number of groups is designated by $n = 1, 2 \ldots n$. Eq. (3.128) was further modified (O'Donnell, 1990) to yield the through-thickness fiber orientation efficiency:

$$\eta_0 = \frac{N_{f1}\cos^3\alpha_1 + N_{f2}\cos^3\alpha_2 + \ldots + N_{fn}\cos^3\alpha_n}{N_{f1}\sec\alpha_1 + N_{f2}\sec\alpha_2 + \ldots + N_{f1}\sec\alpha_n} \tag{3.129}$$

where N_{f1} is the fraction of the total number of fibers orientated at angle α_1 in any field of view. Thus, measuring the through-thickness fiber orientation angles using a series of layers of fields-of-view and determining corresponding efficiency factors, will allow the composite stiffness to be determined through the moulding thickness.

REFERENCES

Agarwal B D, Lifsitz JM, Broutman L J. 1974. Elastic plastic finite element analysis of short fiber composites. Fib. Sci. Tech. 7: 45-62.

Brody H, Ward IM. 1971. Modulus of short carbon and glass fibre reinforced composites. Poly. Eng. and Sci. 11:139.

Cox HL. 1952. The elasticity and strength of paper and other fibrous materials. Brit. J. Appl. Phy. 3: 72- 79.

Giangreco E. 2003. Ingegneria delle strutture. UTET. 2 vol.

Halpin JC, Tsai SW. 1967. In Air Force Material Laboratory technical report.

Halpin JC, Pagano NJ. 1969. The laminate approximation for randomly oriented fibrous composites. J. Comp. Mater. 3:720.

Hill R. 1965. A self-consistent mechanics of composite materials. J. Mech. Phys. Solids. 12: 213-22.

Hill R. 1967. The essential structure of constitutive laws for metal composites and polycrystals. J. Mech. Phys. Solids. 15: 79-95.

Horii H, Nemat-Nasser S. 1983. Overall moduli of solids with microcracks: Load-induced anisotropy. J. Mech. Phys. Solids. 31: 155-177.

Krenchel H. Fibre reinforcement. Copenhagen. Akademisk For- lag. 1964.

Mandel J. 1971. Plasticité classique et viscoplasticité. Springer-Verlag.

O'Donnell B. 1990. Fabrication related variations in property in injection mouldings. Ph.D. Thesis. University of Newcastle-upon-Tyne.

Suquet P. 1981. Sur les equations de la plasticité: existence et régularité des solutions. J. Mécanique. 20: 3-40.

Taya M, Arsenault R J. 1989. Metal Matrix Composites-Thermomechanical Behavior. Pergamon Press.

Toll S. 1992, Interpolative aggregate model for short fibre composites. J. Comp. Maters. 26:1767.

4 BRIEF NOTES ON FINITE ELEMENT METHOD

The finite element method (FEM) is a numerical analysis technique for obtaining approximate solutions to a wide variety of engineering problems. Although originally developed to study stresses in complex airframe structures, it has since been extended and applied to the broad field of continuum mechanics. Because of its diversity and flexibility as an analysis tool, it is receiving much attention in engineering schools and in industry. In more and more engineering situations today, it is necessary to obtain approximate numerical solutions to problems rather than exact closed-form solutions. Without too much effort, the governing equations and boundary conditions for these problems can be written, but no simple analytical solution can be found.

The FEM envisions the solution region as built up of many small, interconnected subregions or elements. A finite element model of a problem gives a piecewise approximation to the governing equations. The basic premise of the FEM is that a solution region can be analytically modeled or approximated by replacing it with an assemblage of discrete elements. Since these elements can be put together in a variety of ways, they can be used to represent exceedingly complex shapes. In a continuum problem of any dimension, the field variable (whether it is pressure, temperature, displacement, stress, or some other quantity) possesses infinitely many values because it is a function of each generic point in the

body or solution region. Consequently, the problem is one with an infinite number of unknowns. The finite element discretization procedures reduce the problem to one of a finite number of unknowns by dividing the solution region into elements and by expressing the unknown field variable in terms of assumed approximating functions within each element. The approximating functions (sometimes called interpolation functions) are defined in terms of the values of the field variables at specified points called nodes or nodal points. Nodes usually lie on the element boundaries where adjacent elements are connected. In addition to boundary nodes, an element may also have a few interior nodes. The nodal values of the field variable and the interpolation functions for the elements completely define the behavior of the field variable within the elements. For the finite element representation of a problem, the nodal values of the field variable become the unknowns. Once these unknowns are found, the interpolation functions define the field variable throughout the assemblage of elements.

Clearly, the nature of the solution and the degree of approximation depend not only on the size and number of the elements used but also on the interpolation functions selected. As one would expect, these functions cannot be chosen arbitrarily, because certain compatibility conditions should be satisfied. The interpolation functions are often chosen so that the field variable or its derivatives are continuous across adjoining element boundaries. This feature is the ability to formulate solutions for individual elements before putting them together to represent the entire problem. This means, for example, that in the case of a problem in stress analysis, the force–displacement or stiffness characteristics of each individual element are first determined and, then, the elements are assembled to find the stiffness of the whole structure. In essence, a complex problem reduces to considering a series of greatly simplified problems. Another advantage of the finite element method is the variety of ways in which one can formulate the properties of individual elements. There are basically three different approaches. The first approach to obtain element properties is called the direct approach because its origin is traceable to the direct stiffness method of structural analysis. Element properties obtained by the direct approach can also be determined by the variational approach. The variational approach relies on the calculus of variations and involves the extremization of a functional. For problems in solid mechanics, the functional turns out to be the potential energy, the complementary energy, or some variant of them. A third and even more versatile approach for deriving element properties has its basis in mathematics and is

known as the weighted residuals approach. The weighted residuals approach begins with the governing equations of the problem and proceeds without relying on a variational statement. This approach is advantageous because it thereby becomes possible to extend the finite element method to problems where no functional is available. The method of weighted residuals is widely used to derive element properties for nonstructural applications such as heat transfer and fluid mechanics.

4.1. INTRODUCTION

The limitations of the human mind are such that it cannot grasp the behaviour of its complex surroundings and creations in one operation. Thus the process of sub-dividing all systems into their individual components or *elements*, whose behavior is readily understood and then rebuilding the original system from such components to study its behavior is a natural way in which the engineer, the scientist or even the economist proceeds.
In many situations an adequate model is obtained using a finite number of well-defined components. We shall term such problems discrete. In others the subdivision is continued indefinitely and the problem can only be defined using the mathematical fiction of an infinitesimal. This leads to differential equations or equivalent statements which imply an infinite number of elements. We shall term such systems continuous.
With the advent of digital computers, discrete problems can generally be solved readily even if the number of elements is very large. As the capacity of all computers is finite, continuous problems can only be solved exactly by mathematical manipulation.
Here, the available mathematical techniques usually limit the possibilities to oversimplified situations. To overcome the intractability of realistic types of continuum problems, various methods of discretization have from time to time been proposed both by engineers and mathematicians. All involve an approximation which, hopefully, approaches in the limit the true continuum solution as the number of discrete variables increases. The discretization of continuous problems has been approached differently by mathematicians and engineers.
Mathematicians have developed general techniques applicable directly to differential equations governing the problem, such as finite difference approximations (Southwell,1946; De G. Allen, 1955) various weighted residual procedures (Crandall, 1956; Finlayson, 1972) or approximate techniques for determining the stationarity of properly defined *functionals*. The engineer, on the

other hand, often approaches the problem more intuitively by creating an analogy between real discrete elements and finite portions of a continuum domain. For instance, in the field of solid mechanics McHenry (1943), Hrenikoff (1941), Newmark (1949), and indeed Newmark (1949), showed that reasonably good solutions to an elastic continuum problem can be obtained by replacing small portions of the continuum by an arrangement of simple elastic bars. Later, in the same context, Argyris (1960) and Turner et al. (1956) showed that a more direct, but no less intuitive, substitution of properties can be made much more effectively by considering that small portions or *elements* in a continuum behave in a simplified manner. It is from the engineering *direct analogy* view that the term *finite element* was born. Clough (1960) appears to be the first to use this term, which implies in it a direct use of a standard methodology applicable to discrete systems. Both conceptually and from the computational viewpoint, this is of the utmost importance.
The first allows an improved understanding to be obtained; the second offers a unified approach to the variety of problems and the development of standard computational procedures. Since the early l960s much progress has been made and today the purely mathematical and analogy approaches are fully reconciled. It is the object of this text to present a view of the finite element method as a general discretization procedure of continuum problems posed by mathematically defined statements.In the analysis of problems of a discrete nature, a standard methodology has been developed over the years. The civil engineer, dealing with structures, first calculates force-displacement relationships for each element of the structure and then proceeds to assemble the whole by following a well-defined procedure of establishing local equilibrium at each 'node' or connecting point of the structure. The resulting equations can be solved for the unknown displacements. Similarly, the electrical or hydraulic engineer, dealing with a network of electrical components (resistors, capacitances, etc.) or hydraulic conduits, first establishes a relationship between currents (flows) and potentials for individual elements and then proceeds to assemble the system by ensuring continuity of flows. All such analyses follow a standard pattern which is universally adaptable to discrete systems. It is thus possible to define a standard discrete system, and this chapter will be primarily concerned with establishing the processes applicable to such systems. Much of what is presented here will be known to engineers, but some reiteration at this stage is advisable. As the treatment of elastic solid structures has been the most developed area of activity this will be introduced first, followed by examples from other fields, before attempting a complete generalization. The existence of a unified treatment of *standard discrete problems* leads us to the first definition of the finite element process as a method of approximation to continuum problems such that:

- the continuum is divided into a finite number of parts (elements), the behavior of which is specified by a finite number of parameters

- the solution of the complete system as an assembly of its elements follows precisely the same rules as those applicable to standard discrete problems.

It will be found that most classical mathematical approximation procedures as well as the various direct approximations used in engineering fall into this category. It is thus difficult to determine the origins of the finite element method and the precise moment of its invention.
The following Figure 4.1 shows the process of evolution which led to the present day concepts of finite element analysis.

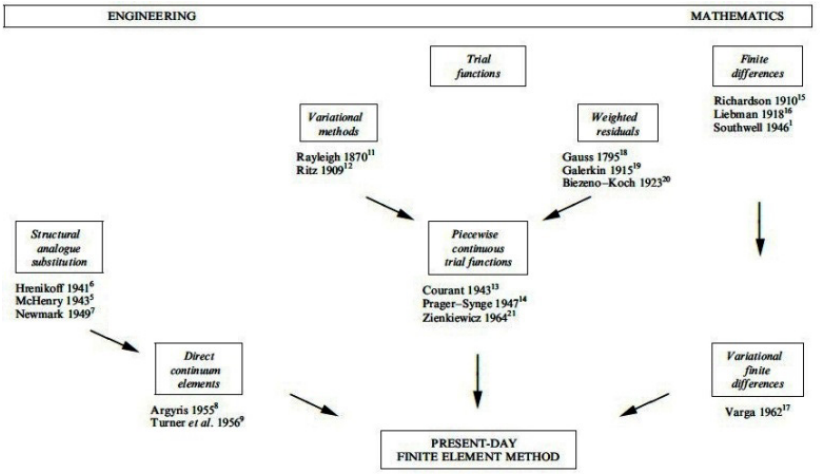

Fig. 4.1 – Evolution of finite element analysis

Regardless of the approach used to find the element properties, the solution of a continuum problem by the finite element method always follows an orderly step-by-step process:

1) *Discretize the Continuum*
   The first step consists in the division of the continuum or solution region into elements. A variety of element shapes may be used and different element shapes may be employed in the same solution region. Indeed, when analyzing an elastic structure that has different types of components such as plates and beams, it is not only desirable but also necessary to use different elements in the same solution.

2) *Select Interpolation Functions*
   The second step, instead, consists in the assignation of nodes to each element and, then, in the choice of the interpolation function to represent

the variation of the field variable over the element. The field variable may be a scalar, a vector, or a higher-order tensor.
Polynomials are often selected as interpolation functions for the field variable because they are easy to integrate and differentiate. The degree of the polynomial chosen depends on the number of nodes assigned to the element, the nature and number of unknowns at each node and certain continuity requirements imposed at the nodes and along the element boundaries. The magnitude of the field variable as well as the magnitude of its derivatives may be the unknowns at the nodes.

3) *Find the Element Properties*
Once the finite element model has been established (that is, once the elements and their interpolation functions have been selected), the matrix equations expressing the properties of the individual elements can be evaluated. For this task, one of the three approaches just mentioned can be used: the direct approach, the variational approach or the weighted residuals approach.

4) *Assemble the Element Properties to Obtain the System Equations*
To find the properties of the overall system modeled by the network of elements all the element properties must be "assembled". In other words, the matrix equations expressing the behavior of the elements are combined to form the matrix equations expressing the behavior of the entire system. The matrix equations for the system have the same form as the equations for an individual element except that they contain many more terms because they include all nodes. The basis for the assembly procedure stems from the fact that at a node, where elements are interconnected, the value of the field variable is the same for each element sharing that node. A unique feature of the finite element method is that the system equations are generated by the assembly of the individual *element* equations. In contrast, in the finite difference method the system equations are generated by writing nodal equations.

5) *Impose the Boundary Conditions*
Before the system equations are ready for solution they must be modified to account for the boundary conditions of the problem. At this stage, nodal values of the dependent variables or nodal loads are imposed.

6) *Solve the System Equations*
The assembly process gives a set of simultaneous equations to be solved to obtain the unknown nodal values of the problem. If the problem describes steady or equilibrium behavior, a set of linear or nonlinear algebraic equations is solved. On the contrary, if the problem

is unsteady, the nodal unknowns are time depending and, so, a set of linear or nonlinear ordinary differential equations must be solved.

7) *Make Additional Computations if Desired*
Many times the solution of the system equations are employed to calculate other important parameters. For example, in a structural problem the nodal unknowns are displacement components. From these displacements, element strains and stresses can be evaluated. Similarly, in a heat-conduction problem the nodal unknowns are temperatures, and from these element heat fluxes are calculated.

4.2. CLASSICAL DISPLACEMENT- BASED MATRIX FORMULATION IN FINITE ELEMENT METHOD.

4.2.1. The Structural Element and the Structural System

In order to define the *stiffness matrix* we shall first consider a structural engineering example of linear elasticity. The following Figure 4.2 represents a two-dimensional structure assembled from individual components and interconnected at the nodes numbered l to 6.

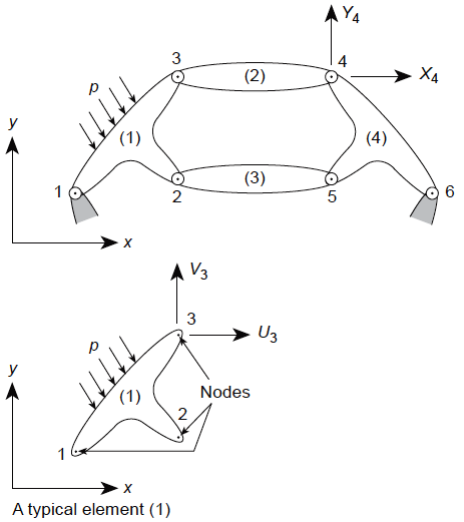

Fig. 4.2 – A typical structure built-up from intyerconnected elements

The joints at the nodes, in this case, are pinned so that moments cannot be transmitted. As a starting point it will be assumed that by separate calculation, or

for that matter from the results of an experiment, the characteristics of each element are precisely known. Thus, if a typical element labelled (l) and associated with nodes l, 2, 3 is examined, the forces acting at the nodes are uniquely defined by the displacements of these nodes, the distributed loading acting on the element (p), and its initial strain. The last may be due to temperature, shrinkage, or simply an initial 'lack of fit'. The forces and the corresponding displacements are defined by appropriate components (U, V and u, v) in a common coordinate system (x, y). Listing the forces acting on all the nodes (three in the case illustrated) of the element (l) as a matrix we have:

$$\mathbf{q}^1 = \begin{Bmatrix} \mathbf{q}_1^1 \\ \mathbf{q}_2^1 \\ \mathbf{q}_3^1 \end{Bmatrix} \quad where: \quad \mathbf{q}_1^1 = \begin{Bmatrix} U_1 \\ V_1 \end{Bmatrix} \tag{4.1}$$

and for the corresponding nodal displacements:

$$\mathbf{u}^1 = \begin{Bmatrix} \mathbf{u}_1^1 \\ \mathbf{u}_2^1 \\ \mathbf{u}_3^1 \end{Bmatrix} \quad where: \quad \mathbf{u}_1^1 = \begin{Bmatrix} u_1 \\ v_1 \end{Bmatrix} \tag{4.2}$$

Assuming linear elastic behaviour of the element, the characteristic relationship will always be of the form:

$$\mathbf{q}^1 = \mathbf{K}^1\mathbf{u}^1 + \mathbf{f}^1 \tag{4.3}$$

in which $\mathbf{f}^1$ represents the nodal forces required to balance any distributed loads acting on the element The first of the terms represents the forces induced by displacement of the nodes. The matrix $\mathbf{K}^e$ is known as the *stiffness matrix* of the element (e). Equation (4.3) is illustrated by an example of an ele ment with three nodes and with the interconnection points capable of transmitting only two components of force. Clearly, the same arguments and definitions will apply generally. An element (2) of the hypothetical structure will possess only two points of interconnection; others may have quite a large number of such points. Quite generally, therefore:

$$\mathbf{q}^e = \begin{Bmatrix} \mathbf{q}_1^e \\ \mathbf{q}_2^e \\ \vdots \\ \mathbf{q}_m^e \end{Bmatrix} \quad and \quad \mathbf{u}^e = \begin{Bmatrix} \mathbf{u}_1 \\ \mathbf{u}_2 \\ \vdots \\ \mathbf{u}_m \end{Bmatrix} \tag{4.4}$$

with each $\mathbf{q}_a^e$ and $\mathbf{u}_a$ possessing the same number of components or *degrees of freedom*.
The stiffness matrices of the element will clearly always be square and of the form:

$$\mathbf{K}^e = \begin{bmatrix} \mathbf{K}_{11}^e & \mathbf{K}_{12}^e & \cdots & \mathbf{K}_{1m}^e \\ \mathbf{K}_{21}^e & \mathbf{K}_{22}^e & & \vdots \\ \vdots & & \ddots & \vdots \\ \mathbf{K}_{m1}^e & \cdots & \cdots & \mathbf{K}_{mm}^e \end{bmatrix} \tag{4.5}$$

in which $\mathbf{K}_{11}^e$, $\mathbf{K}_{12}^e$, etc., are submatrices which are again square and of the size $\ell \times \ell$, where ℓ is the number of force components to be considered at each node. The element properties were assumed to follow a simple linear relationship. In principle, similar relationships could be established for non-linear materials, but the element matrices $\mathbf{K}^e$ will be symmetric.

4.2.2. Assembly and Analysis of a Structure

Consider again the hypothetical structure of Fig. 5.2. To obtain a complete solution the two conditions of:

1) displacement compatibility
2) equilibrium

have to be satisfied throughout. Any system of nodal displacements $\mathbf{u}$:

$$\mathbf{u} = \begin{Bmatrix} \mathbf{u}_1 \\ \mathbf{u}_2 \\ \vdots \\ \mathbf{u}_n \end{Bmatrix} \tag{4.6}$$

listed now for the whole structure in which all the elements participate, automatically satisfies the first condition.
As the conditions of overall equilibrium have already been satisfied within an element, all that is necessary is to establish equilibrium conditions at the nodes of the structure. The resulting equations will contain the displacements as unknowns, and once these have been solved the structural problem is determined. The internal forces in elements, or the stresses, can easily be found by using the characteristics established a priori for each element. If now the

equilibrium conditions of a typical node, a, are to be established, the sum of the component forces contributed by the elements meeting at the node are simply accumulated. Thus, considering all the force components we have:

$$\sum_{e=1}^{m} q_a^e = q_a^1 + q_a^2 + \ldots = 0 \tag{4.7}$$

in which q_a^1 is the force contributed to node a by element 1, q_a^2 by element 2, etc. Clearly, only the elements which include point a will contribute non-zero forces, but for tidiness all the elements are included in the summation.
Substituting the forces contributing to node i from the definition (4.3) and noting that nodal variables $\mathbf{u}_a$ are common (thus omitting the superscript e), we have:

$$(\sum_{e=1}^{m} \mathbf{K}_{a_1}^e)\mathbf{u}_1 + (\sum_{e=1}^{m} \mathbf{K}_{a_2}^e)\mathbf{u}_2 + \ldots + \sum_{e=1}^{m} \mathbf{f}_i^e = 0 \tag{4.8}$$

The summation again only concerns the elements which contribute to node a. If all such equations are assembled we have simply:

$$\mathbf{K}\mathbf{u} + \mathbf{f} = 0 \tag{4.9}$$

in which the submatrices are:

$$\mathbf{K}_{ab} = \sum_{e=1}^{m} \mathbf{K}_{ab}^e \quad and \quad \mathbf{f}_a = \sum_{e=1}^{m} \mathbf{f}_a^e \tag{4.10}$$

with summations including all elements. This simple rule for assembly is very convenient because as soon as a coefficient for a particular element is found it can be put immediately into the appropriate *location* specified in the computer. This general assembly process can be found to be the common and fundamental feature of all finite element calculations. If different types of structural elements are used and are to be coupled it must be remembered that the rules of matrix summation permit this to be done only if these are of identical size. The individual submatrices to be added have therefore to be built up of the same number of individual components of force or displacement.

4.2.3. The Boundary Conditions

The system of equations resulting from Eq. (4.9) can be solved once the prescribed support displacements have been substituted. In the example of Fig.

4.2, where both components of displacement of nodes 1 and 6 are zero, this will mean the substitution of:

$$u_1 = u_6 = \begin{Bmatrix} 0 \\ 0 \end{Bmatrix}$$

which is equivalent to reducing the number of equilibrium equations (in this instance 12) by deleting the first and last pairs and thus reducing the total number of unknown displacement components to eight. It is, nevertheless, always convenient to assemble the equation according to relation (4.9) so as to include all the nodes.
Clearly, without substitution of a minimum number of prescribed displacements to prevent rigid body movements of the structure, it is impossible to solve this system, because the displacements cannot be uniquely determined by the forces in such a situation. This physically obvious fact will be interpreted mathematically as the matrix $\mathbf{K}$ being singular, i.e., not possessing an inverse. The prescription of appropriate displacements after the assembly stage will permit a unique solution to be obtained by deleting appropriate rows and columns of the various matrices.
If all the equations of a system are assembled, their form is:

$$\begin{aligned} &\mathbf{K}_{11}\mathbf{u}_1 + \mathbf{K}_{12}\mathbf{u}_2 + \ldots + \mathbf{f}_1 = 0 \\ &\mathbf{K}_{21}\mathbf{u}_1 + \mathbf{K}_{22}\mathbf{u}_2 + \ldots + \mathbf{f}_2 = 0 \\ &\textit{etc.} \end{aligned} \tag{4.11}$$

and it will be noted that if any displacement, such as $\mathbf{u}_1 = \bar{\mathbf{u}}_1$, is prescribed then the external force $\mathbf{f}_1$ cannot be simultaneously specified and remains unknown. The first equation could then be deleted and substitution of known values of $\mathbf{u}_1$ made in the remaining equations. When all the boundary conditions are inserted the equations of the system can be solved for the unknown displacements and the internal forces in each element obtained.

4.2.4. The Standard Discrete System

In the standard discrete system, whether it is structural or of any other kind, we find that:

1. A set of discrete parameters, say $\mathbf{u}_a$, can be identified which describes simultaneously the behaviour of each element, e, and of the whole system. We shall call these the *system parameters*.

2. For each element a set of quantities $\mathbf{q}_a^e$ can be computed in terms of the system parameters $\mathbf{u}_a$. The general function relationship can be non-linear, for example:

$$\mathbf{q}_a^e = \mathbf{q}_a^e(\mathbf{u}) \tag{4.12}$$

but in many cases a linear form exists giving:

$$\mathbf{q}_a^e = \mathbf{K}_{a_1}^e \mathbf{u}_1 + \mathbf{K}_{a_2}^e \mathbf{u}_2 + \ldots + \mathbf{f}_a^e \tag{4.13}$$

3. The final system equations are obtained by a simple addition:

$$\mathbf{r}_a = \sum_{e=1}^{m} \mathbf{q}_a^e = 0 \tag{4.14}$$

where $\mathbf{r}_a$ are system quantities (often prescribed as zero). In the linear case this results in a system of equations:

$$\mathbf{K}\mathbf{u} + \mathbf{f} = \mathbf{0} = 0 \tag{4.15}$$

such that:

$$\mathbf{K}_{ab} = \sum_{e=1}^{m} \mathbf{K}_{ab}^e \quad and \quad \mathbf{f}_a = \sum_{e=1}^{m} \mathbf{f}_a^e$$

from which the solution for the system variables a can be found after imposing necessary boundary conditions.

In general neither linearity nor symmetry of matrices need exist - although in many problems this will arise naturally. Further, the narrowness of interconnections existing in usual elements is not essential.

4.2.5. Trasformation of coordinates

It is often convenient to establish the characteristics of an individual element in a coordinate system which is different from that in which the external forces and displacements of the assembled structure or system will be measured. A different coordinate system may, in fact, be used for every element, to ease the computation. It is a simple matter to transform the coordinates of the displacement and force components of Eq. (4.3) to any other coordinate system. Clearly, it is necessary to do so before an assembly of the structure can be

attempted. Let the local coordinate system in which the element properties have been evaluated be denoted by a prime suffix and the common coordinate system necessary for assembly have no embellishment. The displacement components can be transformed by a suitable matrix of direction cosines $\mathbf{L}$ as:

$$\mathbf{u}' = \mathbf{L}\mathbf{u} \tag{4.16}$$

As the corresponding force components must perform the same amount of work in either system:

$$\mathbf{q}^T\mathbf{u} = \mathbf{q}'^T\mathbf{u}' \tag{4.17}$$

On inserting (4.16) we have:

$$\mathbf{q}^T\mathbf{u} = \mathbf{q}'^T\mathbf{L}\mathbf{u} \tag{4.18}$$

or:

$$\mathbf{q} = \mathbf{L}^T\mathbf{q}' \tag{4.19}$$

The set of transformations given by (4.16) and (4.19) is called *contravariant*.
To transform stiffnesses which may be available in local coordinates to global ones note that if we write:

$$\mathbf{q}' = \mathbf{K}'\mathbf{u}' \tag{4.20}$$

then by (4.19), (4.20) and (4.16):

$$\mathbf{q} = \mathbf{L}^T\mathbf{K}'\mathbf{L}\mathbf{u} \tag{4.21}$$

or in global coordinates:

$$\mathbf{K} = \mathbf{L}^T\mathbf{K}'\mathbf{L} \tag{4.22}$$

In many complex problems an external constraint of some kind may be imagined, enforcing the requirement (4.16) with the number of degrees of freedom of $\mathbf{u}$ and $\mathbf{u}'$ being quite different. Even in such instances the relations (4.17) and (4.19) continue to be valid. An alternative and more general argument can be applied to many other situations of discrete analysis. We wish to replace a set of parameters $\mathbf{u}$ in which the system equations have been written by another one related to it by a transformation matrix $\mathbf{T}$ as:

$$\mathbf{u} = \mathbf{T}\mathbf{v} \tag{4.23}$$

In the linear case the system equations are of the form:

$$\mathbf{K}\mathbf{u} = -\mathbf{f} \tag{4.24}$$

and on the substitution we have:

$$\mathbf{K}\mathbf{T}\mathbf{v} = -\mathbf{f} \tag{4.25}$$

The new system can be premultiplied simply by $\mathbf{T}^T$, yielding:

$$(\mathbf{T}^T\mathbf{K}\mathbf{T})\mathbf{v} = \mathbf{T}^T - \mathbf{T}^T\mathbf{f} \tag{4.26}$$

which will preserve the symmetry of equations if the matrix $\mathbf{K}$ is symmetric. However, occasionally the matrix $\mathbf{T}$ is not square and expression (4.23) represents in fact an *approximation* in which a larger number of parameters $\mathbf{u}$ is *constrainted*. Clearly the system of equations (4.25) gives more equations than are necessary for a solution of the reduced set of parameters $\mathbf{v}$, and the final expression (4.26) presents a reduced system which in some sense approximates the original one.

4.3. FINITE ELEMENTS WITH NUMERICAL CODE ANSYS®

All the performed analysis have been employed by means of the commercial software Ansys® 11. Ansys® is a general purpose finite element method-based modeling software package for numerically solving of a wide variety of problems. The choice of this software has been dictated first of all by the possibility to use a *batch approach*, creating custom-made macros for the specific problem to solve and personalizing the main menu. In fact, the user can write in a text file a sequence of command lines. This strategy results very advantageous for complex problems because it gives the possibility to easily modify the command lines but, above all, to realize parametric models. Moreover, another important aspect is the possibility to perform multi-physics simulations. In an expanding range of applications, engineers and designers must be able to accurately predict how complex products will behave in real-world environments where multiple types of coupled physics interact. Multi-physics simulation software from Ansys® allows creating virtual prototypes of specific designs operating under real-world multi-physics conditions. This commercial leading software enables to simulate the interaction between structural mechanics, heat transfer, fluid flow and electromagnetics all within a single, unified engineering simulation environment. By incorporating multi-physics

simulation into the design process, engineers reduce error margins, increase product reliability and ultimately create more innovative product designs. Multi-physics simulation from Ansys® provides a portfolio of high-fidelity engineering analysis tools that enable engineers to accurately predict real-world behavior. Ansys® multi-physics solutions combine the most comprehensive set of solver technology for all physics disciplines – structural mechanics, heat transfer, fluid flow and electromagnetics – with an open and adaptive environment, flexible simulation methods and parallel scalability. Together these cutting edge technologies form the foundation for comprehensive multi-physics simulation capable of solving the most complex engineering challenges.
The Ansys® platform is a powerful multi-domain simulation environment that harnesses the core physics from Ansys®, enables their interoperability, and provides common tools for interfacing with CAD, repairing geometry, creating meshes and post-processing results.
Moreover, Ansys® multi-physics solutions deliver proven methods to solve multi-physics problems, including solutions for both direct and sequentially coupled problems. Direct coupled-field elements allow users to solve multi-physics problems by employing a single finite element model with the appropriate coupled-physics options set within the element itself. A direct coupled field solution simplifies the modeling of multi-physics problems by allowing the engineer to create, solve and post-process a single analysis model for a wide variety of multi-physics applications. Sequential coupling, instead, allows engineers to solve multi-physics problems with the automated multi-physics coupling available in Ansys®, which couples multiple single-physics models into one unified simulation.
The platform supports both one-way and two-way sequential solutions for multi-physics problems such as thermal-stress analysis, microwave heating and fluid structure interaction.
The software Ansys® is organized into three modules.

1) ***Preprocessing Module***
   This module allows to model the specific problem in terms of geometry, element type, definition of the material properties of the element and mesh.

2) ***Solution Processor Module***
   In this module, instead, load and constraint conditions are assigned and the specific kind of solution is conveniently selected.

3) ***Post Processing Module***
   The last module furnishes the results of the problem in three different form of visualization: in terms of numerical data lists, with vectorial graphics or through chromatic bands.

The software Ansys® is the most diffuse element finite-based software worldwide; is an open software, it is programmable both for developing macros and menu. From the beginning, in the late 80's, this software has been written in a standard FORTRAN90, one of the first and more used programming language. Knowledge of this language is very helpful. Substantially, it is possible to create macros in a proprietary language called APDL (Ansys Parametric Design Language) having a own proprietary sintax and it is possible to customize menu using a proprietary language called UIDL (User Interface Design Language).
ANSYS Multi-Physics software offers a comprehensive product solution for structural linear or nonlinear and dynamics analysis. The product provides a complete set of elements behavior, material models and equation solvers for a wide range of engineering problems. In addition, ANSYS Multi-Physics offers thermal analysis and coupled-physics capabilities involving acoustic, piezoelectric, thermal-structural and thermoelectric analysis.

REFERENCES

Ansys® Inc. 2007. ANSYS 11 User's Documentation. Canonsburg, PA

Argyris JH. 1960. Energy Theorems and Structural Analysis. Butterworth.Crandall SH. 1956. Engineering Analysis. McGraw-Hill.

Clough RW. 1960. The finite element in plane stress analysis. Proc. 2nd ASCE Conf. on Electronic Computation.

De G. Allen DN. 1955. Relaxation Methods. McGraw-Hill.

Finlayson BA. 1972. The Method of Weighted Residuals and Variational Principles. Academic Press.

Hrenikoff A. 1941. Solution of problems in elasticity by the framework method. J. Appl. Mech. A8: 169-75.

McHenry D. 1943. A lattice analogy for the solution of plane stress problems. J. Inst. Civ. Eng. 21: 59-82.

Newmark NM. 1949. Numerical methods of analysis in bars, plates and elastic bodies. Numerical Methods in Analysis in Engineering. ed. Grinter.

Southwell RV. 1946. Relaxation Methods in Theoretical Physics. Clarendon Press.

Turner MJ, Clough RW, Martin HC, Topp LJ. 1956. Stiffness and deflection analysis of complex structures. J Aero Sci. 23: 805-23.

Zienckiewicz OC, Taylor RL. 2000. The finite element method. Butterworth-Heinemann.

5 TOPOLOGY OPTIMIZATION THEORY

The area of computational variable-topology shape design of continuum structures is presently dominated by methods which employ a material distribution approach for a fixed reference domain in the spirit of the so-called `homogenization method' for topology design, (Bendsøe et al., 1988). That is, the geometric representation of a structure is similar to a grey-scale rendering of an image, in discrete form corresponding to a raster representation of the geometry. This concept has proven very powerful, but it does involve a number of difficulties. One is the issue of existence of solutions, another the issue of solution method.

In many applications, the optimal topology of a structure should consist solely of a macroscopic variation of one material and void, meaning that the density of the structure is given by a $(0-1)$ *integer parametrization (often called a black-and-white design). Unfortunately, this class of optimal design problems is ill-posed in that, for example, nonconvergent, minimizing sequences of admissible designs with finer and finer geometrical details can be found, see (Cheng et al., 1981; Kohn et al., 1986). Existence of black-and-white solutions can be achieved by confining the solution space to limit the complexity of the admissible designs, making the designs dependent on the choice of parameters in the geometrical*

constraint. Such a restriction of the design space can be accomplished in a number of ways, e.g. by enforcing an upper bound on the perimeter of the structure (Ambrosio et al. 1993; Haber, et al.,1996), one can introduce a filtering function that effectively limits the minimum width of a member, (Sigmund, 1994); or one can impose constraints on slopes on the parameters defining the geometry, (Chenais, 1975; Bendsøe, 1983; Niordson, 1983).

For reasonable raster representations of the $(0-1)$ *black-and-white design, the solution of the resulting large-scale integer programming problem becomes a major challenge. Recently, dual methods have been shown to be effective, in the absence of local constraints, (Beckers, 1999). However, the most commonly used approach is to replace the integer variables with continuous variables, and then introduce some form of penalty that steers the solution to discrete* $(0-1)$ *values. A key part of these methods is the introduction of an interpolation function that expresses various physical quantities, e.g. material stiffness, cost, etc., as a function of continuous variables. The continuous variables are often interpreted as material densities, as in the so-called penalized, proportional "fictitious material" model. Inspired by the relaxed formulations that introduce composites, some methods use interpolations derived from employing composite materials of some given form together with penalizations of intermediate densities of material.*

Existence of solutions can also be achieved through relaxation, leaving the concept of a black-and-white design. Relaxation is sometimes attained by expanding the solution space to include microstructures and using homogenized properties to describe their behaviour, as seen in (Bendsøe et al., 1988; Lurie et al., 1982).

In these formulations, the design is allowed to exhibit high-frequency oscillations at an indeterminate, microscopic length scale. Alternatively, we may describe these nonconventional designs through mathematical relaxation, e.g., quasi-convexification, etc. (Goodman et al., 1986). In general, these approaches lead to designs that can only be realized by incorporating microstructure; however, there is no definite length scale associated with the microstructure. Relaxed formulations provide an appropriate basis for direct synthesis where composite materials are allowed to constitute part of the final design, simply because microstructure is admissible. Indeed, the demand for ultimate performance can lead one to consider all possible materials in the design formulation, (Ringertz, 1993; Bendsøe et al., 1994). In general, relaxation yields a set of continuously

variable design fields to be optimized over a fixed domain, so the algorithmic problems associated with the discrete $(0-1)$ *format of the basic problem statement are circumvented; this was one of the main motivations for the initial use of the relaxation concept. Sometimes, a subset of the design fields is optimized analytically, leaving a reduced problem for numerical optimization, (Jog et al., 1994).*

It should be emphasized that the continuum relaxation approach can be very involved theoretically. As of today, it has been mathematically fully worked for minimum compliance design of structures only (for both single and multiple loads) and for a broader class of problems involving the Laplace operator (Goodman et al., 1986).

5.1. INTRODUCTION

The design process of an object is a coherent set of operations that starts from the structure's conception and ends with its realization. One of the most important steps in designing a structure or an element is the definition of its form.
Usually, the traditional approach to this problem is to use geometries that have already been tried or solutions already adopted before; this approach is insufficient in many engineering areas, where the development of new products or new solutions in researching the best structural morphology in relation to design requirements, are very important. A rational approach to this type of problem is known as *optimization*. In a simple way, the word optimization can be defined as the rational procedure that allows reaching the best solution among all admissible ones, according with the required targets and with the physical and geometric constraints and limitations. It is easy to imagine that this concept is not just about the structural field, but it concerns a multitude of fields including bioengineering, fluid mechanics, electromagnetism, optics, natural sciences, economics and many others. The optimization provides engineers a means to determine optimal designs in terms of admissible structural responses (deformation, stress, etc.), through mathematical algorithms. Due to this multidisciplinary approach, most of the results today are obtained by experts from different fields working together. The preliminary operation is to define the geometry of the object, element or structure to be built and it is the most important moment as it can influence all following design choices. Since the '50s, the evolution of the optimization has produced four main classes of distinct problems: sizing optimization, shape optimization, material optimization and topology optimization; the last one is the subject of this thesis work. Actually, these four classes of problems have developed at different times. At the

beginning, the optimization was the search for the "best" sectional properties, after having fixed topology and structural configuration. Later on, in 1950-60, thanks to the development of the Finite Element Method (FEM), shape optimization was introduced; then, in 1980, the topology optimization was developed. Now, the four techniques above mentioned will be briefly described (Cinquini et al., 1995). In the sizing optimization, geometry, material properties and loads are assigned; the designer task is to select the size of the section of all the various parts of the structure. So, the goal is to determine the optimal distribution of the area and the thickness of the structure we want to study.

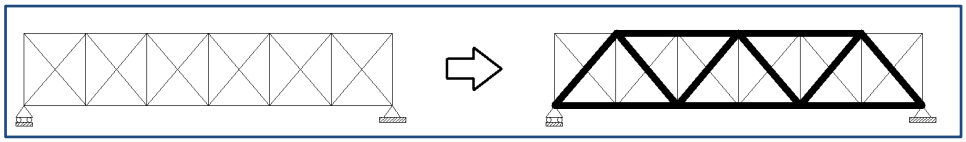

Fig. 5.1 – Sizing optimization

In this case (Fig 5.1), the configuration and topology of the structure are defined beforehand and the optimization process is restricted to research the optimal size of the cross sections of the rods. In the shape optimization the structural topology is established, i.e. the connection level of project domain; optimization becomes the search for "optimal" form, such as inner holes in general or the border of project domain.

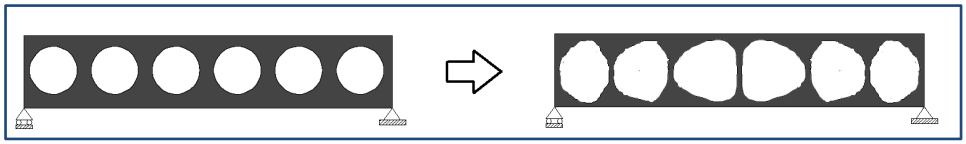

Fig. 5.2 – Shape optimization

Material optimization can be considered as part of a class of problems, but it can be related to topology optimization.
In the case of topology optimization, the connection degree of domain is not fixed beforehand: we only know the form, the constraints and the loads.

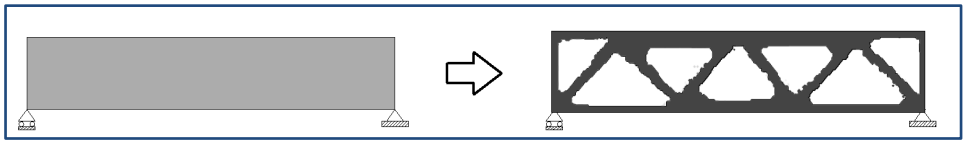

Fig. 5.3 – Topology optimization

Therefore, see Figure 5.3, the aim is to determine the distribution of material (or material properties) that minimizes or maximizes the objective function given for an assigned loads condition and observing appropriate constraints. The topology optimization is the latest in order of development, and compared to other

optimization procedures, it offers several advantages; the most important one consists in the ability to design the domain's level of connection without the need to determine a specific topology in advance, as it occurs in the case of shape optimization. Moreover, a great operational advantage lies in not modifying the discretization of the domain at every step of an iterative process; in this way we have the resolution of the problem (for example through the finite element method). Furthermore, topology optimization can act on several structural levels, allowing the definition of optimal shape at both microstructural (definition of material characteristics) and macrostructural (definition of the structural morphology) (Michell, 1904) levels.

5.2. TOPOLOGY OPTIMIZATION: ETYMOLOGY AND HISTORY

Topology optimization is the search for optimal distribution in the project domain of one or more structural parameters such as density, mechanical properties such as rigidity, microstructural parameters, thickness, and other geometrical and mechanical parameters; for its versatility and potential, this design procedure represents the link between size and shape optimization (Eschenauer et al., 2001). The word *topology* comes from the Greek word *topos* and it means location, space or domain. In mathematical terms, the topology is linked to objects that are deformable in a manner called rubber-like (i.e. as a gum). Topological transformations and topological mapping indicate the topological transformations of a domain in another one that does not destroy or create close links. Two topological domains are called topologically equivalent if there is a topological mapping of one of the other two domains (Fig. 5.4):

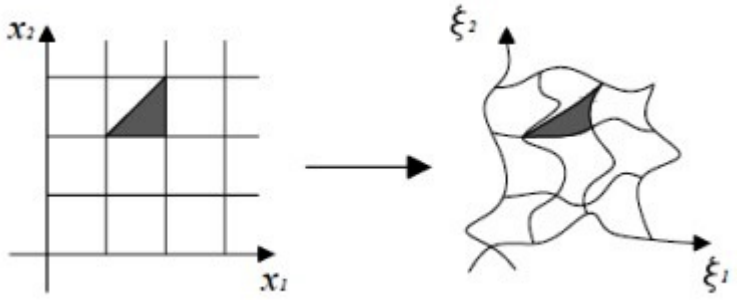

Fig. 5.4 – Topological trasformation

In addition, a topological property is the invariance of all topological mappings. In general, transformations can be formulated as a topological transformation of the continuous, whose inverse transformations are still continuous. Finally, there

is the homomorphism property, by which transformations are reversibly and continuous. The word *optimization* comes from the Greek word *optimus* and it can be defined as the rational procedure that allows reaching the best solution among all admissible ones, according with the required objective and with the physical and geometric constraints and limitations. Topology optimization is a relatively new and rapidly expanding field of structural mechanics that can result in much greater savings than mere cross-section or shape optimization. Owing to its complexity, it is an intellectually challenging field; its progress, however, has often been hampered by conceptual inconsistencies and terminological confusion. For this reason, a critical and systematic re-examination of the relevant issues seems needed. This argument deals mainly with mechanical, structural and computational aspects. For very low volume fractions, important principles of topology optimization were established already at the beginning of the century in the context of trusses, by the versatile Australian inventor Michell (Rozvany, 2001); these principles were extended to grillages (beam systems) more or less seventy years later by Rozvany. Drawing on these applications, the basic principles of optimal layout theory were formulated by Prager and Rozvany (Prager et al. 1977) and generalized considerably by the latter in the eighties and nineties. Topology optimization for higher volume fractions is now called Generalized Shape Optimization (GSO) or Variable Topology Shape Optimization. It involves the simultaneous optimization of the topology and shape of internal boundaries in porous and composite continua. In the context of discretized mechanics, this development was prompted by the observation of Cheng and Olhoff (1981) that optimized solid plates containing systems of ribs which are similar to optimized grillages. For compliance design of perforated plates (disks) in plane stress, optimal microstructures were studied by various mathematicians. The first exact analytical solutions for optimal perforated plates and the correct expressions for the rigidity tensor of homogenized optimal microstructures were obtained by Bendsøe (1983).The birth of practical, FE-based topology optimization for higher volume fractions was brought about by extensive pioneering research of Bendsøe (1989), and his homogenization school. This was followed by a parallel exploration of the SIMP approach, suggested originally by Bendsøe (1989) and used extensively by Zhou (1991) and the author Rozvany (1994), who also suggested the term SIMP.

5.3. FORMULATION PROBLEM

In the mathematical formulation of optimal design problems, we must consider four fundamental aspects (Cinquini et al, 1995):

I. Object function definition
The object function (or *functional*) is represented by a measure indicator (to

maximize or minimize) of the structure quality, where quality is referred to the satisfaction of an assigned requirement. Among the structural properties most often used to define the objective of the optimization procedure, there are:

- the cost (the cost of materials, manufacturing cost, maintenance cost and usage);
- the mechanical properties (global or local);
- the aesthetic qualities.

If more objectives are considered, not in conflict among them, it generates a problem much more complex, precisely defined as a multi-objective optimization problem.

II. Choice of design variables
The design variables are related to the geometry of the structure. The geometry is usually defined by topological variables representing the numerical and spatial sequence of structural elements and nodes position, or through mechanical variables related to structural behaviour. The shape of the structure can be considered as design variables.

III. The formulation of equations governing the problem
The equations controlling the problem, such as the equilibrium and consistency equations and the material's constitutive laws, depend on the nature of the problem.

IV. Definition of the constraints and limitations
From a mathematical point of view, constraints can be classified in equality or inequality and in global or local; from a structural point of view, we can have behaviour or geometric constraints. Constrains limit the domain of admissible solutions.

In summary, in optimal problems all the constraints are written as mathematical expressions (equality or inequality) in order to define the set of possible projects, and then to look for the optimal solution through the minimization (or maximization) of the objective function. In topology optimization of structure, material and mechanisms, parameterization of geometry is often performed by a grey-scale density-like interpolation function (Bendsøe and Sigmund, 1999). This allows to derive simple necessary conditions for the possible realization of grey-scale via composites, leading to a physical interpretation of all feasible designs as well as the optimal one. Thus it is shown that, in many circumstances, the so called artificial interpolation model actually falls within the framework of microstructurally based models. In many applications, the optimal topology of a structure should consist solely of a macroscopic variation of material and void,

meaning that the density of the structure is given by a "0±1" integer parameterization (often called *black and white design*). Unfortunately, this class of optimal design problems is ill-posed in that, for example, non convergent, minimizing sequences of admissible design with finer and finer geometrical details can be found. Existence of black and white solutions can be achieved by confining the solution space to limit the complexity of the admissible designs, making them dependent on the choice of parameters in the geometrical constraint. For reasonable raster representations of the "0±1" black and white design, the solution of the resulting large scale integer programming problem becomes a major challenge. Recently, dual methods have been shown to be effective, in the absence of local constraints (Beckers, 1999). However, the most commonly used approach is to replace the integer variables with continuous variables, and then introduce some form of penalty that steers the solution to discrete "0±1" values. A key part of these methods is the introduction of an interpolation function that expresses various physical quantities, for example material stiffness, cost, etc., as a function of continuous variables. The continuous variables are often interpreted as material densities, as in the so-called penalized, proportional fictitious material model.

5.4. BASIC PROBLEM STATEMENTS

The continuum topology design problems considered are defined on a fixed reference domain Ω in R^2 or R^3. In this domain, we seek the optimal distribution of material, with the term *optimal* being defined through choice of objective functions, constraint functions and through choice of design parametrization. The objective and constraint functions involve some kind of physical modelling that provides a measure of efficiency within the framework of a given area of applications, for example structural mechanics. The basis for the discussion is the minimum compliance problem for a linearly elastic structure in 2-D or 3-D. We thus consider a mechanical element as a body occupying a domain Ω^m which is part of a the reference domain Ω, on which applied loads and boundary conditions are defined Fig. 5.5:

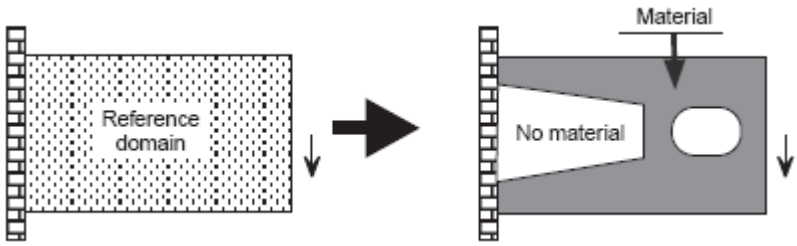

Fig. 5.5 – The shape design problem of finding the optimal material distribution

This reference domain is often referred to as the ground-structure, in analogy with terminology in truss topology design, (Bendsøe, 1995). Referring to the reference domain Ω we can define the optimal topology-shape design problem as a minimization of force times displacement, over admissible designs and displacement fields satisfying equilibrium:

$$\begin{aligned} &\text{minimize} \quad \int_\Omega \boldsymbol{pu}\, d\Omega + \int_{\Gamma_T} \boldsymbol{tu}\, ds \\ &\boldsymbol{u} \in \mathrm{U}, \Theta \end{aligned}$$

subject to:

$$\begin{aligned} &\int_\Omega \boldsymbol{C}_{ijkl}(x)\boldsymbol{\varepsilon}_{ij}(u)\boldsymbol{\varepsilon}_{kl}(v)\, d\Omega = \int_\Omega \boldsymbol{pv}\, d\Omega + \int_{\Gamma_T} \boldsymbol{tv}\, ds, \quad \text{for all } \boldsymbol{v} \in U, \\ &\boldsymbol{C}_{ijkl}(x) = \Theta(x)\boldsymbol{C}^0_{ijkl}, \\ &\Theta(x) = \begin{cases} 1 & \text{if } x \in \Omega^m, \\ 0 & \text{if } x \in \Omega / \Omega^m, \end{cases} \\ &\mathrm{Vol}(\Omega^m) = \int_\Omega \Theta(x)\, d\Omega \le V, \\ &\mathrm{Geo}(\Omega^m) \le K \end{aligned} \tag{5.1}$$

Here, the equilibrium equation is written in its weak, variational form, with U denoting the space of kinematically admissible displacement fields, u the equilibrium displacement, p the body forces, $\boldsymbol{t}$ boundary tractions and $\boldsymbol{\varepsilon}(\boldsymbol{u})$ linearized strains. Moreover, $\mathrm{Geo}(\Omega^m)$ denotes a constraint function limiting the geometric complexity of the domain Ω^m, imposed here to obtain a well-posed problem. In problem (5.1), $\boldsymbol{C}^0_{ijkl}$ denotes the stiffness tensor of a given elastic material from which the structure is to be manufactured, with a total amount of material V; $\Theta(x)$ denotes the pointwise volume fraction of this material and, for a black-and-white design, this can only attain the values zero or one. Problem (5.1) is a discrete optimization problem, and for many applications it is useful to consider reformulations in terms of continuous variables, with the goal of using derivative based mathematical programming algorithms. This means that one changes the model for material properties, i.e., the relations defined in (5.1) as:

$$\boldsymbol{C}_{ijkl} = \Theta \boldsymbol{C}^0_{ijkl} = \begin{cases} \text{either} & \boldsymbol{C}^0_{ijkl}, \\ \text{or} & 0, \end{cases} \tag{5.2}$$

to a situation where the volume fraction is allowed any value between zero and one. It may also involve finding an appropriate method for limiting geometric complexity, for example, exchanging the total variation of a density for the perimeter of a domain.

5.5. ISOTROPIC MODELS FOR SOLID-VOID INTERPOLATION IN ELASTICITY

In this section the so-called penalized, proportional fictitious material model, also names as the *Solid Isotropic Material with Penalization* model (SIMP), is presented (Bendsøe, 1989; Zhou et al., 1991; Mlejnik et al., 1993; Rozvany et al., 1994).
Here, a continuous variable γ, $0 \le \gamma_{\min} \le \gamma$, is introduced, resembling a density of material by the fact that the volume of the structure is evaluated as:

$$\mathrm{Vol} = \int_{\Omega} \gamma(x)\, d\Omega. \tag{5.3}$$

In computations, a small lower bound, $0 < \gamma_{\min} \le \gamma$, is usually imposed, in order to avoid a singular FEM problem, when solving for equilibrium in the full domain Ω.
The relation between this density and the material tensor $\boldsymbol{C}_{ijkl}(x)$ in the equilibrium analysis is written as:

$$\boldsymbol{C}_{ijkl}(\gamma) = \gamma^{p} \boldsymbol{C}^{0}_{ijkl}, \tag{5.4}$$

where the given material is isotropic, i.e. $\boldsymbol{C}^{0}_{ijkl}$ is characterized by just two variables, here chosen as the Young' s modulus E^0 and the Poisson ratio ν^0.
The interpolation (5.4) satisfies that:

$$\boldsymbol{C}_{ijkl}(0) = 0, \quad \boldsymbol{C}_{ijkl}(1) = \boldsymbol{C}^{0}_{ijkl}. \tag{5.5}$$

This means that if a final design has density zero or one in all points, this design is a black-and- white design for which the performance has been evaluated with a correct physical model.
For problems where the volume constraint is active, experience shows that optimization does actually result in such designs if one chooses p sufficiently big (in order to obtain true $(0-1)$ designs, $p \ge 3$ is usually required).
The reason is that, for such a choice, intermediate densities are penalized; volume is proportional to γ, but stiffness is less than proportional.

5.6. MICROSTRUCTURE REALIZING THE SIMP-MODEL

For the SIMP interpolation (5.4), it is not immediately apparent that areas of grey can be interpreted in physical terms. However, it turns out that, under fairly simple conditions on p, any stiffness used in the SIMP model can be realized as the stiffness of a composite made of void and an amount of the base material corresponding to the relevant density. Thus using the term *density* for the interpolation function γ is quite natural. The stiffness tensor $\boldsymbol{C}_{ijkl}(\gamma)$ of the SIMP model is isotropic with a Young's modulus varying with γ.
The Poisson's coefficient also depends from the density but a constant value have been used.
If this tensor is to correspond to a composite material constructed from void and the given material at a real density γ, the bulk modulus k and the shear modulus μ of the tensor $\boldsymbol{C}_{ijkl}(\gamma)$ should satisfy the Hashin-Shtrikman bounds for two-phase materials, (Hashin et al., 1963), written here for plane elasticity and for the limit of one phase being void:

$$0 \le k \le \frac{\gamma k^0 \mu^0}{(1-\gamma)k^0 + \mu^0}, \quad 0 \le \mu \le \frac{\gamma k^0 \mu^0}{(1-\gamma)\left(k^0 + 2\mu^0\right) + k^0} \quad (\text{in } 2D) \tag{5.6}$$

Here k^0, μ^0 are the bulk and shear moduli, respectively, of the base material. This implies that the Young modulus should satisfy (Torquato et al., 1998):

$$0 \le E \le E^* = \frac{\gamma E^0}{(3-2\gamma)} \quad (\text{in } 2D) \tag{5.7}$$

From (5.7), the SIMP model should satisfy:

$$\gamma^p E^0 \le \frac{\gamma E^0}{(3-2\gamma)} \quad \text{for all } 0 \le \gamma \le 1 \tag{5.8}$$

which is true if and only if $p \ge 3$. However, the SIMP model presumes that the Poisson's ratio is independent of the density, and this leads to a stronger condition. From the relationship:

$$k^0 = \frac{E^0}{2\left(1-\nu^0\right)}, \quad \mu = \frac{E^0}{2\left(1+\nu^0\right)} \quad (\text{in } 2D) \tag{5.9}$$

the condition (5.6) for the SIMP model can be written for all $0 \le \gamma \le 1$ as:

$$\begin{aligned} 0 &\le \frac{\gamma^p E^0}{2\left(1-\nu^0\right)} \le \frac{\gamma E^0}{4-2\left(1+\nu^0\right)\gamma} \\ 0 &\le \frac{\gamma^p E^0}{2\left(1+\nu^0\right)} \le \frac{\gamma E^0}{2\left(1-\gamma\right)\left(3-\nu^0\right)+2\left(1+\nu^0\right)} \end{aligned} \tag{5.10}$$

After some algebra, this leads to a condition on the power p in the form:

$$p \ge p^*\left(\nu^0\right) = \max\left\{\frac{2}{1-\nu^0}, \frac{4}{1+\nu^0}\right\} \quad (\text{in } 2D) \tag{5.11}$$

which in itself implies $p \ge 3$. The inequality $p \ge 2/1-\nu^0$ comes from the bulk modulus bound, while the inequality $p \ge 4/1+\nu^0$ is due to the shear modulus bound. Example values of p^* are:

$$\begin{aligned} &p^*\left(\nu^0 = \tfrac{1}{3}\right) = 3; \quad p^*\left(\nu^0 = \tfrac{1}{2}\right) = 4; \quad p^*\left(\nu^0 = 0\right) = 4; \\ &p^*\left(\nu^0 = 1\right) = \infty; \quad p^*\left(\nu^0 = -1\right) = \infty \quad (\text{in } 2D), \end{aligned} \tag{5.12}$$

and $p^* = 3$ holds only for $\nu^0 = 1/3$.

It is important to note that the condition (5.11) implies that the SIMP model can be made to satisfy the Hashin-Shtrikman bounds, so that it makes sense to look for composites which realize the stiffness tensor for the model. The form of this composite can be computed through a design process, where the desired material properties of a periodic medium are obtained by an inverse homogenization process, (Sigmund, 1994; Sigmund, 1995). The geometry of the composite may depend on the density and one can normally not expect to obtain the wanted properties by analytical methods. It is still an open problem if all material parameters satisfying the bounds also can be realized as composites of the given materials. For two materials, one infinitely stiff, one infinitely soft, it is shown in (Milton et al., 1995) that composites can be build for any positive definite material tensor. However, in topology design the stiffness is restricted and the density specified.

In 3-D, there is more geometric freedom to construct microstructures and here the Hashin-Shtrikman bounds lead to the condition:

$$p \ge \max\left\{15\frac{1-\nu^0}{7-5\nu^0}, \frac{3}{2}\frac{1-\nu^0}{1-2\nu^0}\right\} \text{ (in 3D)} \tag{5.13}$$

on the power p in the SIMP model.
Example bounds are here:

$$\begin{aligned} &p \geq 3 \quad \text{per } v^0 = \frac{1}{3}; \quad p \geq 2 \quad \text{per } v^0 = \frac{1}{5}; \quad p \geq \frac{15}{7} \quad \text{per } v^0 = 0; \\ &\text{p} \geq \frac{5}{2} \quad \text{per } v^0 \to -1; \quad p \to \infty \quad \text{per } v^0 \to \frac{1}{2} \quad \text{(in 3-D)} \end{aligned} \tag{5.14}$$

so some lower values of p are possible in dimension three.

Note that for the Poisson's coefficient $\nu = \frac{1}{3}$ we have the same bounds in 2-D and in 3-D.

5.7. TWO MATERIALS WITH NON-VANISHING STIFFNESS

For a topology design problem, where the aim is to seek the optimal distribution of two isotropic, linearly elastic materials with non-vanishing stiffness, the stiffness tensor of the problem (5.1) takes the form:

$$\boldsymbol{C}_{ijkl} = \theta \boldsymbol{C}^1{}_{ijkl} + (1-\theta)\boldsymbol{C}^2{}_{ijkl} = \begin{Bmatrix} 0 & \boldsymbol{C}^1{}_{ijkl} \\ \text{oppure} & \boldsymbol{C}^2{}_{ijkl} \end{Bmatrix} \tag{5.15}$$

where the two materials are characterized by the stiffness tensors $\boldsymbol{C}^1_{ijkl}$ and $\boldsymbol{C}^2_{ijkl}$. Here the material 1 is the stiffer, i.e., $\boldsymbol{C}^1_{ijkl}\boldsymbol{\varepsilon}_{ij}\boldsymbol{\varepsilon}_{kl} \geq \boldsymbol{C}^2_{ijkl}\boldsymbol{\varepsilon}_{ij}\boldsymbol{\varepsilon}_{kl}$ for any strain $\boldsymbol{\varepsilon}$. Note that the volume constraint now signifies the amount of material 1 which can be used, as the total amount of material amounts to the total volume of the domain Ω. The two-material problem has been the focal point of theoretical works on generalized shape design problems, as the possible singularity of stiffness is not an issue. Computational studies are poor with early numerical work concentrating on conduction problems, but this variant of the topology design problem has gained recent interest, mainly as a method for generating microstructures with interesting (and extreme) behaviour.
For the two-material problem, the SIMP model can be expressed:

$$\begin{aligned} &\boldsymbol{C}_{ijkl}(\rho) = \rho^p \boldsymbol{C}^1_{ijkl} + (1-\rho^p)\boldsymbol{C}^2_{ijkl}, \\ &Vol(\text{material 1}) = \int_\Omega \rho(x)\, d\Omega \end{aligned} \tag{5.16}$$

5.8. ANISOTROPIC TOPOLOGICAL OPTIMIZATION

5.8.1. Introduction

Minimization of the strain energy density is of considerable significance when stiff structures or structured materials must be achieved for a given loading, whereas its maximization is an outstanding feature when a large amount of energy absorption under impact loading is demanded. Contrary to isotropic solids, in presence of elastic anisotropy the strain energy density changes when any material element is rotated to the principal directions of stress or strain. Accordingly, the orientation of the material axes can be employed as design variable to achieve the desired maximum or minimum value of the strain energy density. In designing living tissues, nature somehow employs this kind of strategy, and adjusts the microstructure of the material (i.e., its anisotropy), to enhance the mechanical performances. On the other hand, the same idea is artificially adopted when some man-made materials are produced. Among these, fibrous composites represent the most common example of materials intrinsically anisotropic and susceptible to be properly designed for given purposes. In literature some procedures were proposed with the aim to rationalize the problem of finding the *extrema* for the strain energy density, with reference to linear elastic solids in presence of material symmetries (Rovati et al., 2003). Referring to a linearly elastic anisotropic solid, defined by an elasticity tensor with components $\boldsymbol{C}_{ijhk}$, subjected to a constant strain state characterized by given principal strains, this goal can be achieved by answering to the following questions: (a) which conditions must be satisfied by the stress and the strain fields to make the strain energy density stationary, and (b) which are explicitly the corresponding mutual orientations of the strain and the elasticity tensors that satisfy these conditions?
The answer to the first question is partially known. The results obtained up to now, which will be briefly reviewed later, concern essentially the determination of qualitative conditions to be satisfied by absolute maxima and minima for the strain energy density, and the number of such critical points. The problem of the explicit evaluation of the orientations corresponding to all the stationarity values of the strain energy density has only partially been solved. On the last point in following section it is widely explained a procedure proposed by Rovati et al. (2003), where for some classes of anisotropy (namely, tetragonal system, transverse isotropy and cubic symmetry) all the orientations of the principal directions of strain to the material symmetry axes at the critical points are found and discussed.

5.8.2. State of the Art

Pioneering works where extreme values of the strain energy density in anisotropic bodies are sought are those by Banichuk (1981, 1983). Here, the

problem of simultaneously evaluating the most efficient shapes for anisotropic rods in torsion and the orientation of the anisotropy axes which minimize the structural compliance is dealt with. The problem of defining the local values of the elastic coefficients, with fixed directions of material axes, which minimize the energy density is also considered in plane elasticity. These results have been extended in Banichuk and Kobelev (1987) to the case of ideally elastic-plastic solids. Anisotropic plates with variable elastic moduli and material axes orientation have been also studied by Kartvelishvili and Kobelev (1984), referring to optimal design for compliance and natural vibrational frequency.
Beside these structural formulations, the study of the best positioning of elastic symmetry planes in three-dimensional orthotropic bodies for minimum potential energy of deformation has been carried out in a general way in Seregin and Troitskii (1981). In this work, through the application of the Lagrangian multipliers method, it is shown that the solution is locally characterized by a mechanically meaningful condition, that is, *coaxiality of the stress and strain tensors*. Contrary to isotropic elasticity, where the strain and stress tensors are always coaxial, in anisotropic elasticity this feature is, in general, lost. The non-trivial result obtained by Seregin and Troitskii emphasizes a requirement that must always be fulfilled when extreme values of the global stiffness are sought; consequently, it should be assumed as a guidance for an optimal spatial arrangement of the material symmetry axes.
Later, but independently, the same problem has been dealt with in Rovati and Taliercio (1991, 1993) where orientations of the material symmetry axes which maximize or minimize the global elastic stiffness of a general1y anisotropic three-dimensional continuum are sought. Necessary stationarity conditions for the strain energy density are directly computed, assuming the strain state to be given, and their mechanical interpretation (that is, collinearity of principal directions of stress and strain) is highlighted. Some closed form solutions for cubic and transversely isotropic materials are found, and a material parameter, responsible of the relative shear stiffness of the solid, is introduced. It is shown how two classes of solutions can be defined according to its value: one, where stationarity of the strain energy density is accompanied by full collinearity of principal directions of stress, strain and material axes; the other one, where this collinearity is only partially preserved.
Due to pertinence to practical applications, much effort has been devoted to two-dimensional solids. In particular, the elastic problem previously described has been reformulated for plane elasticity in Sacchi Landriani and Rovati (1991), and conditions for absolute maximum and minimum structural stiffness are found; an extension to plates in bending is given as well. Careful investigations in this direction should be mentioned, such as those given by Pedersen (1989), where it is found that the best orientations of the material axes depend on a dimensionless material parameter, plus the ratio of the two principal strains. Coaxiality of the material axes and the principal strain directions always

corresponds to stationary values for the energy density (trivial solutions); however, in some strain conditions, stationarity can also be achieved at some non-trivial orientations. In addition to these considerations referred to any material point, analyses are also carried out for the whole solid (Pedersen, 1990), through applications of sensitivity analysis, finite element analysis, and optimization procedures. Homogenization techniques, coupled with finite element analyses and design for optimal structural performances, have led to the very effective method of topology optimization (Eschenauer and Olhoff, 2001).
A modern formulation of the problem of finding the best orientations of the material symmetry axes in a three-dimensional continuum is given by Banichuk (1996), where the application of spectral methods of tensor analysis makes it possible to clarify general features of the problem itself, and to discuss some qualitative properties. Further accounts on spectral decomposition of the anisotropic elasticity tensor can be found in Sutcliffe (1992) and Theocaris and Sokolis (2000). Banichuk deals with several problems, such as minimization of the compliance functional, the dynamic stiffness and the distortion energy. These problems are then generalized to the case of bodies consisting of several anisotropic phases; accordingly, the medium is represented as a polycrystalline aggregate.
The problem of extremizing the strain energy density by varying the mutual orientation of a fixed stress state to the material symmetry axes (regardless of the considered symmetry class) has also been developed by Cowin (1994). After showing that the stress and strain tensors commute at the stationarity (or critical) points of the strain energy, Cowin looks for absolute maxima and minima of the energy in a subset of orientations at which the gradient of the strain energy density vanishes respect to a second-order orthogonal tensor, representing the coordinate transformation. It is shown that the symmetry coordinate system of cubic symmetry is the only situation in linear anisotropic elasticity for which a strain energy density *extremum* can exist for all stress states. The stationarity conditions for materials with other symmetries depend on the given stress state. In particular, the conditions for the energy *extrema* for transversely isotropic and orthotropic solids are found for uniaxial stress states. In Vianello (1996a) and Sgarra and Vianello (1997a,b) attention is paid to showing the *existence* of rotations of the material axes with respect to the principal directions of strain, at which the energy density is stationary. By means of Weierstrass' theorem the existence of at least two such rotations is proved, which parametrically depend on the strain tensor for any material symmetry. At a first glance, this result seems to contradict the statement given in Cowin (1994); nevertheless, the difference with Cowin's formulation is that here the elastic symmetry is held fixed for a *specific* strain state, whereas in Cowin (1994) a *general* state is considered. This difference is exhaustively clarified in Cowin (1997). The extension to finite anisotropic elasticity is tackled by Blume (1994). and Vianello (1996b), where the properties of the *extrema* are shown to be the same as in the linear case. Further developments in this direction concern the problem

of extremizing the strain energy density, with respect to both the orientation of the anisotropy axes and the type of material symmetry (Cowin and Yang, 2000), for a given, but arbitrary, stress state. This formulation reveals a strict connection with analogous problems concerning the generation of optimal topologies (Eschenauer and Olhoff, 2001), where it is essentially the microstructure of the solid that plays the role of design variable.
Finally, it is interesting to notice that the previously illustrated problems spontaneously arise not only in the study of the behaviour of man-made materials, but also in the mechanics of living tissues. For instance, Fyhrie and Carter (1986) develop a relationship between cancellous bone apparent density, trabecular orientation and applied stress, assuming the bone to be an orthotropic, self-optimizing material. It is shown that the trajectories of the material axes and the apparent density can be described by a unifying minimization principle involving a quadratic functional, similar to the strain energy density, and a purely quadratic Tsai-Wu failure criterion. The results predict the alignment of the material axes to the principal stress directions, in agreement with the previously reviewed results. Mechanisms of local changes in anisotropic properties, that more efficiently allow the living bone to carry the loads, are shown in Cowin (1987, 1995). These results suggest that .the bone is designed by nature to have the greatest stiffness in axial direction and the greatest impact load resistance in the transverse one. The intimate relationship between trabecular architecture of cancellous bone and mechanics is also described by Odgaard et al. (1997).

5.8.3. Topology Optimization Problems for Anisotropic Media

Minimization of the strain energy density plays a crucial role in problems related to the optimization of composites where stiffer properties are needed through the topology rearrangement of the material microstructure (Cowin, 2007; Rovati et al. 2003). Differently from the isotropic case, in elastic anisotropic media the strain energy density changes when any material element is rotated with respect to the principal directions of stress or strain: this requires that the local orientation of the material axes should be employed as design variable in a full TO problem. Living tissues seem to actually exploit this strategy when they adjust their material microstructure (Cowin, 2007; Luo et al.) to achieve, at different scale levels, enhanced mechanical performances and, recently, the same strategy has been artificially introduced for designing man-made materials (Van der Zwaag, 2007).
From the mathematical standpoint, minimize the strain energy means to analyze stationarity properties of the functional and thus finding its critical points. The local orientation of the anisotropy axes is then assumed to be varying from a point to another through the body, and it must be taken as a variable of the

problem. To make this, by explicitly following the approach by Rovati and Taliercio (2003), let us introduce the positive definite strain energy density at a generic point of the anisotropic elastic material as follows:

$$\Psi = \frac{1}{2}\boldsymbol{T} : \boldsymbol{E} = \frac{1}{2}(\mathbb{C} : \boldsymbol{E}) : \boldsymbol{E} > 0, \quad \{\forall \boldsymbol{E} \neq \boldsymbol{0}, \quad C_{ijhk} = C_{hkij} = C_{jihk} = C_{ijkh}\} \quad (5.17)$$

where $C_{ijhk} = [\mathbb{C}]_{ijhk}$ and no restriction on the type of elastic anisotropy is made. However, when the material symmetry axes are locally rotated at any point of the body with respect to an arbitrarily fixed reference frame, any change in the strain energy must be ruled by the equation:

$$\Psi = \frac{1}{2} C_{ijhk} E_{ij} E_{hk} = \frac{1}{2} Q_{im}\, Q_{jn}\, Q_{hp}\, Q_{kq}\, C^{\measuredangle}_{mnpq} E_{ij} E_{hk} \quad (5.18)$$

in which $[\mathbb{C}^{\measuredangle}]_{mnpq} = C^{\measuredangle}_{mnpq}$ are the Cartesian components of the elasticity tensor in its preferred reference system (i.e. the local material symmetry reference frame) and $[\boldsymbol{Q}]_{ij} = Q_{ij}$ represent the usual components of the proper orthogonal tensor, $\boldsymbol{Q}^T = \boldsymbol{Q}^{-1}$, rotating the material axes with respect to the arbitrary system, say – without loss of generality – the system locally coaxial with the principal directions of strain. Then, in order to find critical points for the strain energy density ψ, it is possible to search the stationarity of the following Lagrangian function, $\mathcal{L}$, written as:

$$\mathcal{L} = \mathcal{L}(\boldsymbol{Q}, \boldsymbol{\Lambda}) = \frac{1}{2} C_{ijhk} E_{ij} E_{hk} - \Lambda_{ij} (Q_{ik}\, Q_{jk} - \delta_{ij}) \quad (5.19)$$

where $[\boldsymbol{\Lambda}] = \Lambda_{ij}$ are the components of a symmetric second-rank tensor, $\boldsymbol{\Lambda}$, here utilized as tensor lagrangian multiplier to be used for establishing the orthogonality constraint $\boldsymbol{Q}^T = \boldsymbol{Q}^{-1}$. In fact, stationarity of the functional (5.19) with respect to Λ_{ij} restores the orthogonality condition, while stationarity with respect to the variables Q_{ij}, responsible for the orientation of the anisotropy axes, gives:

$$\frac{\partial \mathcal{L}}{\partial Q_{rs}} = 0 \quad \Rightarrow \quad C^{\measuredangle}_{mspq}\, Q_{im}\, Q_{hp}\, Q_{kq}\, E_{ir} E_{hk} - \Lambda_{rj}\, Q_{js} = 0 \quad (5.20)$$

By means of some algebraic manipulations, the eq. (5.20) finally allows to find:

$$T_{ik} E_{ir} = \Lambda_{rk} \quad \Rightarrow \quad \boldsymbol{T}\,\boldsymbol{E} = \boldsymbol{E}\,\boldsymbol{T} \quad (5.21)$$

where the relations among the elasticity coefficients in (5.18) and the symmetries of stress, strain and $\boldsymbol{\Lambda}$ have been taken into account. The commutativity condition (5.21) implies that the stationarity points of the strain energy can be found when $\boldsymbol{T}$ and $\boldsymbol{E}$ share the same eigenvectors: this is always true in isotropic elasticity, and only applies to anisotropic media characterized by tetragonal, hexagonal and cubic material symmetries, if additional conditions are fulfilled in terms of coaxiality between principal stress, strain and material symmetry axes. On the basis of the above illustrated results, it can be then inferred that analytical models able to describe orthotropic elastic material symmetries due to the local orientation of the microstructure through fabric tensors can be helpfully employed to construct topology optimization strategies for heterogeneous media, identifying both volume fraction and fabric tensors with TO design variables. Accordingly, the most important mathematical steps to find optimal microstructure orientation in heterogeneous media are described below. By making reference to the work by Luo and An (1998) and coherently with the notation previously introduced, let us consider the complementary strain energy, $\mathcal{E}_c$, of a linearly elastic anisotropic heterogeneous materials as follows:

$$\mathcal{E}_c = \int_\Omega \Psi_c \, d\Omega, \qquad \Psi_c = \frac{1}{2}(\mathbb{S}^{\text{hom}} : \boldsymbol{T}) : \boldsymbol{T} \tag{5.22}$$

where Ψ_c is the complementary strain energy density and $\mathbb{S}^{\text{hom}}$ is the overall compliance elasticity tensor assumed in the form:

$$\begin{aligned}
&\mathbb{S}^{\text{hom}} \equiv \frac{\partial^2 \Psi_c(\boldsymbol{T}, \rho, \boldsymbol{M})}{\partial \boldsymbol{T}^2} \equiv \rho^{-p}\, \overline{\mathbb{S}}^{\text{hom}}, \\
&\overline{\mathbb{S}}^{\text{hom}} = k_1 \boldsymbol{I} \otimes \boldsymbol{I} + k_2 \boldsymbol{I} \underline{\overline{\otimes}} \boldsymbol{I} + k_3 \boldsymbol{M} \otimes \boldsymbol{M} + k_4 (\boldsymbol{M} \underline{\overline{\otimes}} \boldsymbol{I} + \boldsymbol{I} \underline{\overline{\otimes}} \boldsymbol{M}) + \\
&\quad + k_5 \boldsymbol{M}^2 \otimes \boldsymbol{M}^2 + k_6 \boldsymbol{M} \underline{\overline{\otimes}} \boldsymbol{M} + k_7 (\boldsymbol{I} \otimes \boldsymbol{M} + \boldsymbol{M} \otimes \boldsymbol{I}) + \\
&\quad + k_8 (\boldsymbol{M} \otimes \boldsymbol{M}^2 + \boldsymbol{M}^2 \otimes \boldsymbol{M}) + k_9 (\boldsymbol{I} \otimes \boldsymbol{M}^2 + \boldsymbol{M}^2 \otimes \boldsymbol{I})
\end{aligned} \tag{5.23}$$

where $\boldsymbol{M}$ is the fabric tensor, $\rho(\boldsymbol{x})$ is the volume fraction, p a positive penalization power and k_i are coefficients to be determined. With reference to the TO problem (5.1), two constraints have been imposed on $\rho(\boldsymbol{x})$, the first one being:

$$\int_\Omega \rho(\boldsymbol{x}) \, d\Omega = \text{Vol}(\Omega^{\text{opt}}) \tag{5.24}$$

and the second one written as:

$$0 < \rho \le 1 \qquad \Rightarrow \qquad \{1 - \rho = a^2, \quad \rho = b^2\} \tag{5.25}$$

where the inequality representing the physical admissible values for the volume fraction is converted into equalities by introducing the real slack variables a and b. Therefore, the augmented objective function, $\mathcal{E}_c^*$, can be formulated as:

$$\mathcal{E}_c^* = \mathcal{E}_c + \lambda\left(\int_\Omega \rho(\boldsymbol{x})\, d\Omega - \mathrm{Vol}(\Omega^{\mathrm{opt}})\right) + \int_\Omega [\alpha(a^2 + \rho - 1) + \beta(b^2 - \rho)]\, d\Omega \quad (5.26)$$

where $\{\alpha, \beta, \lambda\}$ are Lagrangian multipliers. It is possible to prove that stationarity of (5.26) finally leads to the following equations (Luo, 1998):

$$\begin{aligned} & T_{ij}T_{hk}\frac{\partial \overline{S}^{\mathrm{hom}}_{ijhk}}{\partial M_{mn}} = 0, && [\overline{\mathbb{S}}^{\mathrm{hom}}]_{ijhk} = \overline{S}^{\mathrm{hom}}_{ijhk} \\ & -\frac{p}{2\rho^{p+1}} T_{ij}T_{hk}\overline{S}^{\mathrm{hom}}_{ijhk} + \lambda = 0, && \forall \rho < 1 \\ & \rho = 1, && if \quad \rho = 1 \end{aligned} \quad (5.27)$$

The TO problem can be thus formally solved by putting together the eqs. (5.27) with the 15 classical elasticity field equations, the density constraint (5.24), a normalization condition on the first invariant of $\boldsymbol{M}$ (i.e. $tr\,\boldsymbol{M} = 1$) and the boundary conditions, the 23 unknowns being constituted by six stresses, six strains, three displacement components, the volume fraction ρ, the Lagrangian multiplier λ and the six components, $[\boldsymbol{M}]_{ij} = M_{ij}$, defining the symmetrical fabric tensor.

REFERENCES

Ambrosio L, Buttazzo G. 1993. An optimal design problem with perimeter penalization. Calculus and Variation. 1: 55-69

Banichuk NV. 1981. Optimization problems for elastic anisotropic bodies. Archives of Mechanics. 33: 347-363.

Banichuk NV. 1983. Problems and Methods in Optimal Structural Design. Plenum Press.

Banichuk NV, Kobelev VV. 1987. On optimal plastic anisotropy. Prikladnaja Matematika I Mekanika. 51: 489-495. Traslated in: Journal of Applied Mathematics and Mechanics. 51: 381-385.

Banichuk NV. 1996. Optimization of anisotropic properties for continuum bodies and structural elements using spectral methods of tensor analysis. Mechanics of structure and Machines. 24: 71-87.

Beckers M. 1999. Topology optimization using a dual method with discrete variables. Structural Optimization. 17: 14-24.

Bendsøe MP. 1983. G-closure and homogenization problems arising in plate optimization. Optimization Methods in Structural Design. HA Eschenauer & Olhoff eds. 270-275.

Bendsøe MP. 1983. On obtaining a solution to optimization problems for solid elastic plates by restriction of the design space. J. Struct. Mech. 11: 501-521.

Bendsøe MP, Kikuchi N. 1988. Generating Optimal Topologies in Structural Design Using a Homogenization Method. Computer Methods in Applied Mechanics and Engineering. 71: 197-224.

Bendsøe MP. 1989. Optimal shape design as a material distribution problem. Struct. Optim. 1: 193-202.

Bendsøe MP, Diaz AR. 1994. Optimization of material properties for improved frequency response. Struct. Optim. 7: 138-140.

Bendsøe MP. 1995. Optimization of Structural Topology Shape and Material. Springer Verlag

Bendsøe MP, Sigmund O. 1999. Material interpolation schemes in topology optimization. Archive of Applied Mechanics. 69: 635-654.

Blume JA. 1994. Elastic materials with coincident principal stress and strain axes. Journal of Elasticity. 35: 275-280.

Chenais D. 1975. On the existence of a solution in a domain identification problem. J. Math. Anal. Appl. 52: 189-289.

Cheng G, Olhoff N. 1981. An investigation concerning optimal design of solid elastic plates. Int. J. Solids Struct. 16: 305-323.

Cinquini C, Rovati M. 1995. Optimization methods in (structural) engeneering. European Journal of Mechanics A/Solids. 14: 413-437.

Cowin SC. 1987. Torsion of cylinders with shape intrinsic orthotropy. J. Appl. Mech. 109: 778-782.

Cowin, S.C., 1994. Optimization of the strain energy density in linear anisotropic elasticity. Journal of Elasticity 34: 45-68.

Cowin SC. 1995. On the minimization and maximization of the strain energy density in cortical bone tissue. Journal of Biomechanics. 28: 445-447.

Cowin SC. 1997. Remarks on coaxiality of strain and stress in anisotropic elasticity. Journal of Elasticity. 47: 83-84.

Cowin SC. Yang G. 2000. Material symmetry optimization by Kelvin modes. J. Eng. Math. 37: 27-43.

Cowin SC, Doty SB. 2007. Tissue Mechanics. Springer.

Fyhrie DP, Carter DR. 1986. A unifying principle relating stress to trabecular bone morphology. Journal of Orthopaedic Research. 4: 304-317.

Eschenauer HA, Olhoff N. 2001. Topology optimization of continuum structures: a review. Applied Mechanics Review. 4: 331-390.

Goodman J, Kohn RV, Reyna L. 1986. Numerical study of the relaxed variational problem from optimal design. Computer Methods in Applied Mechanics and Engineering. 57:107-127.

Haber RB, Jog CS, Bendsøe MP. 1996. A new approach to variable-topology shape design using a constraint on the perimeter. Structural Optimization. 11: 1-11.

Hashin Z, Shtrikman S. 1963. A variational approach to the theory of the elastic behaviour of multiphase materials. J. Mech. Phys. Solids. 11: 127-140.

Kartvelishvili VM, Kobelev VV. 1984. Rational schemes for reinforcing laminar plates from composite materials. Prikladnaja Matematika I Mekanika. 48: 68-80. Traslated in: Journal of Applied Mathematics and Mechanics. 48: 40-49.

Kohn RV, Strang G. 1986. Optimal design and relaxation of variational problems. Communications on Pure and Applied Mechanics. 39: 1-25, 139-182, 353-357.

Jog CS, Haber RB, Bendsøe MP. 1994. Topology design with optimized self-adaptive materials. International Journal for Numerical Methods in Engineering. 37: 1323-1350.

Lurie KA, Cherkaev AV, Fedorov AV. 1982. Regularization of optimal design problems for bars and plates. Journal of Optimization Theory and Applications. 37: 499-522, 523-543.

Luo ZP, An KN. 1998. Journal of Mathematical Biology. 36:557-568.

Michell A J. 1904. The limits of economy in frame structures. Phil. Mag. Sect. 6. 8: 589-597.

Milton GW, Cherkaev A V. 1995. Which elasticity tensor are realizable? J. Eng. Mat. Tech. 117: 483-493.

Mlejnik HP, Schirrmacher R. 1993. An engineering approach to optimal material distribution and shape finding. Comput. Methods Appl. Mech. Eng. 106: 1-26.

Niordson FI. 1983. Optimal design of plates with a constraint on the slope of the thickness function. International Journal of Solids and Strucutures. 19:141-151.

Odgaard A, Kabel J, van Rietbergen B, Dalstra M, Huiskes R. 1997. Fabric and elastic principal directions of cancellous bone are closely related. J. Biomechanics. 30, 5: 487-495.

Pedersen P. 1989. On optimal orientation of orthotropic materials. Struct. Opt. 1: 101-106.

Pedersen P. 1990. Bounds on elastic energy in solids of orthotropic materials. Struct. Opt. 2: 55-62.

Prager W, Rozvany GIN. 1977. Optimization of structural geometry. In: Bednarek AR, Cesari L. eds. Dynamical systems. 265–293. Academic Press.

Ringertz U. 1993. On finding the optimal distribution of material properties. Struct. Optim. 5: 265-267.

Rovati M, Taliercio A. 1991. Optimal orientation of the symmetry axes of orthotropic materials. In: Eschenauer HA, Mattheck C, Olhoff N. Eds. Engineering Optimization in Design Processes. Springer-Verlag, 127-154.

Rovati M, Taliercio A. 1993. Bounds on the elastic strain energy density in 3-D bodies with material symmetries. In: Herskowits J. Ed. Proceedings of Structural Optimization '93. Rio de Janeiro. 353-360.

Rovati M, Taliercio A. 2003. Stationary of the strain energy density for some classes of anisotropic solids. Int. J. of Solids and Structures. 40: 6043-6075.

Rozvany GIN, Zhou M, Sigmund O. 1994. Topology Optimization in Structural Design. In Adeli H ed. Advances in Design Optimization. 340-399..

Rozvany GIN. 2001. Aims, scope, methods, history and unified terminology of computer-aided topology optimization in structural mechanics. Struct Multidisc Optim. 21, 90–108.

Sacchi Landriani G, Rovati M. 1991. Optimal 2-D structures made of composite materials. J. Eng. Materials Technology. Transactions of the ASME. 113: 88-92.

Seregin GA, Troitskii VA. 1981. On the best position of elastic symmetry planes in an orthotropic body. Prikladnaja Matematika i Mekanik.a 45: 185-189. Translated in: J. Appl. Math. Mech. 45: 139-142.

Sgarra C, Vianello M, 1997. Directions of coaxiality between pure strain and stress in linear elasticity. Journal of Elasticity. 46: 263-265.

Sigmund O. 1994. Materials with prescribed constitutive parameters: an inverse homogenization problem. International Journal of Solids and Strucutures. 31: 2313-2329.

Sigmund O. 1994. Design of Material Structures using Topology Optimization. DCAMM Special report S69.

Sigmund O. 1995. Tailoring materials with prescribed elastic properties. Mech. Mat. 20: 351-368.

Sutcliffe S. 1992. Spectral decomposition of the elasticity tensor. Journal of Applied Mechanics. Transactions of the ASME. 59: 762-773.

Theocaris PS, Sokolis DP. 2000. Invariant elastic constants and eigentensors of orthorhombic, tetragonal, hexagonal and cubic crystalline media. Acta Crystallographica Sect. A. 56: 319-331.

Theocaris. PS, Sokolis DP. 2000. Spectral decomposition of the compliance fourth-rank tensor for orthotropic materials. Archives of Applied Mechanic.s 70: 289-306.

Torquato S, Gibiansky LV, Silva MJ, Gibson LJ. 1998. Effective mechanical and transport properties of cellular solids. Int. J. Mech. Sci. 40: 71-82.

Van der Zwaag S. Self Healing Materials 2007. Springer

Vianello M. 1996. Coaxiality of strain and stress in anisotropic linear elasticity. Journal of Elasticity. 42: 283-289.

Vianello M. 1996 Optimization of the stored energy and coaxiality of strain and stress in finite elasticity. Journal of Elasticity. 44: 193-202.

Zhou M, Rozvany GIN. 1991. The COC Algorithm, Part II: Topological geometrical and generalized shape optimization. Comput. Methods Appl. Mechs. Eng. 89: 309-336.

6 TOPOLOGY OPTIMIZATION IN HIP PROSTHESIS DESIGN

Each year, worldwide, over 800,000 total hip arthroplasty (THA) operations are performed. Due to osteoporosis, rheumatoid arthritis and traumatic events, this number is growing as a consequence of the increase of the average age of the population. Also, a significant number of hip replacements in younger people, who generally are more active and therefore impose more frequent and intensive loads to the joint than elderly people, have been registered in the recent years.

Bad implant position or imprecise indexing of the prosthesis can determine aseptic mobilization phenomena that could result in collateral effects in the long period. After hip replacement, a frequent complication may also occur, represented by a mechanical loosening of the implant. This is revealed by implant movement and remodeling of the bone around the prosthesis, bone remodeling being the physiological dynamic response of the bone to the environmental stress level. The gain or loss of bone within the proximal femur when an orthopedic implant is present is the main factor influencing the performance of the prosthesis and therefore its durability.

Although stress shielding remains one of the main factors responsible for loosening in cementless implants, radiographic evidence based on clinical follow-ups reveals that surface treatments and the use of extensively porous-coated total hip

arthroplasties can significantly limit the influence of stress shielding on the longevity of the implant (Engh et al. 2003).

However, failure of osteointegration does occur in femoral revisions performed with extensively porous-coated stems (Hamilton et al. 2008). On the other hand, in cemented implants, failure of the femoral prosthesis component of a total hip replacement system is mainly attributed to failure of the cement–implant interface and cement mantle in cemented systems (Beckenbaugh and Ilstrup 1978; Maloney 2002; Jasty et al. 1991) and a limited role is therefore played by stress shielding phenomena (Harris 1992). To avoid these types of failures, possible new prosthesis profiles can be envisaged by employing, in common design optimization procedures, objective functions that incorporate a measure of the stress in the cement layer surrounding the prosthesis (Yoon et al. 1989) or at the cement–prosthesis interface (Huiskes and Boeklagen 1989; Katoozian and Davy 2000) with the goal of minimizing stress concentration in these areas, minimizing the probability of prosthesis failure and maximizing prosthesis reliability.

However, the choice of computational strategies based on the design optimization leads to a modified shape design of the implant stem (Nicolella et al. 2006; Tanino et al. 2006) and this produces two main disadvantages. The first one is related to the difficulty of determining geometric compatibility between
implant shape and hosting femur. The second one is due to the necessity of completely modifying surgical instrumentations and consolidated techniques.

Other researchers have approached the problem of improving the hip prostheses performance by trying to understand the phenomenon of loosening (e.g., Rietbergen et al. 1993), as well as relating it to prosthesis design (e.g.,Weinans et al. 1992; Huiskes and Rietbergen 1995), by means of optimization of the implant-femur response in terms of optimal bone remodeling at the interfaces. Usually, these models assume the bone-stem interface to be in contact without friction where the stem is not coated and fully bonded where coated.

Actually, this is a correct approach if one considers complete bone ingrowth in the coated zones, and consequently, the interface bone layer supports both shear and traction without failure.

However, the bone remodeling after a total hip arthroplasty is an evolutionary process, i.e., in a post-operative situation, the bone ingrowth does not exist but, if the local mechanical conditions permit, it can appear. Interface conditions and the bone ingrowth process have been studied in several research contributions (e.g.,

Keaveny and Bartel 1995), as well as methods that integrate ingrowth analysis and bone remodeling (Fernandes et al. 2002).

When the prosthesis is introduced into the femur, the new distribution of the stresses induces bone atrophy and therefore bone resorption can appear in regions near to the implant. Indeed, due to the major overall stiffness, the prosthesis absorbs a significant percentage of the forces transmitted at the acetabular level and the stress in the bone reduces with respect to its physiological magnitude, determining stress shielding (Huiskes et al. 1992) and then implant loosening. Bone would receive more load if the stem were eliminated from the implant. This observation has led to the design of stemless implants.

However, Munting and Verhelpen (1995) have claimed that stemless implants are effective only for short-term fixation. Joshi et al. (2000) investigated the possibility of reducing the shielding in a hip prosthesis by modifying geometry and the system of proximal fixation. In another study, hollow geometry has been introduced by increasing stem inner diameter to reduce stress shielding (Gross and Abel, 2001), but the use of simplified cylindrical shape, load and boundary conditions did not furnish reliable quantitative estimates.

Stress shielding can also be decreased if stem is made from a less stiff material which has Young's modulus equal to bone (Morscher and Dick 1983), but a flexible implant may produce higher stresses along the interface (Huiskes et al., 1992), as would occur with any modulus mismatch.

However, the clinical follow-up suggests that one of the crucial features to study in a pre-clinical evaluation of a new prosthetic design is the primary stability of cementless hip prostheses, essential for long-term durability of the implant. The main factors responsible for primary stability are generally recognized in the shear stresses and micromotions occurring at the interface bone-implant. The amount of motion and the interfacial stresses depend on geometrical and mechanical properties of the prostheses.

As a consequence, for initial stability, the accuracy of host bone preparation and the design of the prosthesis are critical (Gotze et al. 2002). Although there is no agreement in literature for the range of acceptable micro-motion at the bone–implant interface, it seems that interface micro-motion around 40 μm gives partial ingrowth, while micro-motion exceeding 150 μm inhibits bone ingrowth completely (Pettersen et al., 2009).

Bone growing into porous-coated areas on the implant, realized by means of surface treatments with hydroxyapatite or titanium plasma

spray, ensures osteointegration and then determines the so-called secondary stability.

Actually, with reference to aseptic loosening of the implant, it is difficult to distinguish among the factors influencing primary and secondary stability. A good initial fixation, and then the success of a THA, is indeed the result of the combination of different interacting and simultaneously in vivo changing factors, whose synergy gives good chance for the implant to achieve initial stability and to preserve it in the long term (Monti et al., 1999).

From the mechanical point of view, the factors influencing the primary stability of the stem depend on biomechanical interaction between femur and prosthesis. Incorrect loading of the implant after surgery can cause excessive interface shear motions and/or bone resorption, leading to implant debonding and mobilization. The term *incorrect* is here utilized to denote any stress level exceeding a prescribed threshold (for example, the limit shear stress at the bone-implant interface) or below a minimum stress magnitude, necessary to retain a pre-THA physiological stress level in bone and avoiding stress shielding. Then, with the aim of improving primary stability in hip prostheses, we treat the femoral stem as a material to optimize over its volume by locally penalizing the implant stiffness through an updated mass density distribution. The map of the density distribution is obtained by means of an FE topological optimization analysis. By improving the prosthesis-bone stiffness ratio, a higher stress level is reached within the proximal and distal femur regions and, as a consequence, a reduction of stress shielding is obtained.

6.1. ARTHROSIS

Arthrosis is a chronic degenerative disease of the joints related to the degeneration of articular cartilage with a subsequent change in the bony articular surfaces, the development of marginal osteophytes, deformation of the joint, and the development of moderate synovitis. Arthrosis is among the most ancient human and animal diseases. Paleontological studies have found arthrosis in animals and humans from the Stone Age. It is a widespread form of articular pathology seen in 10-12% of the population. The disease correlates with age developing more frequently after 30–35 and seen in 97% of people over 60. Arthrosis appears with the same frequency in men and women with the exception of arthrosis of the interphalangeal joints of the hand, which is seen 10 times more frequently in women. According to information from European and US rheumatologists, this disease makes up 69-70% of all rheumatic diseases.

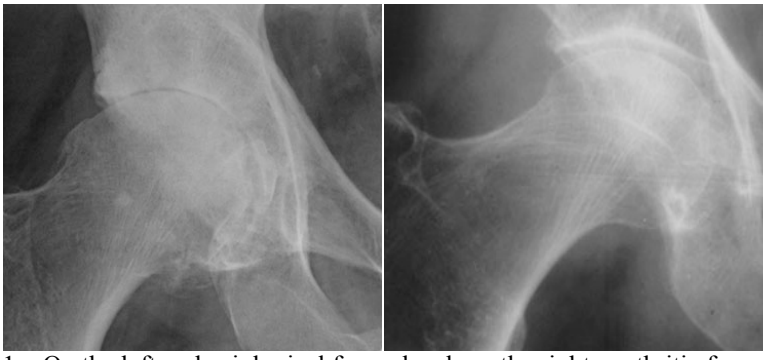

Fig. 6.1 – On the left a physiological femur head; on the right a arthritic femur head

6.2. TOTAL HIP ARTHROPLASTY: A BRIEF HISTORY

During the last century multiple choice of replacing the hip articulation have been tried. From the first pioneer attemps performed by the orthopaedic doctors Smith and Peterson whose objective was the resurfacing of the femur head by means of a metallic cup to the first modular prosthesis proposed by Sir Charnley after the second world war till the modern age when material and manufacturing processes reach high level of performances.
A first hip prosthesis classification is due to the type of fixation inside the femur; the hip implants are usually divided in cemented and cementedless (press-fit), anatomic and revision.

Fig. 6.2 – On the left all the parts componing an hip prosthesis
(stem, head, liner and acetabular cup); on right the assembled hip prosthesis

In order to fix the stem of the prosthesis inside the femur a poly(methyl methacrylate) (PMMA) is utilized. The cementless stem guarantee the primary fixation due to the geometric constraints by means of a press-fit double wedge

situated in proximal part of the stem. Moreover, the proximal surface treatment by means of coating of HydroxyApatite or Titanium Plasma Spray ensure the secondary stability due to osteo-integration. The materials usually utilized are: titanium or stainless alloy for the stem; Co-Cr alloy, ceramics for the head; Ultra High Molecolar Weight Poly-etilene (UHMWPE) and ceramic for the liner; titanium or stainless alloy for the acetabular cup. Finally the head-liner coupling is usually Co-Cr with UHMWPE, ceramic with UHMWPE, ceramic with ceramic; all these couplings are oriented to minimize the wear production during the usual prosthesis life-time. Even if the manufacturing processes and the materials technology improve their quality day by day, a great amount of implant failures happens every year. The following Fig. 6.3 shows a large variety of explanted prostheses.

Fig. 6.3 – A large variety of expianted prostheses

6.3. MODELING FEMUR: MATERIAL PROPERTIES

Considerable attention has been given to the construction of the FE model. Faithful reproductions of actual geometries of the bone and implant were created. Accurate mechanical properties of the materials involved in the analyses and physiological boundary conditions were determined. These efforts were made to insure reliable qualitative and quantitative numerical results. For example, the accuracy in the three-dimensional reconstruction of geometry and mechanical properties of the femur was obtained by direct quantitative computed tomography (QCT) acquisition. This instrumental diagnosis is based on Digital Imaging and Communication in Medicine (DICOM), a standard file format including patient, hospital and instrumentation data. Also contains geometric data about the patient position and densitometric data about the absorption of the X-Ray into the medium. Deeper information will be given in the next chapter. In order to construct the computational FE model, a human femur was scanned by QCT. The QCT scanned the bone along 1mm separated parallel planes and

created 512×512 bitmap images recording the levels of material density. QCT gives density levels in terms of Hounsfield Units (HU), as a function of the X-ray attenuation into the examined material. This information, as well as the image size, is archived in DICOM standard format file. By utilizing the commercial software Mimics®, the density data in terms of Hounsfield Unit (HU) related to the bone have been filtered, polylines have been generated and finally exported to the software Ansys®; a tipical Mimics® window is illustrated in fhe following Fig. 6.4:

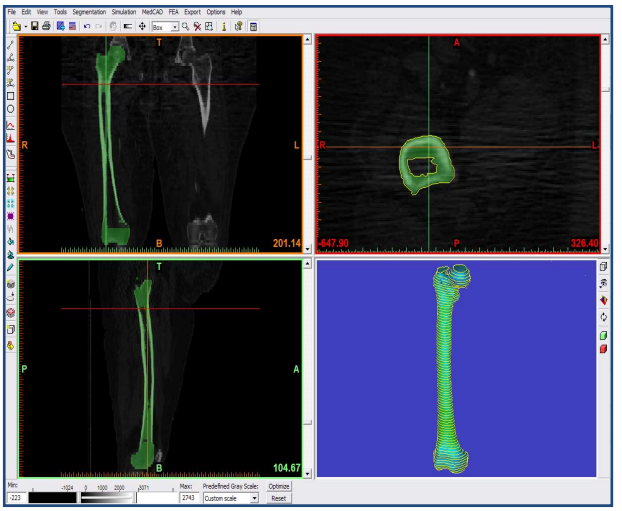

Fig. 6.4 – Polylines from femur filtering density in the range of bone (200-1200 HU)

In Ansys® environment, starting from the imported polylines, the volume of the femur has been created and then meshed.

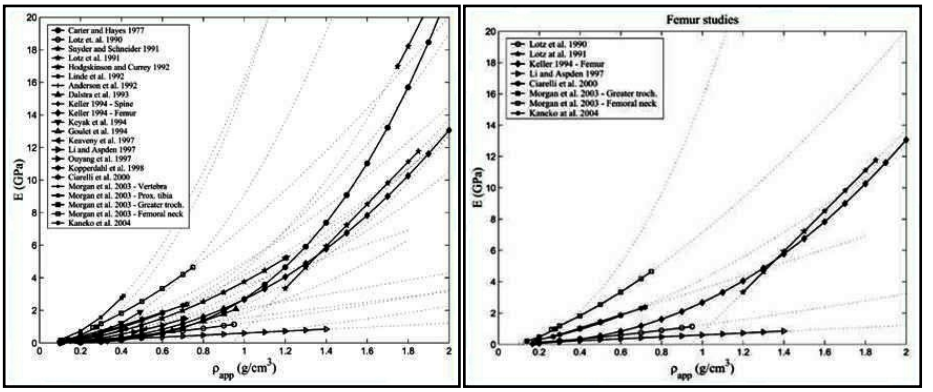

Fig. 6.5 – On the right Young's moduli versus apparent wet density for all human body site; Young's moduli versus apparent wet density for human femur (Helgason et al., 2008)

In order to mechanical characterize the femur volume, the list of elements and nodes has been exported from the software Ansys® to the software Mimics. Finally, each element has been assigned a corresponding elastic modulus by employing the experimentally determined relations of the mechanical properties to the density and CT numbers obtained from literature for human bone (Rho et al. 1995). Indeed, the bone density distribution, with reference to the actual levels of mineralized bone in the trabecular and cortical regions, has been taken into account. As illustrated in Fig. 6.5, Helgason et al. (2208) reviewed all relevant literature on this topic. He included and properly normalized only elasticity-density relationships derived from similarly controlled experiments. The resulting relationships have been grouped according to the most important methodological differences: type of end support during testing, specimen geometry, and anatomical sampling location and some recommendations have been made for the application of elasticity-density relationships to subject-specific finite element studies. With the purpose of identifying density-elasticity relationships suitable for use in subject-specific FE studies, the development of a benchmark study has been also suggestsed. By using the experimental literature tests made on several specimens of trabecular and cortical bone tissues (Rho 1991; Rho et al. 1995), the bone density is converted into material properties, say elastic moduli, using a custom-made algorithm able to relate the HU in output from QCT to corresponding mechanical parameters. The bone cortical regions, selected by means of the HU values, are modeled as transversely isotropic, with in-plane (for example in the plane of the diaphysis cross-section) Young's modulus equal to 17,000 MPa, and the out-plane modulus equal to 22,000 MPa (Turner et al. 1999). Also, we assume isotropy for the spongy bone sites, the spatial variation of the bone density being responsible for the nonhomogenous elastic response. However, the choice of a very fine mesh in the FE-model, see Fig. 6.7, ensures that structural gradients over the RVE are very small because the RVE size is assumed to be coincident with the FE size: this avoids conflicts in terms of the relation between structural gradients and elastic symmetry (Cowin 2002).

6.4. MODELING FEMUR: THE DISCRETIZATION

As shown in the above Fig. 6.6 a model of about 80,000 tetrahedral elements was constructed, from which an FE model of was generated by homogenizing the local material properties over the tetrahedral element volumes. Elements refining zones are employed where geometry and solutions in terms of stress suggest higher accuracy with a very good accuracy for the description of the inhomogeneous mechanical behaviour of the bone. The intact femur model was first created and then sectioned at the trochanteric level for inserting the implant. The accuracy of the FE model compared with QCT images, in terms of effective

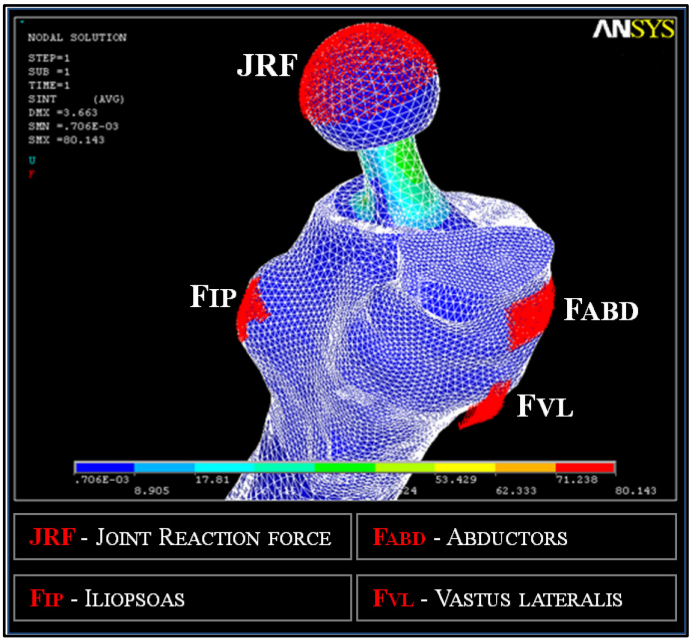

Fig. 6.6 – The final finite element-based model

correspondence of the X-ray density gray levels and density maps obtained by the numerical model, is shown in the following Fig. 6.7.

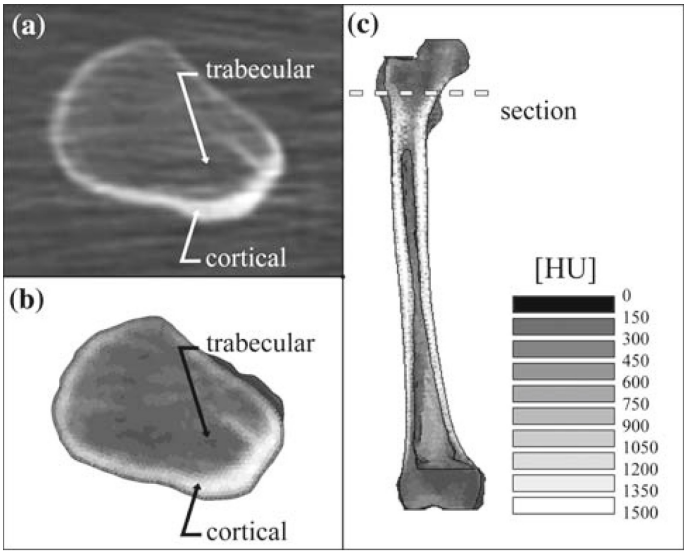

Fig. 6.7 – (a) QCT slice density image at the trochanteric level; (b) gray-scale local density plot of the FE model at the trochanteric level; (c) overall frontal view section of the FE model

The prosthesis (a common cementless Ti-6Al-4V Johnson & Johnson PFC collared stem) was laser scanned, reconstructed by a Computer Aided Design (CAD) system and, then, positioned inside the bone. Its indexing was controlled with reference to the standard surgical protocol.
The elastic properties of the implant are referred to the usual literature values. In particular, the titanium alloy and the CrCo used for the prosthesis head and stem respectively have been modelled as linearly elastic, isotropic and homogeneous with Young's moduli equal to 105 GPa and 210 GPa, in that order, setting 0.3 as the Poisson ratio.

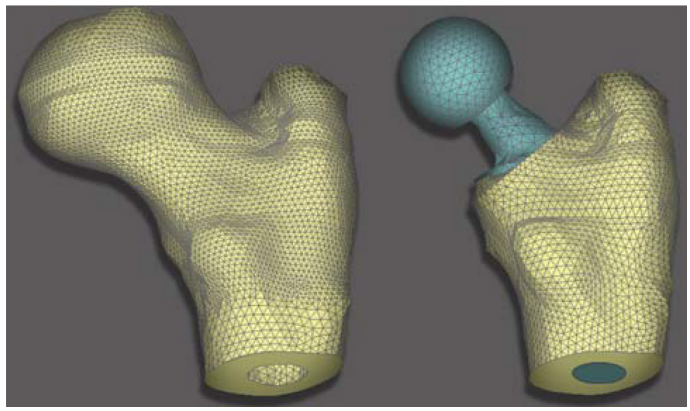

Fig. 6.8 –The three-dimensional reconstruction of the two models. Left: particular of the proximal (intact) femur model and mesh; Right: particular of the proximal femur with implant and mesh

The three-dimensional reconstruction of the two discretized FE models, the intact femur and with the prosthesis, are illustrated in the above Fig. 6.8 where, in order to highlight the accuracy of both the three-dimensional reconstruction and the size of the elements, a detail of the proximal region is shown.

6.5. MODELING FEMUR: LOADS AND CONSTRAINTS

Finally, prescribed loads employed by Simoes et al. (2000), was accomplished to calibrate the numerical model. Simoes et al. (2000) described experiments made on a composite femur monitored with 20 uniaxial strain gauges to determine the response of the bone model under physiological load conditions.
We replicated the force boundary conditions applied to the femur in the experiments of Simoes et al. (2000) in our numerical model taking into account the action of the weight of the patient plus the action of the major muscles, the abductors, the iliopsoas and the vastu lateralis, participating to the standing position, as illustrates in the following Fig. 6.9, where are also listed the directions and the numerical values of the forces acting on the femur.

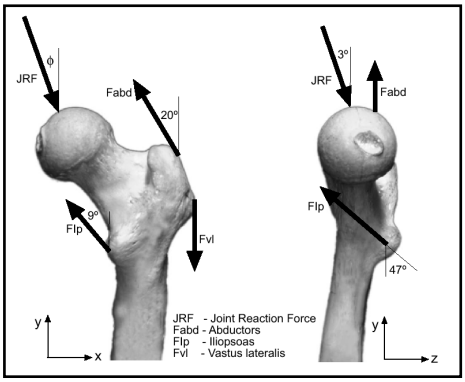

Muscle and joint reaction forces			
	resultant force	angle degree	
	(N)	ϕ	γ
joint reaction force	730	159	7
Abductors	300	20	180
Iliopsoas	188	47	262
vastus lateralis	292	180	-

Fig. 6.9 – Loads conditions applied to the femur taking into account the action of joint reaction force plus abductors, iliopsoas and vastus lateralis muscles.

6.6. TOPOLOGY OPTIMIZATION IN HIP PROSTHESIS DESIGN

6.6.1. Motivation

The basic idea is to use TO for establishing a suitable mass distribution (or arrangement of voids) inside a cementless prosthesis, in order to minimize femur stress-shielding phenomena that are mainly responsible for bone resorption and thus aseptic loosening of the implant. Also, by considering different percentages of prosthesis volume reduction in the maximum stiffness topological optimization analyses, optimal weight and stiffness ratios are determined for reducing stress shielding in both proximal and distal regions, as well as avoiding stress concentrations at the bone–implant interface and inside the optimized prosthesis. As noted above, by improving the prosthesis/bone stiffness ratio, a higher stress level is reached within the proximal and distal femur regions and, as a consequence, a reduction of stress shielding is obtained if the topological optimization is performed over the volume originally occupied by the implant. We chose a grey-scale over a black–white optimization protocol because smooth densities admit the possibility of modeling the removal of material from the original solid domain by making micro-voids (for example, by means of micro-drilling techniques). The point being that the size of the micro-voids could be less than the mesh size (about 1 ÷ 2 mm) that was adopted for the numerical model. This permits the fine-tuning of the prosthesis optimization process. Another rationale that suggests the topological optimization of the prosthesis to obtain a better overall working bone–implant relationship is that maximizing stiffness by means of minimization of the strain energy mimics the biomechanical process, regulated by growth and bone remodeling, in which the

bone tissue is invited to reach its optimal configuration, e.g., remodeling equilibrium (Cowin and Hegedus 1976; Cowin 1994, 1999; Cai et al. 2008; Jang and Kim 2008, 2009; Jang et al. 2009). In this optimization process, the mass distribution of the prosthesis is rearranged; thus, the implant would appear to be obeying its own *Wolff's law*. Moreover, the following figure 6.10 illustrates the rearrangement of the trabeculae (on the left) as the normal scenario (on the right) after a topological optimization of the femur where the bone has been modeled as cortical.

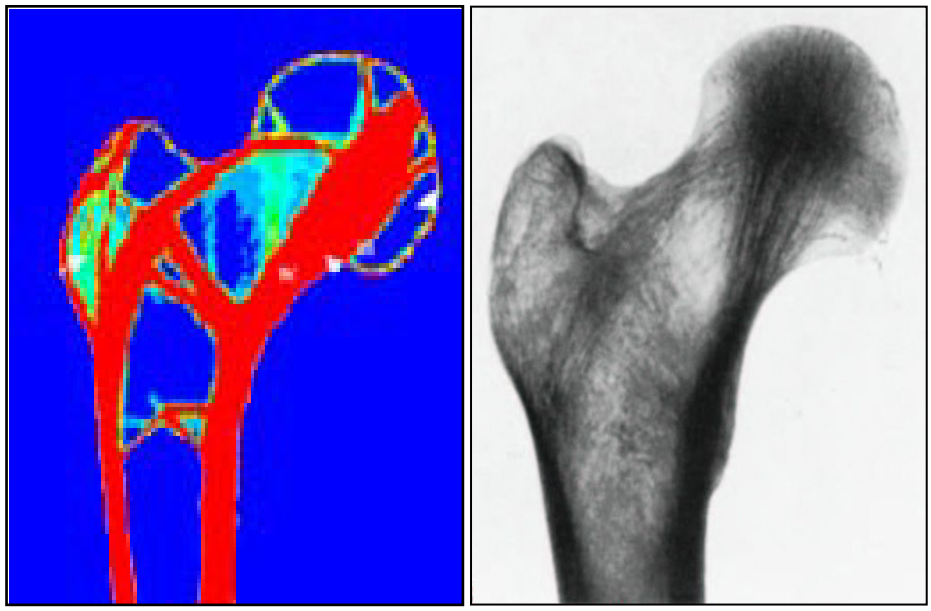

Fig. 6.10 – On the left the rearragment of trabeculae after TO starting from the femur on the right where bone has been modeled as cortical

Huiskes et al. (1987), in order to study the remodeling phenomenon, modeled the microstructure of trabecular bone by means of a fabric tensor, highlighting the behavior of the lamellae and, then, the principal axis of the tensor, oriented in line to the loads applied. Finally, note that, by preserving the integrity of the external shape of the implant, the optimized prosthesis does not require modification of production processes, implanting instrumentation and consolidated surgical procedures. Also, all the surface treatments designed for the femoral stems to promote bone ingrowth and then osteointegration could still be preserved without any conflict with the features needed for the topological optimized implant (Luo et al. 1999; Fernandes et al. 2002).

6.6.2. Non linear FE Analises

Three significant FE analyses have been performed.

The first one was related to the intact femur. This case is studied both for verifying the accuracy of the model and for obtaining results to use as yardsticks for establishing differences in terms of stress distributions in comparison with other analyses where the prosthesis is inserted in the femur. The second study case, named "0", is the one in which the THA is simulated. This is a static analysis performed for the femur with the implant; this is accomplished for two cases, the case of a perfect bond and the case of contact with friction interface conditions. The results of these cases are utilized for estimating stress concentrations and stress shielding in bone in a usual THA situation and are accomplished in the absence of an optimization procedure. The last case treats the topological optimization (maximum stiffness with volume reduction constraints) of the prosthesis, by exploring four different optimization scenarios, that is the scenario "1", where the sole interior of the prosthesis is optimized (e.g., the elements opened onto the boundary of both the prosthesis head and the stem preserve their original mass), the scenario "2", in which the interior of the stem is optimized and the implant head is fully optimized, the scenario "3", representing the case where the stem is fully optimized, while the sole interior of the head is optimized, and finally, the scenario "4", in which the whole prosthesis is optimized. Also, in order to investigate a sufficiently wide range of possible mass configurations inside the optimized implants, for each scenario, the optimized distribution of mass inside the femoral stem model is obtained by imposing four different mass reduction percentages, that is, 55, 65, 75 and 85%. The lower (55%) and upper (85%) selected percentages of volume reduction employed in the topological optimization analyses represent – to a good approximation – the percentages whose corresponding prosthesis volume fractions are 45 and 15%, respectively. These percentages, if homogeneously distributed over the implant domain, would give the equivalent (upper) cortical and (lower) cancellous bone overall stiffness, respectively. These values provide a sufficiently wide and physically reasonable range of possible prosthesis mass reduction. This result is consistent with one of the objectives of this work, namely to reduce the difference between bone and implant stiffness. This result may be verified with mathematical ease if the topological optimization routine is employed with a power law penalization power equal to three to relate Young's modulus to the volume fraction.

6.6.3. Results: Stress Shielding Index

The first analysis was performed for the intact femur. The results in terms of stresses suggest a good accuracy of the numerical model and therefore the effectiveness of employing both a faithful three-dimensional reconstruction of the femur and the elastic non-homogeneity obtained by translating the density map into corresponding material properties. We note that the vector plot of the

principal stresses looks like the trabecular arrangement in the real femur. Also, the magnitude of the stresses never reaches the compressive and tensile yield stresses determined locally by the bone density. In addition, the results obtained in our analysis show that the application of more realistic boundary conditions to the femur model leads to a reduction of bending in the bone and to a more uniform strain distribution, in agreement with the results revealed in experimental, strain gauged, femoral tests by Simoes et al. (2000). Thus, due to this accord and to the accuracy of the numerical model, the results mentioned above have been utilized as reference values (for example in terms of von Mises stresses) for estimating deviations from the physiological stress distribution in the cases where the prosthesis is introduced, for the situations where the implant is optimized and when it is not. The second FE analysis was executed on the femur with an implant, a common cementless titanium alloy collared straight stem. This analysis considered both perfect bond and contact with friction conditions at the interface bone-prosthesis. Several non-linear static analyses were performed in order to investigate the possible influence of friction on the results. As we noted above, friction was considered variable within the range (0, 0.3). However, no significant stress differences were registered between the perfect bond and the contact with friction cases, except for very low friction values (≈ 0). The results show some typical femoral regions where stress shielding actually produces resorption, consistent with those regions revealed by X-rays of post-surgery implantation cases. In particular, part of the great trochanter and some distal cortical areas of the diaphysis exhibit a significant decrease of the vonMises stress, in comparison with the same stress measure read on the corresponding elements of the intact femur. Indeed, to estimate the effect of the prosthesis on the stress distribution in the bone, the von Mises stress, calculated at the centroid of each element, was chosen as the base line.

Rigorously speaking, von Mises stress could be not exactly the most relevant measure of mechanical stimulus in anisotropic, and therefore we should not assume that resorption depends on it. However, this is a relatively convenient, scalar measure of a stress at a point. In addition, a study by Terrier et al. (1997) confirms that bone adaption models using strain energy density and the von Mises criterion give very similar results. With reference to the FE analyses where (maximum stiffness) topological optimization of the implant was evaluated, for different percentages in mass reduction (55, 65, 75, 85%) and for different positioning of the material mass to be optimized (cases “1”, “2”, “3” and “4”), the results were collected and presented as follows. The difference in stress for each element before and after THA was calculated and divided by the stress occurring in the element pre-THA to determine a *Stress Shielding Increase*, (SSI), for that region. The before and after ratios were then volume-averaged over a specific region to calculate SSI for that region. Since the von Mises stress is strictly non-negative, positive stress difference values indicate decrease of the stress level in post-THA situation, therefore, stress shielding.

The explicit expression for SSI is the following:

$$\mathrm{SSI} = \frac{\left\langle \sigma_{VMS}^{pre-THA} \right\rangle - \left\langle \sigma_{VMS}^{THA} \right\rangle}{\left\langle \sigma_{VMS}^{pre-THA} \right\rangle}$$

where $\sigma_{VMS}^{pre-THA}$ is the von Mises stress in the intact femur, σ_{VMS}^{THA} is the von Mises stress in the femur where the implant is introduced, all quantities averaged over the selected volume elements. Vanishing SSI means vanishing stress shielding and indicates an optimal condition. On the contrary, negative values of the SSI indicate an increase of stress when the prosthesis is present and thus they can be interpreted as a measure of stress concentrations, especially, if the actual stress in the bone exceeds yield strength or physiological-based thresholds. Increase of stress shielding (SSI), measured as a ratio between the difference of von Mises stress in the intact and implanted femur and von Mises stress within the intact femur, all quantities being averaged over the element volumes corresponding to the trochanter and diaphysis model regions, are represented. Note that, in comparison with the case "0" where the prosthesis is not optimized, the mean reduction in stress shielding is increasing with the effective mass reduction percentage of the implant and the gain in decrease of stress shielding reaches about 85% (SSI of 15%) for the great trochanter, and up to 99% (SSI less than 1%) for the diaphysis.

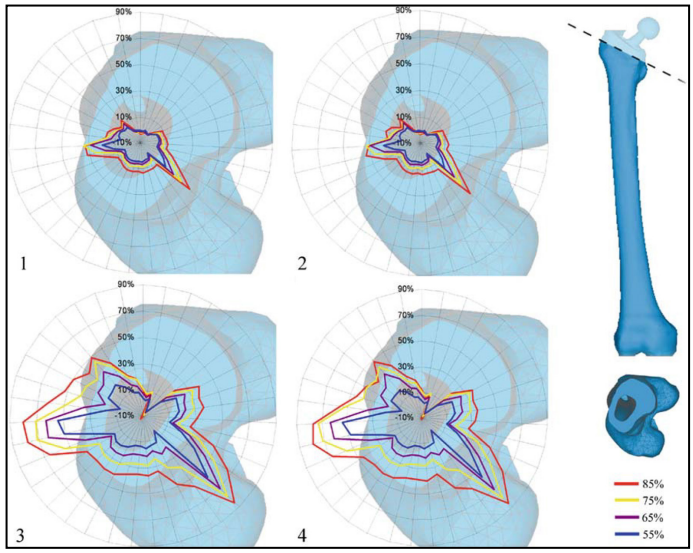

Fig. 6.11 – Polar diagrams show the results of the topological optimization in terms of SSI index at the trochanter level (around the prosthesis) in the 4 cases in terms of percentages.

The previous Figure 6.11 consists of four polar diagrams representing a ratio of the von Mises stresses in these two cases; these ratios are evaluated over a ring

of elements placed at the trochanter level, around the implant, where usually stress shielding phenomena appear. In particular, the polar diagrams show the results of the topological optimization in terms of a ratio between the difference of von Mises stress placed at the trochanter level (around the prosthesis) and von Mises stress in the same elements of the femur with non-optimized implant, and von Mises stress of the femur with non-optimized implant. This estimate differs from the SSI measure as it is calculated at the centroid of each selected element (no overall average on the whole set of elements), comparing the stress shielding in the case where the prosthesis is not optimized (standard case "0") with the results for optimized implants at different prosthesis mass reduction percentages.
It is worthwhile to note that the results show that the von Mises stresses in the femur with optimized implant are 90% greater than the corresponding ones in the femur with non-optimized prosthesis. However, these values are always less than the von Mises stresses in the intact femur in the regions where the same stress is evaluated and, therefore, the stress eigenvalues in the intact femur are less than the compressive and tensile yield stresses.
Finally, the following Figures. 6.12 and 6.13 summarize the results of the topological optimization in terms of resulting densities (RD) over the prosthesis domain and von Mises stresses (VMS) in a frontal section of the femur.

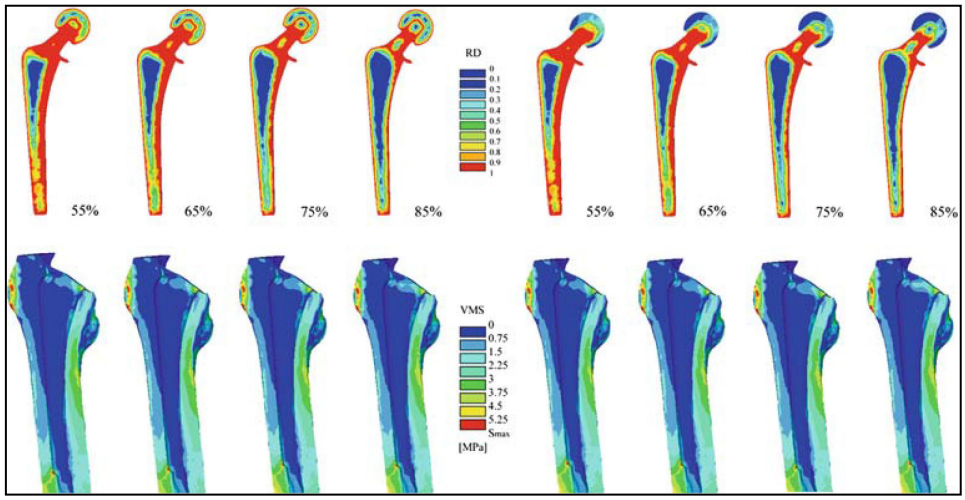

Fig. 6.12 – Results of the topological optimization in terms of resulting densities (RD) over the prosthesis domain and von Mises stresses (VMS) of the femur (as sectioned frontal view projections) for the first 2 cases in terms of percentages.

There, the evolution of the stresses and the decrease in stress shielding with the increase of prosthesis mass reduction percentage is highlighted, as shown in the sequences of the images.
To stress the utility of the wide number of cases examined, it is worthwhile to note that, in classical problems of topological optimization, the regions that exhibit low density as a result of the optimization process are considered as

material to be removed. On the contrary, in the case of optimized prostheses, is not always possible to achieve this.

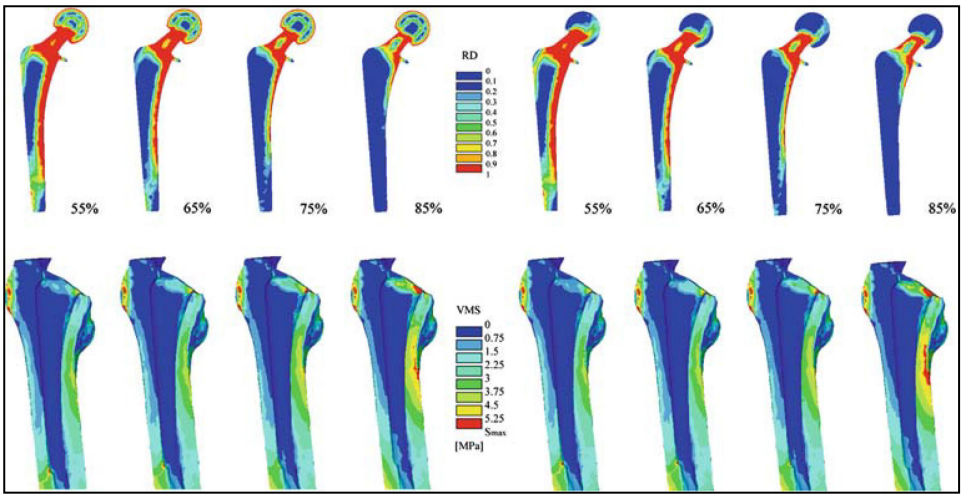

Fig. 6.13 – Results of the topological optimization in terms of resulting densities (RD) over the prosthesis domain and von Mises stresses (VMS) of the femur (as sectioned frontal view projections) for the second 2 cases in terms of percentages.

Indeed, if low densities appear at the interface with the bone (for example, in the cases "2", "3" and "4"), to remove material means to eliminate geometrical continuity and thus loosening would be trivial to predict. Thus, low output densities should be considered as an opportunity of reducing stiffness, not as a requirement. From this point of view, untraditional for TO, one should therefore aim to design prostheses where low densities obtained as TO results suggest where to reduce material stiffness, for example, by decreasing the volume fraction by means of laser micro-drilling of the implant or by defining prostheses in composite materials.

6.7. HIP PROSTHESIS TOPOLOGY OPTIMIZATION STRATEGY LIMITS

6.7.1. Material Properties from Numerical analyses

A large number of mathematical relationships between densitometric measures and mechanical properties have been introduced in the literature. In many published studies, elastic properties of bone are correlated to the bone density, in order to derive an empirical elasticity-density relationship. The accurate determination of such a relationship is of great importance, and while the

relationship between CT attenuation coefficients and ash density can be established with a direct calibration (McBroom et al., 1985; Ciarelli et al., 1991), the determination of a mathematical relationship between density and mechanical properties is more challenging. These proposed relationships are often substantially different one from the other. It is unclear whether such differences in elasticity-density relationships can be entirely explained in terms of methodological discrepancies among studies. This large spread in the predicted Young modulus can partially be explained by the complexity involved in the experimental techniques needed to measure the mechanical properties in a highly porous anisotropic material such as trabecular bone. Commonly, to determine the mechanical compressive properties, a trabecular bone specimen is cut out of a whole bone and loaded in a material testing machine. By recording the load–displacement curve, the stiffness can be calculated. Over time, different testing set-ups were developed and applied, and it was found that different artefacts and source of errors can arise during a mechanical test. In order to solve these problems related to the measurement of the bone mechanical properties, numerical analyses have been performed, considering that, even if the porous media is isotropic, stiffness depends on both volume fraction and cavity morphology. Different kinds of cavity morphology have been considered as shown in Fig. 6.14.

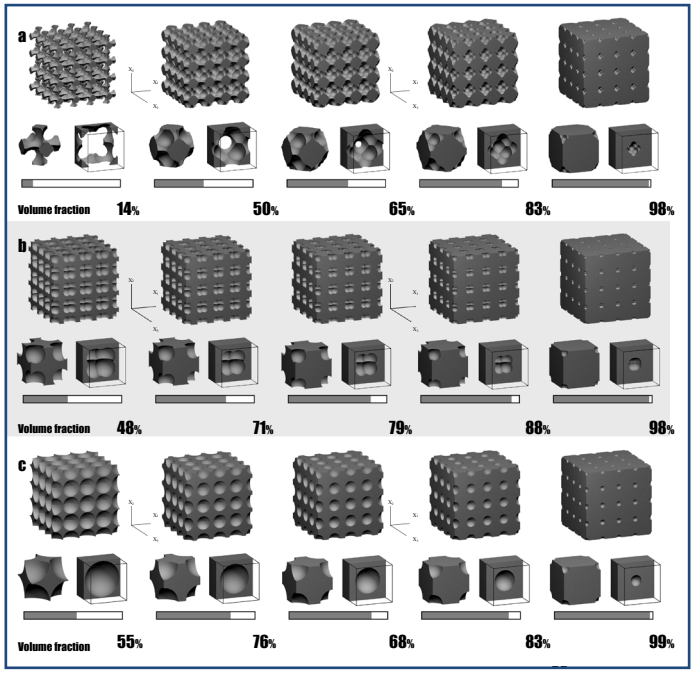

Fig. 6.14 – Different morphology cavities analized

The following Fig. 6.15 regroups the results in terms of Young moduli along density:

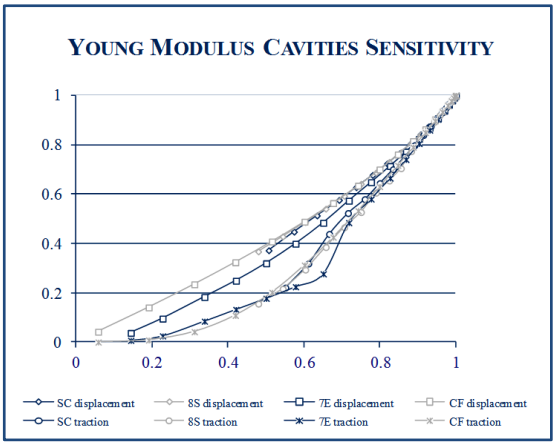

Fig. 5.15 – Young Moduli along density for different cavity morphology

A numerical law correlating Young moduli $E(\gamma)$ with density γ and Poisson coefficient υ have been defined:

$$E(\gamma) = A + B\gamma + C\gamma^2 + D\gamma^3 \tag{6.1}$$

with:

$$A = 0$$

$$B = \frac{2(-2+\upsilon)}{3(-2+\upsilon+\upsilon^2)}$$

$$C = \frac{22+17\upsilon-59\upsilon^2-9\upsilon^3+45\upsilon^4}{6(-7+5\upsilon)(-2+\upsilon+\upsilon^2)}$$

$$D = \frac{-50+17\upsilon+91\upsilon^2-21\upsilon^3-45\upsilon^4}{6(14-17\upsilon-2\upsilon^2+5\upsilon^3)}$$

This relationship will be used to set material properties related to density.

6.7.2. Ansys® Topology Optimization limits

The Ansys® Topological Optimization module has shown evident limits:

1) it is possible to perform only linear static solution
2) the penalization power p of the density ρ is fixed a priori
3) it is not possible to set a minimum value of the density ρ

4) the choice of the objective function is limited
5) there are only two library element types
6) there aren't difference in terms of results in the cases of prescribed displacement and applied loads.

The first limitation doesn't let perform different kinds of analises; in particular thermo-elastic analisis are denied and non-linear analisis both in the case of geometric and constitutive non-linearity are permitted.
The second limitation is relative to the penalization power of the density. As seen in previous chapters in the case of depleted media where it is very important to set a value of the penalization power able to fit in the best way the experimental data; Ansys® Topology Optimization module is a close box respect to this problem.
Manufacuring industries are very sensible to the third limitation because, in order to produce the topology optimized material and-or structure, it is very difficult to realize a density with very low values. The minimum value of the density can be let respect to the technological capabilities.
Usually the objective function is the Total Potential Energy and usually this functional is used to be minimized, but sometimes could be very useful to choice a different objective function as Von Mises Energy or different functional.
Due to particular geometries, materials or physics of the problem, Ansys has a large variety of elements types usable in different multiphysics.The sixth limitation is very absurd; there are only two library element types, one 2D element and one 3D element type able to perform Topology Optimization.
The last limitation, the sixth, is the most significant and will discussed in details in the next chapter.
Due to this limitation, a custom-made algorithm in Ansys® environment has been created and will be shown in details in the next chapter.

REFERENCES

Ansys® Inc. 2007. ANSYS 11 User's Documentation. Canonsburg, PA

Beckenbaugh RD, Ilstrup DM 1978. Total hip arthroplasty. J Bone and Joint Surg Am. 60: 306-313.

Cai K, Chen BS, Zhang HW, Shi J. 2008. Stiffness design of continuum structures by a bionics topology optimization method. J App Mech ASME. 75: 0510061-05100611.

Ciarelli MJ, Goldstein SA, Kuhn JL, Cody DD, Brown MB. 1991. Evaluation of orthogonal mechanical properties and density of human trabecular bone from the major metaphyseal regions with materials testing and computed tomography. J. Orthop. Res. 9: 674-682.

Cowin SC, Hegedus DH. 1976. Bone remodeling I: theory of adaptive elasticity. J Elasticity. 6: 313-326.

Cowin SC. 1994. Optimization of the strain energy density in linear anisotropic elasticity. J Elasticity. 34: 45-68.

Cowin SC. 1999. Bone poroelasticity. J Biomech. 32: 218-238.

Cowin SC. 2002. Elastic symmetry restrictions from structural gradients. In Rational continua: classical and new a collection of papers dedicated to Gianfranco Capriz on the occasion of his 75th birthday. Springer.

Engh CA Jr, Young's AM, Engh CA Sr, Hopper RH Jr. 2003. Clinical consequences of stress shielding after porous-coated total hip arthroplasty. Clin Orthop Relat Res. 417: 157-163.

Fernandes PR, Folgado J, Jacobs C, Pellegrini V. 2002. A contact model with ingrowth control for bone remodeling around cementless stems. J Biomech. 35: 167-176.

Gotze C, Steens W, Vieth V, Poremba C, Claes L, Steinbeck J. 2002. Primary stability in cementless femoral stems: custom- made versus conventional femoral prosthesis. Clin Biomech. 17: 267-273.

Gross S, Abel EW. 2001. A finite element analysis of hollow stemmed hip prostheses as a means of reducing stress shielding of the femur. J Biomech. 34: 995-1003.

Hamilton WG, McAuley JP, Tabaraee E, Engh A. 2008. The outcome of revision of an extensively porous-coated stem with another extensively porous-coated stem. J Arthroplasty. 23: 170-174.

Harris WH. 1992. Will stress shielding limit the longevity of cemented femoral components of total hip replacement? Clin Orthop Relat Res. 274: 120-123.

Helgason B, Perilli E, Schileo E, Taddei F, Brynjolfsson S, Viceconti M. 2008. Mathematical relationships between bone density and mechanical properties: A literature review. Clinical Biomechanics. 23: 135-146.

Huiskes R, Weinans H, Grootenboer HJ, Dalstra M, Fudala B, Slooff TJ. 1987. Adaptive bone-remodeling theory applied to prosthetic-design analysis. J. Biomech. 20: 1135–1150.

Huiskes R, Boeklagen R. 1989. Mathematical shape optimization of hip prosthesis design. J Biomech. 22: 793-804.

Huiskes HWJ, Weinans H, Van Rietbergen B. 1992. The relationship between stress shielding and bone resorption around total hip stems and effects of flexible materials. Clin Orthop. 274: 124-134.

Huiskes R, Rietbergen B. 1995. Preclinical testing of total hip stems, the effects of coating placement. Clin Orthop Related Res. 319: 64-76.

Jang IG, Kim IY. 2008. Computational study of Wolff's law with trabecular architecture in the human proximal femur using topology optimization. J Biomech. 41: 2353-2361.

Jang IG, Kim IY, Kwak BM. 2009. Analogy of strain energy density based bone-remodeling algorithm and structural topology optimization. J Biomeh Eng Trans ASME. 131:0110121-7.

Joshi MG, Advani SG, Miller F, Santare MH. 2000. Analysis of a femoral hip prosthesis designed to reduce stress shielding. J Biomech. 33: 1655-1662.

Katoozian H, Davy DT. 2000. Effects of loading conditions and objective function on three-dimensional shape optimization of femoral components of hip endoprostheses. Med Eng Phys. 22: 243-251.

Keaveny TM, Bartel DL. 1995. Mechanical consequences of bone ingrowth in a hip prosthesis inserted without cement. J Bone Joint Surg. 77: 911-923.

Luo G, Sadegh AM, Alexander H, Jaffe W, Scott D, Cowin SC. 1999. The effect of surface roughness on the stress adaption of trabecular architecture around a cylindrical implant. J Biomech. 32: 275–284.

McBroom, RJ, Hayes WC, Edwards WT, Goldberg RP, White 3rd., AA. 1985. Prediction of vertebral body compressive fracture using quantitative computed tomography. J. Bone Joint Surg. Am. 67: 1206–1214.

Monti L, Cristofolini L, Viceconti M. 1999. Methods for quantitative analysis of the primary stability in uncemented hip prostheses. Artif Organs. 23: 851-859.

Morscher EW, Dick W. 1983. Cementless fixation of isoelastic hip endoprostheses manufactured from plastic materials. Clin Orthop. 176: 77-87.

Munting E, Verhelpen M. 1995. Fixation and effect on bone strain pattern of a stemless hip prosthesis. J Biomech. 28: 949-961.

Nicolella DP, Thacker BH, Katoozian H, Davy DT. 2006. The effect of three-dimensional shape optimization on the probabilistic response of a cemented femoral hip prosthesis. J Biomech. 39: 1265-1278.

Pettersen SH, Wik TS, Skallerud B. 2009. Subject specific finite element analysis of implant stability for a femoral stem. Clin Biomech. 24: 480-487.

Rho JY. 1991. Mechanical properties of human cortical and cancellous bone. Ph.D. Thesis, University of Texas Southwestern Medical Center at Dallas.

Rho JY, Hobatho MC, Ashman RB. 1995 Relations of mechanical properties to density and CT numbers in human bone. Med Eng Phys. 17: 347-355.

Rietbergen B, Huiskes R, Weinans H, Sumner DR, Turner TM, Galante JO. 1993. The mechanism of bone remodeling and resorption around press-fitted THA stems. J Biomech. 26: 369-382.

Simoes JA, Vaz MA, Blatcher S, Taylor M. 2000. Influence of head constraint and muscle forces on the strain distribution within the intact femur. Med Eng Phys. 22: 453-459.

Tanino H, Ito H, Higa M, Omizu N, Nishimura I, Matsuda K, Mitamura Y, Matsuno T. 2006. Three-dimensional computer-aided design based design sensitivity analysis and shape optimization of the stem using adaptive p-method. J Biomech. 39: 1948-1953.

Terrier A, Rakotamanana RL, Ramaniraka AN, Leyvraz PF. 1997. Adaption models of anisotropic bone. Comp Methods Biomech Biomed Eng. 1: 47-59.

Turner CH, Rho J, Takano Y, Tsui TY, Pharr GM. 1999. The elastic properties of trabecular and cortical bone tissues are similar: results from two microscopic measurement techniques. J Biomech. 32 :437-441.

Yoon YS, Jang GH, Kim YY 1989. Shape optimal design of the stem of a cemented hip prosthesis to minimize stress concentration in the cement layer. J Biomech. 22: 1279-1284.

Weinans H, Huiskes R, Grootenboer HJ. 1992. The behavior of adaptive bone-remodeling simulation models. J Biomech. 25: 1425-1441.

7 TOPOLOGY OPTIMIZATION: A CUSTOM-MADE ALGORITHM

In the previous chapter essential limits of the procedure of Optimization have been highlighted in terms of modelling bone material properties, performing Topology Optimization with Ansys® module and building up the finite element-based model.
In order to overcome the significant and intrinsic limitations inside the Topology Optimization Ansys® module, an innovative and original custom-made algorithm, based on analytical formulation, have been proposed.
With the aim of underlining how the numeric code Ansys® is able to perform Topology Optimization only for structure subjected to applied forces, a comparison between Ansys® and custom-made algorithm have been illustrated.
As written before, the Ansys® software is an open environment; it is programmable both for developing macros and menu.From the beginning, in the late 80's this software has been written in a standard FORTRAN90, one of the first and more used programming language. A knowledge of this language is very helpful. Substantially, it is possible to create macros in a proprietary language called APDL (Ansys Parametric Design Language) having a own proprietary sintax and it is possible to customize menu using a proprietary language called UIDL (User Interface Design Language). All the designed menu will be shown in details, emphasizing the different menu used to input data, run

analisis and plot results. In the same way some crucial code lines will be explained in datails underlining the versality of the programming language.

7.1. ANALYTICAL FORMULATION

On the basis of the analytical formulation, a custom made algorithm, totally integrated in Ansys® software environment, has been developed. Three different materials have been taken into account:

- **Depleted Media**
  The first class of material is common called *Depleted Media* with the meaning of a porous material in which the matrix is randomly depleted by voids.

- **Isotropic Inhomogeneous Fiber Reinforced Media**
  The second class of material is Isotropic inhomogeneous fiber reinforced media with the meaning of a matrix in which short reinforced fibers are randomly dispersed.

- **Anisotropic Homogeneous Fiber Reinforced Media**
  The third class of material is Anisotropic inhomogeneous fiber reinforced media with the meaning of a matrix in which short oriented reinforced fibers are randomly dispersed.

For the first two classes of materials, the analytical formulation has been proposed in both cases of prescribed displacements and applied loads. The approach is typical of a functional minimization, normally the Total Potential Energy, using the Lagrange Multiplier Method.

7.1.1. Depleted Media. Prescribed Displacements

As the first case a depleted media subject to prescribed displacements has been considered.
The Deformation Energy, equal in solution to the Total Potential Energy, has been defined in terms of displacements of the single element $\mathbf{u}_e$:

$$U_e = \frac{1}{2}\mathbf{u}_e^T K_e \mathbf{u}_e$$

where K_e is the stiffness matrix.

Then the penalization law for Young Modulus where γ_e is the element density and p the penalization power due to Solid Isotropic Material Penalization (SIMP) (ensoe et al. 1995):

$$E = E_0 \gamma_e^p$$

Finally the volume constraint function g of the system have been written where n is the number of elements and f is the volume fraction:

$$g = \sum_{e=1}^{n} \gamma_e - nf$$

Now, we can define the functional $\Im$ to minimize, according to Lagrange Multiplier Method (Reddy, 1987), containing both the Total Potential energy and the volume constraint function:

$$\Im = U + \lambda g$$

where λ is the Lagrange multiplier. Indeed, from the following equations system generated deriving the functional $\Im$ respect to the density of the single element γ_e and respect to the Lagrange multiplier λ:

$$\frac{\partial \Im}{\partial \gamma_e} = 0 \rightarrow p\gamma_e^{p-1} U_e + \lambda = 0 \rightarrow \gamma_e = \left(-\frac{\lambda}{pU_e}\right)^{\frac{1}{p-1}}$$

$$\frac{\partial \Im}{\partial \lambda} = 0 \rightarrow \sum_{e=1}^{n} \gamma_e = nf \rightarrow \sum_{e=1}^{n} \left(-\frac{\lambda}{pU_e}\right)^{\frac{1}{p-1}} = nf$$

with simple algebraic manipulation, it is possible to find the two unknown variables, first the Lagrange multiplier λ:

$$-\lambda = \left(\frac{nf}{\sum_{e=1}^{n} \left(-\frac{1}{pU_e}\right)^{\frac{1}{p-1}}}\right)^{p-1}$$

and, finally, the analytical expression of the density of the single element γ_e in the case of depleted media subject to prescribed displacements, function of the

Total Potential Energy of the element U_e, the penalization power p, the number of elements n and the volume fraction f:

$$\gamma_e = nf \frac{U_e^{\frac{1}{1-p}}}{\sum_{e=1}^{n} U_e^{\frac{1}{1-p}}} \tag{7.1}$$

7.1.2. Depleted Media. Applied Loads

Following the same reasoning of the previous paragraph, some algebraic passages let find the expression of the density in the case of depleted media subject to applied loads.
First the Deformation Energy, equal in solution to the Total Potential Energy, has been definied in terms of forces $\boldsymbol{f}_e$:

$$U_e = \frac{1}{2} \boldsymbol{f}_e^T K_e^{-1} \boldsymbol{f}_e$$

Then the penalization law for Young Modulus:

$$E = E_0 \gamma_e^p$$

Finally the volume constraint function for the n elements:

$$g = \sum_{e=1}^{n} \gamma_e - nf$$

Now we can define the functional $\Im$ to minimize, according to Lagrange Multiplier Method:

$$\Im = U + \lambda g$$

Indeed, from the following equations system generated deriving the functional $\Im$ respect to the density of the single element γ_e and respect to the Lagrange multiplier λ:

$$\frac{\partial \Im}{\partial \gamma_e} = 0 \rightarrow -p\gamma_e^{-p-1} U_e + \lambda = 0 \rightarrow \gamma_e = \left(\frac{pU_e}{\lambda}\right)^{\frac{1}{p+1}}$$

$$\frac{\partial \Im}{\partial \lambda} = 0 \rightarrow \sum_{e=1}^{n} \gamma_e = nf \rightarrow \sum_{e=1}^{n} \left(\frac{pU_e}{\lambda}\right)^{\frac{1}{p+1}} = nf$$

with simple algebraic manipulation, it is possible to find the Lagrange multiplier λ:

$$\lambda = \left(\frac{\sum_{e=1}^{n} \left(\frac{pU_e}{\lambda}\right)^{\frac{1}{p+1}}}{nf}\right)^{p+1}$$

Finally the analytical expression of the density of the single element γ_e in the case of depleted media subject to applied loads is function of the Total Potential Energy of the element U_e, the penalization power p, the number of elements n and the volume fraction f:

$$\gamma_e = nf \frac{U_e^{\frac{1}{1+p}}}{\sum_{e=1}^{n} U_e^{\frac{1}{1+p}}} \tag{7.2}$$

It is very important to note that the expression of the density of the single element γ_e in the cases of depleted media subject to prescribed displacements (7.1) and to applied loads (7.2) differs only for the sign of penalization power p of the deformation energy U_e.

7.1.3. Isotropic Inhomogeneous Fiber Reinforced Media. Prescribed Displacements

Following the same approach, we first define the Deformation Energy, equal in solution to the Total Potential Energy, in terms of displacements of the single element $\mathbf{u}_e$:

$$U_e = \frac{1}{2} \mathbf{u}_e^T K_e \mathbf{u}_e$$

Then the penalization law for Young Moduli, as described before (5.16), where the subscribe M stands for matrix and the subscribe F for fibers and α is the ratio between E_{0M}, the matrix modulus, and E_{0F} the fiber modulus with usually $\alpha > 1$:

$$E_M = E_{0M}\gamma^p$$
$$E_F = E_{0F}\gamma^p$$
$$E_{0F} = \alpha E_{0M}, \alpha > 1$$
$$E_{2M} = E_{0F}\gamma^p + E_{0M}(1-\gamma^p) = E_{0M}[\gamma^p(\alpha-1)+1]$$

As seen before, E_{2M} is the resulting Young modulus due to the Solid Isotropic Material Penalization homogenization method in the case of two materials proposed by Bensoe (5.16). Finally the volume constraint function for the n elements:

$$g = \sum_{e=1}^{n}\gamma_e - nf$$

Now we can define the functional $\Im$ to minimize, according to Lagrange Multiplier Method:

$$\Im = U + \lambda g$$

Indeed, from the following equations system generated deriving the functional $\Im$ respect to the density of the single element γ_e and respect to the Lagrange multiplier λ:

$$\frac{\partial \Im}{\partial \gamma_e} = 0 \rightarrow p\gamma_e^{p-1}(\alpha-1)U_e + \lambda = 0 \rightarrow \gamma_e = [-\frac{\lambda}{p(\alpha-1)U_e}]^{\frac{1}{p-1}}$$
$$\frac{\partial \Im}{\partial \lambda} = 0 \rightarrow \sum_{e=1}^{n}\gamma_e = nf \rightarrow \sum_{e=1}^{n}[-\frac{\lambda}{p(\alpha-1)U_e}]^{\frac{1}{p-1}} = nf$$

with simple algebraic manipulation, it is possible to find the Lagrange multiplier λ:

$$-\lambda = \{\frac{nf}{\sum_{e=1}^{n}[-\frac{1}{p(p-1)U_e}]^{\frac{1}{p-1}}}\}^{p-1}$$

Finally, the analytical expression of the density of the single element γ_e in the case of isotropic inhomogeneous fiber reinforced media subject to prescribed displacements is function of the Total Potential Energy of the element U_e, the penalization power p, the number of elements n and the volume fraction f:

$$\gamma_e = nf \frac{U_e^{\frac{1}{1-p}}}{\sum_{e=1}^{n} U_e^{\frac{1}{1-p}}} \tag{7.3}$$

7.1.4. Isotropic Inhomogeneous Fiber Reinforced Media. Applied Loads

Following the same approach and with simple algebraic manipulation, the analytical expression of the density of the single element γ_e in the case of isotropic inhomogeneous fiber reinforced media subject to applied loads is:

$$\gamma_e = nf \frac{U_e^{\frac{1}{1+p}}}{\sum_{e=1}^{n} U_e^{\frac{1}{1+p}}} \tag{7.4}$$

It is very important to note that the expression of the density of the single element γ_e for isotropic inhomogeneous fiber reinforced media subject to prescribed displacements (7.3) and to applied loads (7.4) differs only for the sign of penalization power p of the deformation energy U_e. Moreover these expressions are the same of those (7.1) and (7.2) for depleted media.

7.2. THE ANSYS® MENU

A Custom Topo Menu has been developed in Ansys® environment using the UIDL language. As illustrated in the figure on the right (Fig. 7.1), the menu is composed of three parts: in the first, Data Input, it is possible to input all the quantities necessary to the optimization process as the minimum density, the penalization power, the objective function etc; in the second, the Run menu, it is possible to choice the type of the material to be optimized between depleted media, isotropic inhomogeneous fiber reinforced media and anisotropic homogeneous fiber reinforced media, the volume percentage of optimization and the maximum number of iterations.
In the last menu, the output menu, it is possible to plot all the results in terms of densities and orientation of the fibers, stiffness gain, optimized young moduli, etc.

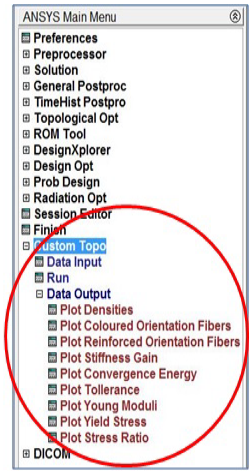

Fig.7.1.The menu

The following Fig.7.2 illustrates the Data Input menu:

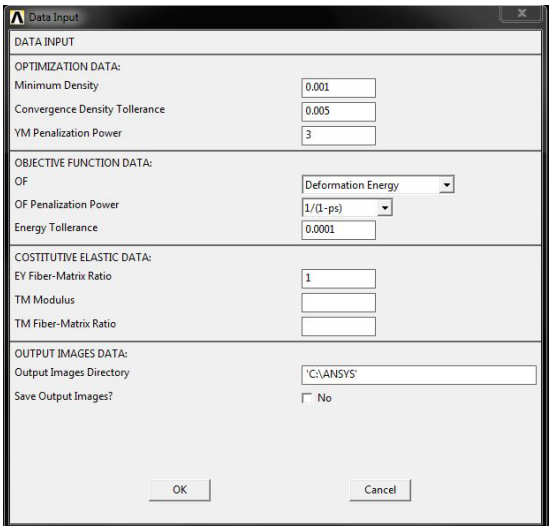

Fig.7.2. The Data Input menu

This menu is divided in four parts: the first one is related to Optimization Data as minimum density, convergence tollerance for density, usually 10^{-4}, and penalization power p; the second part is related to the Objective Function Data and, thus, to the choice of the objective function, to his power and finally to energy tolerance; the third part is related to Constitutive Elastic Data as the ratio between matrix and fiber Young moduli in the case of fiber reinforced media, the matrix tensile modulus and the ratio between matrix and fiber tensile moduli; in the fourth and last part, the Output Image Data, it is possible to set the output image directory, set as default to the Ansys working directory, and a flag used to save the images at the end of each iteration.

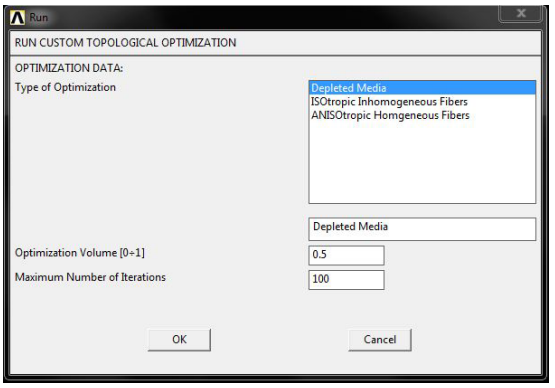

Fig.7.3. The Run menu

The above Fig.7.3 illustrates the Run menu; it is possible to choice the type of optimization in terms of material, related to the analytical formulation discussed in previous paragraphs, the volume to optimize (from 0 to 1) and the maximum number of iterations. Each menu has a numerical call to the relative function both in the case of menu and macros.

7.3. THE ALGHORITHM

The macro named TOPO_CUSTOM.MAC has been developed in Ansys® environment using the APDL language. It as been divided in two parts, the first able to run optimization in the cases of depleted media and isotropic inhomogeneous fiber reinforced media, the second one in the case of anisotropic homogeneous fiber reinforced media. A table of run codes have been designed taking into account errors code too able to generate error messages.
The following codes calculate the total number of elements and that one to be optimized, usually set to type 1:

```
!***** calcola numero elementi totali
    alls
    nummrg,node
    nummrg,elem
    numcmp,node
    numcmp,elem,
    *get,ecount_tot,elem,,count
    *get,emax_tot,elem,,num,max
    *get,emin_tot,elem,,num,min
!*************************************
!***** calcola numero elementi da ottimizzare
!***** type 1 da ottimizzare; type 2 da non ottimizzare
    esel,s,type,,1
    *get,ecount,elem,,count
    *get,emax,elem,,num,max
    *get,emin,elem,,num,min
```

Two array have been set:

```
!***** crea array energie, tolleranze ed iterazioni
    *dim,tolleranza,array,niter,1
    *dim,energia,array,niter,1
```

with the purpose of controlling the density tolerance and the energy of the system at each iteration.
In order to establish if the analisis run in the case of displacement prescribed or

forces applied, a sign have been calculated and a message is produced to let know the user the type of analisis:

```
!***** calcola segno
!***** ottimizzazione U (Reuss), U(gamma=1)>U(gamma=f), segno=+1
!***** ottimizzazione F (Voigt), U(gamma=1)<U(gamma=f), segno=-1
    *if,energia(1),gt,energia(2),then
        segno=1
        msg_segno='U'
    *else
        segno=-1
        msg_segno='F'
    *endif
    *if,alfa,ne,1,then
        segno=-segno
        *if,msg_segno,eq,'U',then
            msg_segno='F'
        *else
            msg_segno='U'
        *endif
    *endif
!***** messaggio segno
    *if,msg_segno,eq,'U',then
        /INPUT,'msgtopo_segnoU','txt',,, 0
    *else
        /INPUT,'msgtopo_segnoF','txt',,, 0
    *endif
```

At the end of each iteration an element table with density data have been created:

```
/post1
etable,gamma,volu
*do,_j,emin_tot,emax_tot,1
    *get,sel,elem,_j,esel
    *if,sel,eq,1,then
        detab,_j,gamma,densita
    *endif
*enddo
finish
```

At the end of each iteration the material properties in terms of Young moduli related to the actual density value are updated and the old density value is

recorded in a element table with the purpose of evaluating the density convergence in terms of difference between two consecutive iterations:

```
tol_tot=0
*do,_j,emin,emax,1
    *get,sel,elem,_j,esel
    *if,sel,eq,1,then
        *get,MP_count,elem,_j,attr,mat
        *get,densita,dens,MP_count
        *get,gamma_elem,elem,_j,etab,gamma
        *if,abs((gamma_elem-densita)/densita),gt,tol_tot,then
            tol_tot=abs((gamma_elem-densita)/densita)
        *endif
        mp,dens,MP_count,gamma_elem
        *if,alfa,eq,1,then
            MP,EX,MP_count,(gamma_elem**p)*E_Young
        *else
            MP,EX,MP_count,E_Young*((alfa-1)*(gamma_elem**p)+1)
        *endif
    *endif
*enddo
```

The macro named PLOTDENS.MAC has been developed to plot results in terms of elements table aswritten in the next numerical code:

```
!PLOTDENS.mac
*if,check_run,eq,1,or,checkrun,eq,2,then
/POST1
/dscale,,off
PLETAB,gamma,ARG1
FINISH
*endif
```

In a similar way the macro named PLOTCE.MAC or PLOTTOLL.MAC let the user plot the convergence energy array and the density tolerance in a graphical fashion:

```
!PLOTCE.mac
*vlen,_i
*vplot,,energia

!PLOTTOLL.mac
*vlen,_i
*vplot,,tolleranza
```

Moreover the macro named PRINTSCREEN.MAC allows the capture of the screen image at the end of every single iteration and is very useful to edit a video containing all the converged densities plot.

```
!PRINTSCREEN.mac
    alls
    /dscale,,off
    pletab,gamma,1                    !0:no average, 1:average
    *if,check_print,eq,1,then
        /SHOW,JPEG,,0
        JPEG,QUAL,100,
        JPEG,ORIENT,HORIZ
        JPEG,COLOR,2
        JPEG,TMOD,1
        /GFILE,800,
        /REPLOT
        /SHOW,CLOSE
        /DEVICE,VECTOR,0
    *endif
```

Moreover, different macros have been developed to send messages to the user, some about errors in inputing data, others about the optimization process in terms of controlling variables, others about output data as for example the value of the stiffness gain. The following codes alert the user to the evolution of the optimization process listing the value of the density tolerance at the end of each iteration:

```
*msg, ui, _i, tol_tot
at the iteration %I tollerance is %G
```

The following lines alert the user in the case of choise of fiber reinforced media topology optimization without inputing the value of α, the ratio between the matrix and fiber young moduli.

```
*msg, ui
ERROR: alfa is equal to 1. You must change this value to have a ISOtropic
Inhomogeneous Fibers TO!!
```

7.4. EXAMPLES

A number of classical mechanical examples have been performed by means of the custom-made topological optimization procedure.

- **Depleted Media Beam with a Center Load**

In the following figure is illustrated the geometry of a depleted media beam subject to a center load:

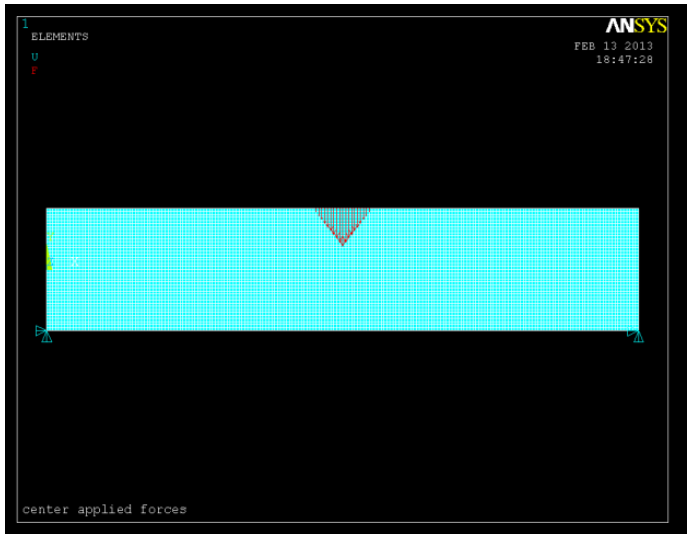

Fig. 7.4 – Geometry of a depleted media beam subject to a center load

In the following figure it is illustrated the topological optimized density map:

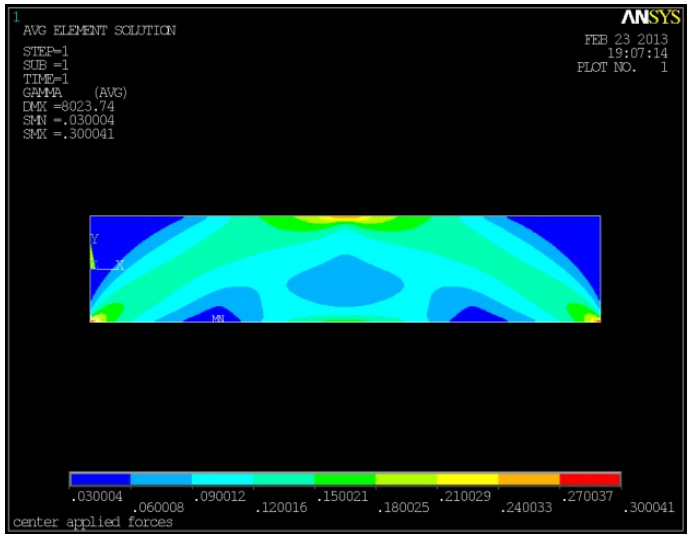

Fig. 7.5 – Topological optimized density map of
a depleted media beam subject to a center load

- **Depleted Media Beam with a Distributed Load**

In the following figure is illustrated the geometry of a depleted media beam subject to a distributed load:

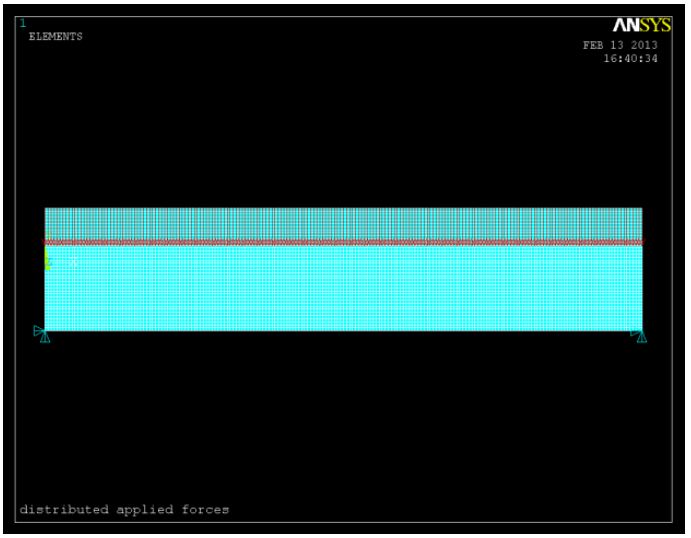

Fig. 7.6 – Geometry of a depleted media beam subject to a distributed load

In the following figure it is illustrated the topological optimized density map:

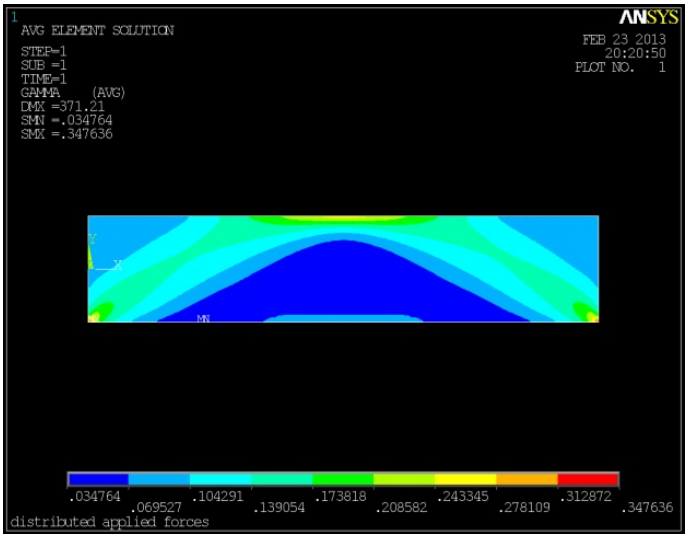

Fig. 7.7 – Topological optimized density map of
a depleted media beam subject to a distributed load

- **Depleted Media Cantilever Beam**

In the following figure is illustrated the geometry of a depleted media cantilever beam:

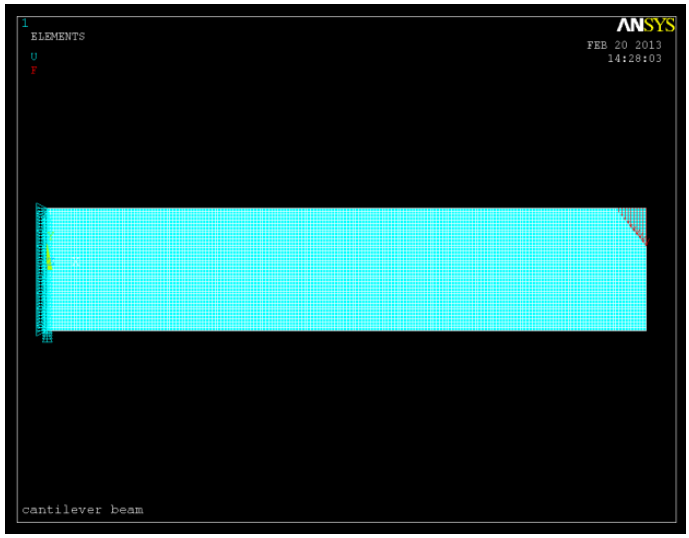

Fig. 7.8 – Geometry of a depleted media cantilever beam

In the following figure it is illustrated the topological optimized density map:

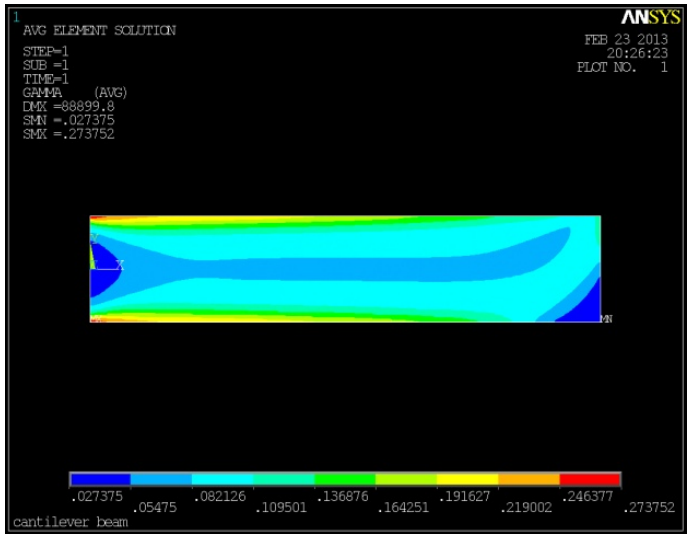

Fig. 7.9 – Topological optimized density map of
a depleted media cantilever beam

- **Depleted Media Beam with a Sinusoidal Load**

In the following figure is illustrated the geometry of a depleted media beam subject to a sinusoidal load:

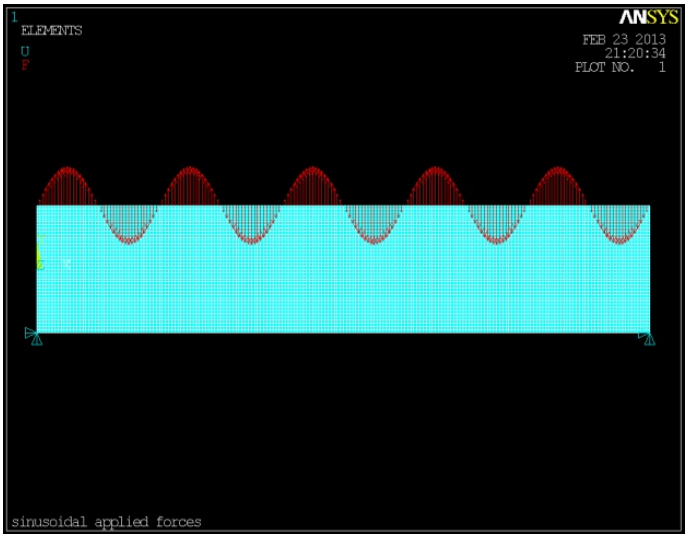

Fig. 7.10 – Geometry of a depleted media beam subject a sinusoidal load

In the following figure it is illustrated the topological optimized density map:

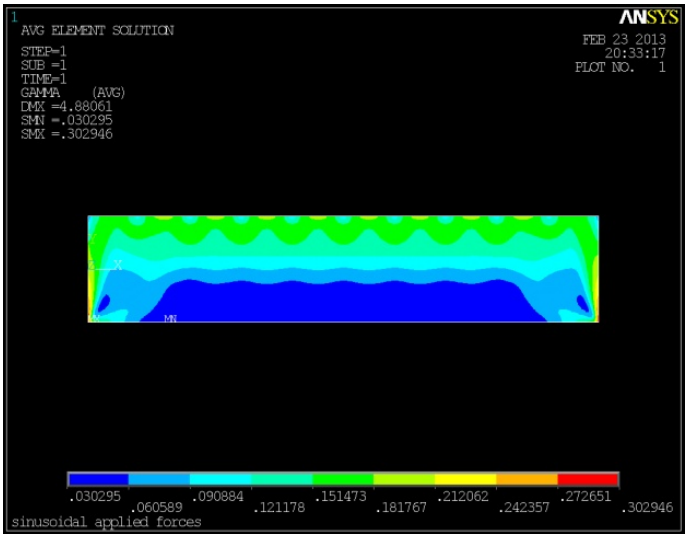

Fig. 7.11 – Topological optimized density map of
a depleted media beam subject to a sinusoidal load

A sensitivity analysis of a depleted media beam subject to a central load has been performed in order to highlight the variation of the density map to the volume of optimization.

- **Volume of Optimization Equal to 10%**

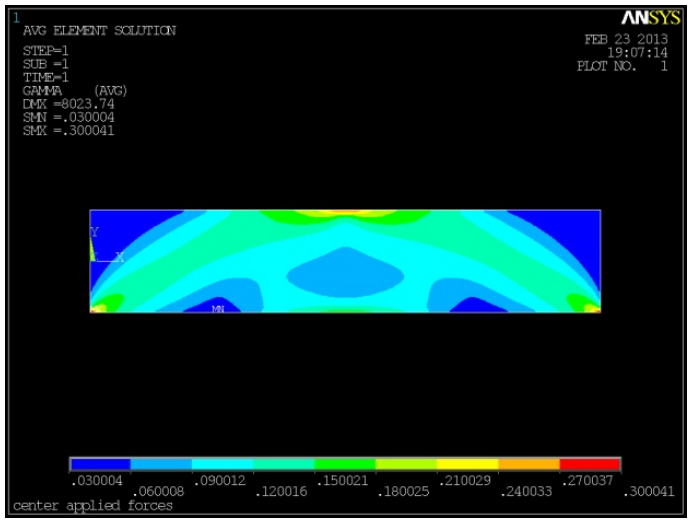

Fig. 7.12 – Topological optimized density map of a depleted media beam subject to a central load with a volume of optimization of 10%

- **Volume of Optimization Equal to 20%**

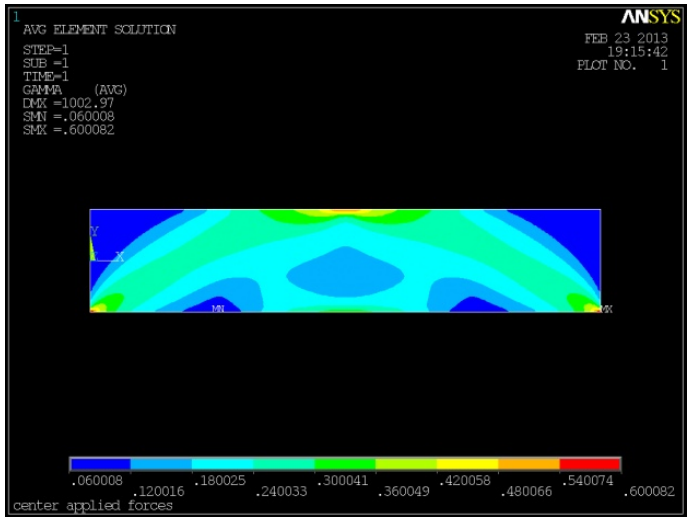

Fig. 7.13 – Topological optimized density map of a depleted media beam subject to a central load with a volume of optimization of 20%

- **Volume of Optimization Equal to 30%**

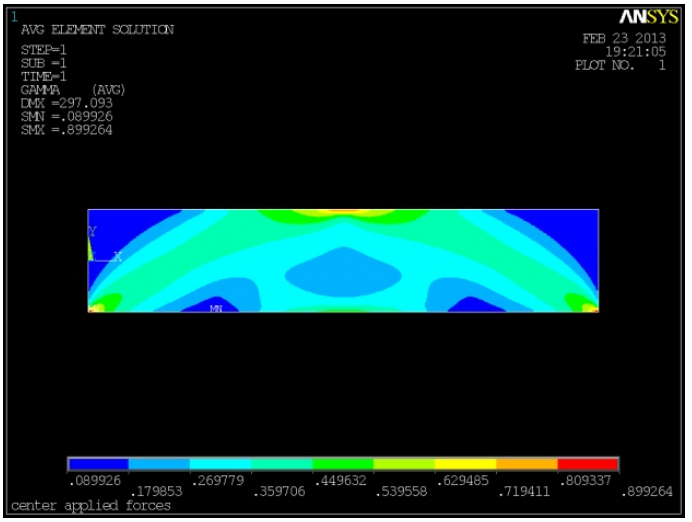

Fig. 7.14 – Topological optimized density map of a depleted media beam subject to a central load with a volume of optimization of 30%

- **Volume of Optimization Equal to 40%**

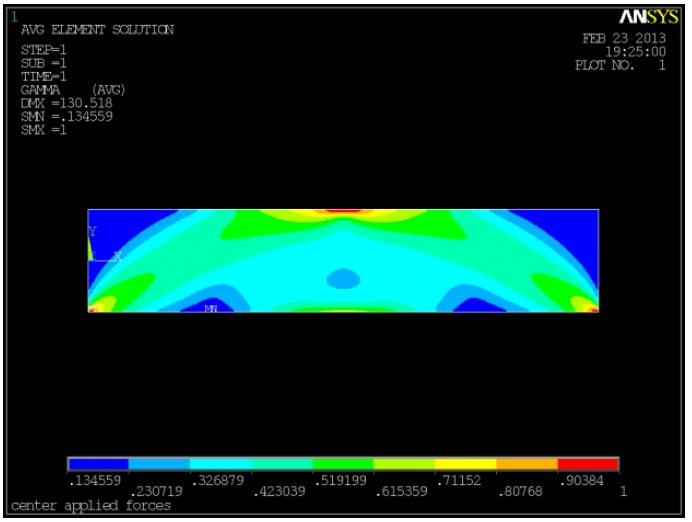

Fig. 7.15 – Topological optimized density map of a depleted media beam subject to a central load with a volume of optimization of 40%

- **Volume of Optimization Equal to 50%**

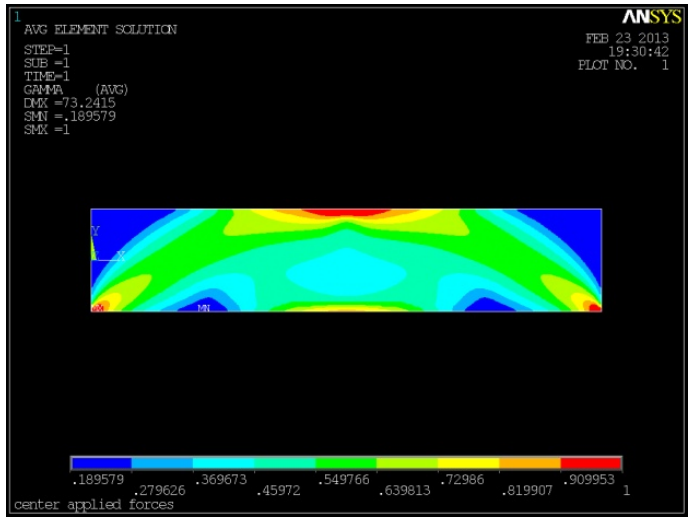

Fig. 7.16 – Topological optimized density map of a depleted media beam subject to a central load with a volume of optimization of 50%

A sensitivity analysis of a depleted media beam subject to a central load has been performed in order to highlight the variation of the density map to the penalization power p of the density.

- **Penalization Power $p = 1.5$**

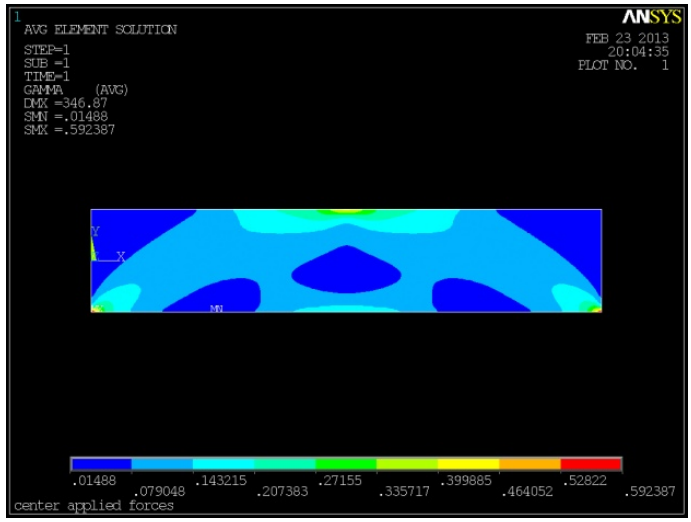

Fig. 7.17 – Topological optimized density map of a depleted media beam subject to a central load with the penalization power $p = 1.5$

- **Penalization Power** $p = 2$

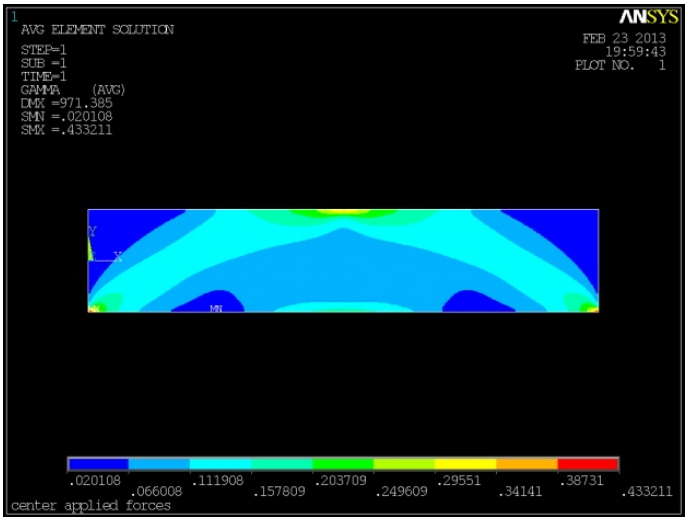

Fig. 7.18 – Topological optimized density map of a depleted media beam subject to a central load with the penalization power $p = 2$

- **Penalization Power** $p = 2.5$

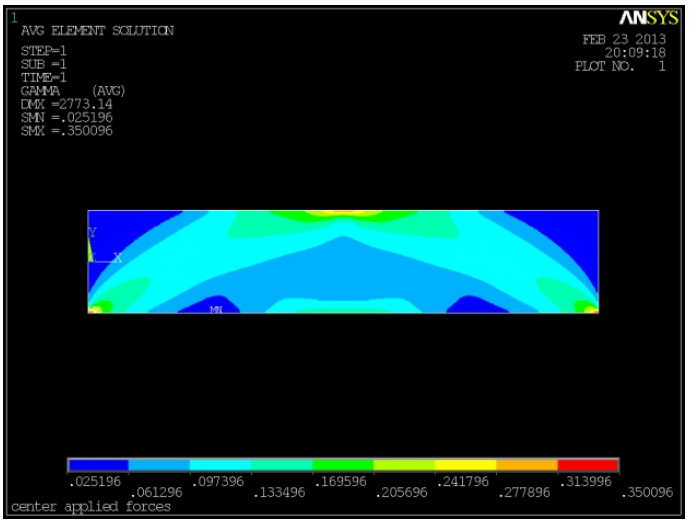

Fig. 7.19 – Topological optimized density map of a depleted media beam subject to a central load with the penalization power $p = 2.5$

- **Penalization Power** $p = 3$

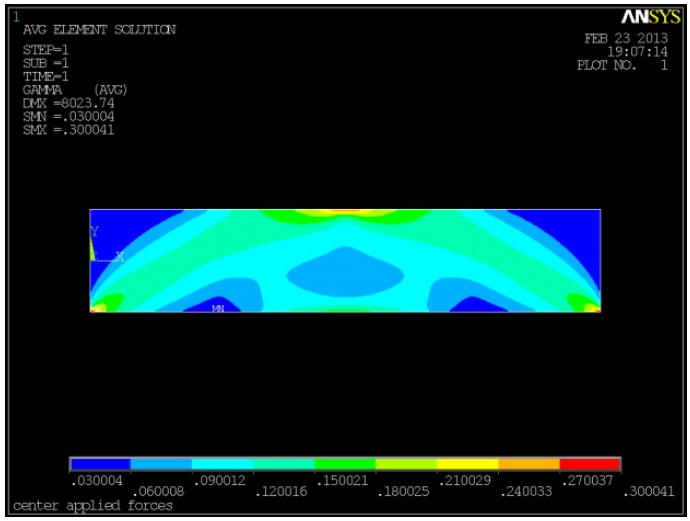

Fig. 7.20 – Topological optimized density map of a depleted media beam subject to a central load with the penalization power $p = 3$

- **Penalization Power** $p = 3.5$

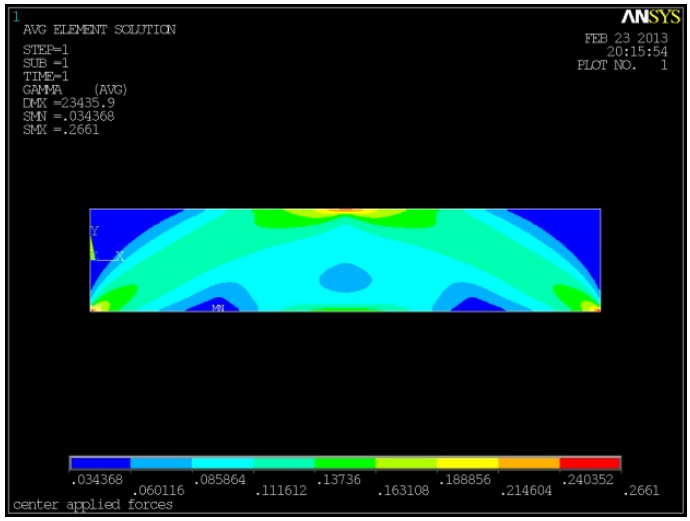

Fig. 7.21 – Topological optimized density map of a depleted media beam subject to a central load with the penalization power $p = 3.5$

It is very clear that, growing p, the resulting density map trends to a black and white representation.

Furthermore, an Isotropic Inhomogeneous Fiber Reinforced beam subject to a center load and to a distributed load, has been optimized.

- **Isotropic Inhomogeneous Fiber Reinforced Beam subject to a Center Load**

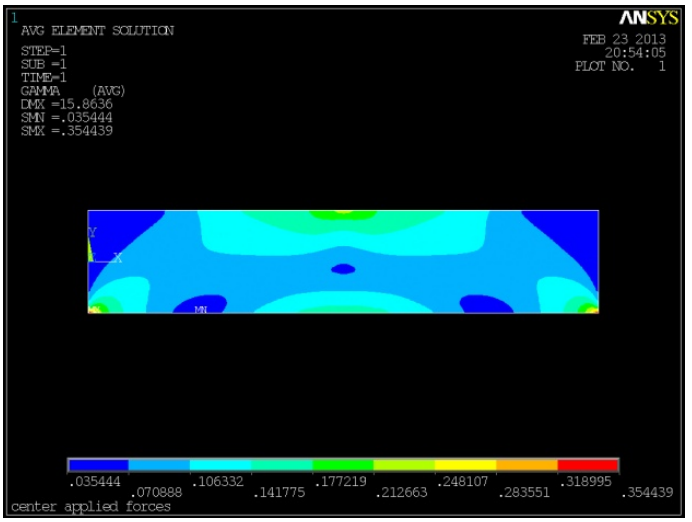

Fig. 7.22 – Topological optimized density map of a Isotropic Inhomogeneous Fiber Reinforced Media beam subject to a center load

- **Isotropic Inhomogeneous Fiber Reinforced Beam subject to a Distributed Load**

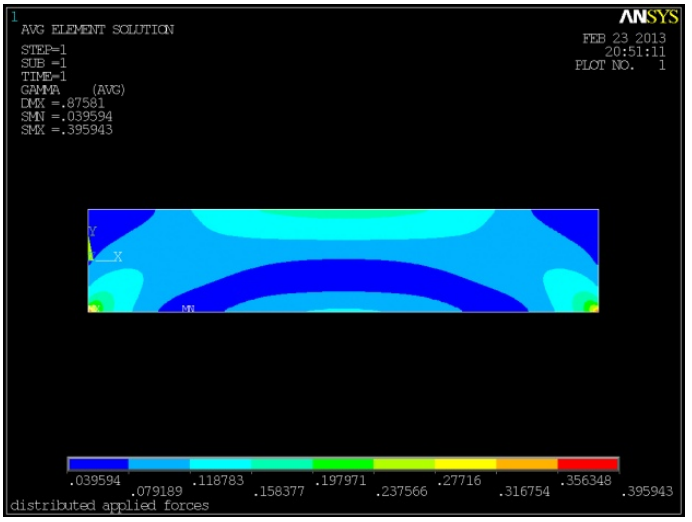

Fig. 7.23 – Topological optimized density map of a Isotropic Inhomogeneous Fiber Reinforced Media beam subject to a distributed load

Finally, an Anisotropic Homogeneous Fiber Reinforced beam subject to a center load and to a distributed load, has been optimized.

- **Anisotropic Homogeneous Fiber Reinforced Media Beam subject to a Center Load**

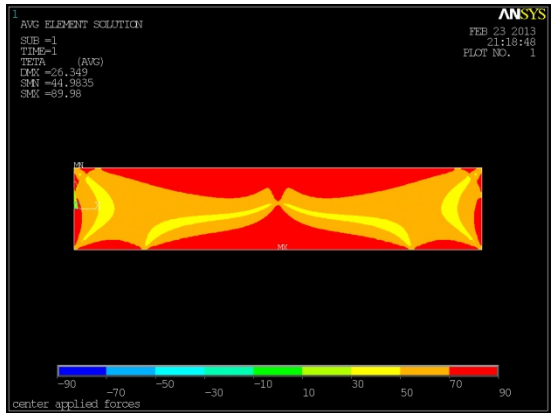

Fig. 7.24 – Topological optimized density map of an Anisotropic Homogeneous Fiber Reinforced Media beam subject to a center load

- **Anisotropic Homogeneous Fiber Reinforced Media Beam subject to a Distributed Load**

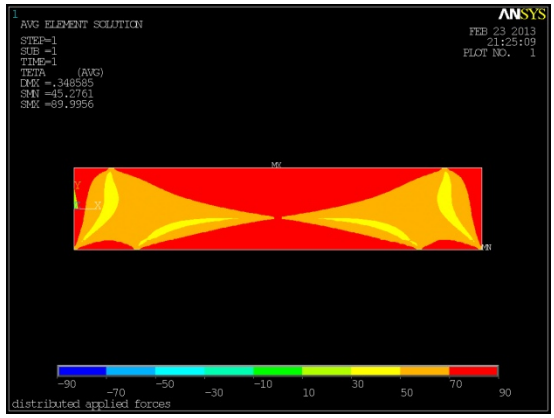

Fig. 7.25 – Topological optimized density map of an Anisotropic Homogeneous Fiber Reinforced Media beam subject to a distributed load

The contour plot maps, in the case of oriented fibers, are not intelligible; with the aim of plotting the orientation of the single fibers the macro PLOTTETA1.MAC have been developed borrowing a reinforced 3D element type usually used to analize concrete behaviour.

For each existing element a new 3D reinforced one has been create, directing the reinforcement bar inside the element with the same orientation of the fibers recorded in the element table.
The following code is used if the angle is between -45 degrees and +45 degrees:

```
*get,teta_elem,elem,_j,etab,teta
!***** -45<teta<+45
    *if,teta_elem,gt,-45,and,teta_elem,le,45,then
        sect,_j,reinf,discrete,fibra1
        e=1
        x1=.5*(1-tan(teta_elem))
        x2=.5*(1+tan(teta_elem))
        secdata,_j+ecount,A,EDGo,e,x1,z0,x2,z0
        esel,s,elem,,_j+ecount
        secnum,_j
        ereinf
    *endif
```

For this element, reinf264, it is necessary to set the section data containing the value of the three angles to define the orinentation into the space.
Other settings are also necessary; in particular the cross sectional area and the location of the reinforcing fibers. The command *ereinf* defines the new reinforcing element.
The left half part of the last case is illustrated in the following figure:

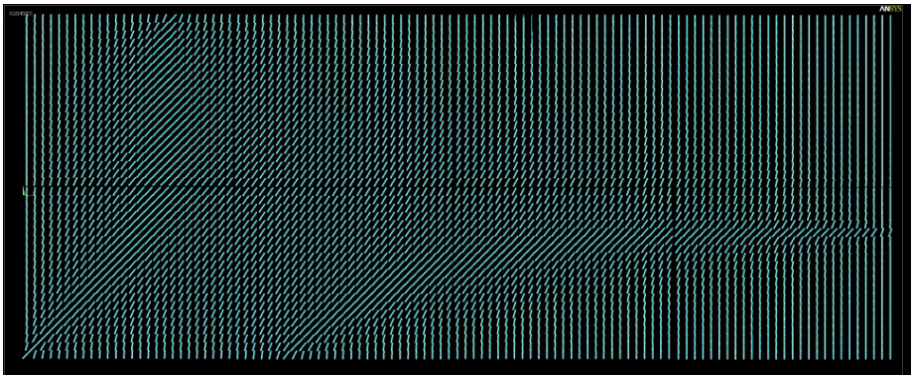

Fig. 7.26 – Particular (half left part) of a topological optimized density map of an Anisotropic Homogeneous Fiber Reinforced beam subject to a distributed load

Finally, it is necessary to underline the procedure at the basis of the choice of the optimal angle, element by element, in both cases of structures subject to displacements prescribed and to applied loads.
Considering a 2-D structure subject to prescribed displacements, so that the flexibility matrix is orthotropic:

$$\mathbb{S} = \begin{bmatrix} \dfrac{1}{E_{\max}} & -\dfrac{\nu_{12}}{E_{\max}} & 0 \\ -\dfrac{\nu_{21}}{E_{\max}} & \dfrac{1}{E_{\max}} & 0 \\ 0 & 0 & \dfrac{1}{G} \end{bmatrix}$$

calculating the principal stresses in every element, it is possible to choice the minimum stress as:

$$\boldsymbol{\sigma}_{\min} = \min\left\{\left|\boldsymbol{\sigma}_{I}\right|, \left|\boldsymbol{\sigma}_{II}\right|\right\}$$

Well, the optimal angle is:

$$\vartheta = \vartheta(\boldsymbol{\sigma}_{\min})$$

and the resulting orthotropic material for this element has the following orthotropic flexibility matrix:

$$\mathbb{S}_{\vartheta} = \mathbf{Q}^{-1}\mathbb{S}\mathbf{Q}$$

where $\mathbf{Q}$ is the typical orthogonal tensor, $\mathbb{S}$ is the flexibility tensor before the single iteration and $\mathbb{S}_{\vartheta}$ is the actualized flexibility tensor at the end of each single iteration.

7.5. ANSYS® VERSUS CUSTOM-MADE TOPOLOGY OPTIMIZATION

Let us considered a depleted media beam of length ℓ in bending regime subject to applied bending moment $\mathfrak{M}$ and prescribed rotation $\dfrac{\varphi}{2}$ such that two loads condition are equivalent.

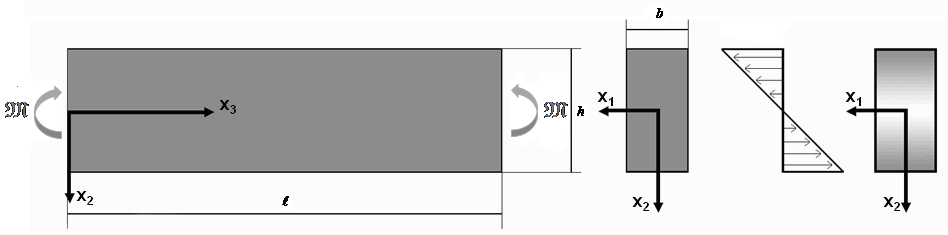

Fig. 7.27 – Depleted media beam in the cases of applied bending moment

The rectangular cross section of the beam have the dimensions b and h. The geometries of the considered beams are illustrated in the fig. 7.27 and 7.28.

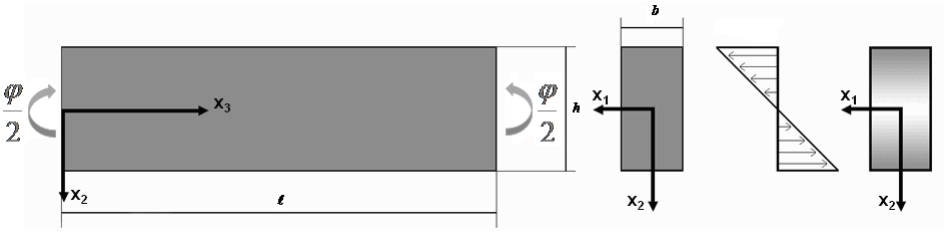

Fig. 7.28 – Depleted media beam in the cases of prescribed rotation

While the topological optimized density map is quite similar when subjected to applied bending moments for both Ansys® and custom-made procedure, as it is illustrated in the following figure:

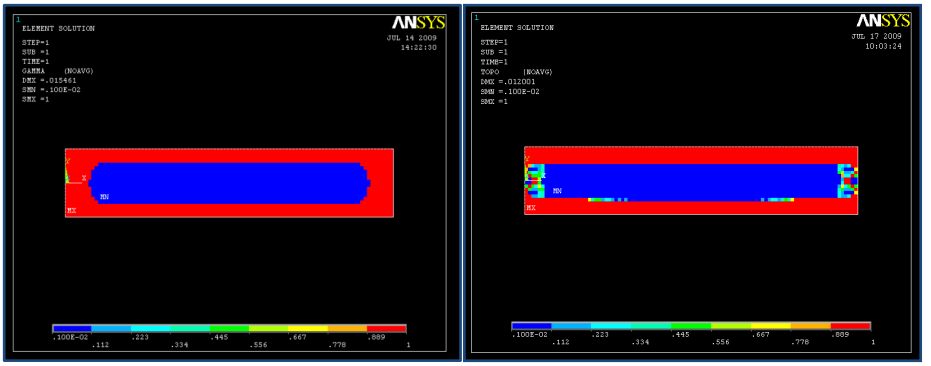

Fig. 7.30 – Topological optimized density map of a depleted media beam in the cases of applied bending moments

when subject to prescribed rotation, the Ansys® topology optimization procedure is not able to catch the real distribution of the resulting density map.
In order to highlight this malfunction, an analytical solution have been performed; the penalization law for Young Modulus is:

$$E = E_0 \gamma^p$$

It is well know that the expression of the stress and, as a consequence, of the strain, depend only on the axis x_3:

$$\boldsymbol{\sigma}_3 = E\gamma^p \boldsymbol{\varepsilon}_3$$

$$\boldsymbol{\varepsilon}_3 = \frac{\mathfrak{M}}{EI} x_2$$

We calculate the Deformation Energy over the volume V :

$$U = \frac{1}{2}\int_{-\frac{b}{2}}^{\frac{b}{2}}\int_{-\frac{h}{2}}^{\frac{h}{2}}\int_{0}^{\ell}\boldsymbol{\sigma}_3\boldsymbol{\varepsilon}_3 dV = \frac{1}{2}b\ell\frac{\mathfrak{M}}{EI^2}\int_{-\frac{h}{2}}^{\frac{h}{2}}\gamma^p x_2^2 dx_2$$

The volume constraint function is:

$$g = b\ell\int_{-\frac{h}{2}}^{\frac{h}{2}}\gamma dx_2 - fhb\ell$$

Now we can define the functional $\mathfrak{I}$ to minimize, according to Lagrange Multiplier Method:

$$\mathfrak{I} = U + \lambda g$$

Indeed, from the following equations system generated deriving the functional $\mathfrak{I}$ respect to the density of the single element γ_e and respect to the Lagrange multiplier λ :

$$\frac{\partial\mathfrak{I}}{\partial\gamma} = 0 \rightarrow Kp\gamma^{p-1}x_2^2 - \lambda = 0 \rightarrow \gamma = [\frac{\lambda}{Kpx_2^2}]^{\frac{1}{p-1}}$$

$$\frac{\partial\mathfrak{I}}{\partial\lambda} = 0 \rightarrow \int_{-\frac{h}{2}}^{\frac{h}{2}}\gamma dx_2 - fh \rightarrow \int_{-\frac{h}{2}}^{\frac{h}{2}}[\frac{\lambda}{Kpx_2^2}]^{\frac{1}{p-1}}dx_2 = fh$$

with easy algebraic manipulation, for a value of penalization power p equal to 2.5, it is possible to find the Lagrange multiplier λ :

$$\lambda = \frac{5K}{2}(-\frac{f}{3})^{\frac{3}{2}}$$

and finally the analytical expression of the density in the case of depleted media subject to prescribed rotation is:

$$\gamma = \frac{f}{3}x_3^{-\frac{4}{3}}$$

This trend is obviously hyperbolic-like.

The following fig. 7.31 illustrates the analytically solved Topological optimized density map of a depleted media beam subject to prescribed rotation:

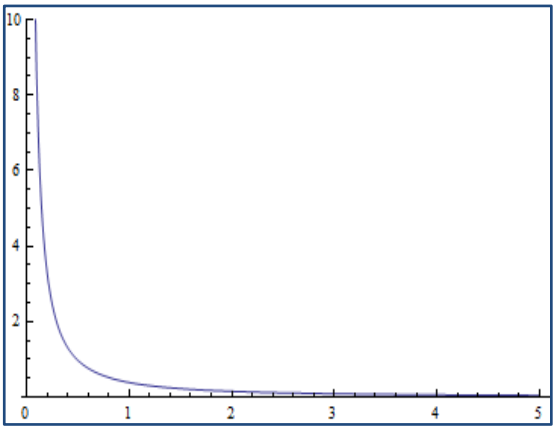

Fig. 7.31 – analytically solved Topological optimized density map of a depleted media beam in the cases of prescribed rotation

The following figure 7.32 shows the Topological optimized density map of depleted media beam in the case of prescribed rotation (left: custom made algorithm; right: Ansys® algorithm):

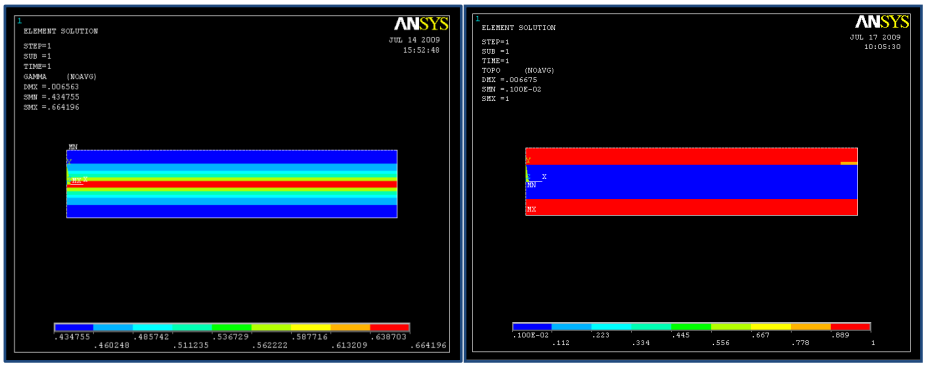

Fig. 7.32 – Topological optimized density map of Depleted media beam in the cases of prescribed rotation (left: custom made algorithm; right: Ansys® algorithm)

While the custom-made algorithm denisty map match the analytical solution, the Ansys® topology optimization density map is substantially equal to that one where the structure is subject to applied bending moments. In the opinion of the author, after the first iteration, Ansys® substantially reads the produced reactions forces and proceeds applying these reaction forces as a case of a structure subject to applied forces; in this way Ansys® always implements the procedure considering the structure subject to of applied forces.

For this reason the resulting density map is significantly the same in both cases of prescribed displacements or applied loads.
The custom-made algorithm is instead able to proceed in the right direction and the resulting density map is significantly the same of that solved analytically.

REFERENCES

Ansys® Inc. 2007. ANSYS 11 User's Documentation. Canonsburg, PA

Bendsøe MP. 1989. Optimal shape design as a material distribution problem. Struct. Optim. 1: 193-202.

Reddy JN. 1987. Applied Functional Analysis and Variational Methods in Engineering, McGraw-Hill.

8 AUTOMATIC MODEL RECONSTRUCTION

Computed tomography (CT) is a methodology to measure both density and structure in a single measurement. Especially, the combination with finite element (FE) analysis, the most widely used computational technique for structural analysis in engineering, seems promising.

CT-based FE models can provide insights into load transfer through the bone architecture and with that help our understanding of how differences in bone microarchitecture influence bone strength. They integrate bone density measurements with bone geometry in a three-dimensional fashion.

The potential of CT-based FE models has been clearly recognized, and over the past years a number of papers have been published on several methodological aspects of FE models, such as mesh type, material properties, failure mechanisms and loading conditions.

Subject-specific finite element (FE) analysis of the skeleton, a very powerful tool for biomechanical research, is now being adopted in clinical applications (Taddei et al., 2003; Viceconti et al., 2005). The most common way of constructing the subject-specific FE models is by deriving information from X-Ray computed tomography (CT) images.

In the previous chapter 6 this aspect has been deeply discussed; moreover the limit relative to the construction of the finite element

model has been underlined. In particular, the procedure related to the construction of the FE model, starting from data recorded in DICOM format files produced by diagnostic instruments described in the previous chapter is complex, long and articulated. Moreover, the continuous passages of data file from software to another could be subject to errors and approximation and the utilization of different software stretch computational times and software costs.
The more crucial aspect is the creation of group of polylines filtering the entire model by HU value; this procedure is totally automatic, but it is uncontrollable and, then, it is full of errors. Often it is necessary a previous step of model segmentation in order to cean data from radiologic artefacts and erroneous geometric reconstruction.
With the aim of simplifying this numerical procedure an automatic model reconstruction algorithm in Ansys® environment has been developed, both developing macros and menu with Ansys® proprietary programming language APDL (Ansys Parametric Design Language) and UIDL (User Interface Design Language) respectively; the automatic reconstruction takes into account both the geometrical and constitutive content recorded in DICOM format files and it is able to build directely the model in one time.
Furthermore this innovative and original procedure can be very useful for the design of composite materials and biomedical implants. Finally the acquisition of bond surfaces by micro-tomography could be processed and constructed with the aim of studying wear and debris production.

8.1. INTRODUCTION TO DICOM FILE

The data format for this kind of instrumental devices is DICOM standard format file. DICOM (Digital Imaging and Communications in Medicine) is a standard for handling, storing, printing, and transmitting information in medical imaging. It includes a file format definition and a network communications protocol. The communication protocol is an application protocol that uses TCP/IP to communicate between systems. DICOM files can be exchanged between two entities that are capable of receiving image and patient data in DICOM format.
DICOM format data is typically utilized for all medical images as X-Ray, CT, magnetic resonance imaging (MRI). The first standard, ACR/NEMA 300, was released in 1985. The DICOM standard is divided into related, but independent parts; DICOM differs from some, but not all, data formats in that it groups information into data sets. That means that a file of a chest x-ray image, for

example, actually contains the patient ID within the file, so that the image can never be separated from this information by mistake. This is guaranteed by the relational data base structure of data.
A DICOM data object consists of a number of attributes, including items such as name, ID, etc., and also one special attribute containing the image pixel data.
There are information related to patient personal data, hospital data, instrumentation data and obviously images related to the scanned patient body site. The CT, instrumental examinations usually used to scan human bone, is a multiple parallel scanning of the body site. As shown in the following fig. 8.1, the patient is positioned inside the radiogen tube and scanned:

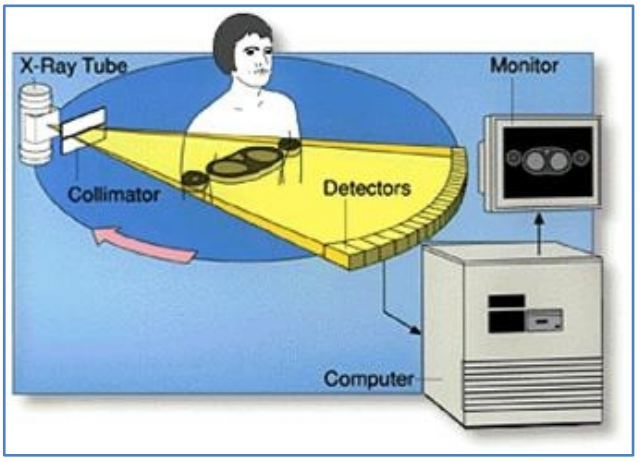

Fig. 8.1 – CT instrumentation

the difference in terms of radiation X-Ray trasmitted and received are related to the density of the crossed medium and expressed in terms of Hounsfield Unit (HU). The Hounsfield unit (HU) scale is a linear transformation of the original linear attenuation coefficient measurement into one in which the radiodensity of distilled water at standard pressure and temperature is defined as zero Hounsfield units, while the radiodensity of air at standard pressure and temperature is defined as 1000 HU. In a voxel with average linear attenuation coefficient μ_X, the corresponding HU value is therefore given by:

$$HU = 1000 \frac{\mu - \mu_{H_2O}}{\mu_{H_2O}}$$

where μ_{H_2O} is the linear attenuation coefficients of water, so the definition for CT scanners are calibrated with reference to water. The following Table 8.1 lists some common substances inside human body in terms of HU values:

SUBSTANCE	HU
Air	−1000
Lung	−500
Fat	−84
Water	0
CSF	15
Blood	+30 to +45
Muscle	+40
Soft Tissue	+100 to +300
Cancellous Bone	+200 to +1200
Cortical Bone	+1200

Table 8.1 – HU values for human substances

In each voxel (volumetric pixel) of each image it is recorded the corresponding densitometric information expressed in terms of HU values.
In addition to densitometric information, DICOM standard has also information related to geometric position of the single slice respect to a cartesian coordinate system. In particular, information like Upper Left Corner (ULC) is the cartesian coordinate point in terms of x_{ULC} ,y_{ULC} , z_{ULC} coordinate and, togheter with the Tilt Orientation information expressed in terms of direction cosines, is the reference point from which it is possible to construct the plane containing the image. In addition, Pixel Spacing along x-axis (PSx), Pixel Spacing along y-axis (PSy), Slice Thickness (ST) are the three dimensions values of the single voxel and, togheter with Image Resolution in terms of number of rows and columns, let construct the volumes corresponding to the voxels which HU value is in the range of interest. Finally by means of the parameters Rescale Intercept (RI) and Rescale Slope (RS) it is possible to trasform the HU values in density values in order to relate the density values to the mechanical properties of the single voxel, as shown in the previous chapter 6, using the following relationship:

$$\gamma = RS \cdot HU + RI \tag{8.1}$$

8.2. AUTOMATIC MODEL RECONSTRUCTION

8.2.1. Complete Integration between Ansys® and Matematica®

The software Ansys® is not able to import DICOM format files; so, in order to get all information, both geometric and constitutive, recorded in every slice (in every file is recorded only one single slice) the software Wolfram Matematica® have been used. A complete integration between the software Ansys® and the

software Wolfram Matematica® have been realized by means of external call from Ansys® to Mathematica and by writing and reading text files containing the information to interchange from a software to the other (see Fig. 8.2).
This type of interface is very useful and can be used whenever it is necessary the utilization of a symbolic mathematical code also to solve systems of equation, derivatives, integrals and whatever mathematical function not included in the Ansys software.

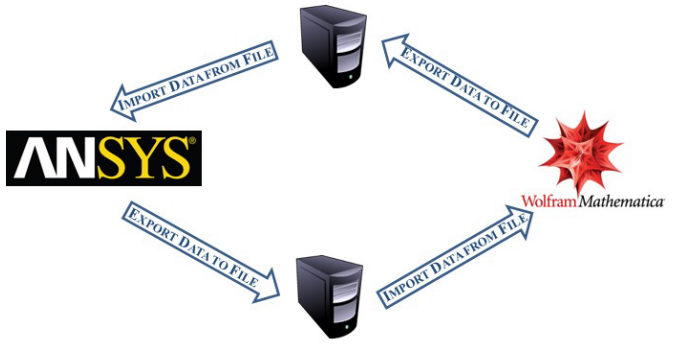

Fig. 8.2 – Integration between software Ansys® and Mathematica®

8.2.2. The Algorithm

The new DICOM menu shown in the Fig. 8.3 on the right have been designed to include all the function relative to automatic model reconstruction.
In Mathematica environment the constitutive information in terms of HU values are first imported from DICOM file and then exported in a comma separated values (CSV) format file; indeed in Ansys® environment the CSV file containing the densitometric information is read and then written in a matrix.
At the same way, in Mathematica environment geometric information necessary to built the model, as discussed in the previous paragraph, are first imported and then exported in a text file; indeed in Ansys® environment the text file containing the geometric information is imported and then written in an array.
The Ansys® importing data format is the typical Fortran format described by precise format

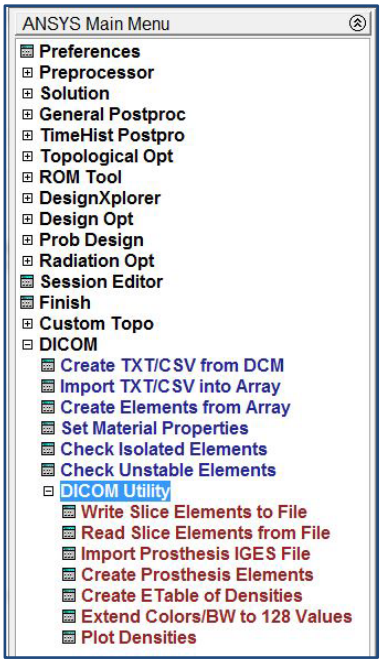

Fig. 8.3 – The DICOM menu

edit descriptors separated by comma and included in parenthesis.
In Ansys® environment, after checking the esistence of the CSV and TXT files produced with Mathematica, the following code is used to import the parametrs in an array:

```
!***** importa parameters slice si-iesima
    nomearray=strcat('par_',chrval(ns))
    *dim,%nomearray%,array,10,1
    arg1=nomearray
    arg2='txt'
    arg3=cartella
    /input,macro_par
    rows=nomearray(1)
    cols=nomearray(2)
```

It is possible to note a call to a temporary macro, *macro_par*, used to read the parameters from file; this macro is listed in the following code:

```
!***** crea macro per l'importazione parametri
    *create,macro_par
*VREAD,%nomearray%,arg1,arg2,arg3,1, , , , , ,
(F8.0)
    *end
```

Similar macro have been produced with the purpose of importing HU values.
The following figure Fig. 8.4 illustrates the menu in Ansys to perform the external call to Mathematica in order to write the DICOM information, both geometric and constituive, in a text (TXT) and comma separated values (CSV) files respectively.

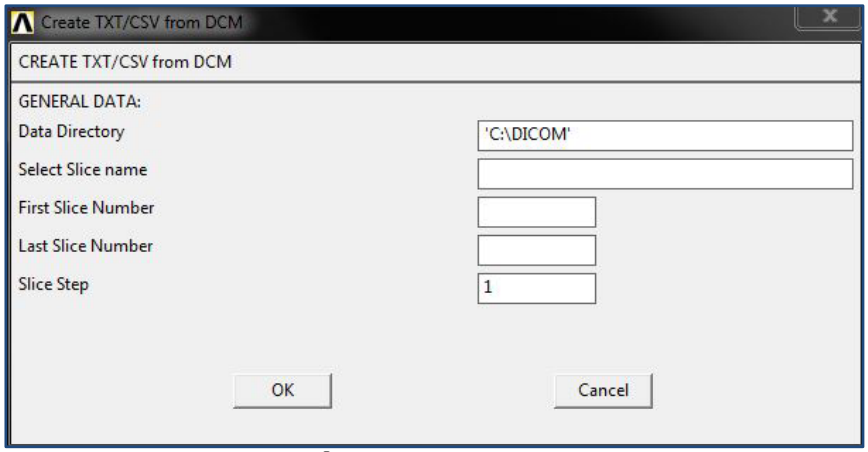

Fig. 8.4 –Ansys® menu Create TXT/CSV from DCM

It is possible to choice the data directory where are recorded the DICOM files, the common suffix of the files and which slices to process with a slice step.
This step value is set to 1 as default and can be used in the case of overlapping.
A similar window let the user to import data, TXT and CSV format files, into Ansys® environment and to record them in an array and a matrix for each slice.
As already said, in addition to these densitometric information, standard DICOM format has also information related to geometric position of the single slice respect to a cartesian coordinate system.
In particular, geometric information like Upper Left Corner (ULC), Pixel Spacing along x-axis (PSx), Pixel Spacing along y-axis (PSy), Slice Thickness (ST), Image Resolution in terms of rows and columns, etc., are utilized to construct the geometry of the model.

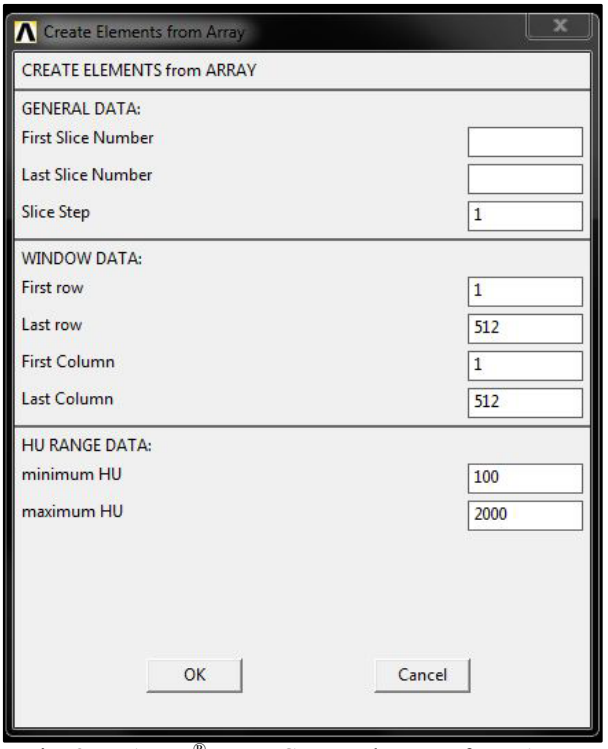

Fig. 8.5 –Ansys® menu Create Elements from Array

The above Fig. 8.5 illustrates the input data necessary to create the elements from array in Ansys; this menu is divided in three parts: in the first part, the general data, the user input the numbers of the slices of interest with the slice step; in the second part, the windows data, in order to minimize computational times due to the model construction, it is possible to choice a sub-window inside the image and, as a consequence, to process only these voxels. The user input the

limit of this window in terms of rows and columns with the default values for a typical resolution from 1 to 512; in the third part, HU range data, the user can input the minimum and maximum values of HU with the purpose of filtering the substances. The macro reads the HU values from the recorded table filtering and creating only the elements whose HU value is in the range of interest (as already said, the bone range is between 200 and 1200 HU).
For each slice, after checking the esistence of the array and matrix of values imported from Mathematica and the absence of the elements component (the esistence of the elements component means that the slice has been already constructed), the macro provides to construct the single element starting from his nodes whose spatial coordinates are function of the imported parameters:

```
*do,i,rigai,rigaf,1
   *do,j,coli,colf,1
      mathu=%nomearray%(i,j)*%nomepar%(10)+%nomepar%(9)
      *if,mathu,ge,HUmin,and,mathu,le,HUmax,then
         xA=%nomepar%(6)+(j-1)*%nomepar%(3)
         xB=%nomepar%(6)+j*%nomepar%(3)
         yA=%nomepar%(7)+(i-1)*%nomepar%(4)
         yC=%nomepar%(7)+i*%nomepar%(4)
         zA=%nomepar%(8)-%nomepar%(5)/2
         zA1=%nomepar%(8)+%nomepar%(5)/2
         n,,xA,yA,zA
         *get,numnode,node,0,num,max
         nodi(1)=numnode
         n,,xB,yA,zA
         *get,numnode,node,0,num,max
         nodi(2)=numnode
         n,,xB,yC,ZA
         *get,numnode,node,0,num,max
         nodi(3)=numnode
         n,,xA,yC,zA
         *get,numnode,node,0,num,max
         nodi(4)=numnode
         n,,xA,yA,zA1
         *get,numnode,node,0,num,max
         nodi(5)=numnode
         n,,xB,yA,zA1
         *get,numnode,node,0,num,max
         nodi(6)=numnode
         n,,xB,yC,ZA1
         *get,numnode,node,0,num,max
         nodi(7)=numnode
         n,,xA,yC,zA1
```

```
        *get,numnode,node,0,num,max
        nodi(8)=numnode
        e,nodi(1),nodi(2),nodi(3),nodi(4),nodi(5),nodi(6),nodi(7),nodi(8)
        emodif,emax,mat,mathu
        emax=emax+1
    *endif
*enddo
```

It is very important to note that every element is constructed if and only if the related value of HU, *matHU*, is in the range of interest (that is HUmin<matHU<HUmax); moreover, in order to construct the volume equal to the voxel, a 8 nodes cubic element have been chosen; the eight nodes where defined as functions of geometrical parameters recorded in the array and the element is defined directly from these nodes.
When all the elements with the density in the range of HU values of interest are constructed, it is possible to set the material properties as function of HU values. Using typical literature mathematical correlation between HU values and density as (8.1), inputting the value of Young modulus of the cortical bone and the value of Poisson coefficient, the algorithm creates a material for each density value using the cubic law (6.1) enveloped for porous media to set the corresponding material properties. The following code has been enveloped to this aim:

```
!SETMATS.mac
!setta le proprietà del materiale in funzione dei valori di HU
    /prep7
!*************************************
!****** calcola massimo HU
    npar=0
    i=0
    nomepar=''
    nomearray=''
    ri=0
    rs=0
    tipo=0
    maxHU=0
    massimo=0
    *get,npar,parm,,max
!****** prendi Rescale Intecept (ri) e Rescale Slope (rs)
    *do,i,1,npar,1
        *get,nomepar,parm,0,loc,i
        *get,tipo,parm,%nomepar%,type
        *if,tipo,eq,1,and,strsub(nomepar,1,4),eq,'PAR_',then
            ri=%nomepar%(9)
```

```
            rs=%nomepar%(10)
            *exit
        *endif
    *enddo
!****** calcola maxHU
    *do,i,1,npar,1
        *get,nomearray,parm,0,loc,i
        *get,tipo,parm,%nomearray%,type
        *if,tipo,eq,1,and,strsub(nomearray,1,3),eq,'HU_',then
            *do,k,1,cols
                *vscfun,massimo,max,%nomearray%(1,k)
                *if,massimo,gt,maxHU,then
                    maxHU=massimo
                *endif
            *enddo
        *endif
    *enddo
    maxHU=maxHU*rs+ri
!*************************************
!****** modello generalizzato RHO:
!****** E(gamma)=A+B*gamma+C*gamma²+D*gamma³ [MPa]
    A=0
    B=2*(-2+ni)/3/(-2+ni+ni**2)
    C=22+17*ni-59*ni**2
    C=C-9*ni**3+45*ni**4
    C=-C/6/(-7+5*ni)/(-2+ni+ni**2)
    D=-50+17*ni+91*ni**2
    D=D-21*ni**3-45*ni**4
    D=-D/6/(14-17*ni-2*ni**2+5*ni**3)
!*************************************
!****** crea materiali
    *do,HU,1,maxHU,1
        gamma=1/2*(1+HU/maxHU)
        EY=(A+B*gamma+C*gamma**2+D*gamma**3)*EY_cort ![MPa]
        MP,EX,HU,EY
        MP,dens,HU,HU                    !!g/cm³
        MP,PRXY,HU,ni
    *enddo
    finish
!*************************************
```

In the last two parts of the exposed macro the cubic law (Generalized RHO model) is chosen and then set with a typical FOR cycle all the *maxHU* materials

starting for the denser material, the cortical bone, whose Young modulus and Poisson coefficient have been taken from literature.
The automatic model reconstruction could create isolated elements as illustrates in the following Fig. 8.6:

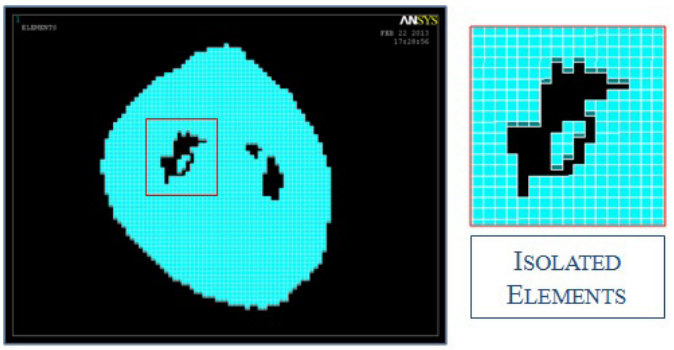

Fig. 8.6 –Isolated elements due to automatic model reconstruction

It is possible to check isolated elements and to erase them. This objective is reached by means of the following code in which, starting from an internal element, all the attached elements were selected and so on up to isolate the separated ones:

```
!***** check elems isolati
    alls
    nummrg,node
    nummrg,elem
    numcmp,node
    numcmp,elem
    *get,ecount,elem,,count
    *get,emax,elem,,num,max
    *get,emin,elem,,num,min
    esel,s,elem,,emin
    *do,i,1,ecount,1
        nsle,s
        esln,s
        *get,ecount_sel,elem,,count
        *if,ecount_sel-ecount_cm,ne,0,then
            cm,elemsiso,elem
        *else
            *exit
        *endif
        cmsel,s,elemsiso
        *get,ecount_cm,elem,,count
```

```
*enddo
```

At the end of the procedure these elements are plotted and the user is asked if they have to be eliminated.

```
*ask,canc,cancellare i %ecount_isol% elementi isolati [0=no 1=si]?,0
*if,canc,eq,1,then
    nsle,s
    edele,all
    ndele,all
*endif
```

Due to automatic model reconstruction also unstable elements, cubic elements with 8 nodes, could be created as shown in the following Fig. 8.7:

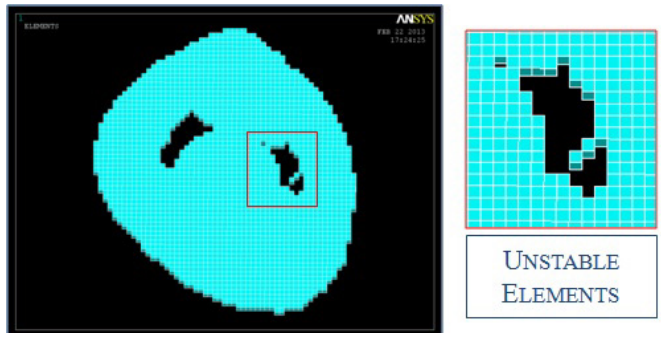

Fig. 8.7 –Unstable elements due to automatic model reconstruction

The following code perform this action:

```
!***** check elems labili
    alls
    nummrg,node
    nummrg,elem
    numcmp,node
    numcmp,elem
    *get,ecount,elem,,count
    esel,inve
    cm,elemslab,elem
    *do,i,1,ecount,1
        esel,s,elem,,i
        nsle,s
        esln,s
        nsle,s
        *get,ncount_tot,node,,count
```

```
        esel,u,elem,,i
        nsle,s
        *get,ncount_at,node,,count
        *if,ncount_tot-ncount_at,gt,5,then
            esel,s,elem,,i
            cmsel,a,elemslab
            cm,elemslab,elem
        *endif
        /INPUT,'msglability','txt'
    *enddo
```

Here too, at the end of the procedure these elements are plotted and the user is asked if they have to be eliminated.
Finally an utility menu have been created as shown in the Fig. 8.8 on the right; the first two procedures let the user write slice elements to file and read elements from file with the aim of constructing different slices of the same model with different computers, performing, thus, a parallel construction of the model; in this way it is possible to drastically reduce computational times related to the construction of the model. This is a very important feature of the procedure because with the more and more increasing of the resolution of the diagnostic instruments the number of elements of the models becomes greater and greater; for this reason the reduction of computational times related to the construction of the model.

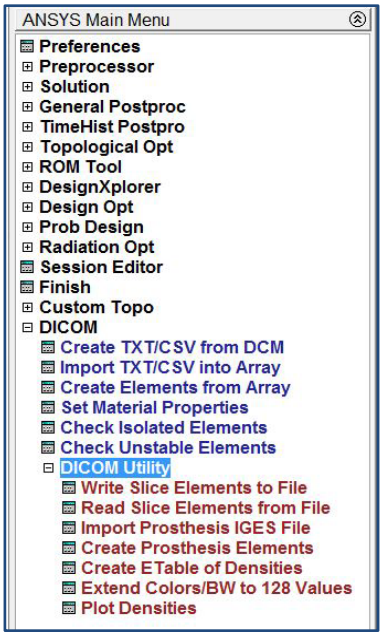

Fig. 8.8 – DICOM Utility menu

Moreover, in the case of designing a prosthesis, in order to verify the mechanical behaviour of the implant inside the bone, it is possible to import the prosthesis IGES file, produced with a Computer Aided Design (CAD) software, and create, slice after slice, the prosthesis elements from the lines.
Finally a procedure have been developed in order to define an element table of densities, plot these densities also expanding the range of colour from typical 9 colours to extended 128 colours or gray scale values.

REFERENCES

ANSYS Inc (2007) ANSYS 11 user's documentation. Canonsburg, PA

Taddei F, Viceconti M, Manfrini M, Toni A. 2003. Mechanical strength of a femoral reconstruction in paediatric oncology: a finite element study. Proc. Inst. Mech. Eng. [H]. 217: 111-119.

Viceconti M, Olsen S, Nolte LP, Burton K.. 2005. Extracting clinically relevant data from finite element simulations. Clin. Biomech. 20: 451–454.

9 TOWARDS MULTI-PHYSICS APPLICATIONS: DUALITY PORO-THERMO-ELASTICITY

The equations of poroelasticity and thermoelasticity are very similar to one another (Zimmerman, 2000) and this correspondence could be a powerful tool to solve poroelastic problems.
The basilar concept of the coupling between poroelasticity and thermoelasticity is that the temperature and the pore pressure play similar roles. In both theories, in fact, the basic constitutive equations relating the stresses and strains are the same of those of standard elasticity, in which some multiple of the pore pressure (or temperature) is subtracted from the normal stresses. Moreover, considering the typical values of these multiple coefficients arising in most rock mechanics applications, both theories are at least partially coupled, that is to say that variations in the pore pressure (or temperature) will appreciably influence the stresses and strains. The pore pressure and temperature are described through diffusion equations, which contain a source-sink type term depending on the time derivative of the bulk strain or mean normal stress. The analogy between the two theories, then, arises from the identical formal structure of the equations governing the two problems, which allows to find a direct relationship between each parameter appearing in the two theories. The strength of the coupling between the mechanical variables, stress and strain, and the pore pressure (or temperature), can be estimated in terms of dimensionless

coupling parameters, as shown in the following. However, an analysis of the typical values for these coupling coefficients shows that the poroelastic coupling effect is usually strong (for a liquid-saturated rock), while the thermoelastic coupling effect is usually negligible.

This result means that the temperature distribution is not affected by the stresses and strains, whereas this is not usually the case for the pore pressure equation. Finally, Zimmerman (2000) emphasized also the existence of other types of thermoelastic couplings, such as the dependence of the constitutive coefficients from stress. The permeability of many fractured rocks, for example, is highly stress-dependent and so, the permeability will be influenced by stress, causing an alteration of the flow field, and, thereby, changes in the pore pressure distribution. Moreover, Zimmerman (2000) underlined also the importance of modeling non-isothermal poroelasticity, characterized by the influence of temperature on stresses, through the following mechanism. An increase in temperature may lead to a large increase in fluid pressure (because this particular coupling is typically large in liquids), which, in turn, will determine mechanical stresses and strains. In this situation, indeed, there will be a coupling between the temperature and the stress and strain fields.

Within the framework of the analogy between poroelasticity and thermoelasticity, a possible strategy to implement a poroelastic problem with a FE code, thus, consists in exploiting this analogy. Since the equations describing the two problems are identical in formal structure, they can be rewritten to draw a direct relationship between each parameter appearing in the two theories.

9.1. COUPLED NON-LINEAR POROELASTIC PROBLEM

The fundamental equations for a poroelastic problem ***P*** can be summarized as follows:

$$\begin{aligned} &\mathrm{P}_1:\ \rho\ddot{\mathbf{u}} - \nabla\cdot\left[\mathbb{C}:\boldsymbol{\varepsilon} - p\mathbf{I}\right] = \rho\mathbf{f} \\ &\mathrm{P}_2:\ \mathbf{I}:\mathbf{I}\dot{\boldsymbol{\varepsilon}} + M^{-1}\dot{p} - \nabla\cdot\left[\left(\rho_{f0}\mathbf{g}\right)^{-1}\mathbf{K}\cdot\nabla p\right] = 0 \end{aligned} \tag{9.1}$$

The field variables involved are the displacement, $\mathbf{u} = \mathbf{u}(\mathbf{x},t)$, the bulk strain, $\boldsymbol{\varepsilon} = sym\nabla\otimes\mathbf{u}$, and the pore fluid pressure, $p = p(\mathbf{x},t)$. In the first equation (9.1), $\rho = \rho_s(1-\phi) + \rho_f\phi$ is the density, $\mathbb{C}$ is the stiffness forth-order tensor, $\mathbf{I}$

is the second order unit tensor and $\mathbf{f}$ is the mass force vector. Note that the Biot tensor is equal to $\mathbf{I}$ for saturated porous media.
In the second equation, instead, the term $\mathbf{I}:\mathbf{I}\dot{\boldsymbol{\varepsilon}}$ can be expressed as $\dot{e} := \nabla \cdot \dot{\mathbf{u}}$ and $\left(\rho_{f0}\mathbf{g}\right)^{-1}\mathbf{K}\cdot\nabla p$ is the filtration velocity vector (Darcy quasi-static approximation law).
This vector depends on the second rank tensor of the filtration coefficients $\mathbf{K}$, which is linked to the second rank permeability tensor, $\mathbf{K}_P$, the initial fluid density, ρ_{f0}, the gravitation acceleration, $\mathbf{g}$, and the fluid viscosity, μ, as shown in the following equation:

$$\mathbf{K} = \frac{\mathbf{K}_P \rho_{f0} \mathbf{g}}{\mu} \tag{9.2}$$

The coefficient M is expressed as $M^{-1} = N^{-1} + K_f^{-1}\phi$, where N^{-1} is the reverse Biot's modulus, K_f is the fluid tangent bulk modulus and ϕ is the porosity.
The change in porosity $\left(\phi - \phi_0\right)$ is directly related to the change in pression $\left(p - p_0\right)$ through the reverse Biot's modulus N^{-1} and the bulk strain $\boldsymbol{\varepsilon}$ the bulk strain, $\boldsymbol{\varepsilon} = sym\nabla \otimes \mathbf{u}$

$$\left(\phi - \phi_0\right) = \mathbf{I}:\boldsymbol{\varepsilon} + N^{-1}\left(p - p_0\right) \tag{9.3}$$

The equations (9.1) are determined starting from the Constitutive Equations:

$$\begin{aligned} &\boldsymbol{\sigma} = \mathbb{C}:\boldsymbol{\varepsilon} - p\mathbf{I} \\ &\phi = \mathbf{I}:\boldsymbol{\varepsilon} + N^{-1}p \qquad \left[\mathbf{I} \leftarrow \mathbf{b}\right] \end{aligned} \tag{9.4}$$

and the Darcy's Law (quasi-static filtration):

$$\mathbf{v}_f = \frac{\mathbf{K}_P}{\mu}\nabla p \tag{9.5}$$

where $\mathbf{v}_f$, the difference between the fluid velocity and the solid matrix one, is responsible of the coupling. The first equation (9.1) is obtained from the equilibrium equation:

$$\rho\ddot{\mathbf{u}} - \nabla\cdot\boldsymbol{\sigma} = \rho\mathbf{f} \tag{9.6}$$

while the second one from the continuity equation:

$$\frac{\partial \rho_f \phi}{\partial t} + \nabla \cdot \left(\rho_f \mathbf{v}_f \right) = 0 \tag{9.7}$$

9.2. COUPLED NON-LINEAR THERMOELASTIC PROBLEM

The fundamental equations for a thermoelastic problem ***T*** can be summarized as follows:

$$\begin{aligned} T_1 &: \ \rho \ddot{\mathbf{u}} - \nabla \cdot \left[\mathbb{C} : \boldsymbol{\varepsilon} - \boldsymbol{\beta} \theta \right] = \rho \mathbf{f} \\ T_2 &: \ T_0 \boldsymbol{\beta} : \dot{\boldsymbol{\varepsilon}} + \rho c_\varepsilon \dot{\theta} - \nabla \cdot \left[\mathbf{K}_T \cdot \nabla \theta \right] = W \end{aligned} \tag{9.8}$$

The field variables involved are the displacement, $\mathbf{u} = \mathbf{u}(\mathbf{x}, t)$, the bulk strain, $\boldsymbol{\varepsilon} = sym \nabla \otimes \mathbf{u}$, and the temperature, $\theta = \theta(\mathbf{x}, t)$. In the first equation (9.8), ρ is the density, $\mathbb{C}$ is the forth order stiffness tensor, $\boldsymbol{\beta} = \mathbb{C} : \boldsymbol{\alpha}$ is the second order "thermal stresses" tensor, $\boldsymbol{\alpha}$ is the second order tensor of thermal expansion and $\mathbf{f}$ is the mass force vector. In the second equation, instead, T_0 is the reference temperature $(T_0 = 1K)$ from which θ is measured and c_ε is the specific heat under constant strain and it can be expressed as:

$$c_\varepsilon = c_\sigma - \frac{T_0}{\rho} \boldsymbol{\alpha} : \boldsymbol{\beta} \tag{9.9}$$

where c_σ is the heat capacity at constant pressure. $\mathbf{K}_T \cdot \nabla \theta$ represents the heat flow vector, $\mathbf{K}_T$ is the second rank tensor of thermal conductivity coefficients and W is the heat source intensity. The equations (9.8) are determined starting from the Constitutive Equations:

$$\begin{aligned} \mathbf{T} &= \mathbb{C} : \boldsymbol{\varepsilon} - \boldsymbol{\beta} \theta \\ \mathbf{S} &= \boldsymbol{\beta} : \boldsymbol{\varepsilon} + \frac{\rho c_\varepsilon}{T_0} \theta \end{aligned} \tag{9.10}$$

The first equation (9.8) is obtained from the equilibrium equation:

$$\rho \ddot{\mathbf{u}} - \nabla \cdot \boldsymbol{\sigma} = \rho \mathbf{f} \tag{9.11}$$

while the second one from the heat flow equation:

$$T_0 \cdot \dot{S}_{ent} + \nabla \cdot \mathbf{h} = W \tag{9.12}$$

where S_{ent} is the entropy density and $\mathbf{h}$ is the heat flow vector, expressed as:

$$\mathbf{h} = -\mathbf{K}_T \cdot \nabla\theta \tag{9.13}$$

$\mathbf{h}$ is responsible of the coupling.
The heat flow equation represents the energy balance from the second thermo-dinamical principle.

9.3. COUPLING BETWEEN POROELASTICITY AND THERMOELASTICITY

As shown in Table 9.1, the fundamental equations for coupled non linear poroelasticity and thermoelasticity are formally very similar.

Poro-Elasticity	*Thermo-Elasticity*
$\rho\ddot{\mathbf{u}} - \nabla \cdot \left[\mathbb{C} : \boldsymbol{\varepsilon} - p\mathbf{I}\right] = \rho\mathbf{f}$	$\rho\ddot{\mathbf{u}} - \nabla \cdot \left[\mathbb{C} : \boldsymbol{\varepsilon} - \boldsymbol{\beta}\theta\right] = \rho\mathbf{f}$
$\mathbf{I} : \dot{\boldsymbol{\varepsilon}} + M^{-1}\dot{p} - \nabla \cdot \left[\left(\rho_{f0}\mathbf{g}\right)^{-1}\mathbf{K} \cdot \nabla p\right] = 0$	$T_0\boldsymbol{\beta} : \dot{\boldsymbol{\varepsilon}} + \rho c_\varepsilon \dot{\theta} - \nabla \cdot \left[\mathbf{K}_T \cdot \nabla\theta\right] = 0$

Table 9.1 – Fundamental Equations for Coupled
Non Linear Poro-Elasticity and Thermo-Elasticity

The objective of this work is to solve poroelastic problems performing thermal analysis. For that purpose, it is necessary to find the connection between the parameters of both theories. The conversion factors introduced to write a poroelastic problem as a thermal one are:

$$\begin{aligned} & p \leftrightarrow \theta; \\ & \mathbf{I} \leftrightarrow \boldsymbol{\beta}; \\ & \frac{T_0}{\rho M} \leftrightarrow c_\varepsilon; \\ & \frac{T_0}{\mu}\mathbf{K}_P \leftrightarrow \mathbf{K}_T \end{aligned} \tag{9.14}$$

Nevertheless, the parameters of the two theories involved in the duality relationships (9.14) have very different order of magnitude, which could cause some problems during the solution of the numerical simulations. For these reasons, the following step consists in the introduction of dimensionless parameters in the fundamental equations written before. Table 9.2 shows the

fundamental equations for coupled non linear poroelasticity and thermoelasticity rewritten in terms of the dimensionless parameters.
The symbol ~ in the equations indicates the dimensionless parameters.

Poro-Elasticity*	***Thermo-Elasticity****
$\tilde{\rho}\frac{\partial^2\tilde{\mathbf{u}}}{\partial\tilde{t}^2}-\tilde{\nabla}\cdot\left[\tilde{\mathbb{C}}:\boldsymbol{\varepsilon}-\mathbf{I}\tilde{p}\right]=\tilde{\rho}\tilde{\mathbf{f}}$	$\tilde{\rho}\frac{\partial^2\tilde{\mathbf{u}}}{\partial\tilde{t}^2}-\tilde{\nabla}\cdot\left[\tilde{\mathbb{C}}:\boldsymbol{\varepsilon}-\tilde{\boldsymbol{\beta}}\tilde{\theta}\right]=\tilde{\rho}\tilde{\mathbf{f}}$
$T_0\mathbf{I}:\frac{\partial\tilde{\boldsymbol{\varepsilon}}}{\partial\tilde{t}}+\tilde{\rho}\tilde{c}_p\frac{\partial\tilde{p}}{\partial\tilde{t}}-\tilde{\nabla}\cdot\left[\tilde{\mathbf{K}}\cdot\nabla\tilde{p}\right]=0$	$T_0\tilde{\boldsymbol{\beta}}:\frac{\partial\tilde{\boldsymbol{\varepsilon}}}{\partial\tilde{t}}+\tilde{\rho}\tilde{c}_\varepsilon\frac{\partial\tilde{\theta}}{\partial\tilde{t}}-\tilde{\nabla}\cdot\left[\tilde{\mathbf{K}}_T\cdot\tilde{\nabla}\tilde{\theta}\right]=0$

Table 9.2 – Fundamental Equations for Coupled Non Linear Poro-Elasticity and Thermo-Elasticity Rewritten in Terms of the Dimensionless Parameters

These equations are written employing the following positions:

$$\begin{aligned}
&\tilde{\mathbf{x}}=\mathbf{x}\,L^{-1};\quad \tilde{\mathbf{u}}=\mathbf{u}\,L^{-1};\quad \tilde{\nabla}=L\nabla;\quad \tilde{t}=T^{-1}t;\quad \tilde{\mathbb{C}}=P^{-1}\mathbb{C};\\
&\tilde{\boldsymbol{\sigma}}=\boldsymbol{\sigma}\,P^{-1};\quad \tilde{\theta}=\theta;\quad \tilde{p}=pP^{-1};\quad \tilde{\rho}=L^2T^{-2}P^{-1}\rho;\\
&\tilde{\mathbf{f}}=T^2L^{-1}\mathbf{f};\quad \tilde{c}_p=T_0PM^{-1}\tilde{\rho}^{-1};\quad \tilde{\mathbf{K}}=T_0PTL^{-2}\mathbf{K}_P\mu^{-1};\\
&\tilde{\mathbf{h}}=-\mathbf{K}_T\cdot\tilde{\nabla}\tilde{\theta}\leftrightarrow\tilde{\mathbf{v}}_f=-\tilde{\mathbf{K}}\cdot\tilde{\nabla}\tilde{p}=-\frac{\mathbf{K}_P}{\mu}\nabla pT_0TL^{-1}=T_0TL^{-1}\mathbf{v}_f
\end{aligned}\tag{9.15}$$

The dimensionless conversion factors are:

$$\begin{aligned}
&\tilde{p}\leftrightarrow\tilde{\theta};\quad \mathbf{I}\leftrightarrow\tilde{\boldsymbol{\beta}}=\tilde{\mathbb{C}}:\boldsymbol{\alpha}=P^{-1}\mathbb{C}:\boldsymbol{\alpha};\\
&\tilde{c}_p\leftrightarrow\tilde{c}_\varepsilon=c_\varepsilon T^2L^{-2};\quad \tilde{\mathbf{K}}\leftrightarrow\tilde{\mathbf{K}}_T=\frac{T}{L^2P}\mathbf{K}_T
\end{aligned}\tag{9.16}$$

where $\alpha=\dfrac{1-2\upsilon}{E}$, L is an enveloping parameter, that is to say the characteristic length of the domain and:

$$\begin{aligned}
&P:=p_{MAX}=\max_{\underline{x},t}\{p\};\\
&T:=t_{MAX}=\max_{\mathbb{R}^+}\{t\};
\end{aligned}\tag{9.17}$$

The dimensionless conversion factors are evaluated referring to the maximum values of length, pressure and time to ensure reasonable values of the parameters involved in the numerical simulations.
Employing the coupling theory presented before, it is possible to solve a transient non linear poroelastic problem as a corresponding thermoelastic problem, interpreting the temperature as a pressure and the temperature gradient

as a velocity. As a consequence it is possible to force a classical commercial code to solve poro-elastic problems utilizing the thermo-elastic module.

9.4. ON THE INFLUENCE OF COUPLING TERMS IN PORO-THERMOELASTICITY

The pore pressure always has an appreciable influence on the deformation field and, so, the equations of linear poroelasticity are always partially coupled (Zimmerman, 2000).
The solution of a coupled poroelastic or thermoelastic problem is of considerable mathematical difficulty, as it combines the theories of elasticity and of heat conduction or fluid flow under transient conditions. Fortunately, in most of the usual engineering applications it is possible to introduce certain simplifying assumptions without error.
The principal such simplifications are the omission of the mechanical coupling term in the energy equation (*uncoupled theory*) and of the inertia terms in the equations of motion (*uncoupled quasi- static theory*). To this purpose, Boley and Weiner (1997) investigated the conditions ensuring that a linear thermoelastic problem can be considered uncoupled or uncoupled quasi-static. In the following, this reasoning is presented and, then, it will be extended to the poroelasticity theory, employing the PTD theory presented before. In the thermoelastic problem, if an external mechanical agency produces variations of strain within a body, the heat conduction equation shows that these variations of strain are, in general, accompanied by variations in temperature and consequently by a heat flow; the whole process, thus, gives rise to an increase of entropy and, therefore, to an increase in the energy stored in a mechanically irrecoverable manner.
This phenomenon, known as *thermoelastic dissipation*, requires for its analysis the use of the coupled heat equation. The mechanical term in the heat equation clearly plays a crucial role in the description of this dissipative process, and its omission would here be meaningless.
However, the deformations due to the external loads are accompanied only by small changes in temperature, and it would, therefore, appear reasonable to calculate these deformation without taking account of the thermal expansion. Similarly, if strain are produced in a body by a non-uniform temperature distribution, it would seem intuitively clear that the influence of these strains on the temperature itself should not be too large. One may therefore anticipate the conclusion that the coupling term appearing in the heat equation can be disregarded for all problem except those in which the thermoelastic dissipation is of primary interest. This matter may be made plausible by the following reasoning. The coupled heat equation may be rewritten as:

$$K_T \Delta T = \rho c_v \dot{T} \left[1 + \delta \left(\frac{\lambda + 2\mu}{3\lambda + 2\mu} \right) \left(\frac{\dot{e}}{\alpha \dot{T}} \right) \right] \tag{9.18}$$

where c_v, the specific heat at constant volume, and c_ε, the specific heat at constant deformation, may be employed interchangeably in the linear theory. The non-dimensional parameter δ is defined by:

$$\delta = \frac{(3\lambda + 2\mu)^2 \alpha^2 T_0}{\rho^2 c_v v_e^{\,2}} \tag{9.19}$$

v_e is the velocity of propagation of dilatational waves in an elastic medium, defined as:

$$v_e = \sqrt{(\lambda + 2\mu)/\rho} \tag{9.20}$$

The term proportional to δ is the coupling term and it is negligible compared to unity if:

$$\frac{\dot{e}}{3\alpha \dot{T}} \ll \left(\frac{\lambda + 2\mu/3}{\lambda + 2\mu} \right) \frac{1}{\delta} \tag{9.21}$$

Equation (9.21) furnishes a comparison between an external factor, $\frac{\dot{e}}{3\alpha \dot{T}}$, directly linked to the thermal-mechanical input, and the intrinsic thermo-mechanical properties of the material, $\left(\frac{\lambda + 2\mu/3}{\lambda + 2\mu} \right) \frac{1}{\delta}$.

To estimate a priori if the problem is uncoupled, both terms of equation (9.21) need to be evaluated.

As already said, the term $\left(\frac{\lambda + 2\mu/3}{\lambda + 2\mu} \right) \frac{1}{\delta}$ depends on thermal, physical and mechanical parameters and, so, it can be determined a priori for the analyzed problem.

For what concerns, instead, the other term, $\frac{\dot{e}}{3\alpha \dot{T}}$, even if it is associated to the thermo-mechanical output, it can be estimated from the thermal-mechanical input.

This term, in fact, represents the ratio between two deformation rates. In the hypothesis of linear thermoelastic theory, $\dot{e}$ can be decomposed in the sum of

two contributions, i.e., $\dot{e} = \dot{e}^{el} + \dot{e}^{t}$, where $\dot{e}^{el}$ is the elastic deformation rate, depending on the constitutive behavior of the material,and $\dot{e}^{t}$ is, instead, the thermal deformation rate, expressed as $3\alpha\dot{T}$. Equation (9.21) can be, thus, rewritten as:

$$\frac{\dot{e}^{el} + \dot{e}^{t}}{\dot{e}^{t}} \ll \left(\frac{\lambda + 2\mu/3}{\lambda + 2\mu} \right) \frac{1}{\delta} \tag{9.22}$$

The order of magnitude of the elastic deformation rate, $\dot{e}^{el}$, can be estimated starting from the loading conditions, while, for the thermal deformation rate, $\dot{e}^{t}$, an estimate can be made considering the boundary conditions on temperature or on its flux. For temperature distributions with no sharp variation or discontinuities in their time histories, it is intuitively expected that the time rate of change of the dilatation is of the same order of magnitude as that of the temperature; thus, the disregarded of coupling as described previously appears to be reasonable. The possibility of omitting the coupling terms depends not only on the fact that the inequality $\delta \ll 1$ must hold (as it does for most metals), but also on the fact that strain rates must be of the same order of magnitude as the temperature rate. The latter condition implies that the time history of the displacement closely follows that of the temperature; in other words, no pronounced lag or vibrations in the motion of the body must arise. It is, therefore, to be expected that the magnitude of inertia effects will also enter this question, so that a close relationship can be anticipated to exist between the two previously mentioned simplifications of the general theory. Starting from equation (9.21), it is possible to extend the same considerations to the poroelasticity theory. The second equation (9.1) can be written as:

$$\frac{K_P}{\mu}\Delta p - \frac{1}{M}\dot{p} - \dot{e} = 0 \tag{9.23}$$

and, then, rearranged in the following form:

$$\frac{K_P}{\mu}\Delta p - \frac{1}{M}\dot{p}\left[1 + \frac{\dot{e}}{\dot{p}}M\right] = 0 \tag{9.24}$$

Following the approach proposed by Boley and Weiner (1997), a poroelastic problem results, thus, uncoupled if the following inequality holds:

$$\frac{\dot{e}}{\dot{p}} << \frac{1}{M} \tag{9.25}$$

However, the simple form of equation (9.25) hides some interesting aspects.
To ensure that a poroelastic problem is uncoupled, it is not sufficient that $\frac{1}{M}$ is very small, but, paradoxically, it should also happen that $\frac{\dot{e}}{\dot{p}} << \frac{1}{M}$. Also in this case, an evaluation a priori of the two terms appearing in the equation (9.25) is necessary. The term $\frac{1}{M}$ is strictly connected to the physical poroelastic properties of the material and it can be easily evaluated *a priori*. The term associated to the poroelastic-mechanical output, $\frac{\dot{e}}{\dot{p}}$, can be estimated starting from the order of magnitude of the loading and boundary conditions. Nevertheless, even if $\frac{\dot{e}}{\dot{p}} M \cong 1$, the problem could result uncoupled. The term $\left[1+\frac{\dot{e}}{\dot{p}} M\right]$ becomes, in fact, equal to 2; if $\frac{1}{M}\dot{p} << \frac{K_P}{\mu}\Delta p$, the poroelastic problem becomes not only uncoupled but also steady-state. Moreover, Boley and Weiner (1997) extended their reasoning considering also the conditions under which a thermoelastic problem can be considered uncoupled and quasi static. They demonstrated, in fact, that when inertial effects are small, also the coupling effects are negligible. The condition on the inertial effects rises from a comparison between the thermal input characteristic time (TICT), t_0^T, and the mechanical t_M, and thermal characteristic times t_T, defined as:

$$t_M = \frac{L}{v_e}; \qquad t_T = \frac{L^2 \rho c_\varepsilon}{K_P} \tag{9.26}$$

where L is the characteristic length of the problem and the term $\frac{K_T}{\rho c_\varepsilon}$ is the thermal diffusivity. The TICT can be evaluated starting from the boundary condition on temperature.
If a temperature profile is assigned in a prescribed point of the boundary, the TICT, t_0^T, can be determined as:

$$t_0^T = \left(\frac{\frac{\partial T(x_0,t)}{\partial t}}{T_{MAX}} \right)^{-1} \tag{9.27}$$

Boley and Weiner (1997) reported that if the following inequalities subsist:

$$t_T \gg t_M, \quad t_0^T \gg t_M \tag{9.28}$$

both coupling effects and inertial effects are small.
To this purpose, in thermoelasticity theory, the following parameter is introduced:

$$h^T = \sqrt{\frac{t_M}{t_T}}\sqrt{\frac{t_M}{t_0^T}} \tag{9.29}$$

and, then, the thermoelastic problem results uncoupled and quasi static if:

$$h^T << 1 \tag{9.30}$$

Replacing the relationships (9.26) in the equations (9.29), the condition (9.30) becomes:

$$\sqrt{\frac{K_T}{(\lambda+2\mu)t_0^T c_\varepsilon}} << 1 \tag{9.31}$$

Employing the coupling between poroelasticity and thermoelasticity, the poroelastic input characteristic time (PICT) can be determined starting from the definition of the thermal one, (9.27), as:

$$t_0^P = \left(\frac{\dfrac{\partial p(x_0,t)}{\partial t}}{P_{MAX}} \right)^{-1} \tag{9.32}$$

Moreover, starting from the definition of the TCT, equation (9.26), and employing the relationships:

$$\begin{aligned} K_T &\leftrightarrow \frac{T_0 K_P}{\mu} \\ \rho c_\varepsilon &\leftrightarrow \frac{T_0}{M} \end{aligned} \tag{9.33}$$

the characteristic time of a poroelastic problem (PCT), t_P, can be, thus, written as:

$$t_P = \frac{L^2 \mu}{K_P M} \tag{9.34}$$

and, from equation (9.29), a poroelastic problem results, indeed, uncoupled and quasi static if:

$$h^P = \sqrt{\frac{t_M}{t_P}} \sqrt{\frac{t_M}{t_0^P}} << 1 \tag{9.35}$$

Replacing the relationships (9.26) and (9.34) in the equations (9.35), the uncoupled quasi-static condition becomes:

$$\sqrt{\frac{\rho K_P M}{(\lambda + 2\mu) t_0^P \mu}} << 1 \tag{9.36}$$

Table 9.3 is a résumé of the conditions presented in this paragraph. It represents, thus, a very important instrument because it allows to estimate a priori if the examined problem is coupled, uncoupled or quasi-static, avoiding, indeed, excessive computational costs in the analyses performed.
The first step of this analysis consists, thus, in the evaluation of the input time, t_0^T or t_0^P, starting from the boundary conditions. Then, the parameters h^T, for the thermoelastic problem, and h^P, for the poroelastic one, are evaluated to determine if the problem is uncoupled quasi static. If the conditions (9.31) or (9.36) do not hold, the conditions (9.21) and (9.25) are investigated, to verify if the problem is uncoupled.
Finally, if also these two last conditions do not subsist, the problem results coupled.

	Poro-Elasticity	***Thermo-Elasticity***
t_0	$t_0^P = \left(\frac{\frac{\partial p(x_0,t)}{\partial t}}{P_{MAX}} \right)^{-1}$	$t_0^T = \left(\frac{\frac{\partial T(x_0,t)}{\partial t}}{T_{MAX}} \right)^{-1}$
Uncoupled Quasi static	$\sqrt{\frac{\rho K_P M}{(\lambda + 2\mu) t_0^P \mu}} << 1$	$\sqrt{\frac{K_T}{(\lambda + 2\mu) t_0^T c_\varepsilon}} << 1$
Uncoupled	$\frac{\dot{e}}{\dot{p}} << \frac{1}{M}$	$\frac{\dot{e}}{3\alpha \dot{T}} \ll \left(\frac{\lambda + 2\mu/3}{\lambda + 2\mu} \right) \frac{1}{\delta}$

Table 9.3 – Résumé of the Uncoupled-Quasi Static Conditions for Thermo-Elastic and Poro-Elastic Problems

REFERENCES

Boley BA., Weiner JH. 1997. Theory of thermal stresses. Dover Pubblications.

Zimmerman RW. 2000. Coupling in poroelasticity and thermoelasticity. International Journal of Rock Mechanics and Mining Sciences. 37: 79-87.

10 PERSPECTIVES

Many analytical and numerical approaches have been proposed in order to solve poroelastic problems describing the behavior of biological tissues. The main difficulty associated to numerical strategies concerns the solution of the coupled poroelastic equations for determining the solid response in terms of deformation and filtration. The proposal of this work is to find a strategy to numerically solve poroelastic problems employing the Finite Element Method (FEM). In particular, the strategy presented is based on the well known similarity between thermoelasticity and poroelasticity theories. This analogy allows to solve transient poroelastic problems as corresponding thermoelastic ones, interpreting the temperature as a pressure and thermal gradients as velocities. With this aim, the relationship between thermoelasticity and poroelasticity is formulated in terms of dimensionless parameters to ensure numerical stability, because the elasticity moduli, filtration coefficients and porosity have essentially different orders of magnitude. Thus, the dimensionless equations obtained are implemented in numerical FEM-based computations. Such transferring to equivalent thermoelastic problems enables to apply the FEM package Ansys® 11, which provides opportunities to solve coupled thermoelastic problems in transient non linear settings. Two numerical examples are presented. The first one is concerning

a very important problem of drug delivery in solid tumors. The second example is, instead, related to the investigation of the role played by trigonal-like microstructure in osteons in bone adaptive, growth and remodeling processes.

10.1. INTRODUCTION TO OSTEONS

The analysis of the role of bone microstructure in bone mechano-trasduction process have been investigated utilizing Finite Element Method. Bone is a living tissue, hierarchically organized, constituted by liquid and solid components, strictly interacting to optimize the structure for its functions (Knothe Tate, 2003). Bone cells actively recognize and respond to mechanical and chemical stimuli in the process known as *mechano-chemical transduction*. Human bone is continuously renewed by basic multicellular units (BMUs), working in a coordinate fashion to reabsorb old bone and, then, filling the gap with new bone tissue organized in osteons in cortical bone. The mechanical properties of these secondary osteons are crucial for the stability of the entire bone. The cells involved in the remodeling process are the osteoblasts, actively engaged in the production of extracellular matrix (Cowin et al., 1991) and the osteoclasts, bone reabsorbing cells, coordinated by the osteocytes, considered the underestimated conductors of bone orchestra (Bonucci, 2009). Osteocytes are thought to be the mechanosensory cells in bone because they detect physical stresses, translating them into autocrine and paracrine signals. Mechanical stimuli can be transmitted through the solid matrix of the tissue or indirectly via fluid pressure and shear stresses caused by fluid moving through the lacunocanalicular system due to load-induced fluid flow. Moreover, also chemical signals, associated to diffusive, convective and active transport mechanisms, arrive intracellularly or through the extracellular fluid in which the cells live. A central role in the mechanotrasduction process is carried out by the lacunocanalicular system, which serves as fluid reservoir and, thus, is determinant for the signals transmission. Pericellular fluid in this network is the coupling medium for the translation of mechanical forces into biochemical, mechanochemical, mechanobiological and electromechanical effects in cells, the *machine tools* for bone remodeling. Different biophysical and electrochemical mechanisms can cause bone fluid motion. Apart from endogenous mechanisms, such as active transport in osteocytes, pressure gradients associated to osmotic or pulsatile pressures and exogenous mechanisms induced by mechanical loading can determine fluid motion. Bone tissue behaves like a hierarchically organized stiff, dense, fluid-filled sponge and, as a consequence, Biot's theory of poroelasticity enables to describe the interactions between the solid matrix and the fluid phase (Cowin et al., 2009). Mechanical loading in bone is associated to a tissue stress

state comprising cyclic dilatational and deviatoric components. The dilatational component kindles the fluid pressure, inducing the fluid flow through deformation of the fluid-filled lacunocanalicular and intermatrix porosities within bone tissue.
According to Biot's theory, compression deforms the solid matrix of a porous material, raising instantaneously a pressure increase in the fluid within the pores. The differences in pressure between the interior and exterior of a porous solid cause a net flow of fluid. Removal of load results, instead, in a pressure gradient which guides the fluid inward, until it reduces to zero. Bone formation induced by mechanical loading is site-specific and, so, it depends on the stimuli perceived by the skeleton. Different possible remodeling stimuli have been considered, such as strain magnitude, strain rate, strain frequency and the strain tensor. Recently, Gross et al. (1997) indicated that peak magnitude strain gradients, deducible from bone load environment and geometry, are strictly correlated with the sites of bone formation. Moreover, strain gradients are associated to fluid flow in the canalicular network. Ruimerman et al. (2005) considered both the effects of the volumetric strain, representing the actual load on the osteocytes, and of its gradient, related to the mechanical effects on fluid flow. As illustrated, osteon microstructure plays a fundamental role in guiding fluid flow and is optimized for the functions it has to fulfill. Bone is an intelligent material and its architecture is a consequence of the loads acting on it. The cylindrical osteons design can be seen as the response to the load history. Their distribution in compact bone, in fact, corresponds to the distribution of principal stresses acting on bone. Osteons structure ensures maximum load-bearing capacity and resistance to weakness induced by fatigue and microdamage (Weiner et al., 1999). Bàca et al. (2007) analyzed the course of osteons of the human proximal femur, underlying that osteons are present above all in the regions subjected to high stress and absent in all regions where loading of the bone is not significant. Osteons enable bone to respond optimally to the stress applied thanks to their peculiar mechanical properties, determined by the specific pattern of collagen fibers. Tests of macroscopic samples have demonstrated that collagen fibers orientation is correlated to the mechanical properties of long bones, independently of the type of species. Ramasamy et al. (2006) argued that collagen fibers orientation is a potential result of a microarchitectural adaptation process to the load environment and that the specific orientation is determined by the mineralization that freezes the collagen fibers in the directions dictated by physiological strains. Collagen fibers orientation is considered an important predictor of the tensile strength of cortical bone and a measure of toughness. Skedros et al. (2009) noted that longitudinal oriented collagen fibers determine greater strength in tension and also a grater elastic modulus, while transverse collagen fibers are optimized for compressive stresses. Fibers orientation obviously changes within the bone segments. Beraudi et al. (2009) analyzed the collagen orientation in human femur, tibia and fibula shaft by circularly polarized light. They found, indeed, that transverse fibers

become predominant moving versus epiphyses where the compressive physiological forces are more aligned with the shaft cross section, confirming that the collagen pattern is strictly dependent on the loads to bear. Besides, collagen orientation is a fundamental factor also in fracture initiation and arrest (Weiner et al., 1999).
Microdamage in bone occurs in the form of microcracks as a result of everyday cyclical loading activities (Mohsin et al., 2006) and it represents a stimulus for remodeling. Porosity, mineralization, collagen fibers orientation are all factors which promote cracks initiation, but hinder their growth.
Gupta et al. (2006) considered osteons as mechanically modulated laminates of mineralized collagen fibril layers, characterized by the alternance of a wide band of stiffer mineralized matrix with thin bands of softer material. This mechanical modulation provides an example of a natural crack stopping mechanism. Moreover, also the stiffness variation of single lamellae may serve as a crack trapping mechanism inside osteons, preventing cracks running in the interstitial bone from propagating toward the inner Haversian canal. However, lamellar interface in bone is weak and, so, it is the principal site of shear damage formation, but it is also highly effective in keeping cracks isolated from each others. Some authors also proposed that the cement lines, surrounding osteons, can be seen as barriers to crack growth (O'Brien et al., 2007), because they can reduce the shear strength of osteonal bone. O'Brien et al. explained the osteons crack-stopping mechanism comparing them to composite materials. Also osteons, in fact, provide numerous sites for crack initiation, but the fibers act as barriers and prevent further growth. Another important aspect of osteons microstructure needs to be considered. Wagermaier et al. (2006) hypothesized a three-dimensional spiraling of collagen fibrils in osteonal bone. They argued that the helicoidal structure provides more resistance to mechanical loads and enables a higher extensibility in tension and compression. They proposed that one of the advantages of such a helicoidal plywood structure could be the protection of the blood vessels against failure of the surrounding matrix. Nevertheless, at the best author knowledge, no works have been presented in literature where the helical microstructure of lamellae in osteons has been interpreted as a significant factor for driving nutrients.

10.2. FE SIMULATION OF A TYPICAL OSTEON UNIT

A poroelastic steady-state analysis has been conducted on a FEM model of osteons to demonstrate that osteons microstructure itself is a key element to understand bone adaptive, growth and remodeling processes, employing the Poro-Thermo Duality theory. Numerical simulations have been carried out considering that the osteon length and its internal radius are respectively 300 μm

and 30 μm. In this model, the osteon is constituted by 10 lamellae with a thickness of about 5 μm. For the wrapping angle, nine different values are considered to simulate T-type osteons $(\theta = 0)$, L-type osteons $(\theta = \frac{\pi}{2})$ and oblique-type osteons $\left(\theta = i \cdot \frac{\pi}{12},\ \ i \in \{1,2,3,4,5\} \right)$.

A parametrical custom-made Ansys® environment macro was developed to assign different anisotropic properties to the lamellae. The FEM based model was constructed by means of hexahedral 8 nodes elements with linear shape functions generating a 364.800 elements and 380.182 nodes mesh with 4 elements in each lamella thickness; the model is shown in Figure 10.1. The boundary conditions and the constraints imposed in the model reflect osteons physiological conditions. The osteon is constrainted on the basis, simulating bone typical *packaging* at the microstructural level. A pressure is applied on the internal surface, simulating the interstitial pressure in the Haversian channel, while the pressure on the external surface is zero.

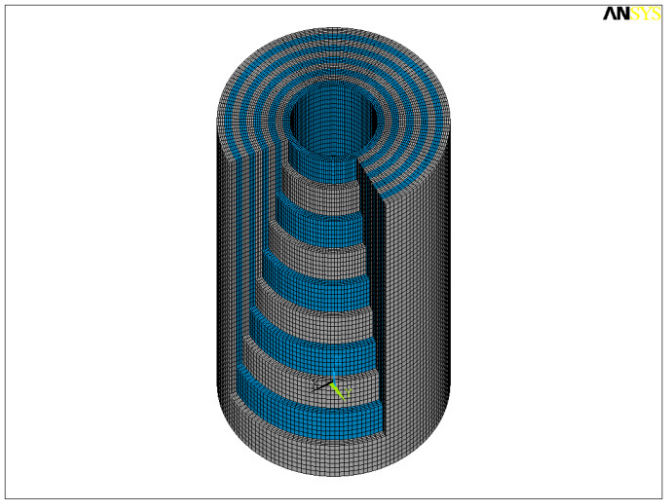

Fig. 10.1 – Finite Element Mesh of the osteons model

Due to the trigonal microstructure, the applied pressure may induce the osteon rotation, but the presence of other osteons in the environment thwarts the osteon to move. This aspect is simulated by imposing zero tractions on the internal surface and a prescribed traction acting on the external one as boundary conditions.

The elastic constants of the osteon are summarized in Table 10.1 and Table 10.2 in terms of elastic moduli and Poisson's coefficients respectively.

Finally Table 10.3 reports the estimated bone matrix elastic constants of a single lamella for type L osteon (Yoon and Cowin 2008), used as starting point to

evaluate the lamellar elastic constants for osteons with different values of the wrapping fibers angle.

	ELASTIC MODULI [GPa]
E_1^m	16.4
E_2^m	18.7
E_3^m	22.8
G_{12}^m	7.2
G_{13}^m	7.1
G_{23}^m	8.4

Table 10.1 – Estimated bone matrix elastic moduli of a single lamella for type L osteon (Yoon and Cowin 2008)

	POISSON'S COEFFICIENTS
υ_{12}^m	0.334
υ_{12}^m	0.237
υ_{12}^m	0.381
υ_{12}^m	0.247
υ_{12}^m	0.330
υ_{12}^m	0.301

Table 10.2 – Estimated bone matrix Poisson's coefficients of a single lamella for type L osteon (Yoon and Cowin 2008)

The material parameters employed in the analysis are reported in Table 10.3 (Rémond et al., 2008).

$K^p[m^2]$	$\mu[Pa]$	$M[GPa]$
10^{-18}	10^{-18}	40

Table 10.3 – Material parameters (Rémond et al., 2008)

Nature always optimizes structures to the specific functions to fulfill.
The helicoidal pattern of the collagen fibers results, thus, a key element for understanding osteonal behavior. It will be shown that, together with the qualitative results, the apparently negligible difference in trigonal elastic constants with respect to the orthotropic ones produces significant differences in

terms of poroelastic behavior and, then, in terms of biomechanical consequences. The resulting trigonal microstructure, in fact, is crucial for many aspect associated to osteons functions, such as fluid velocity magnitude.
Figure 10.2 shows the different velocity profiles for the trigonal (blue line) and orthotropic model (red line).

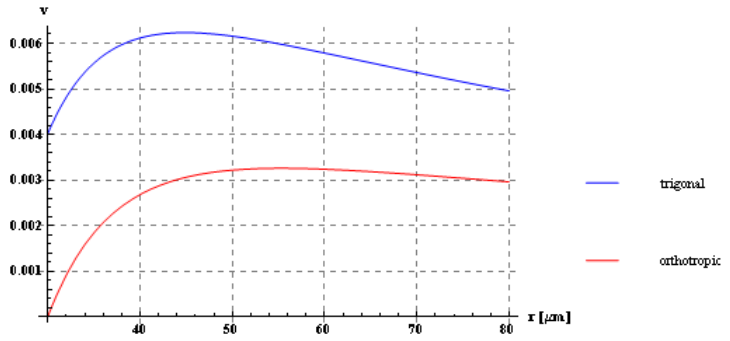

Fig. 10.2 – Comparison between velocity profiles for the trigonal (blue line) and the orthotropic model (red line)

The analyses of the velocity profiles reveals that the trigonal model appears to generate significant increases of velocity and, then, fluid shear stresses can be envisaged to activate mechanosensory in osteocytes and BMU activities as a cell response. Fluid shear stresses, in fact, play a crucial role in bone remodeling process. Fluid flow induces shear stress on cell membranes, a well-known stimulus for bone remodeling (Smit et al., 2002). Bone cells are particularly sensitive to fluid shear stress, which cause the release of different kinds of substances, ensuring the transmission of biochemical signals. Strain induced fluid flow results, thus, a powerful regulator of cells behavior and, so, a determinant factor in bone mechanotrasduction. The bone mechanosensor cells, i.e. the osteocytes, are, in fact, actively stimulated by fluid shear stresses. Moreover, according to Darcy's Law, velocity is directly linked to pressure gradients. As a consequence, trigonal microstructure determines also a significant increase in pressure gradients, responsible of fluid motion. However, trigonal model appears to generate also significant increases in volumetric strain gradients respect to the values obtained employing an orthotropic osteon model.
This result has very important implications because strain gradients have been proposed as a possible remodeling stimulus (Gross et al. 1997). Moreover, also volumetric strain is influenced by trigonal microstructure, as shown in Figure 10.3. In the volumetric strain profiles, in fact, a 20% increase can be highlighted by taking into account trigonal symmetry of the osteon.
This can be a factor that participates to the well-known mechanism of strain amplification, here induced by the helicoidal arrangement of lamellae.
In bone physiology, in fact, an important paradox exists, associated to the strain levels perceived in bone at the cellular level. Strains applied to the macroscopic

bone are, in fact, smaller then the strains necessary to activate mechanotrasduction processes and, thus, an amplification phenomenon should exist to ensure sufficient magnitude stimuli to bone cells (Cowin, 2002).

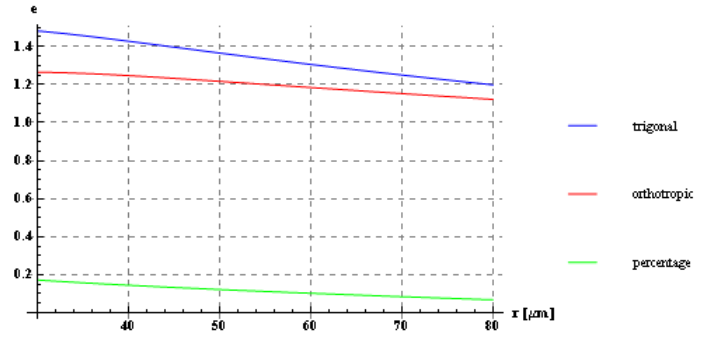

Fig. 10.3 – Comparison between volumetric strain profiles for the trigonal (blue line) and the orthotropic model (red line). Green line represents the percentage difference between the two models

An answer to this interesting paradox has not been found yet, even if different possible models have been proposed.
Han et al. (2004) suggested, for example, a possible strain amplification mechanism associated to the fluid flow through the pericellular matrix at the lacunar-canalicular porosity level.
However, our results envisage that trigonal microstructure aids the strain amplification phenomenon, ensuring the strain levels needed to activate signaling in bone.

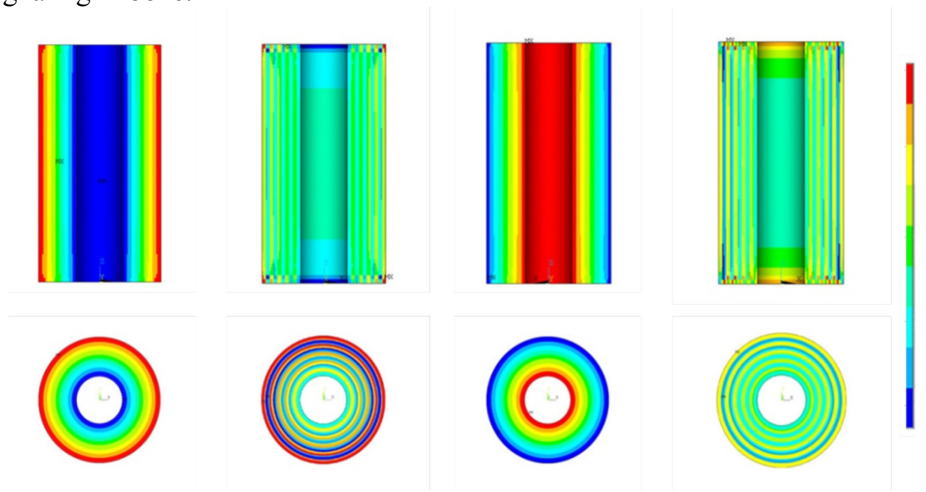

Fig. 10.4 – Variation of the volumetric strain in frontal and transverse osteon sections at one half of the overall length for $\theta = \frac{\pi}{4}$

Figure 10.4 is, instead, a sketch of the variation of the volumetric strain in a frontal section, highliting what happens in the longitudinal direction, and in a transverse section, emphasizing the behavior in the radial direction. These sections are obtained at one half of the overall osteon length for $\theta = \frac{\pi}{4}$.

Another important consequence of trigonal microstructure is associated to the change in sign and jumping at the interface of the in-plane shears, reported in Figure 10.5.

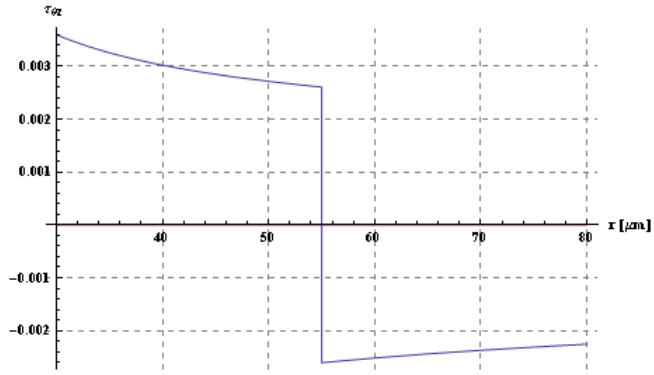

Fig. 10.5 – In plane-shears for the trigonal model

This phenomenon has important effects for what concerns osteocytes stimulation. Osteocytes are placed within niches of calcified matrix, the osteocyte lacunae, at the lamellae interfaces. As well known, different stimuli induce different pathways of biological signals. Moreover, mechanical loading induce also a rapid osteocytes production of nitric oxide and prostaglandin. It has been demonstrated that these substances are released as a consequence of the wall shear stresses (Bonucci, 2009). Finally, trigonal microstructure could also explain how osteons can act as microcracks barriers. Microdamage in bone occurs in the form of microcracks as a result of everyday cyclical loading activities (Mohsin et al. 2006) and it represents a stimulus for remodeling and repair. However, bone microstructure is also optimized to prevent microcracks propagation, slowing or altering their propagation direction and velocity. Microcracks, in fact, usually initiate in interstitial bone and stop when encountering cement lines, acting as weak interfaces, or somewhere within the osteon (Huang et al., 2006). Some authors proposed that the cement lines, surrounding osteons, can be seen as barriers to crack growth (O'Brien et al. 2007), because they can reduce the shear strength of osteonal bone. Moreover, also osteons themselves act as microcracks barriers. To this purpose, O'Brien et al. explained the osteons crack-stopping mechanism comparing them to composite materials. Also osteons, in fact, provide numerous sites for crack initiation, but the fibers act as barriers and prevent further growth. Osteons crack stoppers function can be material induced, i.e. associated to their intrinsic

material properties, or stress induced, i.e. associated to the stress levels experienced. For what concerns the material properties, Gupta et al. (2006) considered osteons as mechanically modulated laminates of mineralized collagen fibril layers, characterized by the alternance of a wide band of stiffer mineralized matrix with thin bands of softer material. This mechanical modulation provides an example of a natural crack stopping mechanism. Moreover, also the stiffness variation of single lamellae may serve as a crack trapping mechanism inside osteons, preventing cracks running in the interstitial bone from propagating toward the inner Haversian canal. Obviously, this kind of behavior is highlighted also when an orthotropic osteon model is employed. However, as just said before, the crack stopping behavior do not depend exclusively on the material properties, but also on stress intensity. Stresses profiles for trigonal and orthotropic osteons models have been investigated, with the purpose of showing the consequences of the different trends on the crack stopping mechanism. For a mode I crack, propagating in the radial direction, the comparison between the hoop stresses profiles for the two models emphasizes that trigonal microstructure ensures a crack stopping behavior .
As shown in Figure 10.6, the hoop stress gradients, in fact, decrease respect to the orthotropic case and, so, also the crack propagation velocity decreases. For a mode III crack, instead, referring to Figure 6.19, the analysis of shear stresses shows that an in-plane torque-induced shear stress kindles within the lamellar structure of trigonal osteons only, as a consequence of the kinematical constraint on the twisting angle, while this stress is zero for an orthotropic model.

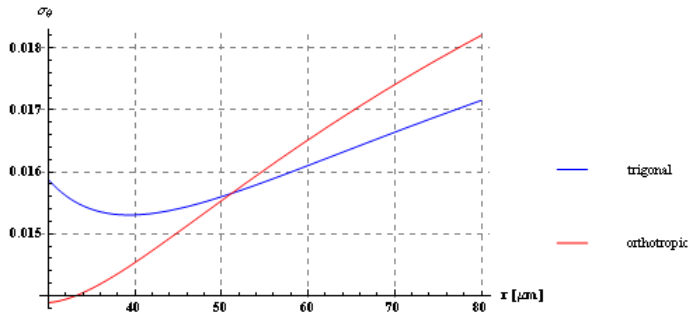

Fig. 10.6 – Comparison between the hoop stresses profiles
for the trigonal (blue line) and the orthotropic model (red line)

As shown in Figure 10.6, the hoop stress gradients, in fact, decrease respect to the orthotropic case and, so, also the crack propagation velocity decreases. For a mode III crack, instead, referring to Figure 10.5, the analysis of shear stresses shows that an in-plane torque-induced shear stress kindles within the lamellar structure of trigonal osteons only, as a consequence of the kinematical constraint on the twisting angle, while this stress is zero for an orthotropic model.

Moreover, in-plane shears change sign and jump passing from a lamella to the following one, revealing a stress induced crack stopping mechanism.
All these considerations support the idea that osteons trigonal microstructure is fundamental for bone adaptive and survival functions. Moreover, the trigonal microstructure ensures also the signaling far away the site of emission, creating a pathway for the fluid which can flow interlamellar and also in the osteon network. Figure 10.7 represents the organization of osteons in a cross section of a human femur. The inner region is reported on the left, while the outer one on the right. Dark osteons are indicated with A, Bright osteons with B, Alternating ones with C and hooped osteons, containing a thick portion of the peripheral boundary with a bright appearance under polarized light, with DThe different kinds of osteons showed in this image suggest that they are not only the bone answer to mechanical stimuli but also a system to optimize fluid flow and, thus, signaling in bone.

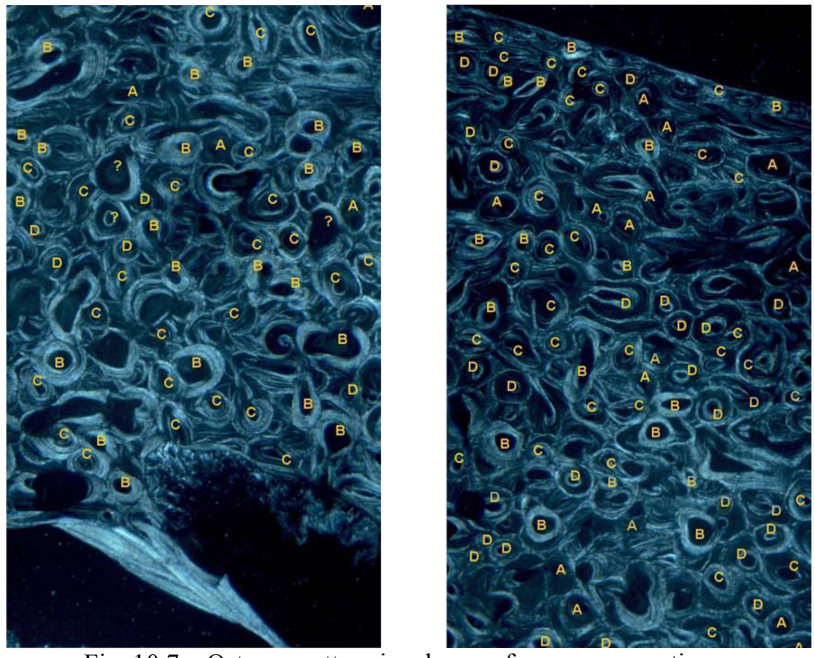

Fig. 10.7 – Osteons pattern in a human femur cross section.

Finally the next figures illustrate the shear stress in the case of $\theta = 0$ and $\theta = \frac{\pi}{4}$ respectively.
Considering the position of the osteocytes between contiguous lamellas, the value of the shear stress in the cases of $\theta = 0$ differ of two order of magnitude less then the case of $\theta = \frac{\pi}{4}$. This so big difference suggest the important role of mechano-trasduction in the phenomenon regulating the bone process and, in

particular, the importance of the angle of wrapping of the fibers in determining the action of the osteocytes which will active theirself, starting the usual bone process, depending of the value of the mechanical stress they fill.

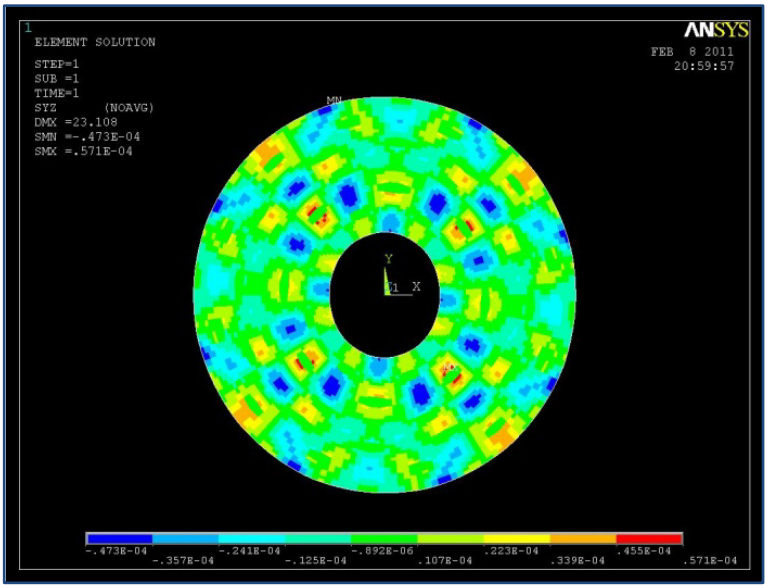

Fig. 10.8 – Shear stress in Osteons with $\theta = 0$.

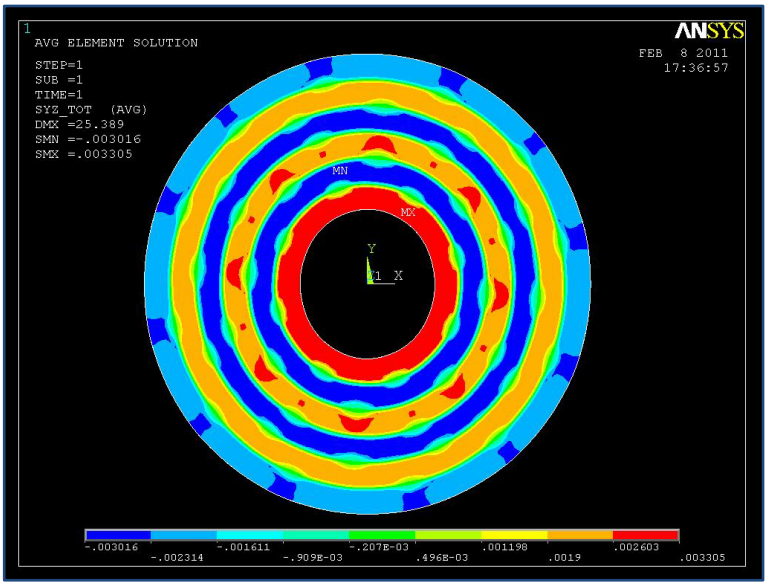

Fig. 10.9 – Shear stress in Osteons with $\theta = \frac{\pi}{4}$.

10.3. INTRODUCTION TO DRUG DELIVERY TO SOLID TUMORS

This second FEM application concerns the analysis of the Convection-Enhanced Delivery (CED) technique for the delivery of drugs to brain tissue. Primary central nervous system tumors are the second cause of cancer death in younger population (Allard et al, 2009). The difficulties in cancer treatment are associated to its characteristic features, such as the uncontrolled cell growth, not regulated by external signals, and the capacity to invade tissues, metastasize and colonize at distant sites. There are several modes of therapy for brain tumors. The first treatment is, usually, the tumor resection, associated to radiotherapy and chemotherapy. The major difficulties in the treatment of brain tumors is the effectiveness of the delivery of therapeutic agents. Drug delivery in vivo results difficult because of the presence of physiological barriers, drug resistance of tumor cells, tissue tolerance and so on (Yuan, 1998). In brain, the two major obstacles for drug delivery are represented by the blood-brain barrier (BBB), almost impermeable to drugs (Baxter and Jain, 1989), and the interstitial fluid pressure (IFP), which is high in the solid tumor and decreases abruptly in the tumor periphery (Jain, 1988), caused by the disorganized vascular network and the absence of functional lymphatics. Many efforts have been made to model the phenomena involved in the delivery of drugs to solid tumors and to understand how to ride out physiological obstacles. Walker et al. (1996), for example, proposed an analytical model to investigate the effect of the protocols to overcome the blood brain barrier on the different drug transport processes, focusing on the role of convection and the influence of the changing parameters. Netti et al. (1995) proposed a poroelastic model of a solid tumor to investigate the mechanisms which regulate the interstitial fluid pressure, looking for a possible strategy to overcome this physiological barrier. Supporting the analytical approach with experimental data, they found that the periodic administration of vasoactive agents improve the effectiveness of the macromolecular delivery. Moreover, also tumor blood flow plays a crucial role in tumor therapy and it is characterized by temporal and spatial heterogeneities (Netti et al., 1996), probably due to the coupling between interstitial fluid pressure and tumor microvascular pressure (Mollica et al., 2003). Infusion-based techniques seem to be promising approaches for the delivery of therapeutic agents to brain tissue because convection enhances drug transport, ensuring the drug release in larger regions respect to pure diffusion. Based on these considerations, the Convection-Enhanced Delivery (CED) technique has been recently proposed. It is defined as the continuous delivery of a therapeutic fluid agent simply guided by pressure gradients (Allard et al., 2009). CED enables the drugs to cross the BBB and supplements diffusion in the delivery of large drugs over required distances, determining greater in situ drug concentrations and reducing systemic toxicity. A wide range of substances can be locally delivered with this technique, such as monoclonal antibodies, conventional chemotherapeutic agents, proteins, nanocarriers, targeted toxins and viruses. The

effectiveness of CED is strictly connected to the different parameters proper of this technique. For this reason, CED protocols need to take into account the infusate concentration, the volume of the infusate, the infusion rate and site, the backflow mechanism. To improve CED protocols and to predict drug distribution profiles, analytical and numerical models have been developed. To this purpose, the poroelasticity theory is a very useful instrument to describe soft tissue mechanics (Biot, 1955) and it can also be used to model the coupling between fluid flow and solid deformation in tumors.

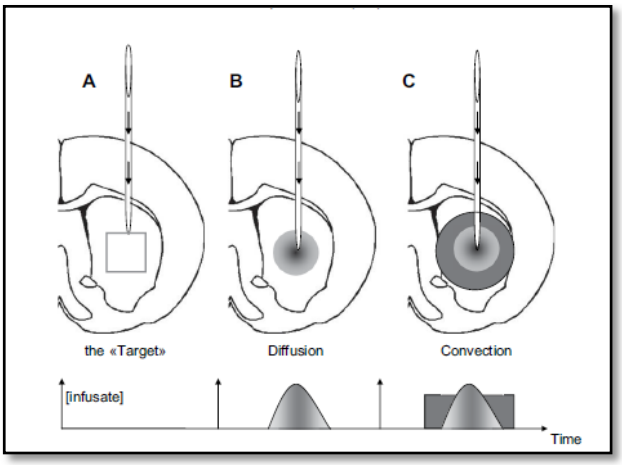

Fig. 10.10 – Schematic representation of CED mechanism (Allard et al., 2009)
A: identification of the target site with correct placement of the catheter according to specific coordinates. B: Diffusion occurs all the time but is rigorously dependent of the infusate nature. C: Convection (or bulk flow) is strictly dependent on the pressure gradient and occurs during all the establishment of the pressure gradient.

Basser (1992) presented an analytical model of infusion-induced swelling in brain, treating white and gray matter as linear poroelastic isotropic media. He found an analytical steady-state solution to estimate interstitial fluid pressure and fluid velocity profiles during infusion into brain. Smith and Humphrey (2007) proposed a model for the CED in brain tissue, deriving the interstitial fluid pressure and fluid velocity induced by infusion into brain tissue and in a tissue-isolated tumor. They determined steady-state and transient solutions for the proposed model.
Also Netti et al. (1997) employed the poroelasticity theory to describe fluid movement in soft tissues at macroscopic and microscopic scales, specializing the model to a local analysis of blood flow around a single blood vessel. Moreover, they applied the model to determine an analytical solution for a spherical solid tumor, obtaining the interstitial fluid pressure and fluid velocity profiles. Roose et al. (2003), instead, employing a poroelastic model, investigated solid stress associated to a spheroid tumor growth in order to better understand the effects of

the growth on the surrounding environment. The model, validated by experimental results, suggests that the range of stresses created by tumor growth are considerable and could collapse blood and lymphatics vessels, contributing to the lack of vessels in the middle of the tumor. Moreover, to take into account transient evolution of the phenomena associated to the drug delivery to solid tumors, Netti et al. (2003) proposed a poroviscoelastic model for a spherical geometry to analyze how mechanical stresses and deformations influence macromolecular distribution in a gel, in order to simulate an intratumoral infusion. Also biphasic theory has been used to develop an analytical model to describe drug delivery to solid tumors. Garcia and Smith (2008), in fact, employed a biphasic hyperelastic model to describe infusion into brain, attributing the differences between linear solution and nonlinear analyses to geometric nonlinearities. However, the interest of the scientific community is increasingly addressed to numerical approaches. FE models, in fact, allow to describe more realistic infusion protocols and geometries and to perform parametric analysis. Linninger et al. (2008) proposed a computational technique to rigorously predict the distribution of drugs in brain tissue, based on the three-dimensional reconstruction from patient-specific images. This approach allows to take into account brain heterogeneity and anisotropy. Chen and Sarntinoranont (2007) employed the software package ADINA to study the effects of pressure-induced swelling on the macromolecular transport, modeling brain tissue as a biphasic isotropic medium. They validated their results comparing them to the analytical solution of Basser (1992) and developed a sensitivity analysis to quantify the effect of the changes in the material parameters on the pressure-controlled infusion. As highlighted in this introduction, the CED technique has been investigated by many authors because it represents a challenging approach to overcome the physiological barriers in brain tumors treatment. In this chapter, a FE computational model of CED protocols, based on the PTD theory, is presented. However, this approach presents some limits. The model employed, in fact, is linear and isotropic, for both the constitutive behavior and the permeability. These assumptions are the same used by Basser (1992). The other limit is that the therapeutic fluid agent is simply guided by pressure gradients, modeled employing the Darcy's law, and not by a diffusion process, described by Fick's law. On the contrary, an advantage of the approach proposed is the possibility to perform FEM analyses, by starting from mechanical, geometrical and infusion data reported in the scientific literature. Following this way, a parametrical custom-made Ansys® environment macro is used to perform steady state and transient poroelastic analyses employing the PTD theory. Another important advantage of this model consists in the possibility of simulating in silico sensitivity analyses to determine the effects of different parameters on the effectiveness of the infusion protocols.

10.4. FE MODEL OF DRUG DELIVERY TO SOLID TUMORS

This FEM analysis has been performed to compare the analytical steady state solution presented by Basser (1992) for a step brain infusion from a pressure source into a spherical cavity of radius *a*, with the solutions obtained with the software Ansys®.

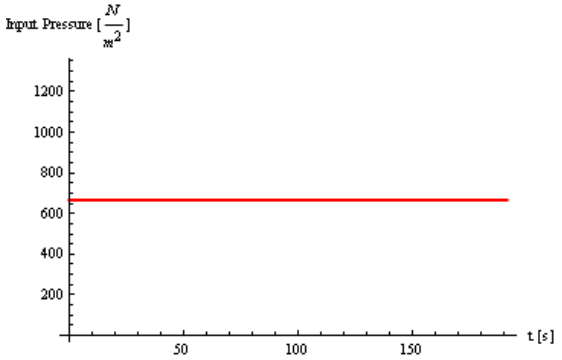

Fig. 10.11 – Input Pressure in the cavity

As just said before, brain tissue is modeled as an isotropic poroelastic medium. Starting from Biot's poroelasticity theory, the solution is found imposing that the pressure in the cavity suddenly jumps from zero to P_0, i.e. $P(a,t) = P_0 H(t)$, as illustrated in Figure 10.11.

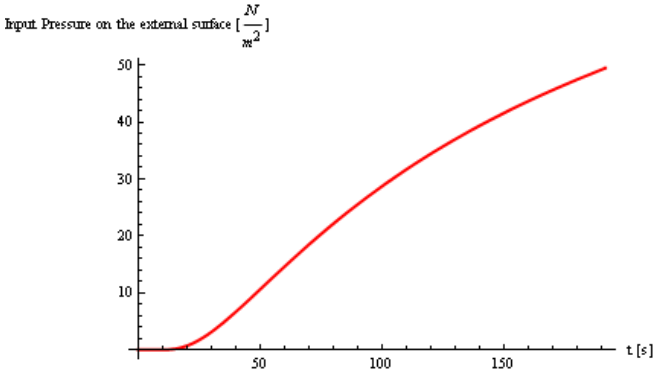

Fig. 10.12 – Input Pressure on the external surface

The resulting pressure distribution for $r \gg a$ is:

$$P(r,t) = P_0 \frac{a}{r}\left(1 - erf\left(\frac{r-a}{2\sqrt{ct}}\right)\right) \qquad (10.1)$$

where $c = \frac{K_P}{\mu}\left(\lambda + 2\mu_{solid}\right)$ is the consolidation coefficient.

Moreover, because the solution found by Basser (1992) refers to an infinite medium, the numerical solution is evaluated imposing on the external surface the pressure profile obtained from equation (10.1) when $r = 5a$, as shown in Figure 10.12.

The infusionparameters , the gray and white matter parameters employed by Basser (1992) are reported in Table 10.4, 10.5 and 10.6 respectively.

INFUSION PARAMETERS	
Infusion Pressure	P_0=6664 [dynes/cm^2]
Infusion flow rate	Q_0=10^{-5} [cm^3/s]
Radius of spherical cavity	a=0.03 [cm]
Radius of tissue sample	R_0=2 [cm]
Solute diffusivity	D=10^{-7} [cm^2/s]

Table 10.4 – Infusion parameters employed by Basser (1992)

GRAY MATTER	
Shear modulus	G=2 10^4 [dynes/cm^2]
Lamé constant	λ=9 10^5 [dynes/cm^2]
Permeability	κ=5 10^{-9} [cm^4/dynes s]
Pore fraction	f=0.2

Table 10.5 – Gray matter parameters employed by Basser (1992)

WHITE MATTER	
Shear modulus	G=9 10^3 [dynes/cm^2]
Lamé constant	λ=4 10^5 [dynes/cm^2]
Permeability	κ=7.5 10^{-9} [cm^4/dynes s]
Pore fraction	f=0.2

Table 10.6 – White matter parameters employed by Basser (1992)

To compare analytical and numerical results, brain tissue is modeled as a sphere with an infusion cavity of radius *a*.

After the definition of the geometry of the problem, the domain has been discretizatized. The Finite Elements Method based model is constructed by means of hexahedral 8 nodes elements with linear shape functions generating a 16875 elements and 18746 nodes mesh. The element chosen for the mesh, i.e.

SOLID70, requires that opposites sides of the discretized domain have the same number of divisions.
Moreover, in order to optimize the mesh, the element size increases with the sphere radius.
Figure 10.13 illustrates the number of divisions along the radius, *m*, and along the circular arches, *n*.

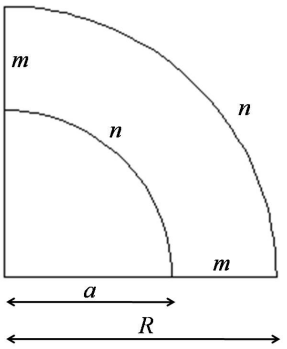

Fig. 10.13 – Division numbers along the radius, *m*, and along the circular arches, *n*

To this purpose, if $\alpha = \frac{a}{R}$, the number of divisions *m* along the radius is evaluated as the geometrical average, i.e.,

$$m = \frac{2n}{\pi}\frac{1-\alpha}{\sqrt{\alpha}} \tag{10.2}$$

The relationship (10.2) allows to determine, starting from *n*, the number of

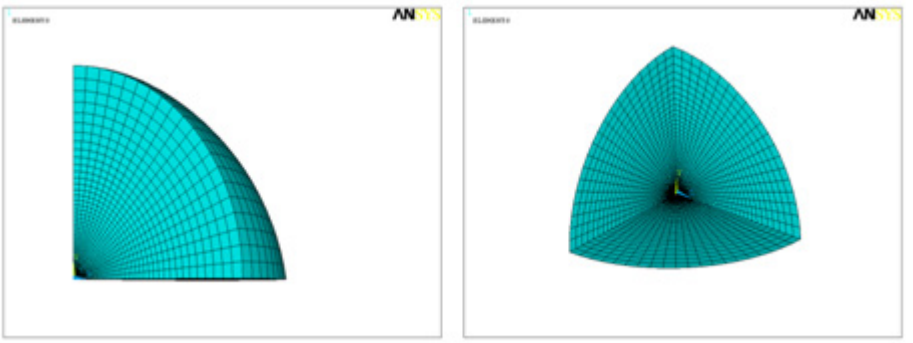

Fig. 10.14 – Finite Element mesh of the model

divisions *m*, as function of the ratio between the cavity radius and the sphere

one.
The Finite Element Mesh of the model proposed is shown in Figure 10.14. Because the problem is axial-symmetrical, only $\frac{1}{4}$ of the whole geometry is represented.
The steady state solutions for the analytical and numerical analyses overlap, as shown in Figure 10.15.

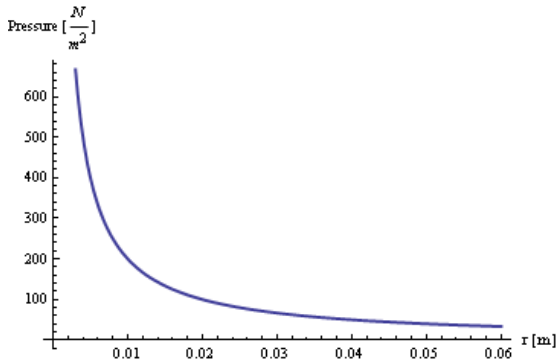

Fig. 10.15 – Steady state solution for an infinite, isotropic medium

Moreover, adopting the same geometry and mesh as well as the same input conditions, a transient analysis has also been performed, making reference to the physical parameters reported in Table 10.7.
The transient analysis has been conducted in 40 substeps, with a time substep of 2 seconds.

INPUT PARAMETERS	
Tissue sample radius R	$2\ 10^{-2}$ [m]
Hydraulic conductivity	$5\ 10^{-12}$ [m^2/Pa s]
Elastic shear modulus	$2\ 10^{3}$ [Pa]
Lamé constant	$9\ 10^{4}$ [Pa]
Storage Modulus	$1.8356\ 10^{-8}$ [Pa]
Density	1000 [Kg/m^3]
Reference Temperature	1 [K]

Table 10.7 – Finite Parameter values used in the model

In the following Figure 10.16. it is shown the pseudo-hyperbolic variation of the pressure along the radius for different values of the time; in particular it is illustrated the curves for a time value equal to 2 seconds and from a time value equal to 10 seconds to a time value equal to 80 seconds with a substep time value of 10 seconds.
All the curves are differently coloured.

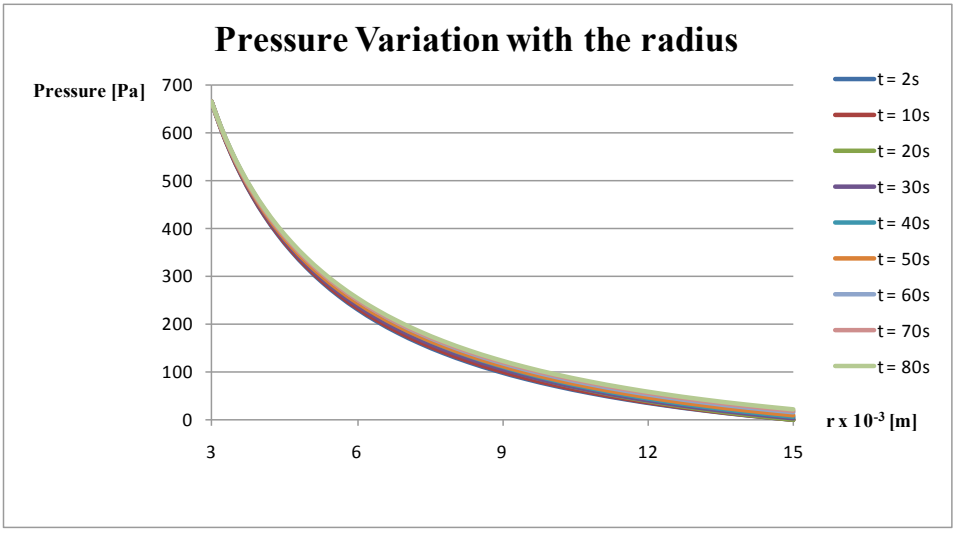

Fig. 10.16 – Pressure variations with the radius for different time substeps

It has to be noticed that these profiles show an oscillatory effect, as illustrated in Figure 10.17, because pressure values increase or decrease in an alternative way, passing from a time value to the following one.

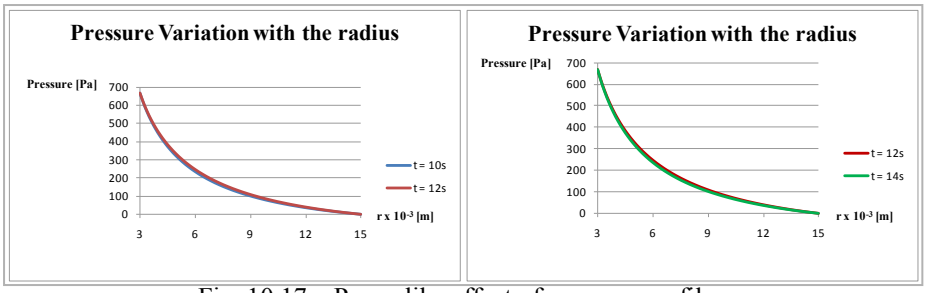

Fig. 10.17 – Pump-like effect of pressure profiles

In particular the graphics illustrate in the figure 10.15 describe the variation of the pressure along the radius in different times, that is for t equal 10, 12 and 14 second.
The figure highlights the alternative way of increasing or decreasing of the curves and so the oscillatory effect due to the variation with time.
Indeed, it is very interesting to investigate also pressure variation with time for different radius values.
In the following graphics in Figure 10.18 it is illustrated, in fact, the decreasing weight of the transitory waves when the radius increases.
Pressure profiles, in fact, are more affected by the oscillatory behavior induced by the transitory presence for radius values next to the infusion cavity then for radius values far from it.

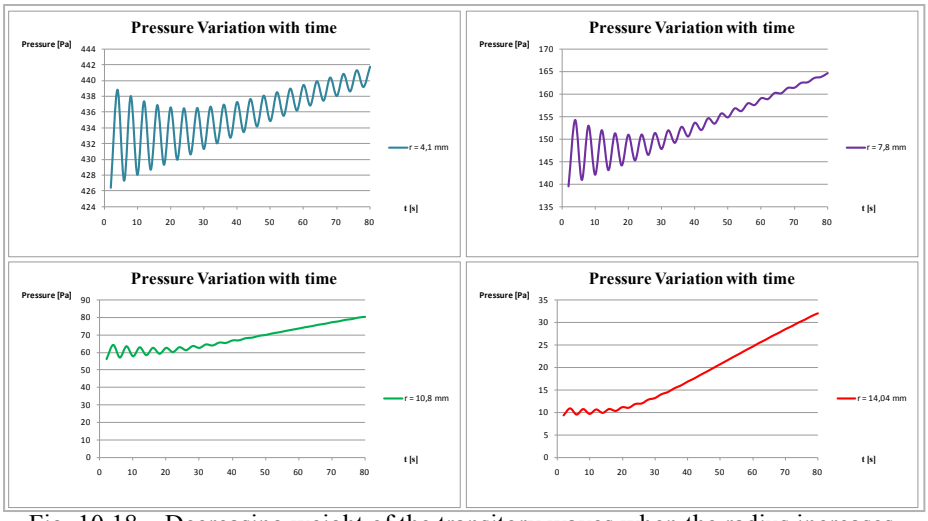

Fig. 10.18 – Decreasing weight of the transitory waves when the radius increases

The following figure 10.19, instead, concerns the pressure map for a selected time substep.
Extending the analysis to the whole temporal range, also in this case the oscillatory behavior outcrops.

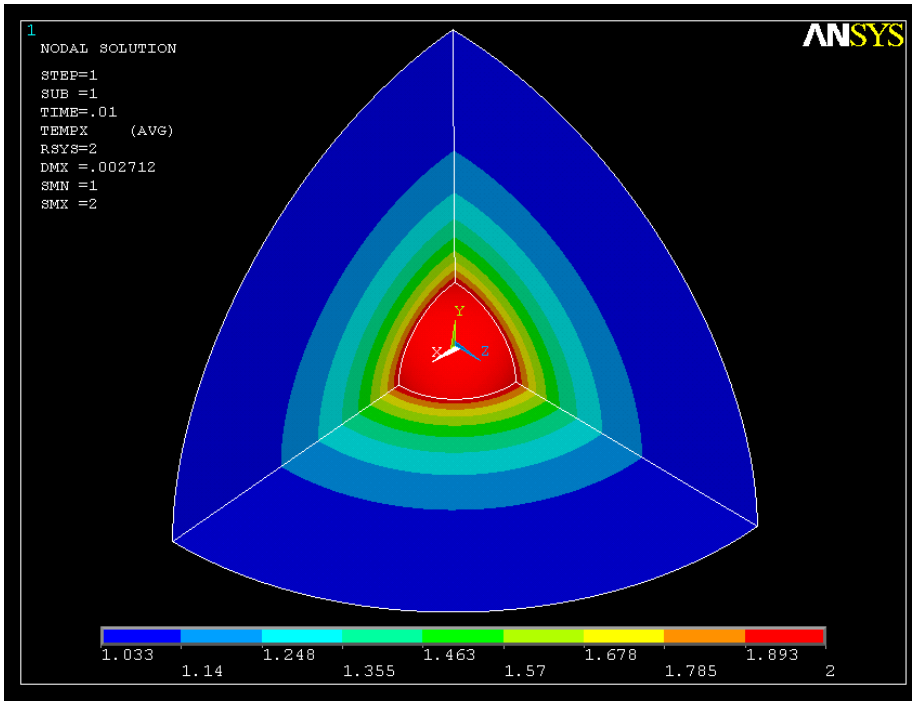

Fig. 10.19 – Pressure Map

Moreover, it has to be noticed that Figure 10.19 – 10.21 are associated to the output of the thermo-mechanical analysis and, so, all the values need to be multiplied for the appropriate coefficients to transform them into poroelastic output.
The following figure 10.20 illustrates the deformation maps in the spherical coordinates system.

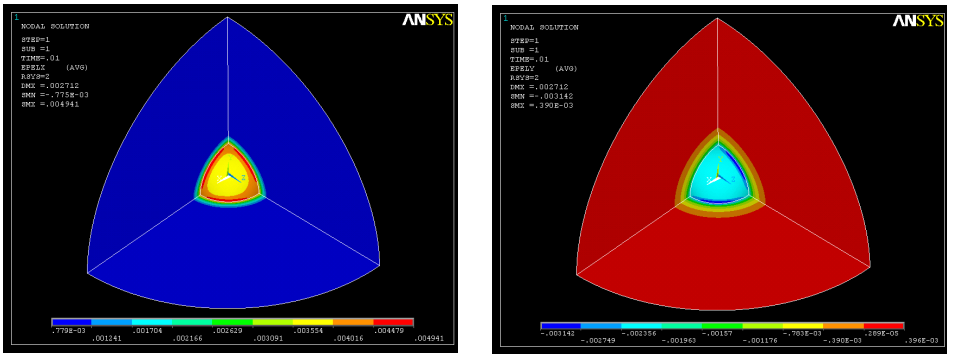

Fig. 10.20 – Deformation Mapsin spherical coordinates system

The next figure 10.21 reports the radial displacement map.

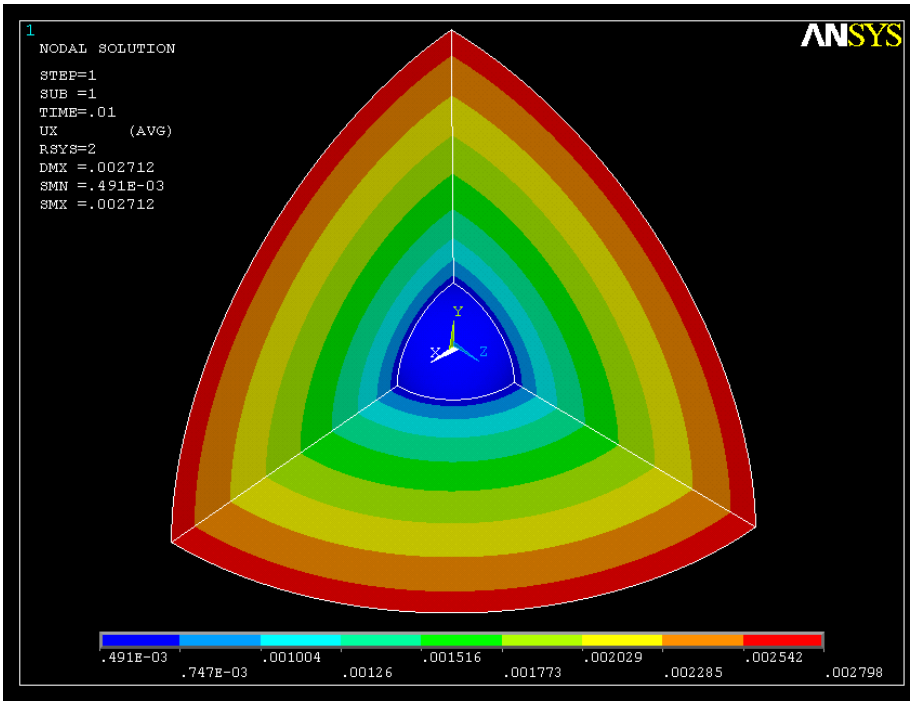

Fig. 10.21 – Radial Displacement Map

Finally, Figure 8.22 reports the Von Mises stress map. Von Mises stresses are very important parameters in order to ensure that the infusion input applied to brain do not cause the tissue failure. These stresses could, in fact, be used to introduce a stretch ratio, defined as the ratio between the stresses experienced by the tissue and the brain yield stress, referring, for example, to the work of Velardi et al. (2006). Values of the stretch ratio less than one ensure that the infusion procedure adopted preserves tissue integrity.

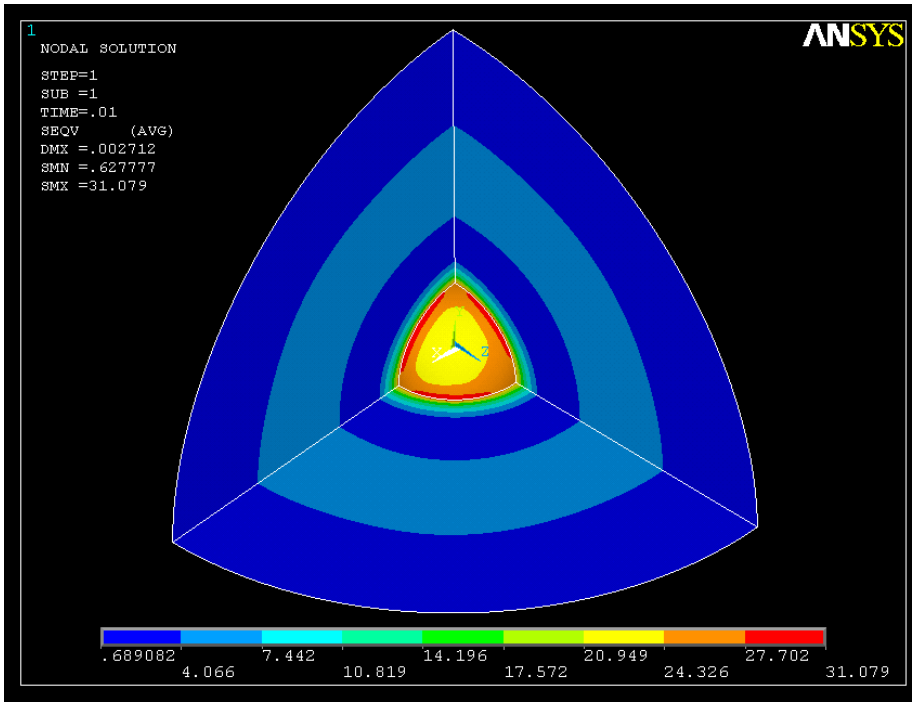

Fig. 8.22 – Von Mises stress Map

It is worth to note that replacing the values reported in Table 8.7 in the expression (9.35) and considering t_0^P as 80 s, the inequality $h^P << 1$ subsists and, thus, the problem results uncoupled and quasi static.

As highlighted before, the purpose of these analyses concerns the improvement of CED protocols. The back-flow mechanism occurring in CED will be objet of further investigations. By CED, in fact, the drug delivery is driven by the pressure gradient, due to the difference between the skull pressure and the infusion one and, so, the injection flow is a crucial parameter for the effectiveness of the infusion. Moreover, the infusion rate is limited by the back-flow mechanism. Back-flow can cause the release of the drug in not targeted brain regions and it can also induce a drug lack where necessary. Back-flow depends, above all, on three parameters: the catheter placement, the injection rate and the catheter diameter. Moreover, for the constancy of the fluid

discharge, the injection rate and the catheter diameter are strictly connected and, thus, only the diameter can be considered as a crucial parameter in the induction of the back-flow. Two different kinds of backflow can be envisaged. First of all, backflow can occur because the catheter placement can cause the mechanical disruption of the tissue and the formation of voids, determining the reflux of the therapeutic infused agent through that gap. However, backflow can be also intrinsic, associated to the tissue separation from the catheter induced by the pressure guiding the infusion process. This phenomenon stops only when this pressure is balanced by the shear forces in the tissue (Raghavan et al., 2006). The FE software *Ansys*® could be employed to investigate the transient profiles of pressure and velocity and the influence of different parameters on the back-flow mechanism occurring in CED. This aspect is very important because, even if CED technique ensures larger volumes of drug distribution, its clinical application is not widespread for some obstacles, such as backflow itself, responsible of the uncontrolled drug release (Ivanchenko et al., 2010).

REFERENCES

ANSYS Inc (2007) ANSYS 11 user's documentation. Canonsburg, PA

Allard E, Passirani C, Benoit JP. 2009. Convection-enhanced delivery of nanocarriers for the treatment of brain tumors. Biomaterials. 30: 2302-2318.

Bàca V, Kachlìk D, Horàk Z, Stingl J. 2007. The course of osteons in the compact bone of the human proximal femur with clinical and biomechanical significance. Surgical and Radiologic Anatomy. 29: 201-207.

Basser PJ. 1992. Interstitial pressure, volume, and flow during infusion into brain tissue. Microvascular Research. 44: 143-165.

Baxter L, Jain RK. 1989. Transport of fluid and macromolecules in tumors I. Role of interstitial pressure and convection. Microvascular Research. 37: 77-104.

Beraudi A, Stea S, Montesi M, Baleani M, Viceconti M, 2009. Collagen orientation in human femur, tibia and fibula shaft by circularly polarized light. Bone. 44: S253-S338.

Biot MA. 1955. Theory of elasticity and consolidation for a porous anisotropic solid. Journal of Applied Physics. 26: 182-185.

Bonucci E. 2009. The osteocyte: the underestimated conductor of the bone orchestra. Rendiconti Lincei Scienze Fisiche e Naturali. 20: 237-254.

Chen X, Sarntinoranont M. 2007. Biphasic Finite Element Model of solute transport for direct infusion into nervous tissue. Annals of Biomedical Engineering. 35: 2145-2158.

Cowin SC, Moss-Salentijn L, Moss ML. 1991. Candidates for the Mechanosensory System in Bone. Journal of Biomechanical Engineering. 113: 191-197.

Cowin SC. 2002. Mechanosensation and fluid transport in living bone. Journal of musculoskeletal & neuronal interactions. 2: 256-260.

Cowin SC, Gailani G, Benalla M. 2009. Hierarchical poroelasticity: movement of interstitial fluid between porosity levels in bones. Philosophical Transactions of the Royal Society A. 13: 3401-3444.

Garcia JJ, Smith JH. 2008. A Biphasic Hyperelastic Model for the Analysis of Fluid and Mass Transport in Brain Tissue. Annals of Biomedical Engineering. 37: 375-386.

Gross TS, Edwards JL, McLeod KJ, Rubin CT. 1997. Strain Gradients correlate with sites of periosteal bone formation. Journal of Bone and mineral Research. 12: 982-988.

Gupta HS, Stachewicz U, Wagermaier W, Roscherger P, Wagner HD, Fratzl P. 2006. Mechanical modulation at the lamellar level in osteonal bone. Journal of Materials Research. 21: 1913-1921.

Han Y, Cowin SC, Schaffler MB, Weinbaum S. 2004. Mechanotrasduction and strain amplification in osteocyte cell processes. PNAS. 101: 16689-16694.

Huang J, Rapoff AJ, Haftka RT. 2006. Attracting cracks for arrestment in bone-like composites. Materials and Design. 27: 461-469.

Ivanchenko O, Sindhwani N, Linninger A. 2010. Experimental techniques for studying poroelasticity in brain phantom gels under high flow microinfusion. Journal of Biomechanical Engineering. 132: 1-8.

Knothe Tate ML. 2003. Whither flows the fluid in bone? An osteocyte's perspective. Journal of Biomechanics. 36: 1409-1424.

Jain RK, 1988. Determinants of tumor blood flow: a review. Cancer Research. 48: 2641.

Linninger AA, Somayaji MR, Erickson T, Guo X, Penn RD. 2008. Computational methods for predicting drug transport in anisotropic and heterogeneous brain tissue. Journal of Biomechanics. 41: 2176-2187.

Mohsin S, O'Brien FJ, Lee TC. 2006. Osteonal crack barriers in ovine compact bone. Journal of Anatomy. 208: 81-89.

Mollica F, Jain RK, Netti PA. 2003. A model for temporal heterogeneities of tumor blood flow. Microvascular Research. 65: 56-60.

Netti PA, Baxter LT, Boucher Y, Skalak R, Jain RK. 1995. Time-dependent behavior of interstitial fluid pressure in solid tumors: implications for drug delivery. Cancer Research. 55: 5451-5458.

Netti PA, Roberge S, Boucher Y, Baxter LT, Jain RK. 1996. Effect of Transvascular fluid exchange on pressure-flow relationship in tumors: a proposed mechanism for tumor blood flow heterogeneity. Microvascular Research. 52: 27-46.

Netti PA, Baxter LT, Boucher Y. 1997. Macro- and Microscopic fluid transport in living tissues: application to solid tumors. AIChE Journal. 43: 818-834.

Netti PA, Travascio F, Jain RK. 2003. Coupled Macromolecular Transport and Gel Mechanics: Poroviscoelastic Approach. AIChE Journal. 49: 1580-1596.

O'Brien FJ, Taylor D, Lee TC. 2007. Bone as a composite material: The role of osteons as barriers to crack growth in compact bone. Internation Journal of Fatigue. 29: 1051-1056.

Raghavan R, Brady ML, Rodriguez-Ponce MI, Hartlep A, Pedain C, Sampson JH. 2006. Convection-enhanced delivery of therapeutics for brain disease, and its optimization. Neurosergery focus. 20: 1-13.

Ramasamy JG, Akkus O. 2006. Local variations in the micromechanical properties of mouse femur: the involvement of collagen fiber orientation and mineralization. Journal of Biomechanics. 40: 910-918.

Rémond A, Naïli S, Lemaire T. 2008. Interstitial fluid flow in the osteon with spatial gradients of mechanical properties: a finite element study. Biomechanics and Modeling in Mechanobiology. 7: 487-495.

Roose T, Netti PA, Munn LL, Boucher Y, Jain RK. 2003. Solid stress generated by spheroid growth estimated using a linear poroelasticity model. Microvascular Research. 66: 201-212.

Ruimerman R, Van Rietbergen B, Hilbers P, Huiskes R. 2005. The effects of Trabecular-Bone Loading Variables on the Surface Signaling Potential for Bone Remodeling and Adaptation. Annals of Biomedical Engineering. 33: 71-78.

Skedros JG, Mendenhall SD, Kiser CJ, Winet H. 2009. Interpreting cortical bone adaptation and load history by quantifying osteon morphotypes in circularly polarized light images. Bone. 44: 392-403.

Smit TH, Burger EH, Huyghe JM. 2002. A case for strain-induced fluid flow as a regulator of BMU-coupling and osteonal alignment. Journal of Bone and Mineral Research. 17: 2021-2029.

Smith JH, Humphrey JAC. 2007. Interstitial transport and transvascular fluid exchange during infusion into brain and tumor tissue. Microvasecular Research. 73: 58-73.

Velardi F, Fraternali F, Angelillo M. 2006. Anisotropic constitutive equations and experimental tensile behavior of brain tissue. Biomechanical Modeling in Mechanobiology. 5: 53-61.

Yoon YJ, Cowin SC. 2008. The estimated elastic constants for a single bone osteonal lamella. Biomechanics and Modeling in Mechanobiology. 7: 1-11.

Yoon YJ, Cowin SC, 2008. An estimate of anisotropic poroelastic constants of an osteon. Biomechanics and Modeling in Mechanobiology. 7: 13-26.

Yuan F. 1998 Transvascular drug delivery in solid tumors. Seminars in Radiation Oncology. 8: 164-175.

Wagermaier W, Gupta HS, Gourrier A, Burghammer M, Roscheger P, Fratzl P. 2006. Spiral twisting of fiber orientation inside bone. Biointerphases. 1: 1-5.

Walker WL, Cook J. 1996. Drug delivery to brain tumors. Bulletin of Mathematical Biology. 58: 1047-1074.

Weiner S, Traub W, Wagner HD. 1999. Lamellar Bone: Structure-Function Relations. Journal of Structural Biology. 126: 241-255.